



A National Center of Excellence in Advanced Technology Applications

ISSN 1520-295X

Experimental Investigation and Computational Modeling of Seismic Response of a 1:4 Scale Model Steel Structure with a Load Balancing Supplemental Damping System

by

Gokhan Pekcan, John B. Mander and Stuart S. Chen

University at Buffalo, State University of New York

Department of Civil, Structural and Environmental Engineering

Ketter Hall

Buffalo, New York 14260-4300

Technical Report MCEER-99-0006

April 2, 1999

This research was conducted at the University at Buffalo, State University of New York and was supported in whole or in part by the National Science Foundation under Grant No. CMS 96-16624.

NOTICE

This report was prepared by the University at Buffalo, State University of New York as a result of research sponsored by the Multidisciplinary Center for Earthquake Engineering Research (MCEER) through a grant from the National Science Foundation and other sponsors. Neither MCEER, associates of MCEER, its sponsors, University at Buffalo, State University of New York, nor any person acting on their behalf:

- a. makes any warranty, express or implied, with respect to the use of any information, apparatus, method, or process disclosed in this report or that such use may not infringe upon privately owned rights; or
- b. assumes any liabilities of whatsoever kind with respect to the use of, or the damage resulting from the use of, any information, apparatus, method, or process disclosed in this report.

Any opinions, findings, and conclusions or recommendations expressed in this publication are those of the author(s) and do not necessarily reflect the views of MCEER, the National Science Foundation, or other sponsors.



**Experimental Investigation and Computational Modeling
of Seismic Response of a 1:4 Scale Model
Steel Structure with a Load
Balancing Supplemental Damping System**

by

Gokhan Pekcan¹, John B. Mander² and Stuart S. Chen²

Publication Date: April 2, 1999

Submittal Date: November 6, 1998

Technical Report MCEER-99-0006

Task Number 97-5000

NSF Master Contract Number CMS 96-16624

University at Buffalo Foundation Contract Number UBFS-9103-374825

- 1 Post Doctoral Research Associate, Department of Civil, Structural and Environmental Engineering, University at Buffalo, State University of New York
- 2 Associate Professor, Department of Civil, Structural and Environmental Engineering, University at Buffalo, State University of New York

MULTIDISCIPLINARY CENTER FOR EARTHQUAKE ENGINEERING RESEARCH
University at Buffalo, State University of New York
Red Jacket Quadrangle, Buffalo, NY 14261

Preface

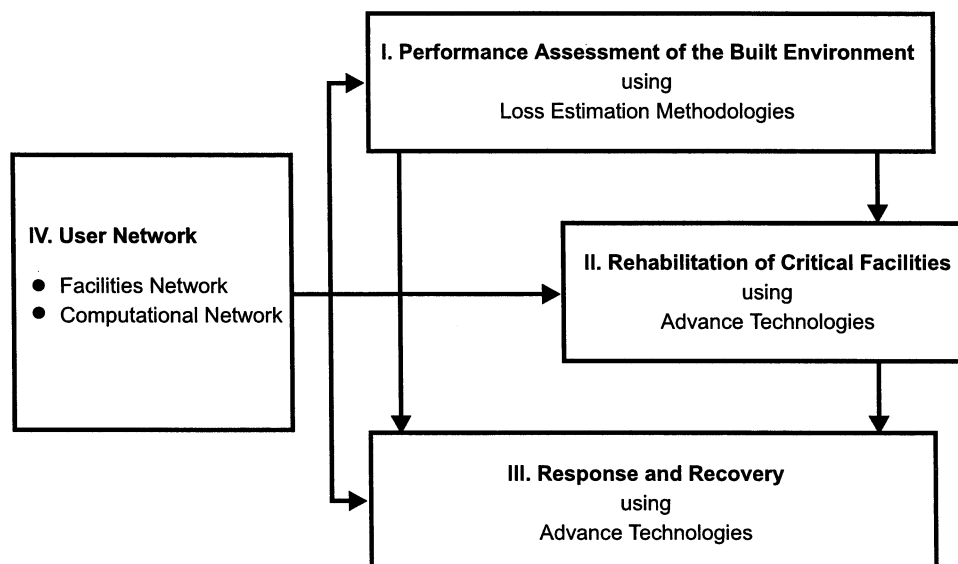
The Multidisciplinary Center for Earthquake Engineering Research (MCEER) is a national center of excellence in advanced technology applications that is dedicated to the reduction of earthquake losses nationwide. Headquartered at the University at Buffalo, State University of New York, the Center was originally established by the National Science Foundation in 1986, as the National Center for Earthquake Engineering Research (NCEER).

Comprising a consortium of researchers from numerous disciplines and institutions throughout the United States, the Center's mission is to reduce earthquake losses through research and the application of advanced technologies that improve engineering, pre-earthquake planning and post-earthquake recovery strategies. Toward this end, the Center coordinates a nationwide program of multidisciplinary team research, education and outreach activities.

MCEER's research is conducted under the sponsorship of two major federal agencies: the National Science Foundation (NSF) and the Federal Highway Administration (FHWA), and the State of New York. Significant support is derived from the Federal Emergency Management Agency (FEMA), other state governments, academic institutions, foreign governments and private industry.

The Center's NSF-sponsored research is focused around four major thrusts, as shown in the figure below:

- quantifying building and lifeline performance in future earthquake through the estimation of expected losses;
- developing cost-effective, performance based, rehabilitation technologies for critical facilities;
- improving response and recovery through strategic planning and crisis management;
- establishing two user networks, one in experimental facilities and computing environments and the other in computational and analytical resources.



This report describes the development of a novel idea for placement of damping systems in structures to reduce their vibrations and eliminate damage even in the case of high velocity pulses expected near a fault. The work presents a detailed study of the new concept supported by rigorous nonlinear analytical modeling and simulations and moreover, supported by a consistent experimental study of scaled models tested on the shaking table. The study discusses the advantages of the proposed system and the remaining challenges to be resolved in the future, thus providing a base for further expansion of knowledge. The solution suggested in this study helps to advance the engineering knowledge of innovative structural applications.

ABSTRACT

An experimental study to investigate the seismic behavior of steel structures under the simulated ground motions is described. It is argued that damper distribution should be based on: (i) either the interstory deformations or story shears, and (ii) the overturning moments generated by the lateral inertia loads. The former method was implemented in a non-ductile reinforced concrete frame (Pekcan et al., 1995), while for the latter method an innovative prestressed load-balancing tendon system was introduced in this report. Approximate alternatives were experimentally explored on a model steel structure. This load-balancing supplemental system consists of prestressed-draped tendons in the shape of the overturning moment diagram. The tendons are connected in series with the nonlinear dampers and sacrificial fuse-bars. It is concluded that the load-balancing tendon-fuse+damper system is an appropriate cost-effective method of mitigating the earthquake induced demands on a steel frame. By careful detailing, it is possible to ensure that under design earthquake loads the structure remains elastic, while under maximum credible motions fracture of the steel frame welded connections can be avoided.

ACKNOWLEDGEMENTS

Financial support was primarily provided by Jarret Inc. of Cannonsburg, PA. Funding under the “year 11” program was also provided by the National Center for Earthquake Engineering Research (NCEER). Both sources of support are gratefully acknowledged. The scaled model building was constructed and initially tested by A.M. Reinhorn and T.T. Soong and under partial financial support of the NCEER. Seismic laboratory technicians, Mark Pitman, assisted with conducting the shaking table tests, Dick Cidziel and Dan Walch, helped during the preparation of the experiments. All are gratefully acknowledged.

TABLE OF CONTENTS

ABSTRACT	v
ACKNOWLEDGEMENTS	vii
SECTION 1 INTRODUCTION	
1.1 Background	1
1.2 Objectives and Scope	2
1.3 Organization of this Report	3
SECTION 2 PROPERTIES AND ANALYTICAL MODELING OF ELASTOMERIC SPRING DAMPERS (ESD)	
2.1 Introduction	5
2.2 Properties of Elastomeric Spring Dampers	5
2.2.1 ESDs used in the Previous Studies	6
2.2.2 ESDs used in the Present Study	11
2.3 Analytical Characterization and Implementation of the Damper Behavior	11
2.3.1 Development of the Analytical Model	12
2.3.2 Solution of the Equations of Motion	16
2.3.2.1 One-Step Correction Method	16
2.3.2.2 Iterative Solution Method	17
2.3.3 Solution of the Differential Damper Force Equation	18
2.4 Verification of the Analytical Model	24
2.4.1 Comparison of Nonlinear Viscous Damper ($\alpha < 1$) Model with SAP 2000	24
2.5 Summary and Conclusions	29
SECTION 3 DAMPER CONFIGURATION AND PLACEMENT: CONCEPT DEVELOPMENT	
3.1 Introduction	31
3.2 Seismic Shears and Overturning Moments Imposed on Structural Frames	31
3.3 Damper Placement to Resist Interstory Shear Forces: Truss Solution (DTR)	32
3.3.1 Effective Damping and Device Distribution	36
3.4 Damper Placement to Resist Overturning Moments: Load Balancing Pre-stressed Tendon-Fuse+Damper Solution (LPTFD)	37

TABLE OF CONTENTS – CONT'D

3.4.1 The Load Balancing Approach: Pre-stressed Concrete Beam Analogy	37
3.4.2 The Load Balancing Approach: Application to Cantilever Frames	39
3.4.3 Tendon Layout to Balance Lateral Loads and Supplemental System Deformation	41
3.4.4 Damper Deformation and Provided Effective Damping	44
3.4.5 Approximate Load Balancing Solution – Straight Tendon	45
3.5 Discussion of the Proposed Configuration	47
3.5.1 Tendon Layout and Higher Mode Effects	47
3.5.2 Three Dimensional Response with LPT System	47
3.5.3 Floor Slab Detail	50
3.5.4 The Benefits of Pre-stressing	50
3.6 Summary and Conclusions	52
 SECTION 4 TEST STRUCTURE AND SHAKING TABLE TEST PROGRAM	
4.1 Introduction	53
4.2 Test Setup and Instrumentation	59
4.3 Test Program	59
4.4 Computational Modeling of the Test Structure	66
4.4.1 Modeling of the Braced Frame	66
4.4.2 Modeling of the Structure with the Load Balancing Tendon-Fuse+Damper System	67
 SECTION 5 SHAKING TABLE TEST RESULTS	
5.1 Introduction	69
5.2 Discussion of Previous Related Work	69
5.3 Properties of the ESD Devices and Fuse-Bars Used in the Experimental Study	71
5.4 Shaking Table Test Results	73
5.4.1 Comparison of Structural Dynamics Characteristics of Various Configurations	73
5.4.2 Tests on the Structure with Various Bracing Configurations	83
5.4.3 Tests on the Structure with ESDs and Fuse-Bars	100
5.4.3.1 Top Three Stories Braced (B4# Configurations)	100

TABLE OF CONTENTS – CONT'D

5.4.3.2 Moment Frame (B5# Configurations)	125
5.5 Summary and Conclusions	137
SECTION 6 DISCUSSION OF STRUCTURAL RESPONSE AND COMPARATIVE EVALUATION	
6.1 Introduction	153
6.2 Discussion of Structural Response and Analytical Evaluation	153
6.3 Effect of Tendon Profile	160
6.4 Summary and Conclusions	167
SECTION 7 SUMMARY, CONCLUSIONS AND RECOMMENDATIONS	
7.1 Executive Summary	169
7.2 Conclusions	171
7.3 Future Research Recommendations	173
SECTION 8	
REFERENCES	175

LIST OF FIGURES

Figure	Title	Page
2-1	Elastomeric Spring Damper – Modified for Double Acting	7
2-2	Selected Force-Deformation Relationships of a Model BC1C Damper	8
2-3	Selected Force-Deformation Relationships of a Prototype BC5A Damper	9
2-4	Selected Force-Deformation Relationships of a Model BC1C Damper: Present Study	10
2-5	Modeling of Dampers	13
2-6	Force-Deformation Modeling of Dampers	13
2-7	Various Damper Force-Deformation Relationships	21
2-8a	Comparison of Drain-2DX and SAP2000 Nonlinear Damper Models-Sinusoidal Input	26
2-8b	Comparison of Drain-2DX and SAP2000 Nonlinear Damper Models-Sinusoidal Input	27
2-9	Comparison of Drain-2DX and SAP2000 Nonlinear Damper Models-Earthquake Input	28
3-1	Seismic Shears and Overturning Moments Imposed on Structural Frames	33
3-2a	Damper Placement to Resist Interstory Shear Forces: Truss Solution	35
3-2b	Force Coefficients for Unit Base Shear	35
3-3	Prestressed Concrete Beam Analogy with Load Balancing Tendons	38
3-4	Load Balancing Prestressed Tendon-Fuse+Damper Solution (LPTFD)	40
3-5	Determination of Tendon Layout	42
3-6	Approximate Load Balancing Solution	46
3-7	Three-dimensional View of LPTFD System	48
3-8	Tendon-Floor Slab Detail	49
3-9	Effect of Initial Prestressing on the Behavior of Fuse-Bars	51
4-1	General View of Test Structure	54
4-2	Load Balancing Tendon-Fuse+Damper System and Third Floor Connection Details	55
4-3	Photograph of the ¼ Scale Model Test Structure	56
4-4	Photograph of the Third Floor-Tendon Connection	57
4-5	Photograph of the Supplementary System Detail	58

LIST OF FIGURES – CONT'D

Figure	Title	Page
4-6	Instrumentation of the Test Structure	60
4-7	Acceleration Records (1/2 time scaled)	62
4-8	Tested Configurations	63
4-9	Drain-2DX Computational Model of the Tendon System	67
5-1	Selected ESD Specimen Tests	72
5-2	Average Stress-Strain Relationship of Fuse-Bars	72
5-3	Comparison of story level transfer functions obtained from white noise experiments – Braced configurations and moment frame	75
5-4	Comparison of identified mode shapes – Braced configurations and moment frame	76
5-5	Comparison of story level transfer functions obtained from white noise experiments – Top three stories braced with supplementary system	77
5-6	Comparison of identified mode shapes – Top three stories braced with supplementary system	78
5-7	Comparison of story level transfer functions obtained from white noise experiments – Moment frame with supplementary system	79
5-8	Comparison of identified mode shapes – Moment frame with supplementary system	80
5-9	Experimental and Analytical Displacement Time Histories: B20EL12	84
5-10	Experimental and Analytical Displacement Time Histories: B20TA12	85
5-11	Experimental and Analytical Displacement Time Histories: B20HA08	86
5-12	Experimental and Analytical Displacement Time Histories: B30EL08	87
5-13	Experimental and Analytical Displacement Time Histories: B30TA08	88
5-14	Experimental and Analytical Displacement Time Histories: B30HA08	89
5-15	Experimental and Analytical Displacement Time Histories: B40EL12	90
5-16	Experimental and Analytical Displacement Time Histories: B40TA12	91

LIST OF FIGURES – CONT'D

Figure	Title	Page
5-17	Experimental and Analytical Displacement Time Histories: B40HA08	92
5-18	Experimental and Analytical Displacement Time Histories: MOMEL08	93
5-19	Experimental and Analytical Displacement Time Histories: MOMTA08	94
5-20	Experimental and Analytical Displacement Time Histories: MOMHA08	95
5-21	Maximum response envelopes for the braced and moment frame configurations subjected to El Centro ground motion at various PGA levels	96
5-22	Maximum response envelopes for the braced and moment frame configurations subjected to Taft ground motion at various PGA levels	97
5-23	Maximum response envelopes for the braced and moment frame configurations subjected to Hachinohe ground motion at various PGA levels	98
5-24	Five percent displacement, velocity and acceleration spectra for El Centro, Kobe and Sylmar ground motions (Note that these motions have been time scaled such that $T_{table}=T_{field}/2$)	99
5-25	Experimental and Analytical Displacement Time Histories: B41EL12	103
5-26	Experimental and Analytical Displacement Time Histories: B41TA12	104
5-27	Experimental and Analytical Displacement Time Histories: B41PA18	105
5-28	Experimental and Analytical Displacement Time Histories: B41SY17	106
5-29	Experimental and Analytical Displacement Time Histories: B41KO17	107
5-30	Experimental and Analytical Displacement Time Histories: B43EL20	109
5-31	Experimental and Analytical Average Tendon Force-Deformation: B43EL20	110
5-32	Experimental and Analytical Displacement Time Histories: B43TA20	111
5-33	Experimental and Analytical Average Tendon Force-Deformation: B43TA20	112
5-34	Experimental and Analytical Displacement Time Histories: B43PA20	113
5-35	Experimental and Analytical Average Tendon Force-Deformation: B43PA20	114
5-36	Experimental and Analytical Displacement Time Histories: B43SY20	115
5-37	Experimental and Analytical Average Tendon Force-Deformation: B43SY20	116
5-38	Experimental and Analytical Displacement Time Histories: B43KO20	117

LIST OF FIGURES – CONT'D

Figure	Title	Page
5-39	Experimental and Analytical Average Tendon Force-Deformation: B43KO20	118
5-40	Experimental and Analytical Displacement Time Histories: B44EL30	119
5-41	Experimental and Analytical Average Tendon Force-Deformation: B44EL30	120
5-42	Experimental and Analytical Displacement Time Histories: B44SY30	121
5-43	Experimental and Analytical Average Tendon Force-Deformation: B44SY30	122
5-44	Experimental and Analytical Displacement Time Histories: B44KO30	123
5-45	Experimental and Analytical Average Tendon Force-Deformation: B44KO30	124
5-46	Experimental and Analytical Displacement Time Histories: B47EL40	126
5-47	Experimental and Analytical Average Tendon Force-Deformation: B47EL40	127
5-48	Experimental and Analytical Displacement Time Histories: B47SY40	128
5-49	Experimental and Analytical Average Tendon Force-Deformation: B47SY40	129
5-50	Experimental and Analytical Displacement Time Histories: B47KO40	130
5-51	Experimental and Analytical Average Tendon Force-Deformation: B47KO40	131
5-52	Maximum response envelopes for the structure with top three stories braced and supplementary system active configurations subjected to El Centro ground motion at various PGA levels	132
5-53	Maximum response envelopes for the structure with top three stories braced and supplementary system active subjected to Sylmar ground motion at various PGA levels	133
5-54	Maximum response envelopes for the structure with top three stories braced and supplementary system active subjected to Kobe ground motion at various PGA levels	134
5-55	Experimental and Analytical Displacement Time Histories: B51EL40	138
5-56	Experimental and Analytical Average Tendon Force-Deformation: B51EL40	139
5-57	Experimental and Analytical Displacement Time Histories: B51SY40	140
5-58	Experimental and Analytical Average Tendon Force-Deformation: B51SY40	141
5-59	Experimental and Analytical Displacement Time Histories: B51KO40	142
5-60	Experimental and Analytical Average Tendon Force-Deformation: B51KO40	143

LIST OF FIGURES – CONT'D

Figure	Title	Page
5-62	Experimental and Analytical Displacement Time Histories: B52EL40	144
5-63	Experimental and Analytical Average Tendon Force-Deformation: B52EL40	145
5-63	Maximum response envelopes for the moment frame structure and supplementary system active subjected to El Centro ground motion at various PGA levels	146
5-64	Maximum response envelopes for the moment frame structure and supplementary system active subjected to Sylmar ground motion at various PGA levels	147
5-65	Maximum response envelopes for the moment frame structure and supplementary system active subjected to Kobe ground motion at various PGA levels	148
6-1	Comparison of response of the test structure subjected to severe ground motions (top three stories braced and damper only cases obtained analytically) – El Centro, PGA=0.419	156
6-2	Comparison of response of the test structure subjected to severe ground motions (top three stories braced and damper only cases obtained analytically) – Sylmar, PGA=0.505	157
6-3	Comparison of response of the test structure subjected to severe ground motions (top three stories braced and damper only cases obtained analytically) – Kobe, PGA=0.432	158
6-4	Comparison of response of the test structure subjected to severe ground motions (moment frame and damper only cases obtained analytically) – El Centro, PGA=0.307	159
6-5	Load Balancing Draped Tendon Profile used in the Analytical Study	161
6-6	Comparison of response of the test structure retrofitted with straight and draped tendon profile with dampers only and subjected El Centro, PGA=0.307	162
6-7	Comparison of response of the test structure retrofitted with straight and draped tendon profile with dampers only and subjected to Kobe, PGA=0.432	163
6-8	Comparison of response of the test structure retrofitted with straight and draped tendon profile with dampers+fuses and subjected to El Centro, PGA=0.307	164

LIST OF FIGURES – CONT'D

Figure	Title	Page
6-9	Comparison of response of the test structure retrofitted with straight and draped tendon profile with dampers+fuses and subjected to Kobe, PGA=0.432	165
6-10	Balanced Inertial Loads Based on the Triangular Distribution and Proportional to the 1st Mode Shape for Unit Base Shear	166

LIST OF TABLES

Table	Title	Page
2-1	Solution Algorithm Using Nonlinear Damper Force Relationship	19
2-2	FORTTRAN Code for the Solution of Differential Damper Force Equation	22
2-3	Variable Definitions	23
2-4	Parameters for BC1C and BC5A Dampers	23
2-5	Nonlinear Damper Properties used in Drain-2DX – SAP 2000 Comparison	25
4-1	Description of Instrumentation	61
4-2	Schedule of Shaking Table Experiments	64
5-1	Mode Shapes of the Moment Frame	74
5-2	Comparison of 1st Mode Natural Periods and Viscous Damping Ratios	82
5-3	Summary of Experimental Response – Braced Configurations	82
5-4	Comparison of 1st Mode Natural Periods and Viscous Damping Ratios Top 3 stories braced – Tendon system active	101
5-5	Summary of Experimental Response – Top 3 stories braced – Tendon system active	101
5-6	Comparison of 1st Mode Natural Periods and Viscous Damping Ratios Moment Frame - Tendon system active	136
5-7	Summary of Experimental Response – Moment Frame – Tendon system active	136
6-1	Comparison of Maximum Responses – Upper Three Stories Braced	155
6-2	Comparison of Maximum Responses – Bare Frame Only	155

SECTION 1

INTRODUCTION

1.1 BACKGROUND

Since steel moment frame structures did not perform particularly well in the recent 1994 Northridge earthquake, it is necessary for the profession to investigate both direct and indirect means of mitigating inherently faulty welded steel beam-column connection designs that were designed prior to the 1994 Northridge earthquake. Direct methods principally involve strengthening and/or enhancing the ductility of the welded beam-column connections. Much research sponsored by SAC has been directed to this end (SAC, 1995). It is the premise of the research presented here that indirect methods of mitigation should be investigated as an alternative or supplement to direct strengthening. Indirect methods embrace supplemental damping and/or bracing.

Another important consideration in the earthquake resistant design and retrofit of the structures is the near-source ground motions and their damage potential especially on flexible buildings. Since the 1994 Northridge earthquake, there have been a considerable number of studies on the effects of near-source ground motions. This type of ground shaking, which is generally accompanied by large velocity and displacement pulses, has a greater damage potential than those adopted in current design codes. In one recent study (Hall et al., 1995), it was pointed out that the displacement pulses at or near the natural period of vibration of the structure may cause severe damage to the structure as excessive interstory drifts are to be expected. If such pulses occur during the first cycle of response, maximum response is generally not a function of the damping in the structure. Furthermore, it can be shown that maximum deformation is attained at the end of the pulse. Therefore, the effect of damping in reducing the maximum response will be minimal since the dissipated energy will only be about one-fourth of that expected in one full cycle of response. This becomes an important issue in the design of structures with energy dissipation systems that rely merely on the added damping. For pulse-like ground motions such as those mentioned above, damper only systems will damp out the response after the initial peak response achieved but may only be of marginal value in mitigating the peak response.

Therefore, it follows that some additional and/or alternative means of damping is needed to arrest the impulse response. This experimental study investigates a system that employs strengthening through post-tensioned bracing coupled with a supplementary damping system. It consists of an approximate load-balancing tendon system with sacrificial fuse-bars which are used in parallel to elastomeric spring dampers (ESD). ESD devices were previously used to retrofit a three story – 1:3 scale lightly reinforced concrete structure tested under simulated earthquake loading on the shaking table at the State University of New York at Buffalo (Pekcan et al., 1995). The fuse-bars with a predefined yield load level provide a high (controllable) initial stiffness and limit displacements. However, the damping devices are still effective to attenuate the remaining motion following the first large peak and yielding of the fuse-bars. The system tested in this experimental study was designed to work only in tension. This had the advantage of being light-weight (no buckling problems), relatively unobtrusive and easy to install.

1.2 OBJECTIVES AND SCOPE

In the present study a type of single-acting damper device previously employed in the railroad and steel industries is used. These stock off-the-shelf devices, referred to here in as *elastomeric spring dampers (or ESD)*, exhibit a distinct re-centering characteristic and were modified to operate in a double-acting fashion and used to retrofit a lightly reinforced, previously damaged 1/3 scale model of an office building (Pekcan et al., 1995).

In the experimental part of the study, a 1:4 scale model steel structure was tested under various simulated ground motions using the shaking table in the State University of New York at Buffalo. Previously, the first experimental study on this model structure involved the testing of an active tendon system and active mass dampers (Reinhorn et al., 1989). This previous experimental study was primarily intended to investigate the effectiveness of a simple active control system in response control of complex structures under earthquake type excitations. Various active tendon configurations were tested both in strong and weak directions under simulated ground motions which had peak ground accelerations up to 0.09 g. Mokha et al (1990) tested the six-story moment frame supported on rigid beams with four Friction Pendulum System (FPS) isolators. Al-Hussaini et al. (1994) removed the rigid base and added an additional story with FPS isolators to further investigate the effectiveness of the FPS isolation system with various bracing configurations.

In this study, ESDs (as well as fuses) were installed in a series arrangement with a tension-only working tendon system. The model structure was tested under various simulated ground motions using the shaking table at the State University of New York at Buffalo. The principal objectives of investigating the performance of the proposed supplemental system are:

- i) to determine the mechanical properties of ESDs and improve the previously developed analytical model (Pekcan et al., 1995),
- ii) to investigate the experimentally-observed and analytically-predicted response characteristics of the model steel building structure with various supplemental system configurations,
- iii) to analytically study the effect of various tendon configurations on the overall response of the structure.

1.3 ORGANIZATION OF THIS REPORT

The primary emphasis is put on the experimental investigation of the proposed supplemental tendon system configuration (approximate load balancing tendon-fuse+damper system). The organization of the report is summarized in what follows.

Section 2 presents the improved computational modeling of the type of supplemental energy dissipation device (ESD) that was used in this study. Its implementation in one of the most widely used nonlinear structural dynamic analysis program namely, DRAIN-2DX is given. An innovative design/retrofit alternatives using supplementary systems are introduced in Section 3, following a general discussion of current design methodologies and retrofit strategies for reinforced concrete and steel structures. In Section 4, details of the test structure, test program and analytical modeling are presented. In Section 5, shaking table experiment results are given in comparison with the analytical predictions for the tested configurations. A discussion of the experimental results and observations are presented in Section 6 which is followed by subsequent analytical studies. Finally, conclusions are drawn and recommendations are made in Section 7.

SECTION 2

PROPERTIES AND ANALYTICAL MODELING OF ELASTOMERIC SPRING DAMPERS (ESD)

2.1 INTRODUCTION

In the present study, a type of single acting damper device previously employed in the railroad and steel industries is used. These stock off-the-shelf devices, called elastomeric spring dampers (ESD), exhibit a distinct re-centering characteristic and were modified to operate in double-acting fashion. ESDs were previously used to retrofit a lightly reinforced, previously damaged 1:3 scale model of an office building (Pekcan et al., 1995).

Previously developed, two-component velocity-dependent model to simulate the force-deformation behavior of ESD devices (Pekcan et al., 1995) is modified to improve the numerical stability of the solution of the equations of motion. The analytical model is implemented in the well-known nonlinear structural dynamic analysis program Drain-2DX (Parakash et al. 1992). Two alternative methods of solution for the nonlinear equations of motion are given in the following paragraphs. The analytical model and the solution methods are compared and discussed in detail. Finally, nonlinear viscous damper model is compared with that implemented in recently released commercially available SAP 2000 program.

2.2 PROPERTIES OF ELASTOMERIC SPRING DAMPERS

Over the last three decades the type of elastomeric spring damper investigated in the present study has enjoyed much use in a wide range of industrial, defense and civilian applications. Railway engineering applications in various parts of the U.S. and Europe for this class of shock absorbing device include end-of-track buffers and part of the car-to-car coupling systems on rapid transit trains. The dampers are used in many industrial applications including steel mills, manufacturing and process treatment industries, as well as heavy-duty material handling systems such as cranes. Military applications include shock absorption devices on missile and torpedo launching systems, gun recoil systems, and suspension systems for tanks. This class of shock absorber has also been applied to a wide range of civil engineering systems including the seismic protection of highway and railroad bridge systems, swing and lift bridges,

sliding roof and lock gate protection systems, and offshore drilling platforms. It is thus evident that this type of damper has historically exhibited good reliability and longevity in a variety of chemically and thermally hostile environments. It is therefore considered, based on this previous track record, that this class of shock absorber that utilizes the unique compressibility characteristics of the silicon elastomer, is a viable candidate for the seismic protection of buildings.

The dampers used in this study contain a silicone-based elastomer that has the appearance of silly-putty. The consistency of this material gives both compressibility and viscous attributes. Thus dampers can be designed to give both spring and hysteretic behavior. The performance of the elastomeric spring dampers results from the interaction of the following parameters; i) the precharge pressure of the elastomer, ii) the compressibility characteristic of the elastomer, iii) the viscosity and shear characteristics of the elastomer, iv) the design of the piston head, v) the size and the shape of the plunger, vi) the piston rod/plunger cavity volume relationship, and vii) seal friction. These parameters can be modified to produce a wide variety of required damper performance characteristics and energy absorption capabilities.

2.2.1 ESDs used in the Previous Studies

Single-acting (compression only) dampers were modified to enable the application for seismic protection of building structures, by building a housing around the damper to give similar tension and compression attributes as shown in figure 2-1. These model BC1C dampers were previously used to retrofit a 1:3 scale reinforced concrete model structure. The dampers were tested prior to shaking table experiments at varying displacement-controlled amplitudes (6.5-24 mm) and frequencies (6.5-2 Hz.). A total of twenty tests were performed on six damper specimens. Some selected force-deformation relationships from these specimen test results are plotted in figure 2-2.

Also tested was the prototype damper (BC5A). Force-deformation relationships for two different test amplitudes with various testing frequencies are plotted in figure 2-3. When compared to plots of figure 2-2, frequency dependency is more pronounced for BC5A type damper. The specimen test results were used to identify the computational model parameters introduced in the following paragraphs.

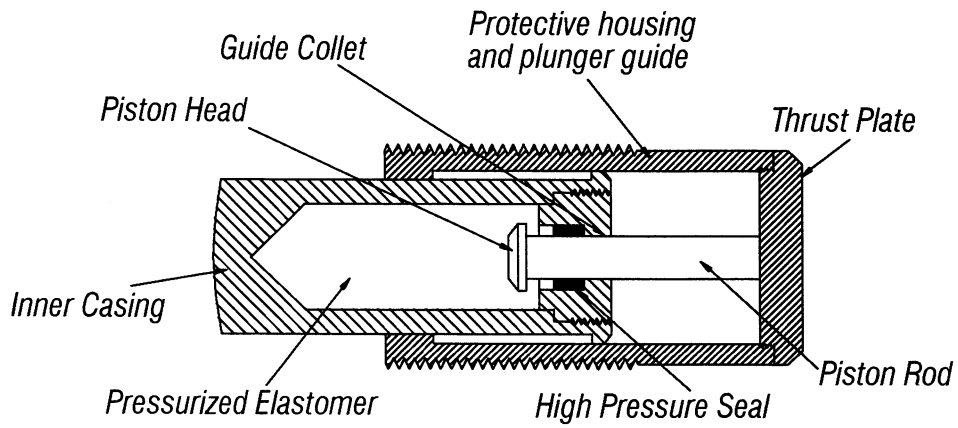
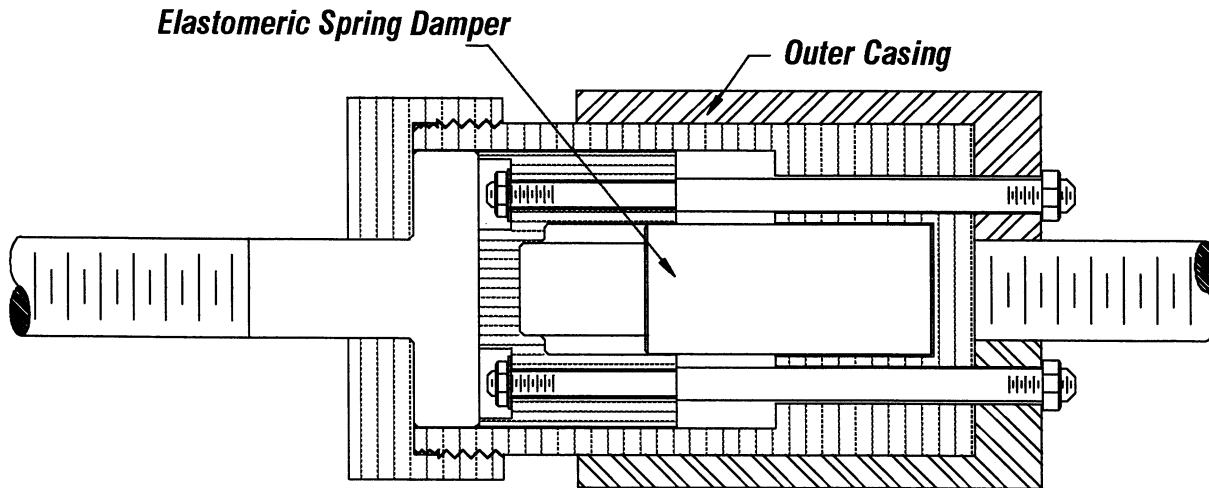


Figure 2-1 Elastomeric Spring Damper – Modified for Double Acting

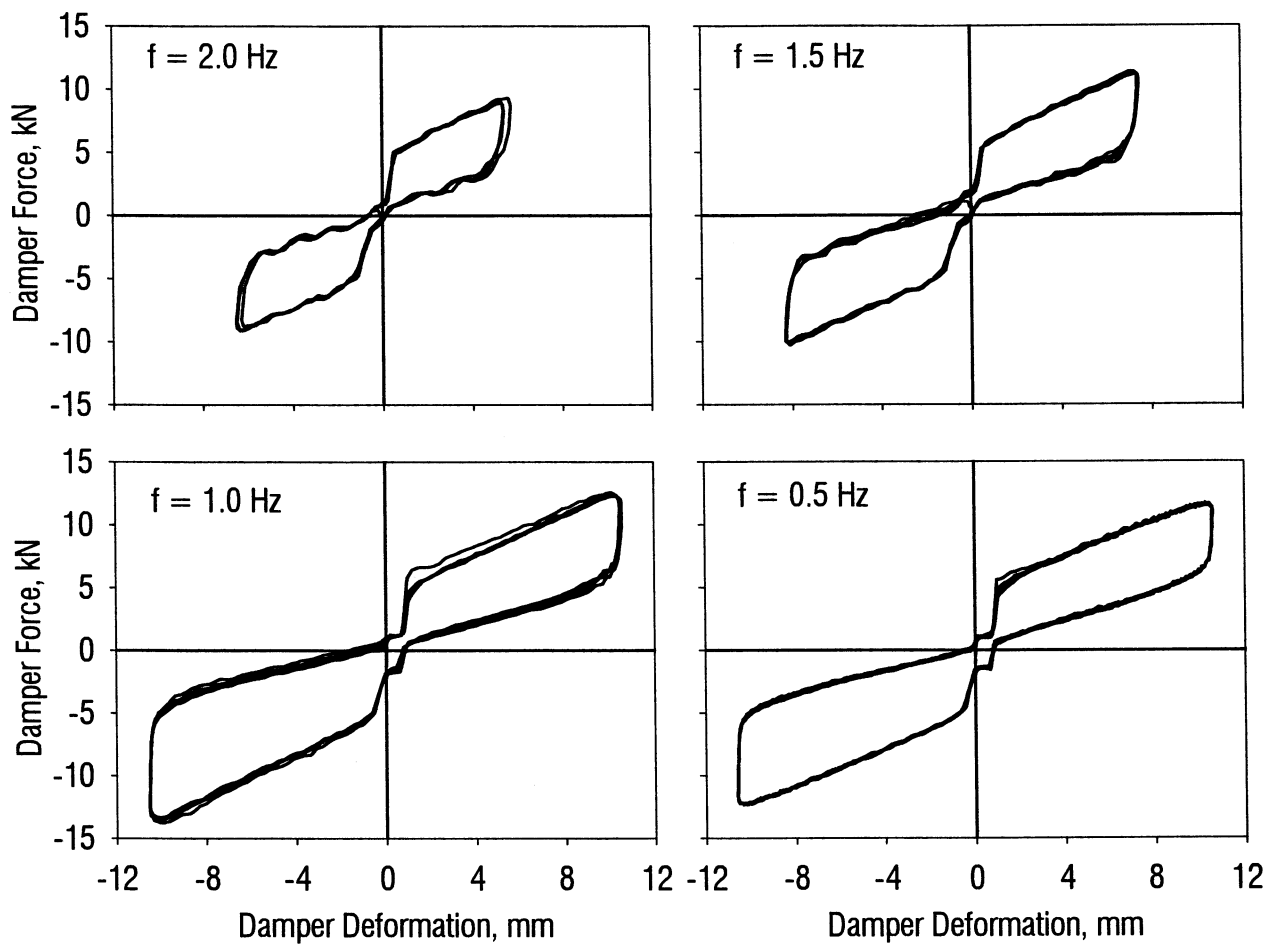


Figure 2-2 Selected Force-Deformation Relationships of a Model BC1C Damper

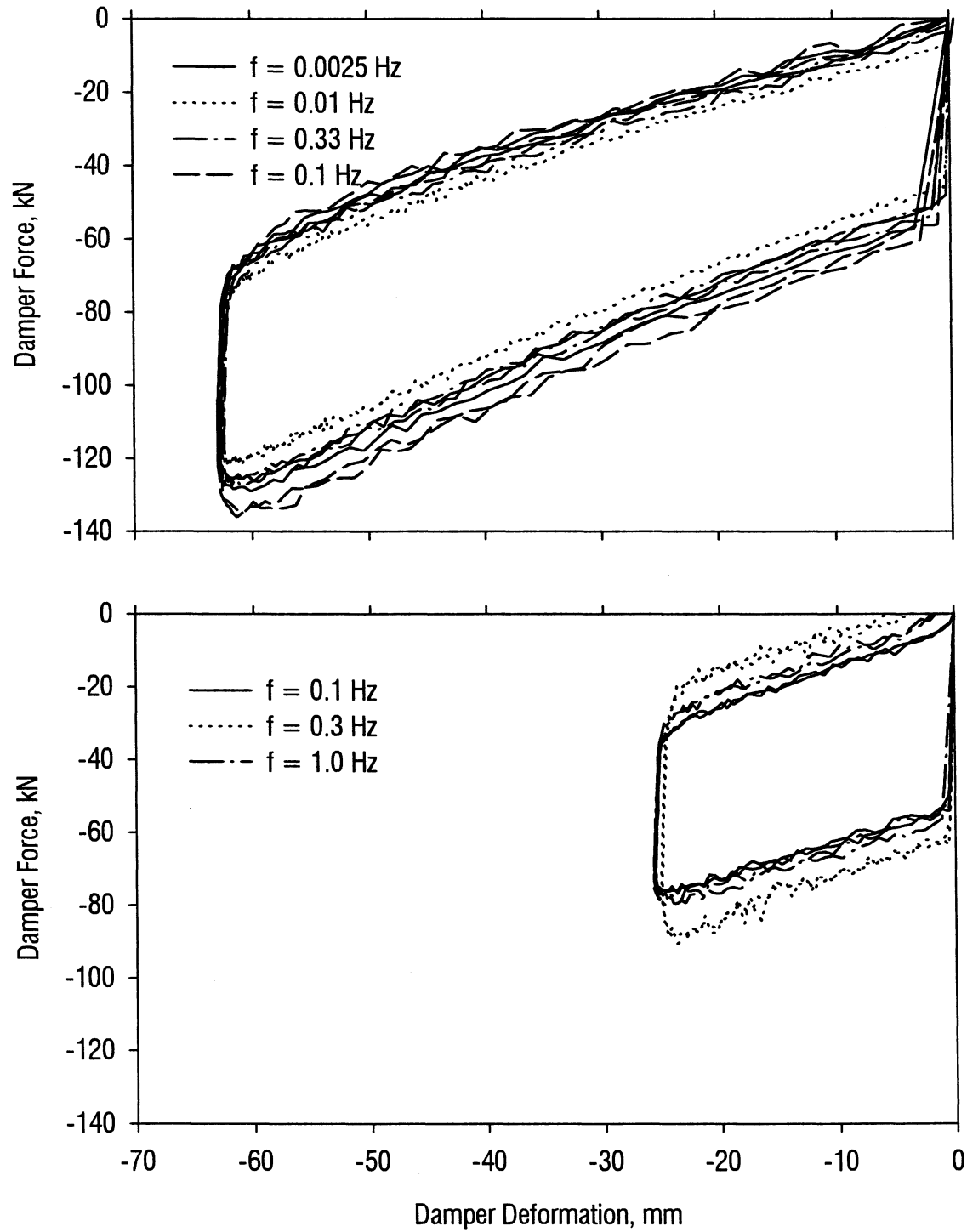
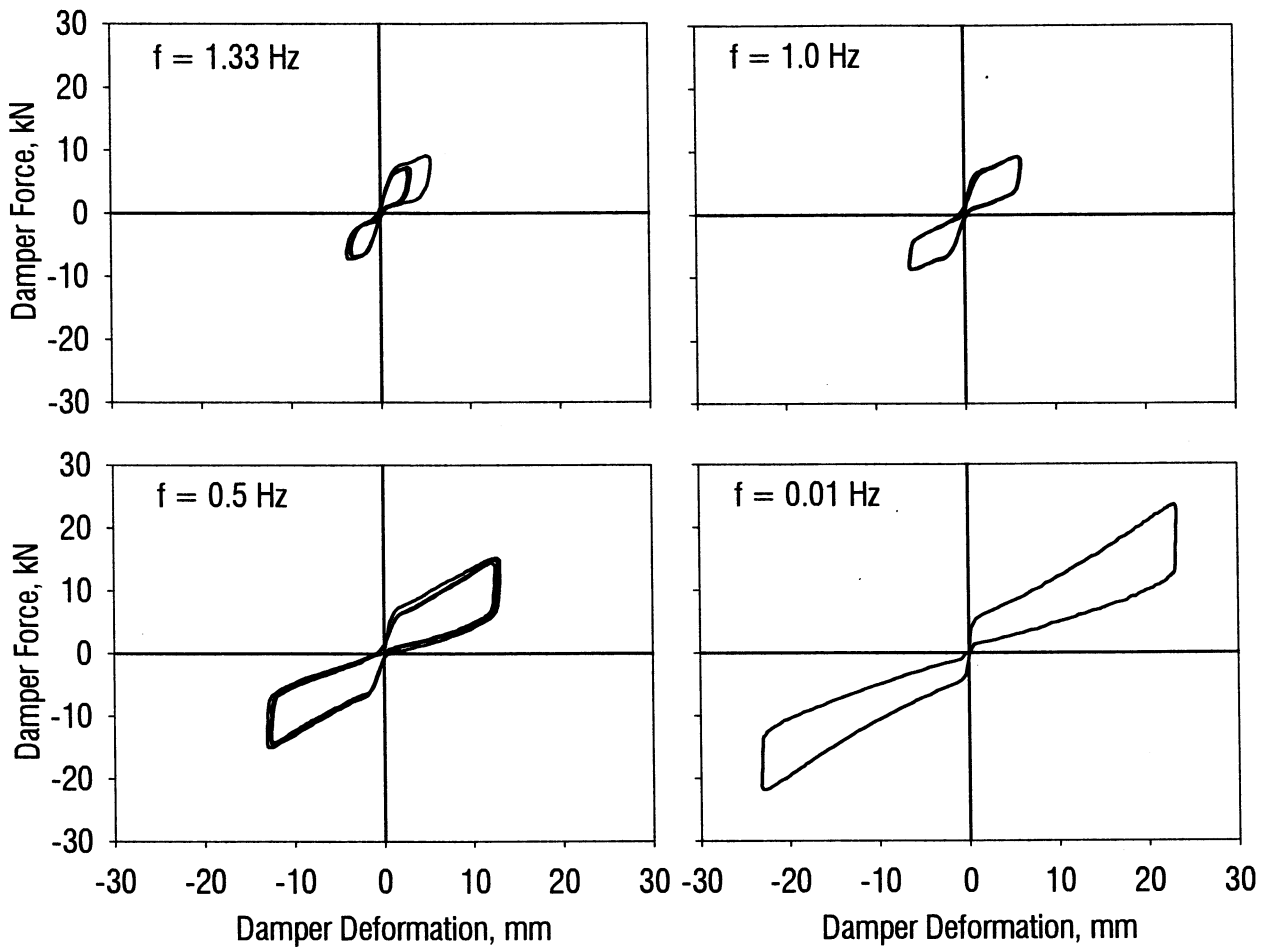


Figure 2-3 Selected Force-Deformation Relationships of a Prototype BC5A Damper



**Figure 2-4 Selected Force-Deformation Relationships of a Model BC1C Damper:
Present Study**

2.2.2 ESDs used in the Present Study

A different set of ESDs was used in the present study in the same mechanical configuration shown in figure 2-1. These devices are in fact model BC1C dampers with slightly less pre-load level. Each device was tested under displacement-controlled sinusoidal motions at specific frequencies and amplitudes. Force deformation relationships obtained from the specimen tests are shown in figure 2-4. The slight increase in the damper stiffness is due to the fact that elastomer pressure increases as the piston rod is forced into the plunger cavity, further tightening the seal shown in figure 2-1. In general, the post-yield stiffness can be altered during design by varying the piston rod/plunger cavity volume relationship and elastomer compressibility.

An improved analytical model and corresponding properties of the ESD devices used in this study are given in what follows.

2.3 ANALYTICAL CHARACTERIZATION AND IMPLEMENTATION OF THE DAMPER BEHAVIOR

The need for a better engineering understanding of the nonlinear response of various structural elements subjected to earthquake ground motions brought modeling issues to the attention of researchers. In most of the cases, it is important to simulate the behavior of these elements to establish dependable design guidelines since analytical/mathematical models allow one to study various possible cases. Hence, many studies have been performed to develop mathematical models for concrete, steel and composite structural as well as nonstructural elements. These models were then used to predict the overall structural response after being properly implemented in dynamic analysis programs.

In general, simplified piecewise linear hysteretic models such as bi-linear and tri-linear force-deformation relationships provide satisfactory simulations of real behavior. However, continuous models can be developed that more factfully capture actual behavior, yielding more accurate predictions. One of the major considerations in choosing between a piecewise linear and smooth continuous model for an application is whether it can easily be implemented in computational analysis tools. Historically, experience has shown that that piecewise linear models tend to be more robust and therefore more desirable than their smooth continuous counterparts unless they are supported by powerful solution methodologies. With these facts in mind, a two component velocity dependent model described in the following paragraphs is

developed to simulate the force-deformation behavior of elastomeric spring dampers. However, it can easily be used to model a wide range of nonlinear as well as linear viscous based energy dissipation devices as will be pointed out in the next section. Two alternative methods of solution for the nonlinear equations of motion are described in detail.

2.3.1 Development of the Analytical Model

It was observed from the specimen (BC1C) test results that elastomeric spring dampers (ESDs) exhibit a significant velocity dependency that was due to the nature of the elastomeric material and orificing. Therefore, a two component-velocity dependent model (figure 2-5a) which conveniently de-couples the spring and damping characteristics is proposed. According to the model, the total damper force can be calculated as the sum of the "bi-linear" spring force, F_S and velocity-dependent (viscous) force F_V :

$$F_{TD} = F_S + F_V \quad (2-1)$$

The spring force, F_S (figure 2-5a) has in essence a bi-linear relationship. The four-parameter model proposed first by Menegotto and Pinto (1973) is used herein to model the skeleton curve:

$$F_S = K_2 x_D + \frac{(K_1 - K_2) x_D}{\left[1 + \left| \frac{K_1 x_D}{P_y} \right|^R \right]^{\frac{1}{R}}} \quad (2-2)$$

in which x_D = the damper displacement or stroke, K_1 = the initial stiffness when the damper and connecting rod are fully extended, K_2 = elastomeric stiffness that is activated when the prestress has been overcome, P_y = damper static prestress force, and R = curvature shape parameter. However, it must be noted here that in implementing the model in DRAIN-2DX, a bi-linear link element with elastic loading-unloading option was used to model the spring force as shown in figure 2-6.

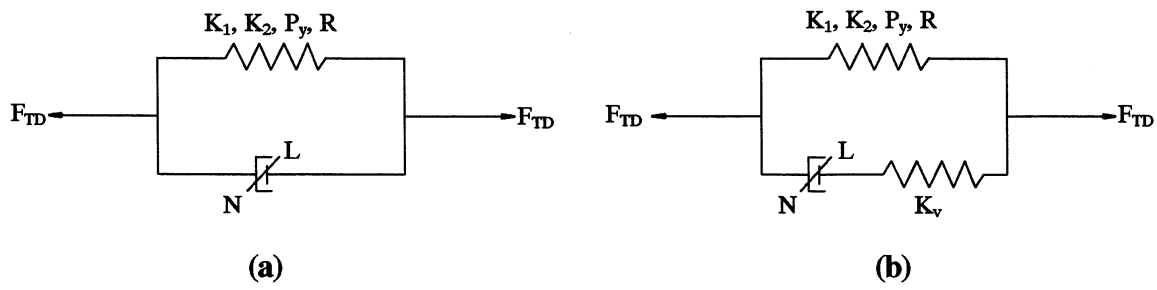


Figure 2-5 Modeling of Dampers

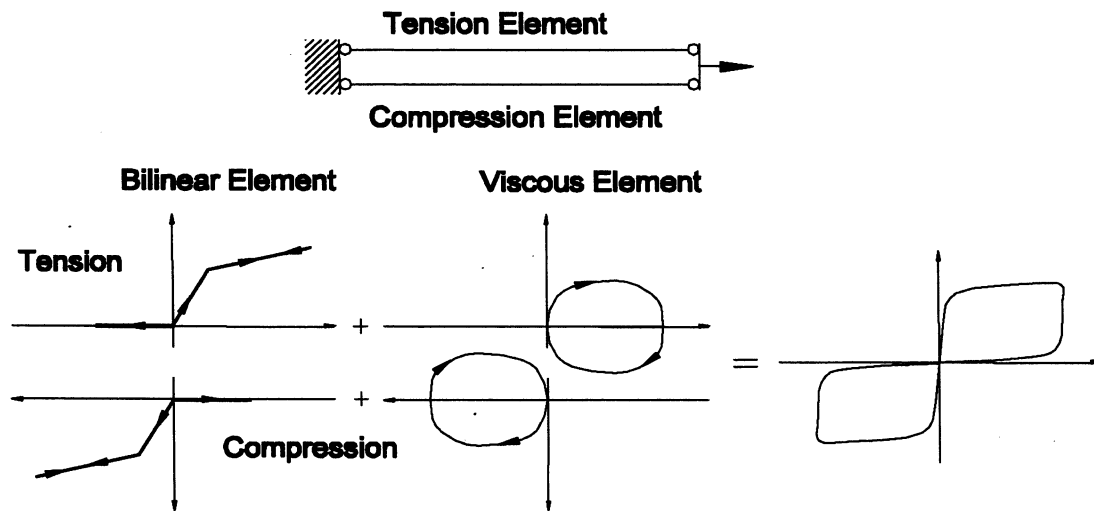


Figure 2-6 Force-Deformation Modeling of Dampers

The viscous part of the hysteretic model (equation 2-1) should reflect the self-centering characteristic of the dampers as well as the velocity dependency. Therefore, a nonlinear viscous-rate dependent model was modified to include the self-centering characteristics of the damper as follows:

$$F_V = \text{sgn}(\dot{x}_D) c_D |\dot{x}_D|^\alpha \left| \frac{x_D}{x_R} \right|^\beta \quad (2-3)$$

in which c_D = the damper constant, \dot{x}_D = the damper velocity, x_R = the damper stroke capacity, and α, β are positive real exponents. It should be noted here that α is the velocity exponent while β is a mechanical configuration exponent. It was found that $\alpha = \beta$ for double-acting damper modified from a single acting unit.

The first proposed velocity dependent model for ESDs is modified to improve the numerical solution of the equations of motion. Figure 2-5b shows this modified model which in fact is a combined Maxwell-Kelvin model. Derivation of "differential force- displacement" relationship for this model is given in the following:

The following set of relationships can be written modeling the nonlinear dashpot and spring in series arrangement shown on figure 2-5b:

$$x_V = x_D + x_K, \quad \dot{x}_V = \dot{x}_D + \dot{x}_K \quad (2-4)$$

in which x_V = the total deformation of the nonlinear damper and spring x_D = the deformation of the dashpot element, x_K = the deformation of the spring element. The dot over these quantities represents the derivatives with respect to time. The force response of the dashpot F_V and spring in series F_K are equal to each other:

$$F_V = F_D = F_K \quad (2-5)$$

Therefore F_V can be written as

$$F_V = K_V x_K = \text{sgn}(\dot{x}_D) c_D |\dot{x}_D|^\alpha \left| \frac{x_D}{x_R} \right|^\beta \quad (2-6)$$

Equation 2-6 can be solved for \dot{x}_D and after substituting x_D, \dot{x}_D from equation 2-4, it takes the following form:

$$\text{sgn}(\dot{x}_V - \dot{x}_K) |\dot{x}_V - \dot{x}_K|^\alpha = \frac{F_V}{C_D \left| \frac{x_V - x_K}{x_R} \right|^\beta} \quad (2-7)$$

The time derivative of the first equality in equation 2-6 is:

$$\dot{F}_V = \dot{F}_K = K_V \dot{x}_K \quad (2-8)$$

Consequently, substituting these two relationships (equations 2-6 and 2-8) for x_K and \dot{x}_K in equation 2-7 and rearranging:

$$\dot{F}_V = K_V \dot{x}_V - \text{sgn}(F_V) K_V \frac{|F_V|^{1/\alpha}}{\left| C_D \left| \frac{x_V - \frac{F_V}{K_V}}{x_R} \right|^\beta \right|^{1/\alpha}} \quad (2-9)$$

Equation 2-9 conforms to the class of differential equations mentioned in the following subsection. A general semi-implicit Runge-Kutta method of solution is described in Section 2.3.3 for the numerical solution of this type of equation.

The first model (figure 2-5a) and the latter (figure 2-5b) yield identical results for high stiffness values, K_V . Both models can be used to model nonlinear viscous ($K_1 \approx K_2 \approx 0$) as well as viscoelastic damper ($K_1 = K_2$) behavior without any difficulty. However, due to the nature of the mathematical model of the nonlinear dashpot, virtually infinite stiffness values take place at near zero velocity (maximum displacement, i.e. where the velocity changes sign). This is in fact physically not possible and induces numerical instability in analysis as will be explained in the next section. The modified model, however, is both more powerful and realistic due to the presence of the added spring element in series with the dashpot. Linear behavior of this spring element simulates the unloading characteristics of elastomeric material providing numerical stability to the solution of the equations. Moreover, it can be used to model damper-brace configurations as in real life applications dampers are usually installed on braces that have finite stiffness.

2.3.2 Solution of the Equations of Motion

Newmark's (1959) constant acceleration procedure ($\gamma = 1/2, \beta = 1/4$) was adopted in DRAIN-2DX. In general, the equation of motion can be written in incremental form as follows:

$$m\Delta\ddot{x} + [\alpha m + \beta K_0]\Delta\dot{x} + K_T \Delta x + \Delta F_v(\dot{x}_{i+1}, x_{i+1}; \dot{x}_i, x_i) = -m\Delta\ddot{x}_g \quad (2-10)$$

in which $\Delta x, \Delta\dot{x}, \Delta\ddot{x}$ = incremental displacement, velocity, acceleration, respectively, m = mass, K_0 = initial stiffness of the system at the beginning of the excitation, K_T = tangent stiffness of the system, $\Delta F_v = F_{v_{i+1}} - F_{v_i}$. It must be noted here that viscous damping of the structural system is considered to be proportional to mass and stiffness. The solution of equation 2-10 requires the damper force, F_v at the $i+1$ th time step. Two alternative solutions will be presented in the next paragraphs.

2.3.2.1 One-Step Correction Method

Equations of motions are solved in the same manner, i.e. by transferring the nonlinear damper force quantity to the right-hand side of the equation. However, zero damper force increment ΔF_v is assumed and the equations of motions are solved as mentioned above. The damper force is then calculated using equation 2-9 that is in the form of

$$\dot{F}_v = f(F_v, x_i, \dot{x}_i) \quad (2-11)$$

The solution of this differential equation is described in the next section. The calculated damper force, therefore, is treated as the unbalanced load vector and applied back to the structure in the next time step as the global unbalanced load is calculated by (Park et al., 1987):

$$F_{UNB} = \{Applied\ Load\} - \{Internal\ Resistance\} - \{Inertial\ Response\} \quad (2-12)$$

In equation 2-12, the applied load vector is the product of the ground acceleration and the story masses, and where internal resistance also includes the calculated damper force.

2.3.2.2 Iterative Solution Method

Solution of the incremental equation of motion starts with the assumed damper force $F_{v_{i+1}}^a$ at the end of the previous time step. After the first iteration damper response $F_{v_{i+1}}^c$ can be calculated solving the differential-damper force equation after which the error term is calculated as

$$\varepsilon = \left| \frac{F_{v_{i+1}}^c - F_{v_{i+1}}^a}{F_{v_{i+1}}^c} \right| \quad (2-13)$$

If ε is smaller than a prescribed limit, the solution routine proceeds to the next time step initializing the damper force vector to the average of the last calculated and assumed values as:

$$F_{v_{i+1}} = \frac{F_{v_{i+1}}^c + F_{v_{i+1}}^a}{2} \quad (2-14)$$

In cases where ε is not acceptable, the equation of motion is re-solved at the current time step by setting the assumed damper force equal to:

$$F_{v_{i+1}}^a = \frac{F_{v_{i+1}}^c + F_{v_{i+1}}^a}{2} \quad (2-15)$$

and the state is initialized to the state at the beginning of the current time step.

A schematic algorithm for the solution of the equations of motion with nonlinear dampers whose force displacement behavior can be modeled with equation 2-9, is given in table 2-1.

As is clear from the above discussion, in applying the viscous damper force effects, no modification is made to the structure stiffness. Instead, a set of damper forces is calculated at the end of each integration time step and added to the loads in the succeeding time step. These forces are computed at the element level and transferred to the global system coordinates through proper transformation matrices.

One-step correction method was implemented for the unmodified model (figure 2-5a) for which the damper forces were calculated using the relationship given in equation 2-3. Because the damper forces acting during $i+1$ th time step are based on the conditions at the end of i th

step, there may be a tendency for numerical oscillations developed in the integration process to be amplified with consequent numerical error or instability. Another source of numerical instability is that the unloading stiffness becomes practically infinite and this causes convergence oscillation effects (with aggravated unbalanced load) especially in the analysis of large size dampers (hence large damper forces).

The modified model avoids most of the above mentioned problems. However, an iterative solution scheme is suggested if the overall structural model has too many nonlinear elements other than the damper elements. This is because, when yielding takes place, large equilibrium unbalances occur within the structural elements. Unbalanced forces cause inaccurate results when combined with the damper forces, unless they are calculated iteratively. It should also be noted here that due to high nonlinearities very fine time steps ($\sim 0.001 - 0.0001$ sec) should be selected for the analysis, especially when high spring stiffness, K_v values are used. This is due to the fact that in the damper force-deformation space, if the change in force values from one time step to the next becomes large, high unbalanced loads and/or flip-flops may take place.

2.3.3 Solution of the Differential Damper Force Equation

A general semi-implicit Runge-Kutta method of solution for the equations of the form:

$$\dot{F}_v = f(F_v, x, \dot{x})$$

was first proposed by Rosenbrock (1963) and later utilized by Reinhorn et al. (1995) for the solution of equations of similar nature, in incremental time-history analysis:

$$\Delta F_v = R_1 k_r + R_2 l_r + R_3 m_r + \dots \quad (2-16)$$

in which coefficients R_i are real constants and k_r , l_r , m_r , ... defined as

Table 2-1 Solution Algorithm Using Nonlinear Damper Force Relationship

- A.1. Average acceleration method $\gamma = 1/2$, $\beta = 1/4$
 Linear acceleration method $\gamma = 1/2$, $\beta = 1/6$

- A.2. Newmark-Beta integration constants:

$$a1 = \frac{1}{\beta(\Delta t)^2}, a2 = \frac{1}{\beta(\Delta t)}, a3 = \frac{1}{2\beta}, a4 = \frac{\gamma}{\beta\Delta t}, a5 = \frac{\gamma}{\beta}, a6 = \Delta t \left(\frac{\gamma}{2\beta} - 1 \right)$$

- B.1. Form the global initial stiffness matrix, K_o (stiffness matrix will be updated after each time step for the changes in element stiffnesses) of the structure from the element contributions, and form the global mass matrix, M .
- B.2. Form the mass and stiffness proportional damping matrix, $C = \alpha M + \beta K_o$.
- B.3. Initialize nonlinear damper force vector, $\{F_v\}_o = 0$.
- B.4. Form the effective stiffness matrix, $K^* = a1M + a4C + K_o$.

It should be noted here that the first two terms on the right hand side of the above equation stay constant for the whole computation. Therefore, it can be stored permanently, however tangent stiffness matrix K_T replaces the initial stiffness matrix, K_o as the stiffness matrix of the nonlinear structural elements changes.

- C.1. Assume the damper force, $\{F_v^a\}_{i+1} = \{F_v\}_i$.
- C.2. Therefore, damper force increment vector becomes, $\{\Delta F_v^a\}_{i+1} = \{F_v^a\}_{i+1} - \{F_v\}_i$.
- C.3. Form the effective load vector at $t = i + 1$;

$$P^*_{i+1} = \{P_{i+1} - (M \ddot{x}_i + C \dot{x}_i + K_T x_i + F_{vi})\} + (a2M + a5C) \dot{x}_i + (a3M + a6C) \ddot{x}_i - \Delta F^a_{vi+1}$$

Note that, the first term in brackets is in fact the unbalanced load vector from the previous time step.

- C.4. Solve for the displacement increment Δx from;
 $P^* = K^* \Delta u_{i+1}$
 where $K^* = K_T + a2C + a1M$
- C.5. Calculate the corresponding velocity and acceleration increments and overall deformation vectors:

$$\Delta \dot{x} = a4 \Delta x_{i+1} - a5 \dot{x}_i + a6 \ddot{x}_i,$$

$$\Delta \ddot{x} = a1 \Delta x_{i+1} - a2 \dot{x}_i - a3 \ddot{x}_i \text{ and}$$

$$x_{i+1} = x_i + \Delta x_{i+1}, \dot{x}_{i+1} = \dot{x}_i + \Delta \dot{x}_{i+1}, \ddot{x}_{i+1} = \ddot{x}_i + \Delta \ddot{x}_{i+1}$$

- D.1. If modified model (figure 2-6b) is used, calculate the damper force vector $\{F_v^c\}_{i+1}$ using the solution technique described in Section 2.3.3. Otherwise, use the relationship given in equation 2-3 to calculate the damper force vector. Analysis proceeds to step D2 if iterative solution method is adopted. If however one-step correction method is used, proceed to the next time step
- D.2. Calculate the error term ϵ :

$$\epsilon = \left| \frac{F_{vi+1}^c - F_{vi+1}^a}{F_{vi+1}^c} \right|$$

- D.3. If $\epsilon < \bar{\epsilon}$ proceed to the next time step or else update the assumed damper force vector as:

$$F_{vi+1} = \frac{F_{vi+1}^c + F_{vi+1}^a}{2}$$

and go to step C.2. initializing the current state to that at the beginning of the time step $i + 1$.

$$\begin{aligned}
k_r &= \Delta t \left[f(F_v, x, \dot{x})_{t-\Delta t} + a_1 \frac{\partial f(F_v, x, \dot{x})_{t-\Delta t}}{\partial F_v} k_r \right] \\
\ell_r &= \Delta t \left[f(F_v + b_1 k_r, x, \dot{x})_{t-\Delta t} + a_2 \frac{\partial f(F_v + c_1 k_r, x, \dot{x})_{t-\Delta t}}{\partial F_v} \ell_r \right] \\
m_r &= \Delta t \left[f(F_v + b_2 k_r + d_1 \ell_r) + a_3 \frac{\partial f(F_v + c_2 k_r + e_1 \ell_r)_{t-\Delta t}}{\partial F_v} m_r \right] \\
&\vdots
\end{aligned} \tag{2-17}$$

Linear implicit equation 2-16 can be solved successively to yield k_r , ℓ_r , m_r , etc. The relationships amongst the coefficients, R_i , a_i , b_i , c_i , etc. can be established by comparing the power series of equation 2-16 in Δt and Taylor's series. In a two stage process, i.e., when only k_r , ℓ_r , R_1 and R_2 are involved, it can be shown that the six adjustable constants a_1 , a_2 , b_1 , c_1 , R_1 , and R_2 in equations 2-16 and 2-17 are defined by the solution of the following system of equations:

$$\begin{aligned}
R_1 + R_2 &= 1 \\
R_1 a_1 + R_2 (a_2 + b_1) &= \frac{1}{2} \\
R_1 a_1^2 + R_2 [a_2^2 + (a_1 + a_2) b_1] &= \frac{1}{6} \\
R_2 (a_2 c_1 + \frac{1}{2} b_1^2) &= \frac{1}{6}
\end{aligned} \tag{2-18}$$

Reinhorn et al. (1995) suggested the following values for the fourth order truncation error that satisfy equation 2-18:

$$R_1 = 0.75, R_2 = 0.75, a_1 = a_2 = 0.7886751, b_1 = -1.1547005 \text{ and } c_1 = 0 \tag{2-19}$$

It must be noted here that since $\partial f(F_v, x, \dot{x}) / \partial F_v$ may not be available or too complex, it can conveniently be calculated using finite difference equation without losing too much significant accuracy for small analysis time steps.

A FORTRAN source code for the solution of the differential equations described in this section is given in table 2-2 and the variable parameters are described in table 2-3. A single-degree-of-freedom system subjected to sinusoidal input motion was analyzed with four different dampers, namely one linear viscous ($\alpha=1$), two nonlinear ($\alpha=0.5$ and $\alpha = 0.2$) and one ESD ($\alpha = \beta=0.2$). Corresponding damper force-displacement responses

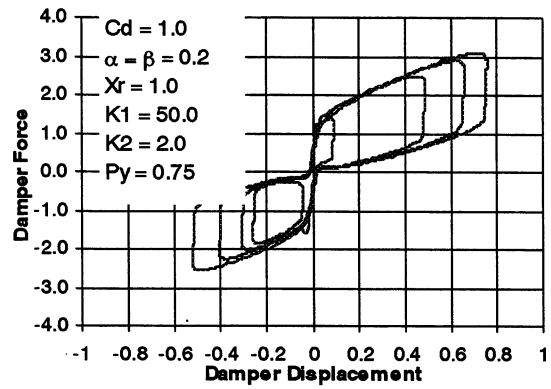
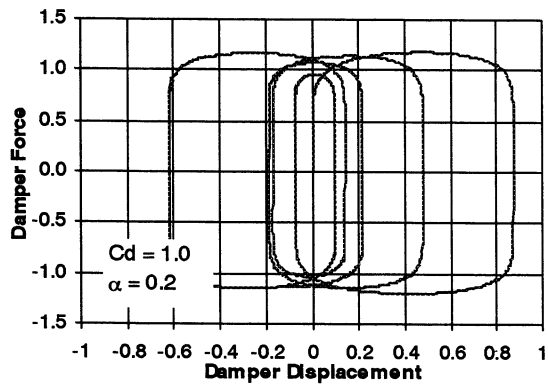
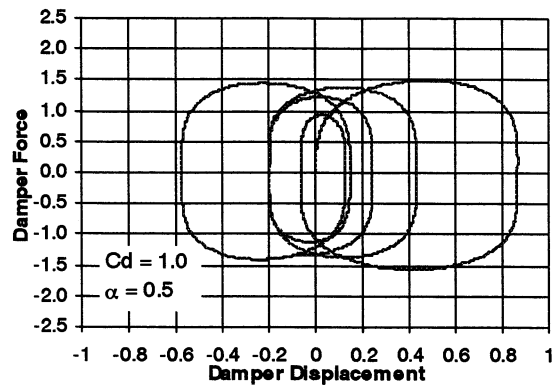
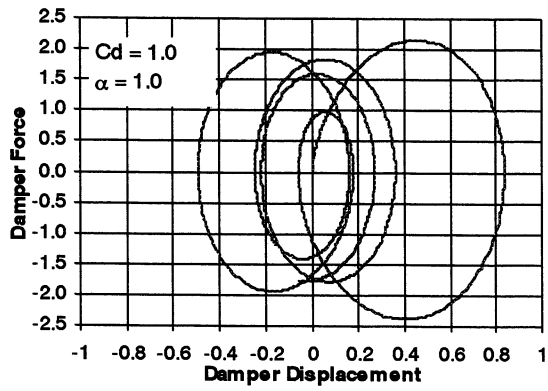


Figure 2-7 Various Damper Force-Deformation Relationships

Table 2-2 FORTRAN Code for the Solution of Differential Damper Force Equation

```
SUBROUTINE INT_DAMP (DIS,VELO,ACCL,CD,AL,BE,XR,aKS,tst,FVAL0,DELF0)
c DOUBLE PRECISION / LARGE
include 'double.h'

DATA RR1,RR2 /0.75,0.25/
DATA AA1,AA2,BB1 /0.7886751,0.7886751,-1.1547005/

signf = dsign(1.,fval0)
if (dabs(fval0).gt.0.) then
  ddelf = signf * fval0 * 1.d-5
else
  ddelf = signf * 1.d-10
end if

CALL FUNC (dis,velo,cd,al,be,xr,aks,fval0,func0)
fval1 = fval0 + ddelf
CALL FUNC (dis,velo,cd,al,be,xr,aks,fval1,func1)
dderiv1 = (func1-func0) / (fval1-fval0)
cons1 = 1. - AA1*tst*dderiv1
VKK = (1./cons1) * func0 * tst
fval2 = fval1 + BB1*VKK
CALL FUNC (dis,velo,cd,al,be,xr,aks,fval2,func2)
fval3 = fval2 + ddelf
CALL FUNC (dis,velo,cd,al,be,xr,aks,fval3,func3)
dderiv2 = (func3-func2) / (fval3-fval2)
cons2 = 1. - AA2*tst*dderiv2
VLK = (1./cons2) * func2 * tst

DELF0 = RR1*VKK + RR2*VLK

RETURN
END

SUBROUTINE FUNC (DIS,VELO,CD,AL,BE,XR,aKS,FF,FV)
c DOUBLE PRECISION / LARGE
include 'double.h'

diff = dsign(1.,FF)
FV = aKS*velo- diff*aKS*
1 abs(FF/(cd*dabs((dis-FF/aKS)/XR)**be))**(1./al)

RETURN
END
```

Table 2-3 Variable Definitions

VARIABLE NAME	DESCRIPTION
INPUT	
DIS	Current deformation
VEL	Current velocity
AL	α
BET	β
XR	Damper stroke capacity
aKS	Stiffness of the spring in series
TST	Time step increment
FVAL0	Previous damper force
OUTPUT	
DELF	Damper force increment

Table 2-4 Parameters for BC1C and BC5A Dampers

Damper	LoadingDi rec.	C (kN/mm/sec) ^a	α	β	P_y (kN)	K_1 (kN/mm)	K_2 (kN/mm)	x_{max} (mm)
BC1C (previous)	Comp.	2.26	0.2	0.2	3.3	7.0	0.66	23
	Tension	2.53	0.2	0.2	2.7	5.3	0.79	23
BC1C (present)	Comp./ Tens.	1.09	0.35	0.35	2.8	4.4	0.60	25
BC5A	Comp.	25.5	0.2	0.15	26.7	62	1.14	101

are plotted on figure 2-7. Damper parameters are given on the figure. The stiffness of the spring (in series, see figure 2-5b) was taken as 500 kN/m for the viscous dampers and 200 kN/m for the ESD.

2.4 VERIFICATION OF THE ANALYTICAL MODEL

The parameters defined in equations 2-2 and 2-3 were determined from the experimentally observed force-deformation results. Average values of the parameters for BC1C type damper subsequently used in the previous experimental study (Pekcan et al., 1995) and in the present study are given in table 2-4. Also included in the table are the corresponding values for the BC5A damper.

2.4.1 Comparison of Nonlinear Viscous Damper ($\alpha < 1$) Model with SAP 2000

General-purpose nonlinear computational model, which was developed in mid 1995 (as introduced above) and implemented in Drain-2DX, is compared with that implemented in recently released commercially available SAP 2000 (version 6.11) program. It must be noted here that only nonlinear damper elements whose force-deformation behaviors are governed by the equation 2-20 are available in SAP 2000 nonlinear element library.

$$F_D = \text{sgn}(\dot{x})c|\dot{x}|^\alpha \quad (2-20)$$

Hence, equation 2-19 is a special case of equation 2-3 with $\beta = 0$ ($\beta \neq 0$ is used to model elastomeric spring dampers).

Several linear SDOF systems with natural periods of $T = 0.75$ and 1.5 sec. are modeled with linear as well as nonlinear damper elements. Inherent viscous damping is assumed to be 5%. The damper exponents $\alpha = 1.0, 0.5$ and 0.2 are used with various damper coefficients $c = 10$ and 50 whose units depend on the damper exponent α . Comparisons are made using sinusoidal as well as ground motion inputs. The sinusoidal input used had an amplitude, $A=1.0$ g and input frequency $\omega = 6.28$ rad/sec. ($T = 1.0$ sec.) where 1994 Northridge – Arleta ground motion is used for the comparisons. Complete list of the cases for which comparisons are plotted in figures 2-8 and 2-9 is listed in table 2-5. As can be seen from the figures that Drain-2DX and SAP 2000 results compare very well.

Table 2-5 Nonlinear Damper Properties used in Drain-2DX - SAP 2000 Comparison

Input	T (sec)	c (kN/(m/sec)^α	α	K_{spr} (kN/m)
Sinusoidal	0.75	50	1.0	100000
“	0.75	50	0.5	100000
“	1.50	10	0.2	50000
“	1.50	50	0.2	100000
Arleta	1.50	50	0.5	100000
“	1.50	50	0.2	100000

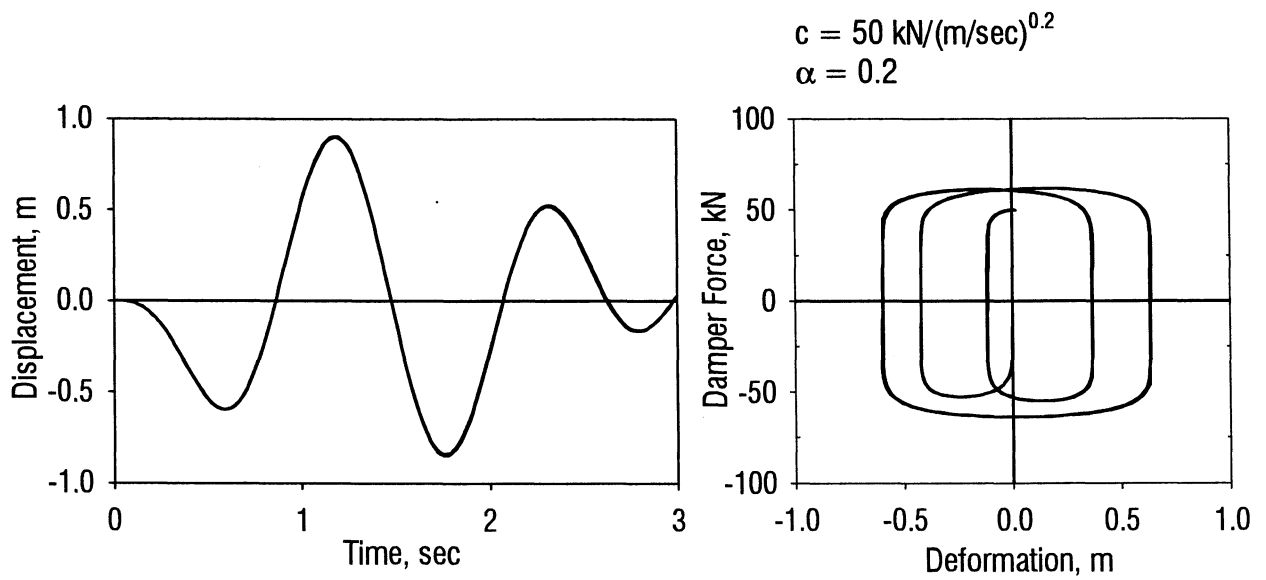
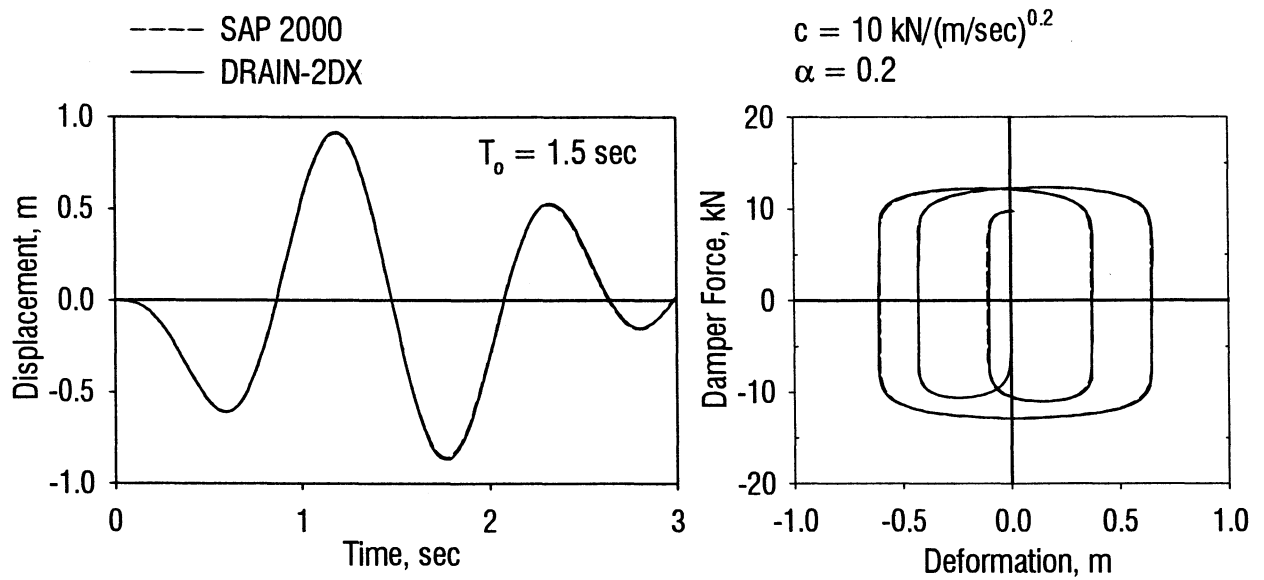


Figure 2-8a Comparison of DRAIN-2DX and SAP 2000 Nonlinear Damper Models - Sinusoidal Input

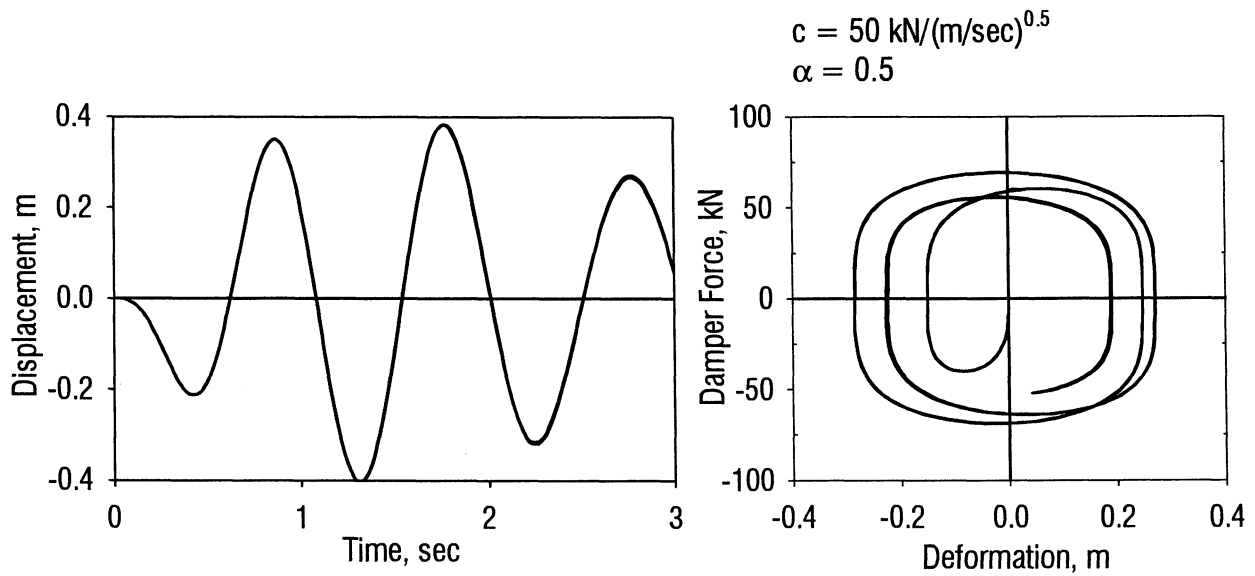
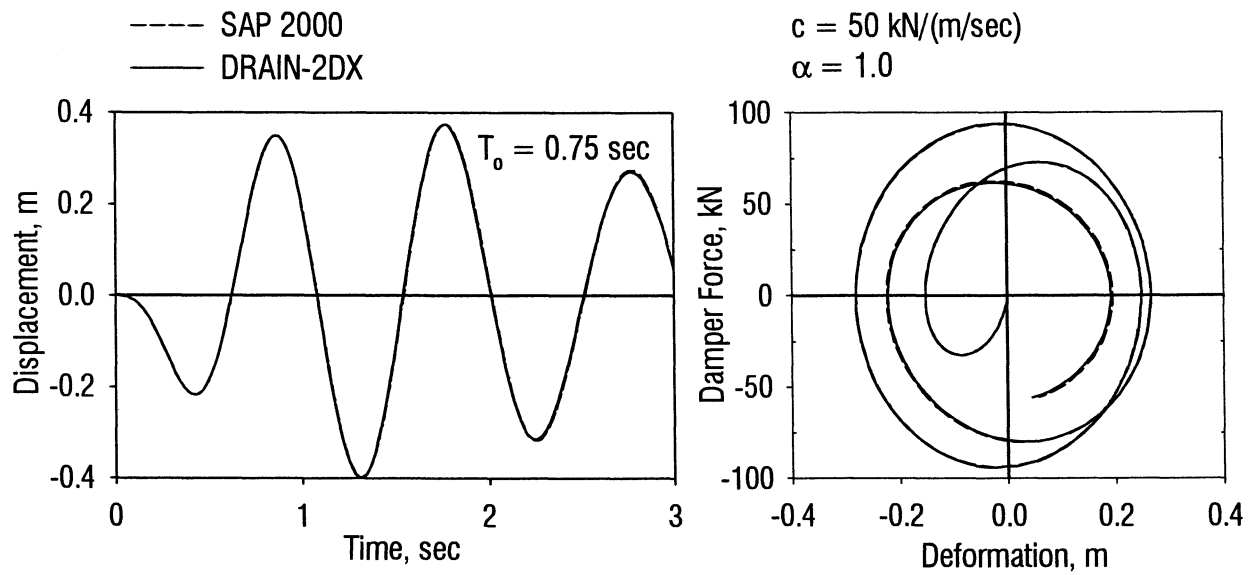


Figure 2-8b Comparison of DRAIN-2DX and SAP 2000 Nonlinear Damper Models - Sinusoidal Input

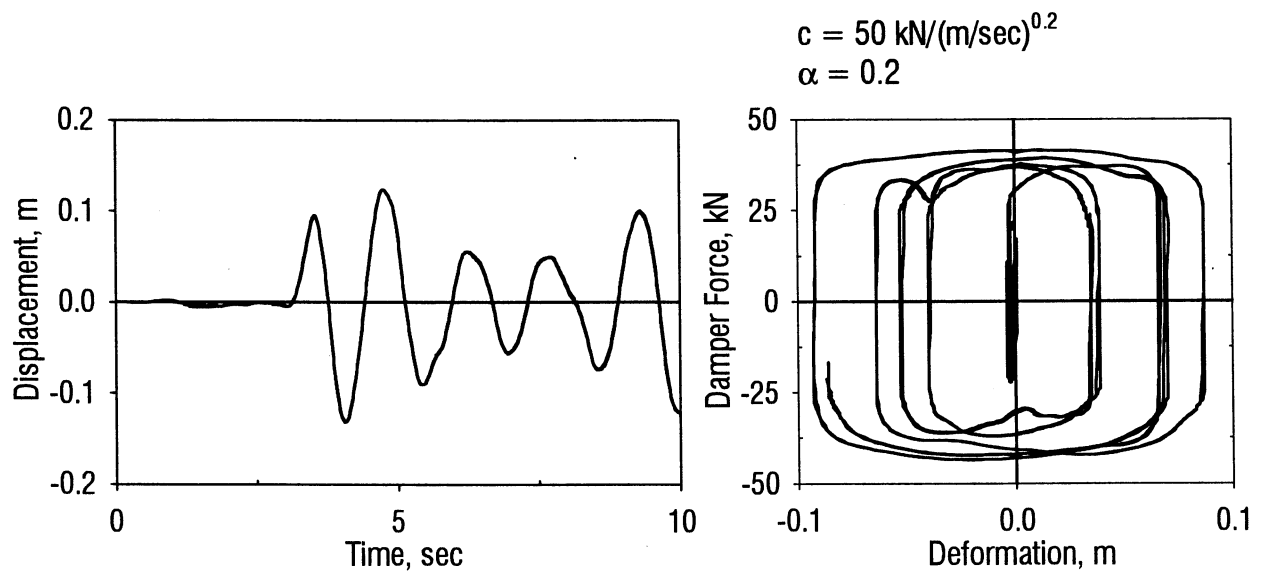
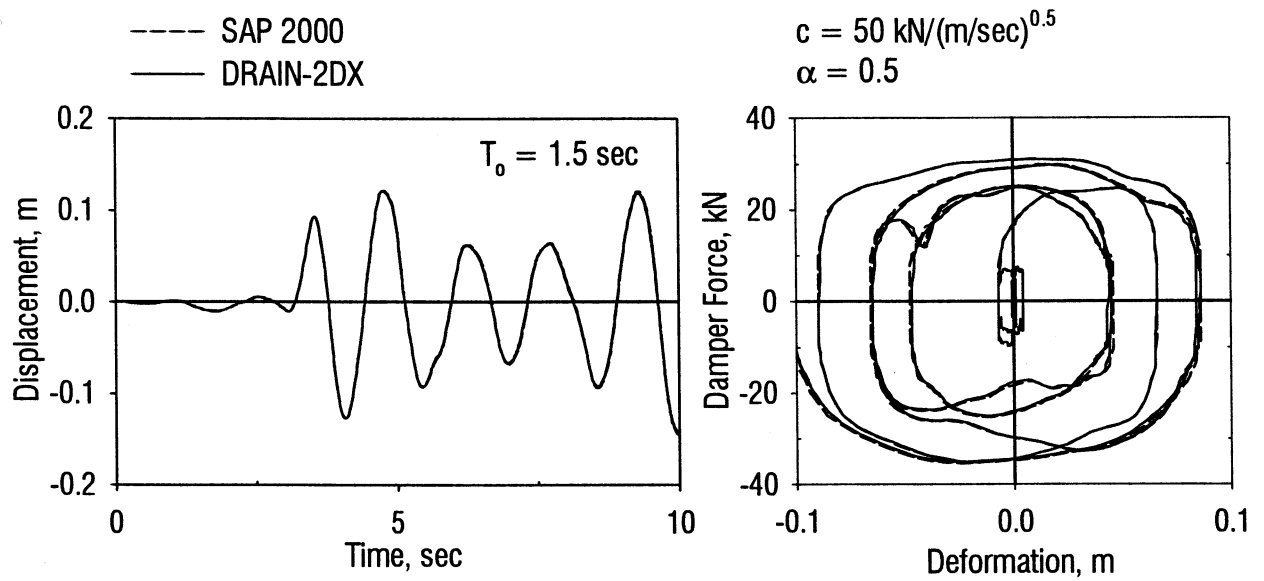


Figure 2-9 Comparison of DRAIN-2DX and SAP 2000 Nonlinear Damper Models - Earthquake Input

2.5 SUMMARY AND CONCLUSIONS

A new class of supplemental energy dissipation devices, namely elastomeric spring dampers was introduced. A nonlinear-two component computational model was developed and relevant parameters were identified experimentally. Four-parameter Menegotto-Pinto model was used to model the first component of the computational model that captures the spring nature of the elastomeric spring dampers. The second component described is in fact a modified Maxwell-Kelvin model and is intended to capture the nonlinear viscous nature of the devices. A fourth order Runge-Kutta method was used to solve the differential damper-force equations.

Two different solution techniques for the nonlinear differential equations of motion were given, namely; one-step correction and iterative solution. It was noted that in the latter, iterations were performed on the above-mentioned nonlinear model. The model was successfully implemented in the well-known nonlinear structural dynamic analysis program DRAIN-2DX and verified using experimentally obtained deformation histories. Finally, nonlinear model was compared with that implemented in the recently released structural analysis program SAP 2000.

SECTION 3

DAMPER CONFIGURATION AND PLACEMENT: CONCEPT DEVELOPMENT

3.1 INTRODUCTION

The main objective of this section is to present a new design and/or retrofit concept that deals with the placement and functional attributes of dampers. The new approach is firstly contrasted with the concept that is presently used by designers and advocated in FEMA 273/274 (1997). Herein, the present practice of using story-by-story cross-braced damper configuration will be referred to as a “Damper-Truss Solution”. The damper-truss system can be thought as an extension to conventional bracing system in building structures. The bracing elements are replaced with the so-called damper braces whose capacities are determined based on the corresponding story shear distribution. The load-path is then implicitly defined by the damper braces so as to reduce the story shear demand on the columns. Apart from the desired load path, benefits of added damping can be identified as a function of the damper properties and interstory deformations and velocities. The configuration for the proposed new retrofit/design concept is based on notions of load-balancing and uses a combination of tendons, fuse-bars and dampers preferably with re-centering (hence pre-load) characteristics. It is believed that the system has a direct effect in balancing the overturning moment demand on the structure.

3.2 SEISMIC SHEARS AND OVERTURNING MOMENTS IMPOSED ON STRUCTURAL FRAMES

Seismic design concepts require consideration of two basic principles: i) visualization of the general nature of the deflected shape of the structure under dynamic loads as a function of dominant response parameters, and, ii) understanding and being able to identify the continuous load path traveled by the lateral forces. Any design should then proceed in a way to *oppose* or *negate* the undesired effects of ground motion (deformations, forces etc.) imposed on the structural system.

Earthquake ground motions are time dependent and create inertia or lateral forces by shaking the structure back and forth. The deformation of the structure at any instant of time is a function of the stiffness and damping of the structure and of the characteristics of the ground motion. However, what is of more concern in seismic design are the maximum response

quantities observed during ground shaking. Therefore, the maximum forces and deformations can be idealized with the equivalent lateral forces shown in figure 3-1. This is similar to saying: horizontal forces induced by the ground motion and transmitted to the structure cause a set of story deformations Δ_i . This in turn corresponds to story forces F_i that act upon the structure to cause the same deformations. A general seismic design approach is to develop these forces numerically so that they best represent the maximum ground motion as well as structural characteristics. This kind of representation of seismically induced forces allows one to determine story shear force distribution and overturning moment at the peak structural response as shown in figure 3-1.

Story shears (ΣF_i) of the equivalent static system shown in figure 3-1 can be readily determined from the horizontal force equilibrium requirements. Similarly, externally applied overturning moments ($F_i h_i$) are resisted by the structure due to either moment frame action, cantilever shear wall action, braced-truss action or connections of the former. This observation is thought to be the first step in determining a realistic load path traveled by the externally applied seismic loads. At this point, it is of great relevance that characteristics of bracing systems that include axial load paths be reviewed. A braced frame in a building is in essence a vertical cantilever beam. Therefore, shear and moment demands at any level are known from the statically determinate equilibrium conditions. Hence, for the design of braced frames the size of the bracing elements can be determined directly from the maximum design story shears.

The supplemental damping devices for the seismic protection of building structures are most commonly implemented as the interstory bracings. Based on the above discussion, an alternative sizing of these supplemental damping devices when used in cross-braced configurations is discussed in the following paragraphs. Next, a new *load balancing tendon-fuse+damper* system is introduced.

3.3 DAMPER PLACEMENT TO RESIST INTERSTORY SHEAR FORCES: TRUSS SOLUTION (DTR)

Irrespective of the type of device used, adding supplemental devices to a frame structure always involves increasing the lateral stiffness of the structure. However, a reduction in the lateral stiffness may also be observed when a braced-frame structure is replaced by a damper-braced-frame structure. Lateral forces as well as deformations may increase or decrease in the structure, depending on the effect of devices and connections on the dynamic characteristics of

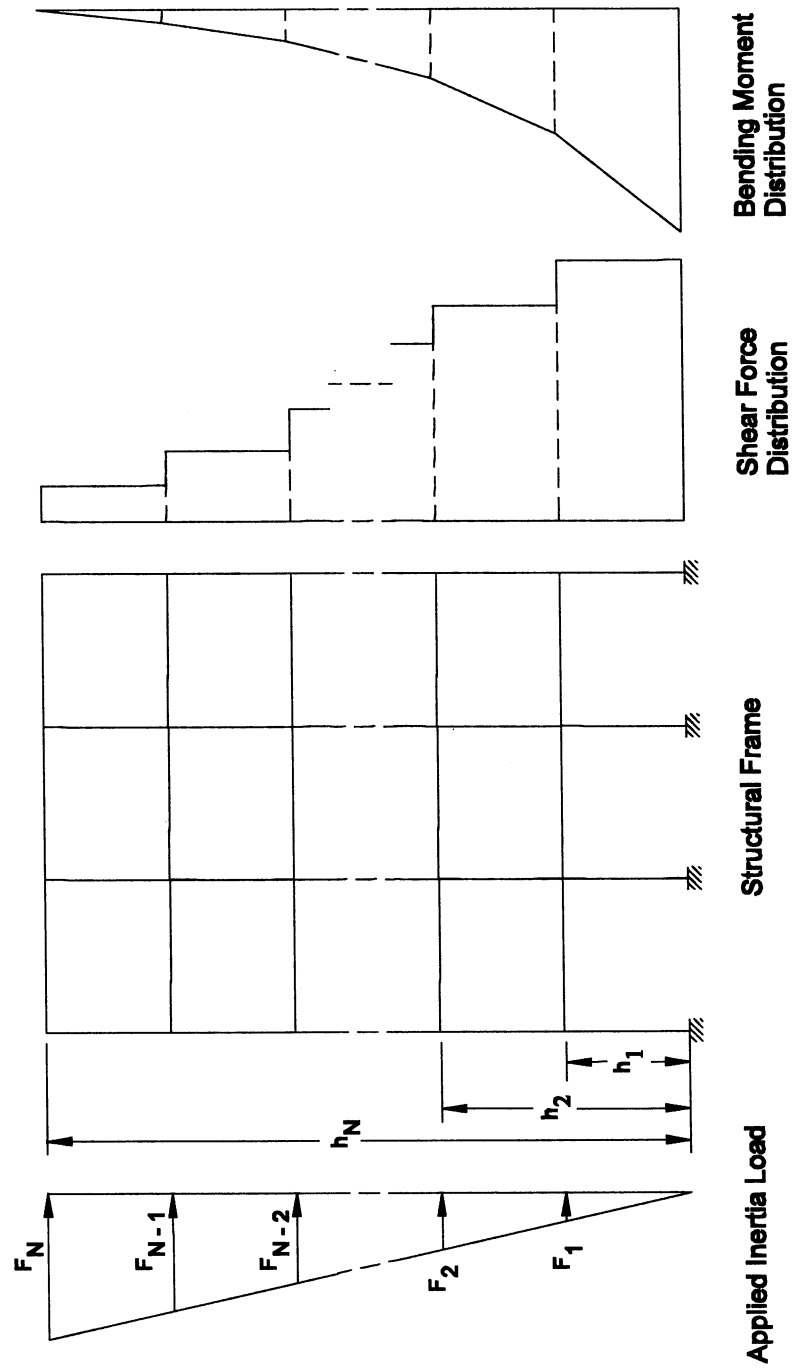


Figure 3-1 Seismic Shear and Overturning Moments Imposed on Structural Frames

the structure, and on the characteristics of the ground motions. Moreover, the magnitude of the increased lateral stiffness in a typical structure varies depending on the type of device used. In all cases, however, the intensity of ground motion induced lateral forces is a function of the overall lateral stiffness of the structure. Consequently, these forces must be resisted by supplemental damping devices.

Most building structures tend to have a fundamental mode of vibration, the distribution of supplemental devices is typically based on the level of maximum device forces and on the requirements as to how these forces are transferred within the structural system. It follows that devices should be distributed throughout a structure to ensure the stiffness regularity and redundancy. However, it is not essential that devices should be distributed over the full height of a structure. There may be cases in which supplemental devices can be installed only in the lower stories from a more economical design point of view. Moreover, interstory drifts and velocities will in general be less in the upper stories, which reduces the efficiency of such devices. The above statements are in fact supported by experimental findings (Pekcan et al., 1995)

Another important fact is that lateral resisting forces increase cumulatively going from the top level to lower levels and finally to the foundation (base shear). Therefore, it implies that supplemental devices that *resist* and *transfer* the lateral seismic forces to the ground level should likely have capacities in proportion to the story shears at which they are installed. This forms the basis for the DTR solution.

One of the most commonly used design methods is in fact based on the interstory deformations along the height of the building (figure 3-2a). Damping devices are sized to achieve required damping ratio at the design interstory deformations. Since a constant interstory drift is generally the objective for a regular building structure which has a first-mode dominant response, a uniform – one size damper would be dictated by this design. However, it is realized that if the total damper size is distributed in proportion to the design story shears, a desired *moment frame-truss action* can be achieved. Typical shear force distribution and corresponding force coefficients for unit base shear are shown in figure 3-2b. In application to the building structures, lateral seismic forces are transferred by the dampers installed on the gravity load-carrying interior frames in all directions, therefore reducing the demand on the moment frames. This approach is supported by experimental studies conducted on model structures (Pekcan et al., 1995).

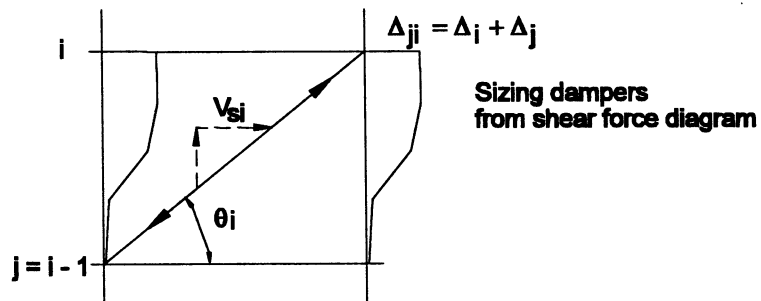
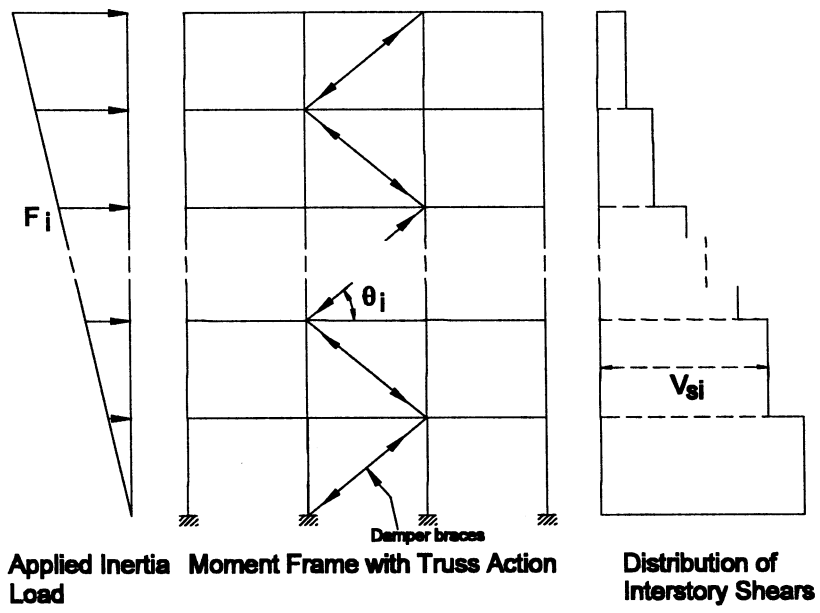


Figure 3-2a Damper Placement to Resist Interstory Shear Forces: Truss Solution

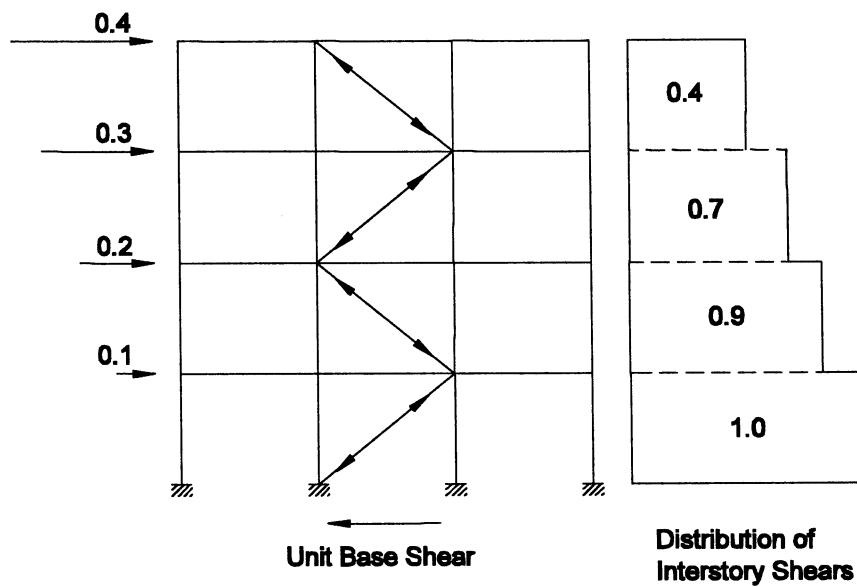


Figure 3-2b Force coefficients for Unit Base Shear

Various design methods for building structures with supplementary damping systems in DTR configuration have been suggested by Shen and Soong (1996), and Gluck et al. (1996). Shen and Soong proposed a design method for multistory reinforced concrete structures that is based on the concept of damage control. In their study, they used equivalent SDOF system properties in determining damage index recommended by Park and Ang (1985) and included the effect of energy dissipating devices implicitly through maximum deformation and hysteretic energy quantities. Gluck et al. adopted optimal control theory using a linear quadratic regulator to design linear viscous or visco-elastic devices. It was proposed that the gain matrix obtained by minimizing a performance index that ensures optimality can be used to determine the damping system properties in terms of constant stiffness and damping coefficients.

3.3.1 Effective Damping and Device Distribution

Firstly, practical formulations should be established for added damping due to supplemental damping devices. For a linear viscous damping device, added damping due to linear viscous damping can be calculated from energy considerations as (Constantinou et al., 1993):

$$\xi_d = \frac{W_d}{4\pi E_s} \quad (3-1)$$

in which W_d = total dissipated energy is given in terms of interstory deformations,

$$W_d = \pi\omega_k \sum_i c_i \cos^2 \theta_i \Delta_{ri}^2 \quad (3-2)$$

where ω_k = circular frequency of the k^{th} mode of vibration, c_i = linear viscous damper coefficient located at the i^{th} story, Δ_{ri} = relative-interstory deformation between $i-1^{\text{th}}$ and i^{th} floors, as shown in figure 3-2a.

Similarly, maximum strain energy E_s , can be determined as it equals to the maximum kinetic energy,

$$E_s = \frac{1}{2} \sum_i m_i \Delta_{ri}^2 \omega_k^2 \quad (3-3)$$

Finally, equivalent viscous damping can be calculated by substituting equations (3-2) and (3-3) into (3-1) as,

$$\xi_d = \frac{1}{2} \frac{\sum_i c_i \cos^2 \theta_i \Delta_i^2}{\omega_k \sum_i m_i \Delta_i^2} \quad (3-4)$$

in which θ_i = damper brace inclination angle at the i^{th} story.

An effective damper coefficient C , which is determined for an equivalent SDOF system can be distributed assuming story shear forces as shown in figure 3-2a:

$$c_i = \frac{V_{si}}{\sum_{j=1}^N V_{sj}} \frac{C \dot{x}_i^\alpha}{(\dot{\Delta}_i \cos \theta_i)^\alpha} \quad i = 1 \dots N \quad (3-5)$$

where V_{si} = story shear at story i , C = total (equivalent SDOF) damper coefficient, \dot{x}_i = equivalent SDOF design velocity and N = number of stories.

The above mentioned damper-truss solution is not the most desired configuration for relatively stiff structural systems as the interstory deformations are small. However, an innovative configuration based on the load-balancing concept can be employed in flexible as well as stiff structural systems.

3.4 DAMPER PLACEMENT TO RESIST OVERTURNING MOMENTS: LOAD BALANCING PRE-STRESSED TENDON-FUSE+DAMPER SOLUTION (LPTFD)

Prior to introducing the proposed load balancing approach to mitigate lateral loads in buildings, it is considered desirable to review a well-known analogous scenario.

3.4.1 The Load Balancing Approach: Pre-stressed Concrete Beam Analogy

Consider the design of a post-tensioned pre-stressed concrete beam. Using post-tensioning along with a draped parabolic tendon profile it is possible to balance gravity loads as shown in figure 3-3. This approach was first developed by Lin (1963). If the tendon profile has a draped parabolic profile similar to the moment diagram then the gravity loads are balanced and deflections removed when

$$Fe = \frac{wL^2}{8} \quad (3-6)$$

where F = tendon force, w = distributed load per unit length, L = length of the beam, e = maximum eccentricity as shown in figure 3-3.

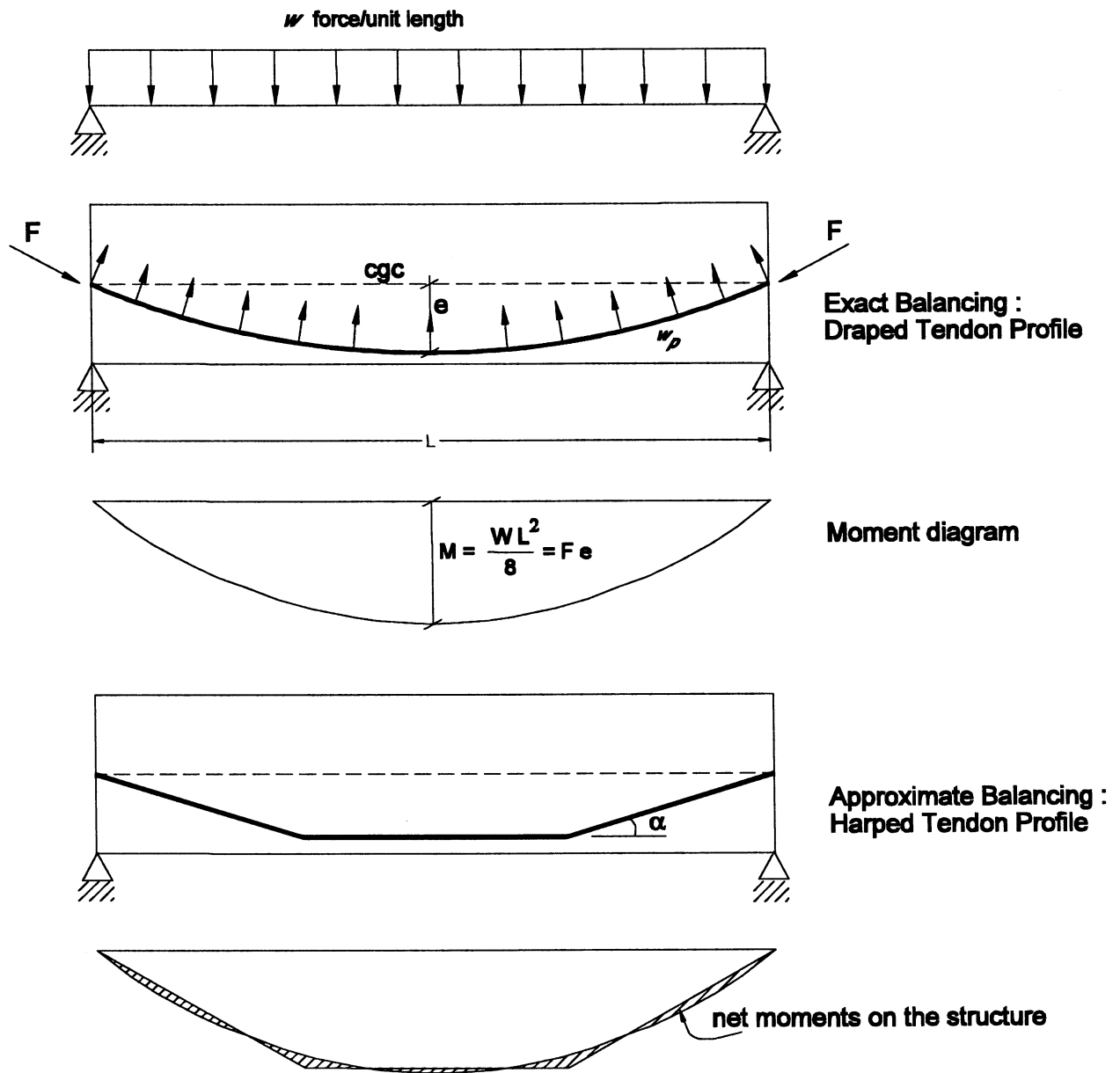


Figure 3-3 Prestressed Concrete Beam Analogy with Load Balancing Tendons

Alternatively, if it is not possible to use a draped tendon profile (such is the case for pre-tensioning) deflections can be minimized by using a harped profile as shown in figure 3-3. Deflections only arise due to the difference between the parabolic shape of the gravity moment diagram and the piece-wise linear shape of the harped tendon profile (This is shaded region in figure 3-3). It should be noted that the harped tendon profile provide point forces where the tendon suddenly changes direction; the point force (P) being equal to

$$P = F \sin \alpha \quad (3-7)$$

where, α = angle of deviation of the cable profile (that is the angle change where it is kinked).

3.4.2 The Load Balancing Approach: Application to Cantilever Frames

A second alternative configuration is proposed in which tendons are draped so as to generate lateral horizontal forces that balance the overturning moments. The proposed system works in tension only and is composed of two major components; pre-stressed tendons with high axial stiffness, and a supplementary damping system located at the foundation level. The draped tendon is anchored at one end and connected to the supplementary damping system in series at its other end (preferably at the foundation level). The tendon layout is designed to be piecewise continuous, i.e. in straight-line segments, so that each segment diagonally spans between holes bored (or cast in the case of a new structure) in the floor slab. Tendons are allowed to slide through these holes. The damping forces are therefore transferred in the horizontal direction by bearing of the tendons to the floor slab/transfer beams. Therefore, if the dominant load path for the structure is considered to be overturning moments, the “load balancing” concept can be ideally employed, which is reviewed in what follows.

If a geometrically feasible system can be used in a building structure such that it exerts forces in equal magnitude and opposite direction to the applied lateral seismic forces, it will be referred to as a *load balanced system* (figure 3-4). It must be noted here that such systems when pre-stressed will enhance the ability of the overall structural system to initially resist lower levels of lateral loading with little or no deformation. This is especially desirable for structures subjected to wind loading.

After the 1994 Northridge and 1995 Kobe earthquakes, engineers realized that the near-source ground motions may be detrimental for tall flexible building structures due to high initial pulse in the ground acceleration history (Hall et al., 1995). Traditional supplemental damping

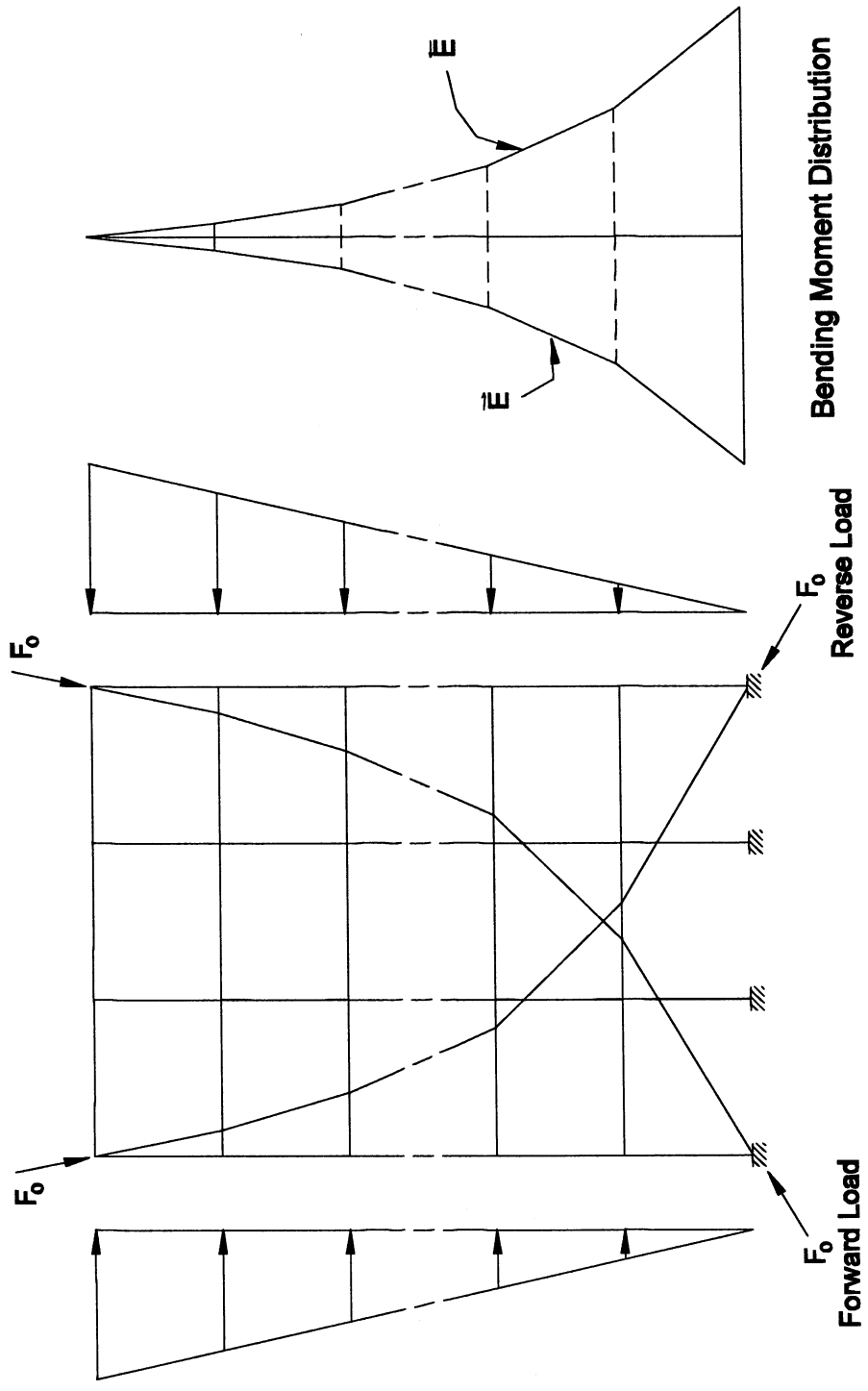


Figure 3-4 Load Balancing Prestressed Tendon-Fuse+Damper Solution (LPTFD)

devices may be ineffective in mitigating the effects of this type of ground motion. In general, since the damping related terms on the left-hand side of general equation of motion (equation 3-8) would physically be not sufficient for dampening the response, it becomes clear that stiffness characteristics of the building structure should be improved.

$$m\ddot{x} + c\dot{x} + kx = -m\ddot{x}_g \quad (3-8)$$

Uniform stiffening may not be attractive, as stiffer structures attract larger forces that in turn should be resisted by the structural elements. Therefore, it is desirable to provide a system with a passively controllable or adaptive stiffness. Better still, a system can be controlled in such a way that the required amount of opposing force is induced in the system when the seismic impulse hits the building structure. Consequently, a load balancing pre-stressed tendon-fuse+damper system that has the above-mentioned characteristics which can resist the reversing inertial loads is proposed. In this system, shown in figure 3-4, sacrificial yielding fuse-bars are used in parallel to the main supplemental damping devices. The fuse-bars provide a high initial stiffness and also limit displacements. The damping devices are primarily used to attenuate the response after the maximum displacement has occurred.

Once the lateral design loads are determined, a tendon layout described above can be determined based on the assumed deformed shape and the lateral forces as shown in figure 3-4. Details of the derivation of the design equations for the load balancing tendon layout geometry and supplemental system deformation are given next.

3.4.3 Tendon Layout to Balance Lateral Loads and Supplemental System Deformation

The horizontal force equilibrium at a node (figure 3-5) can be written by assuming very rigid beam and column elements.

$$F_{Ti} \cos \theta_i = \sum_{j=i+1}^N F_j \quad i = 0, \dots, N-1 \quad (3-9)$$

in which F_{Ti} = force in the tendon at the i^{th} level, θ_i = the angle of inclination of the i^{th} floor tendon, F_j = horizontal lateral loads or story shear at level i . It must be noted here that the above equilibrium relation can be written for each level i as shown in figure 3-5 and as implied in equation (3-9).

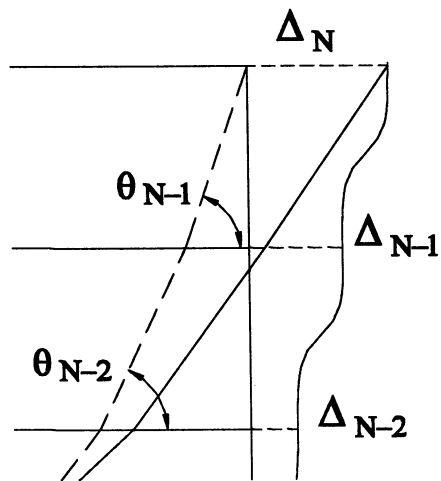
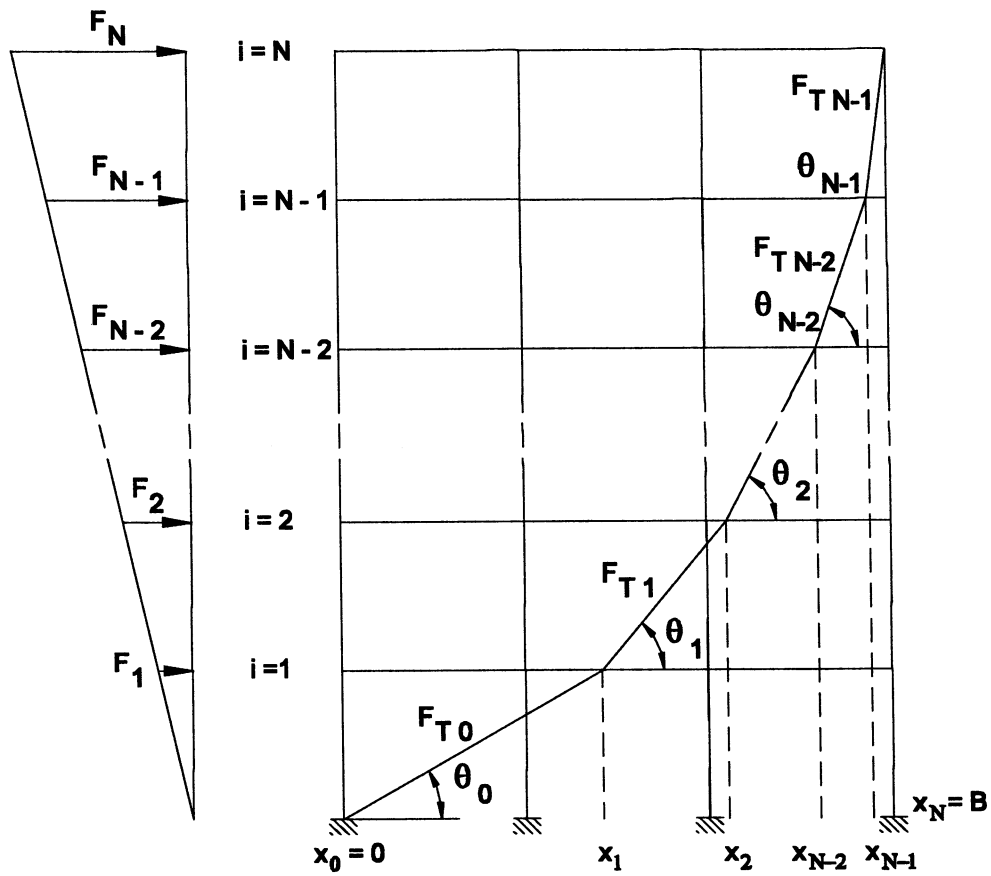


Figure 3-5 Determination of Tendon Layout

Vertical force equilibrium at each floor level can be written similarly, noting that the resultant should equal 0 (zero) force:

$$F_{T_i} \sin \theta_i = F_{T_{i+1}} \sin \theta_{i+1} \quad i = 0, \dots, N-2 \quad (3-10)$$

Equation (3-10) can be rearranged by pre-multiplying and dividing both sides by $\cos \theta_i / \cos \theta_{i+1}$:

$$\frac{F_{T_i} \cos \theta_i}{F_{T_{i+1}} \cos \theta_{i+1}} = \frac{h_{i+2} / (x_{i+2} - x_{i+1})}{h_{i+1} / (x_{i+1} - x_i)} = \frac{\tan \theta_{i+1}}{\tan \theta_i} \quad (3-11)$$

Equation (3-9) can now be substituted in equation (3-11) to give:

$$\frac{h_{i+1}}{h_{i+2}} R_{i,i+1} = \frac{x_{i+1} - x_i}{x_{i+2} - x_{i+1}} \quad i = 0, \dots, N-2 \quad (3-12)$$

in which h_{i+1} = story height between levels i and $i+1$ and, $R_{i,i+1} = \frac{\sum_{j=i+1} F_j}{\sum_{j=i+2} F_j}$ is the ratio of the story shear at the i^{th} to that at the $i+1^{\text{th}}$ level.

Equation (3-12) in fact defines a system of $N-1$ simultaneous equations with $N-1$ unknowns, x_i :

$$\begin{aligned} x_0 - \left(\frac{h_1}{h_2} R_{0,1} + 1 \right) x_1 + \frac{h_1}{h_2} R_{0,1} x_2 &= 0 \\ x_1 - \left(\frac{h_2}{h_3} R_{1,2} + 1 \right) x_2 + \frac{h_2}{h_3} R_{1,2} x_3 &= 0 \\ &\vdots \\ x_{N-3} - \left(\frac{h_{N-2}}{h_{N-1}} R_{N-3,N-2} + 1 \right) x_{N-2} + \frac{h_{N-2}}{h_{N-1}} R_{N-3,N-2} x_{N-1} &= 0 \\ x_{N-2} - \left(\frac{h_{N-1}}{h_N} R_{N-2,N-1} + 1 \right) x_{N-1} &= x_N \end{aligned} \quad (3-13)$$

where $x_0 = 0$, and $x_N = B$, width of the frame structure.

Finally, the tendon layout can be determined by solving the tri-diagonal matrix equation defined by equation (3-13). Assuming equal story heights (i.e. $h_i = h_{i+1}$):

$$[R]\{X\} = \{D\} \quad (3-14)$$

where,

As can be seen from figure 3-5, deformation of the supplemental system at the foundation level can be written as the sum of all the tendon segment elongations assuming zero tendon stiffness and subtracting the sum of all the actual tendon elongations due to tendon forces, F_{Ti} :

$$X_{\text{sup}} = \sum_{i=0}^{N-1} \left\{ \left[\sqrt{1 - \left[\left(\frac{\delta_{i+1}}{L_i} \right) \sin \theta_i \right]^2} + \left(\frac{\delta_{i+1}}{L_i} \right) \cos \theta_i \right] - 1 \right\} L_i - \frac{F_{Ti} L_i}{A_i E_i} \quad (3-16)$$

where A_i = cross-sectional area, E_i = Young's Modulus and, $L_i = h_{i+1} / \sin \theta_i$ is the length of tendon segment i .

Finally equivalent damping based on the equivalent power consumption approach introduced by Pekcan et al. (1998) for nonlinear viscous nature dampers:

$$\xi_{eq} = \frac{1}{1+\alpha} \frac{c_\alpha x_o^{\alpha-1} \omega_o^{\alpha-2}}{M} \quad (3-17)$$

can be used along with the pseudo-exact velocity transformation (Pekcan et al., 1998) to determine the added damping due to dampers in the load balancing tendon configuration as:

$$\xi_d = \frac{1}{1+\alpha} \left(\frac{2\pi}{T_k} \right)^{\alpha-2} \left(\frac{T_k}{0.75} \right)^{0.15\alpha} \frac{\sum_i c_{di} \Delta_i^{1+\alpha}}{\sum_i m_i \Delta_i^2} \quad (3-18)$$

but $F_{Ti,h} = c_{di} \Delta_i^\alpha \left(\frac{T_k}{0.75} \right)^{0.15\alpha} \left(\frac{2\pi}{T_k} \right)^\alpha$ is the horizontal component of the damping force at level i .

Therefore, equation (3-18) can be simplified using equation (3-11) as:

$$\xi_d = \left(\frac{1}{1+\alpha} \right) \left(\frac{T_k}{2\pi} \right)^2 \frac{\sum_{i=1}^{N-1} (F_{Ti-1} \cos \theta_{i-1} - F_{Ti} \cos \theta_i) \Delta_i + F_{TN} \cos \theta_{N-1} \Delta_{rN}}{\sum_i m_i \Delta_i^2} \quad (3-19)$$

where F_{Ti} = force in the tendon between floor levels $i-1$ and i .

3.4.5 Approximate Load Balancing Solution – Straight Tendon

An approximate load balancing solution can be employed in which the draped tendon system is replaced with a straight tendon as shown in figure 3-6. It must be realized that the straight tendon layout does not provide damping forces that fully oppose the inertial forces and

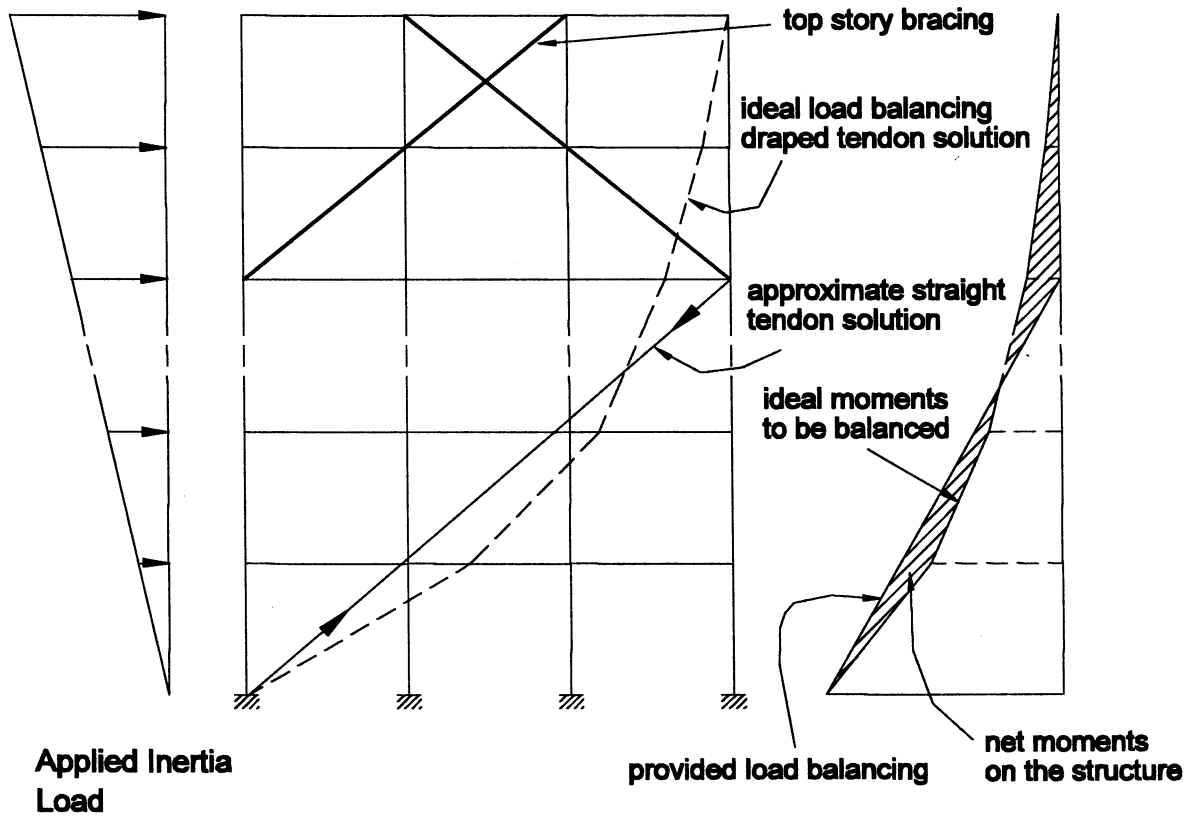


Figure 3-6 Approximate Load Balancing Solution

oppose the overturning moments induced in the structure. Hence, this approach is analogous to the approximate load balancing with harped tendon mentioned previously for the pre-stressed concrete beam. However, the net moments on the structure (shaded area in figure 3-6) can be minimized by carefully designing the tendon layout. As can be seen in the figure, overturning moment demand on the columns can still be significantly reduced. However, a potential disadvantage of this approach may be that a single point application of the damping forces may cause a so-called whipping action in the upper stories, and therefore excite higher modes. However, this undesired response can be effectively overcome by bracing the levels above the tendon system. Moreover, the bracing elements should ensure a continuous load path as shown in figure 3-6.

3.5 DISCUSSION OF THE PROPOSED CONFIGURATION

Various aspects of proposed load balancing tendon system are questioned and discussed in what follows.

3.5.1 Tendon Layout and Higher Mode Effects

Determination of tendon layout for building structures is not an easy task for especially tall-flexible building structures for which the higher mode effects are in general significant. If the tendon layout is designed based on the first mode vibration characteristics, possible higher mode contribution in the overall response is expected to adversely affect the performance of the proposed configuration. However, it is possible to iteratively determine a tendon layout based on the altered first mode characteristics to minimize the higher mode effects. Moreover, a hybrid bracing system can be efficiently designed for relatively tall building structures which would ensure a dominant response, hence improving the load-balancing tendon efficiency in terms of balanced loads.

3.5.2 Three Dimensional Response with LPT System

Three-dimensional response of structures with load balancing tendons may pose important problems if it is not carefully considered in the design. A three dimensional view of tendons placed on the interior frames of a building structure is schematically shown in figure 3-7. Two pairs of tendons work in the XZ plane and only one tendon is shown in the YZ plane for clarity of the figure. Supplemental system is preferably (but not necessarily) placed at the lower

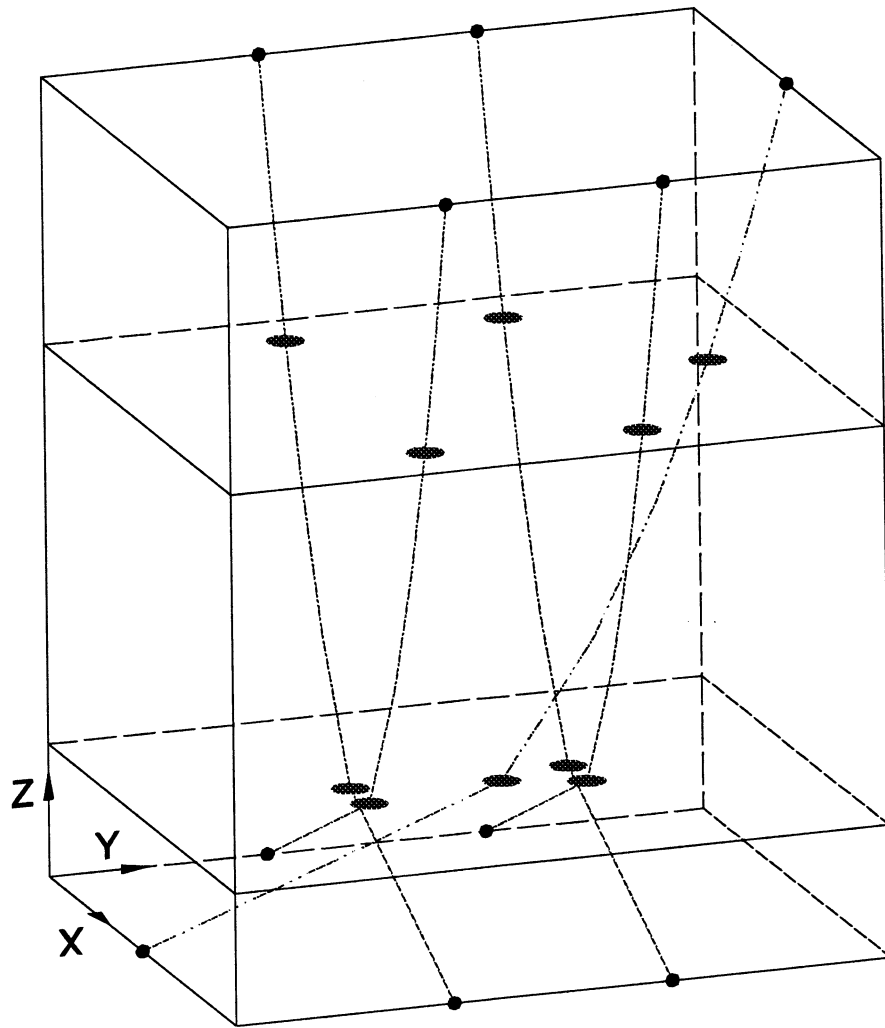


Figure 3-7 Three-dimensional View of LPTFD System

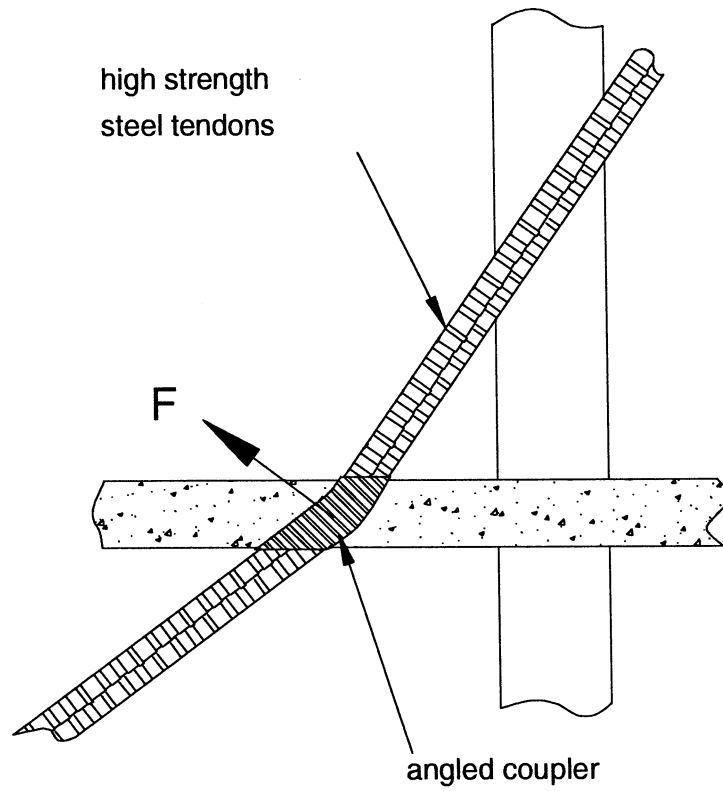


Figure 3-8 Tendon-Floor Slab Detail

end of the draped tendon. When fuse-bars are used in parallel with the supplemental damping devices, they are designed to yield under a major ground shaking. Hence, after yielding of the fuse-bar(s), stiffness characteristics and distribution within the structural system will be modified. Since the simultaneous yielding may not take place, the stiffness change is likely to promote torsional response. Therefore, the overall supplemental system with the draped tendon profile should be designed to accommodate the undesired torsional effects. On the other hand, it must be noted that the proposed supplemental system can also be designed to eliminate any initial plan irregularities. Consequently, three dimensional nonlinear analysis tools should be developed and used in the analytical investigation of this phenomenon.

3.5.3 Floor Slab Detail

As was previously mentioned, the tendon layout is designed to be in piecewise continuous segments that span between holes bored in the floor slab. A typical detail is schematically shown in figure 3-8. As can be seen from the figure, the damping forces are transferred in the horizontal direction by bearing of the tendons to the floor slab. In fact, the bearing force F , has a horizontal as well as a vertical component which must be reacted by the floor slab action. Therefore, the magnitude of the vertical component bearing forces must be carefully considered and the floor slabs around these holes must be reinforced if necessary. Another alternative to reduce the effect of vertical forces is to avoid friction at the contact surfaces by means of either a proper lubrication or durable-specially treated surfaces.

3.5.4 The Benefits of Pre-stressing

Initially, tendons may be either slack or pre-stressed. If tendons are used, only one tendon of the diametrically opposing pair will work at any given time. However, if the tendon is stressed to say 50 percent of the fuse-bar yield stress, then the initial stiffness is doubled, as both tendons will act together, doubling the effectiveness of the system. The pair of tendons will continue to work together until the tendon on the compression side becomes slack. This relaxes the structure and as the composite system is more flexible, the demand is reduced.

If the fuse-bars are pretensioned to a pre-determined level such that they start yielding at the onset of impulse load, they also contribute to the energy dissipation. The effect of pre-stressing is in fact to produce a shift in the axis of the axial load-elongation relationship for the fuses as shown in figure 3-9. The shift results in an apparent compressive strength of the fuses

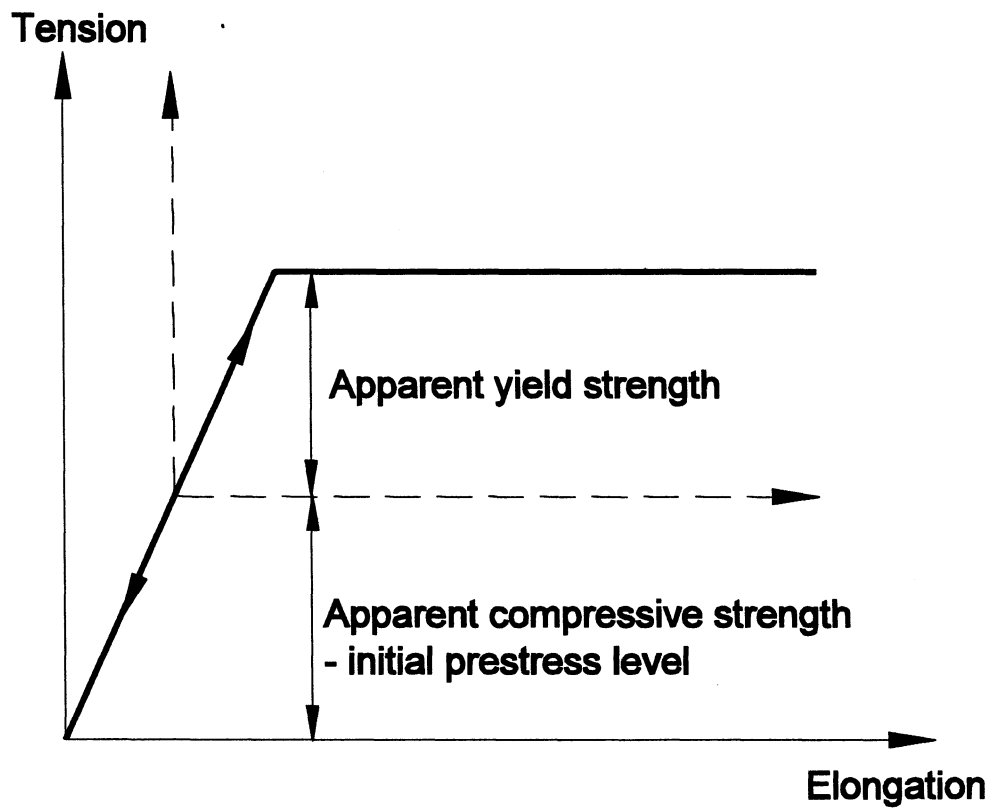


Figure 3-9 Effect of Initial Pre-stress on the Behavior of the Fuse-Bars

equal to the pre-stressing level. Similarly, apparent yield strength in tension is equal to the yield strength of the fuse minus the initial pre-stressing force. Various levels of pre-stress and its effects on the structural response should be investigated both experimentally and analytically. However, it can readily be said that the initial pre-tension should not exceed the initial pre-load level (if any) of damping devices and the deformation capacity should be carefully designed.

It is further recommended that re-centering devices should be used as part of the supplemental system. A class of re-centering devices (Elastomeric Spring Damper, ESD) was previously investigated and tested on a 1:3 scale reinforced concrete model structure in DTR configuration (Pekcan et al., 1995). The unique characteristic of ESD is that it is strongly re-centering due to the initial pre-load. In fact, it is a very desirable feature especially in applications to flexible-yielding structures. It can be readily said that the re-centering forces can be uniformly (as desired) distributed when these devices are used in the load balancing tendon configuration. Moreover, the pre-load level can be designed to accommodate the pre-tensioning forces and therefore avoids pre-stress losses.

3.6 SUMMARY AND CONCLUSIONS

The primary purpose of this section was to propose a new concept for mitigating lateral loads imposed on building frames – that is to balance the lateral loads with a pre-stressing tendon-fuse+damper system. The proposed system, which balances the applied overturning moments, is in contrast to the present vogue of using a damper-truss solution. The damper-truss solution reduces interstory shear deformations within a structure through added damping. However, due to the need to place dampers on each story, the damper-truss solution is evidently a more costly proposition than the proposed pre-stressed load balancing approach. Design formulations are given for the LPT system and various aspects are discussed. However, it must be noted that LPT system is designed to balance inertia forces whose distribution is based on the dominant mode of vibration of the structure. When considering various choices of dampers and their installation configuration open to designer, the LPT solution may not be the optimal approach for structures with significant higher mode effects. Nevertheless, a creative way of solving the higher mode response problem may be to install a secondary LPT system(s) for a particular higher mode(s). However, the efficacy of such a strategy should be both subject to future research and case-by-case design studies.

SECTION 4

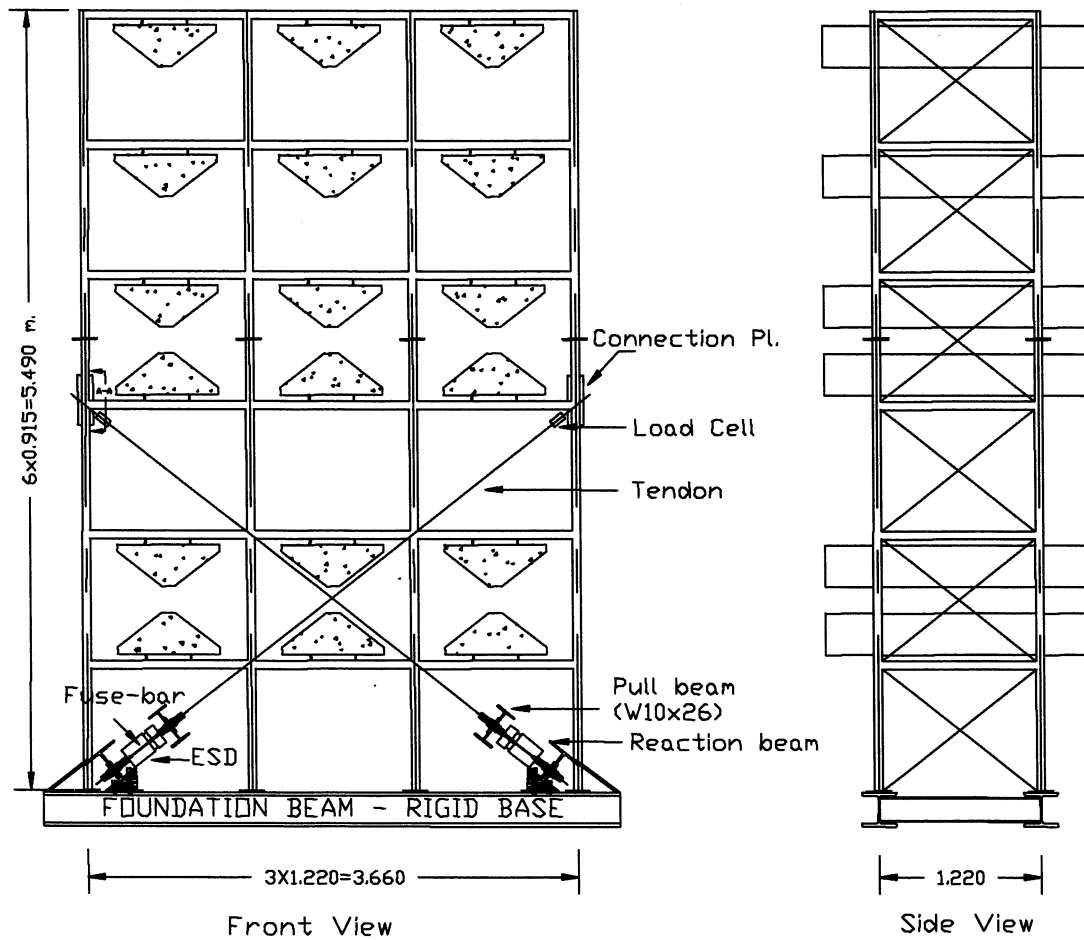
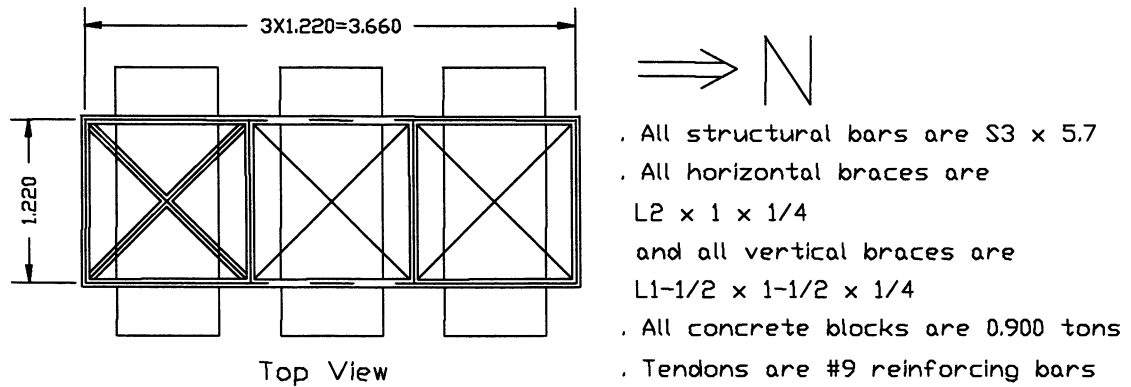
TEST STRUCTURE AND SHAKING TABLE TEST PROGRAM

4.1 INTRODUCTION

The model structure is a one-fourth scale, 6-story, space frame as shown in figure 4-1. *Load balancing tendon-fuse+damper* system and third floor connection details are shown in figure 4-2. This structure has been used previously in extensive experimental studies described below. The test structure represents a slice of a full-scale prototype of a moment resisting frame of a building structure. It has three bays in the strong (tested) long direction and one bay in the weak (short) transverse direction. Kentledge weights (ballast for similitude purposes) consisting of concrete blocks were used to ensure constant acceleration mass similitude requirements.

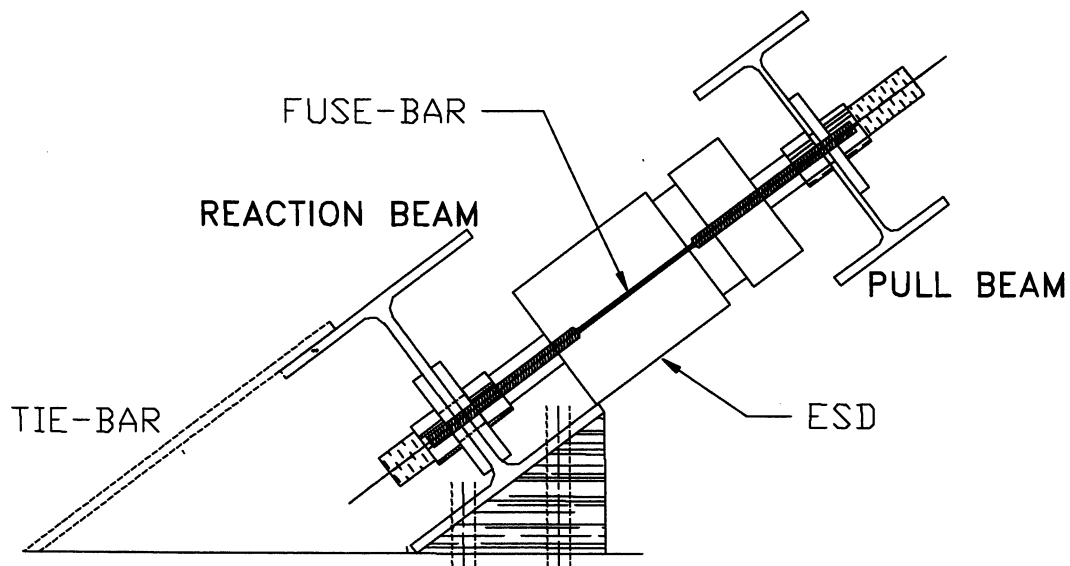
This model structure was constructed and tested under various simulated ground motions using the shaking table at the State University of New York at Buffalo. The first experimental study on this model structure involved the testing of an active tendon system and active mass dampers (Reinhorn et al., 1989). This experimental study was primarily intended to investigate the effectiveness of a simple active control system in response control of complex structures under earthquake type excitations. Various active tendon configurations were tested both in strong and weak directions under simulated ground motions which had peak ground accelerations up to 0.09 g. Mokha et al (1990) tested the six-story moment frame supported on rigid beams with four Friction Pendulum System (FPS) isolators. Al-Hussaini et al. (1994) removed the rigid base (figure 4-1) and added an additional story with FPS isolators to further investigate the effectiveness of the FPS isolation system with various bracing configurations.

In this study, ESDs (as well as fuses in parallel with ESDs) were installed in a series arrangement with a tension only working tendon system as shown in figure 4-1 and in the photographs of figure 4-3 through 4-5. Fuse-bars were fixed at their lower ends to the reaction beam in parallel to the ESD devices. Large washers were placed at both sides of the beams where fuse-bars were connected to the reaction and pull-beams. One washer was used on the pull side of the pull-beam to ensure the activation in tension only. Details of the test setup, instrumentation and testing program are given in the following subsections.

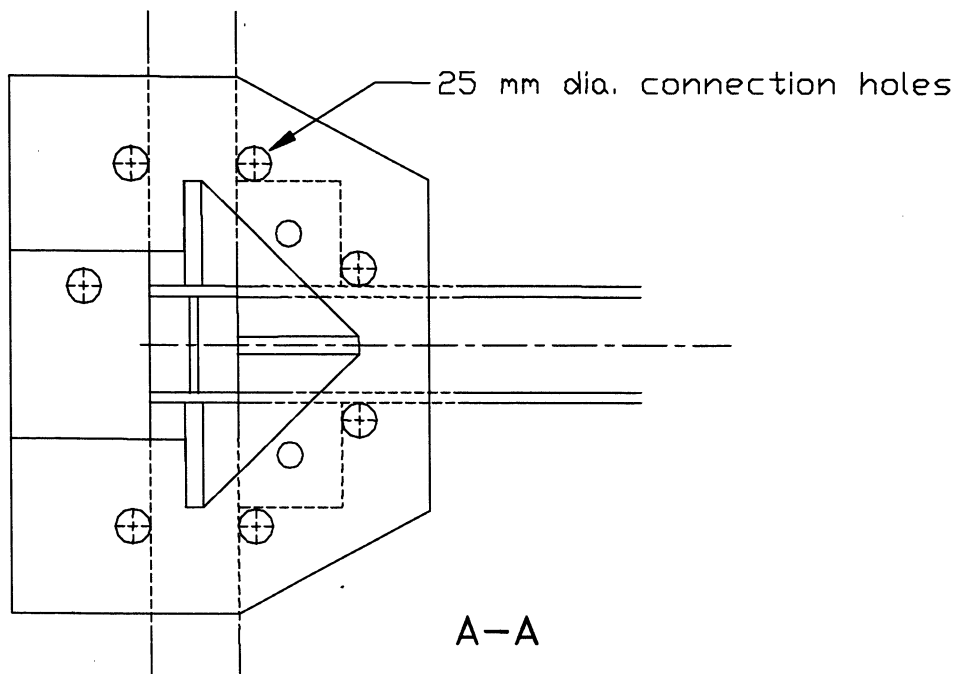


* All dimensions are in meters

Figure 4-1 General View of Test Structure



(a) Supplemental system detail



(b) Third floor connection detail

Figure 4-2 Load Balancing Tendon-Fuse+Damper System and Third Floor Connection Details

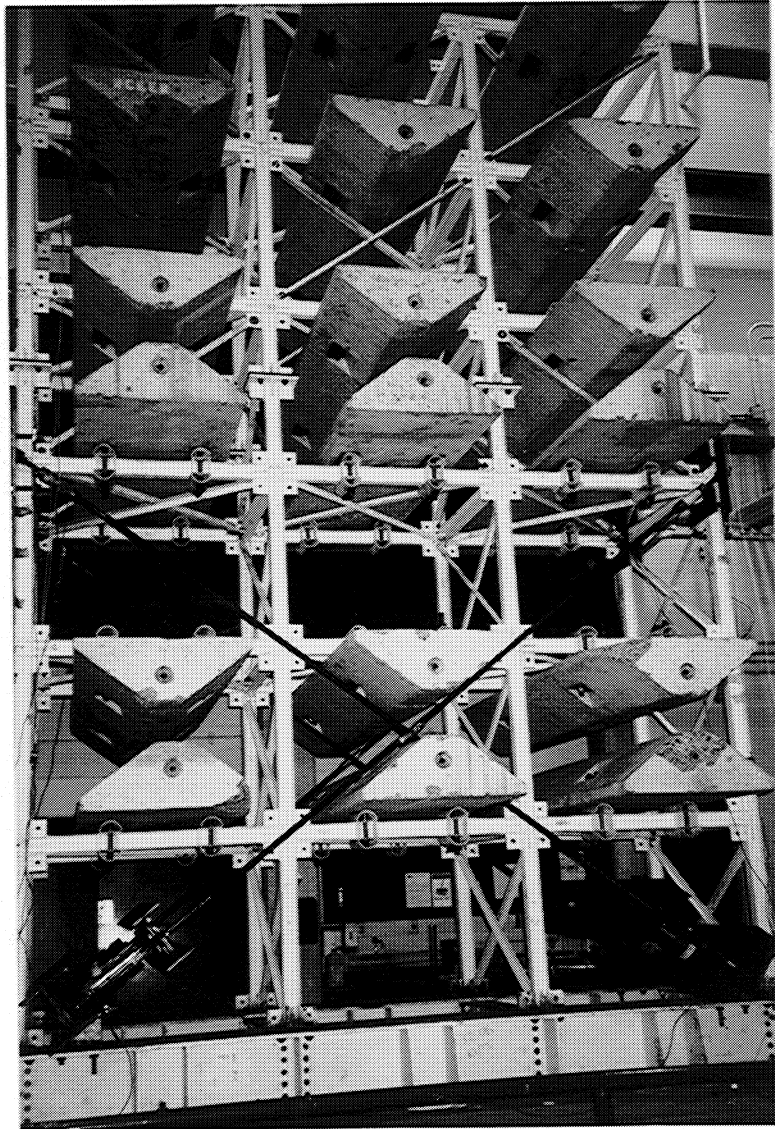


Figure 4-3 Photograph of the $\frac{1}{4}$ Scale Model Test Structure: Rigid foundations (I-beams) were fixed to the shaking table platform and, the test structure with the supplementary system were placed on these foundation beams.



Figure 4-4 Photograph of the Third Floor-Tendon Connection: Load cells with a capacity of ± 130 kN were installed in series with the tendon in order to record the supplementary system forces at this level. $\Phi 25$ mm-high strength threaded rods were used in the plate connections as shown.

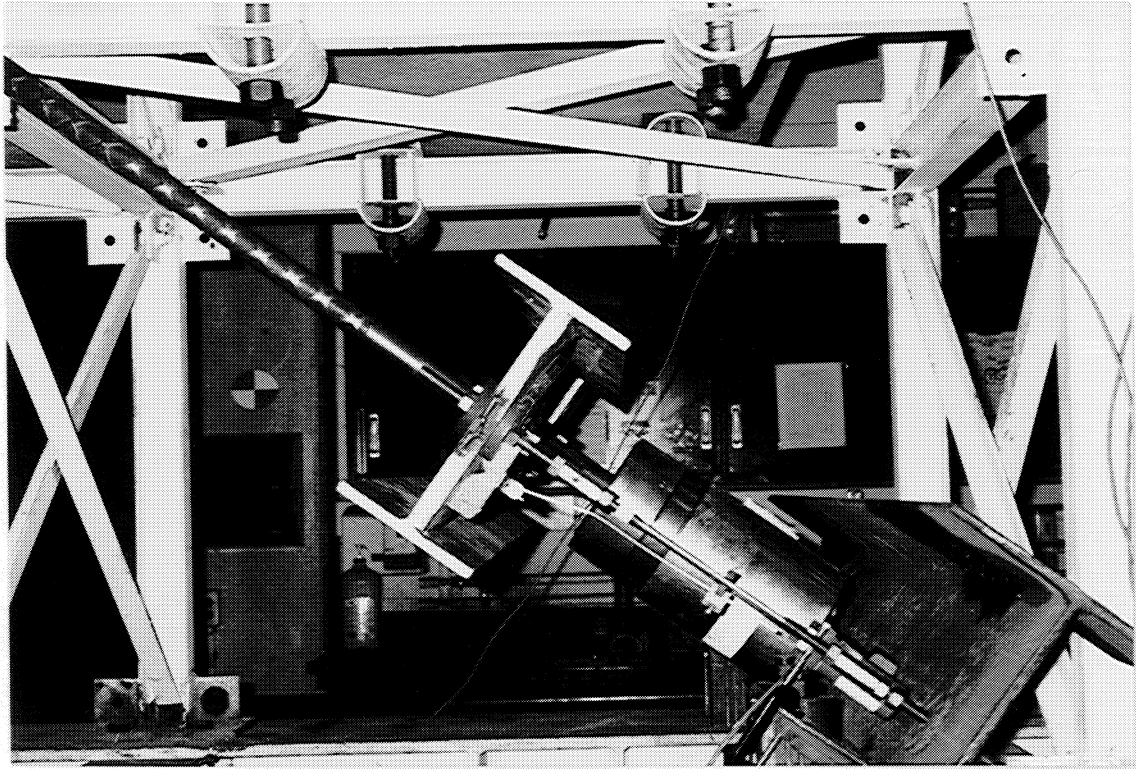


Figure 4-5 Photograph of the Supplementary System Detail: ESD devices and the fuse-bars were attached rigidly to the (lower) reaction beam. At the pull-end tendons had plate washers only on the pull side of the pull-beam, therefore worked in tension only. Note the fuse-bars in parallel to the ESD devices and the displacement transducers at the tendon-end.

4.2 TEST SETUP AND INSTRUMENTATION

A total of 55 channels were used to monitor the model structure response. A complete list of these channels and corresponding descriptions are given in table 4-1. A schematic view of the instrumentation on the test structure is shown in figure 4-6.

After the test structure was fixed on the foundation beams on the shaking table platform, a set of displacement potentiometers and, horizontal, vertical and transverse accelerometers were installed. Linear transducers (displacement transducers) were used to measure the absolute displacement response in the longitudinal (N-S) direction of the base and each story level of the model. Four additional displacement transducers were installed to monitor the relative translation between reaction beam and pull beam (hence, average damper/fuse deformations, figure 4-1) at the tendon's lower end. Horizontal accelerometers (in the direction of shaking) were installed on every floor level on both east (AHE#) and west (AHW#) frames to monitor torsional response (if any). Vertical (AV) and transverse (AT) accelerometers were only used on the base, 2nd, 4th and 6th floors.

Four #9 bars were provided to act as rigid tendons (one pair on each side) which had a nominal cross sectional area of 645 mm² and weight per unit length of 0.05 kN/m.

4.3 TEST PROGRAM

In the experimental study, numerous shaking table tests were performed using seven different ground motions at various peak ground acceleration (PGA) levels with and without a *load balancing tendon-fuse+damper* system:

- (i) 1952 Kern County - Taft N21E,
- (i) 1968 Tokachi-Oki - Hachinohe NS,
- (ii) 1971 San Fernando - Pacoima Dam S16E and S74W,
- (iii) 1940 Imperial Valley - El Centro NS,
- (iv) 1994 Northridge - Sylmar County 360 deg.,
- (v) 1995 Great Hanshin - Kobe.

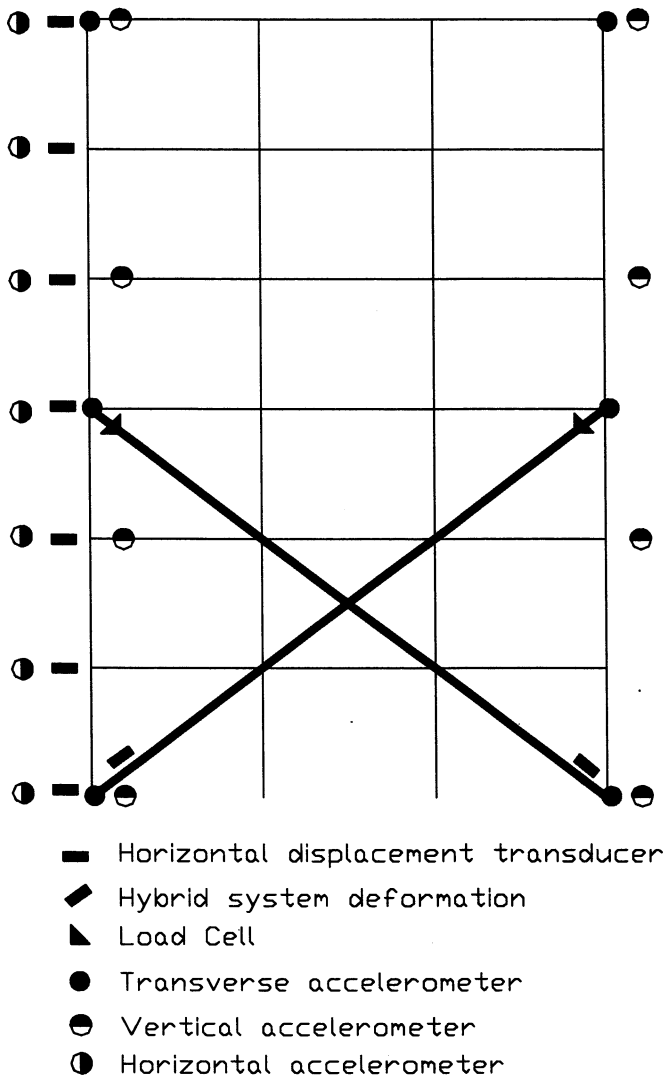


Figure 4-6 Instrumentation of the Test Structure

Table 4-1 Description of Instrumentation

Channel Name	Units	Description/Remarks
AH#E	G's	Horizontal acceleration at the floor levels – on the east frame (0-6)
AH#W	G's	Horizontal acceleration at the floor levels – on the west frame (0-6)
AT#N	G's	Transverse acceleration at alternating floor levels – on the north end (0,2,4,6)
AT#S	G's	Transverse acceleration at alternating floor levels – on the south end (0,2,4,6)
AV#N	G's	Vertical acceleration at the base, mid height and roof – on the north end (0,3,6)
AV#S	G's	Vertical acceleration at the base, mid height and roof – on the south end (0,3,6)
D#E	mm.	Horizontal (in the direction of shaking) displacement - on the east frame (0-6)
D#W	mm.	Horizontal (in the direction of shaking) displacement - on the west frame (0-6)
DD#	mm.	Fuse+damper system deformation - 1-2 on south end, 3-4 on north end
LC#	kN	Tendon force (load cell) – 1-2 on south end, 3-4 on north end
DLAT	mm.	Shaking table horizontal displacement
ALAT	G's	Shaking table horizontal acceleration
DVRT	mm.	Shaking table vertical displacement
AVRT	G's	Shaking table vertical acceleration

Ground motions were time scaled (by a factor of $1 / \sqrt{4}$) in order to meet the constant acceleration similitude requirements. Time scaled acceleration-time histories of some of the ground motions used are shown in figure 4-7. The latter three records mentioned above were extensively used to form the basis for the comparison of various configurations tested. The first four ground motions were mainly used to gather enough experimental information to establish dependable models for further analytical studies. Various bracing configurations were tested using these ground motions of minor to moderate levels. A wide-band (0 to 50 Hz) white noise base excitation (0.05 g) was used before and after each configuration change to determine the dynamic characteristics of the test structure. A complete list of shaking table test program is given in table 4-2. A total of seven configurations were tested as schematically shown in figure 4-8.

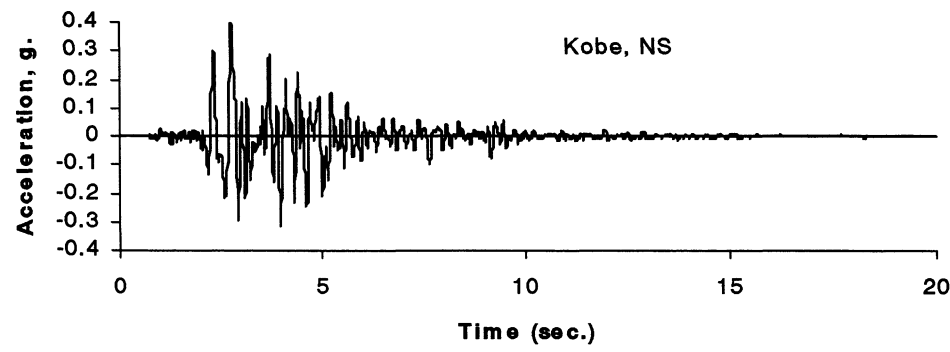
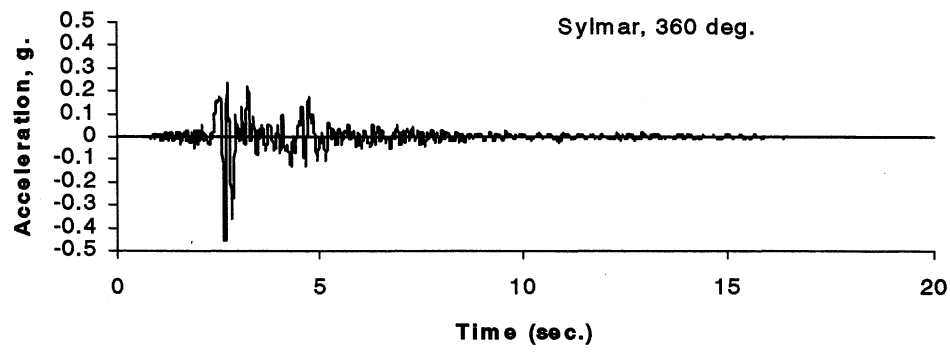
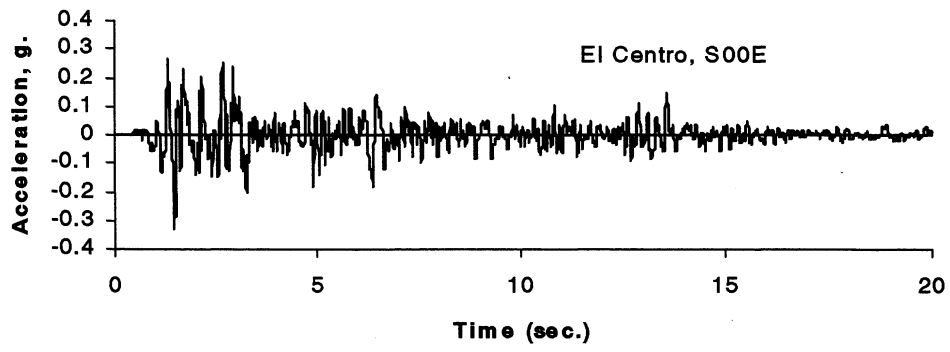


Figure 4-7 Acceleration Records (1/2 time scaled)

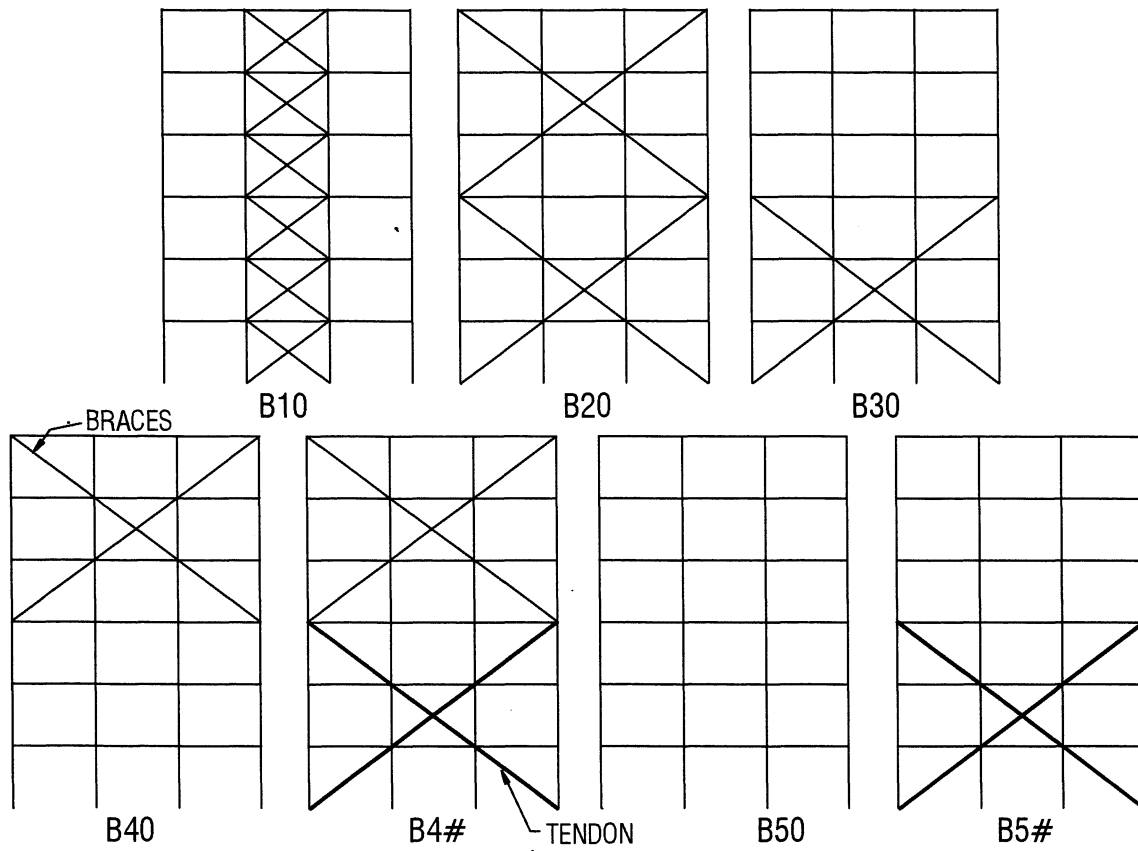


Figure 4-8 Tested Configurations

Table 4-2 Schedule of Shaking Table Experiments

Test #	Ground Motion	PGA (g)	File Name	Remarks
1	White Noise	0.050	B10AW05	"B1" configuration
2	El Centro, S00E	0.080	B10EL07	
3	"	0.130	B10EL12	
4	Taft,N21E	0.073	B10TA08	
5	"	0.115	B10TA12	
6	Hachinohe, NS	0.075	B10HA08	
7	White Noise	0.050	B10BW05	
8	White Noise	0.050	B20AW05	"B2" configuration
9	El Centro, S00E	0.121	B20EL12	
10	Taft,N21E	0.101	B20TA12	
11	Hachinohe, NS	0.082	B20HA08	
12	White Noise	0.050	B20BW05	
13	White Noise	0.050	B30AW05	"B3" configuration
14	El Centro, S00E	0.084	B30EL08	
15	Taft,N21E	0.077	B30TA08	
16	Hachinohe, NS	0.088	B30HA08	
17	White Noise	0.050	B30BW05	
18	White Noise	0.050	B40AW05	"B4" configuration
19	El Centro, S00E	0.108	B40EL12	
20	Taft,N21E	0.108	B40TA12	
21	Hachinohe, NS	0.079	B40HA08	
22	White Noise	0.050	B40BW05	
23	White Noise	0.050	MOMAW05	"B5" config - Moment frame only
24	El Centro, S00E	0.074	MOMEL12	
25	Taft,N21E	0.067	MOMTA12	
26	Hachinohe, NS	0.063	MOMHA08	
27	White Noise	0.050	MOMBW05	
28	White Noise	0.050	B41AW05	"B4" config with all fixtures on but dampers not active
29	El Centro, S00E	0.110	B41EL12	
30	Taft,N21E	0.114	B41TA12	
31	Hachinohe, NS	0.089	B41HA08	
32	Pacoima, S74W	0.160	B41PA16	
33	Pacoima, S16E	0.180	B41PA18	
34	Sylmar, 360 deg.	0.175	B41SY17	
35	Kobe, NS	0.168	B41KO17	
36	White Noise	0.050	B41BW05	

Table 4-2 Cont'd

Test #	Ground Motion	PGA (g)	File Name	Remarks
37	White Noise	0.050	B43AW05	"B4" config - dampers active prestressed to 1.5+ kips
38	El Centro, S00E	0.183	B43EL20	
39	Taft, N21E	0.218	B43TA20	
40	Pacoima, S16E	0.200	B43PA20	
41	Sylmar, 360 deg.	0.218	B43SY20	
42	Kobe, NS	0.193	B43KO20	
43	White Noise	0.050	B43BW05	
44	White Noise	0.050	B44AW05	"B4" config - dampers active prestressed to 1.5+ kips
45	El Centro, S00E	0.306	B44EL30	
46	Sylmar, 360 deg.	0.350	B44SY30	
47	Kobe, NS	0.265	B44KO30	
48	White Noise	0.050	B44BW05	
49	White Noise	0.050	B47AW05	"B4" config - dampers and fuses active prestressed to 5+ kips
50	El Centro, S00E	0.418	B47EL40	
51	Sylmar, 360 deg.	0.495	B47SY40	
52	Kobe, NS	0.373	B47KO40	
53	White Noise	0.050	B47BW05	
54	White Noise	0.050	B50AW05	"B5" config with all fixtures on but dampers not active
55	El Centro, S00E	0.172	B50EL20	
56	Sylmar, 360 deg.	0.162	B50SY20	
57	Kobe, NS	0.164	B50KO20	
58	White Noise	0.050	B50BW05	
59	White Noise	0.050	B51AW05	"B5" config - dampers active prestressed to 1.5+ kips
60	El Centro, S00E	0.280	B51EL30	
61	El Centro, S00E	0.332	B51EL40	
62	Sylmar, 360 deg.	0.456	B51SY40	
63	Kobe, NS	0.397	B51KO40	
64	White Noise	0.050	B51BW05	
65	White Noise	0.050	B52AW05	"B5" config - dampers and fuses active prestressed to 5+ kips
66	El Centro, S00E	0.307	B52EL40	Table malfunction

4.4 COMPUTATIONAL MODELING OF THE TEST STRUCTURE

Main load carrying structural elements (beams and columns) of the test structure were modeled using the beam-column elements with a specified P-M interaction that are available in the DRAIN-2DX element library. Modeling of the structure with *load balancing tendon-fuse+damper* system is somewhat different and more involved than that of with various bracing configurations. Although, most of the modeling techniques and assumptions are still applicable to both systems, specific details are given in following two subsections, respectively.

4.4.1 Modeling of the Braced Frame

The braces were modeled using truss elements that have axial-bilinear force-deformation characteristics. The main assumptions considered in the analytical model with the braced configurations are as follows:

- (i) One of the two moment frames is modeled as a plane frame with rigid floor diaphragms,
- (ii) Half the total weight of the structure, hence masses are assumed to be lumped at the nodes of the elements at each floor level,
- (iii) Elastic axial deformations of the column members and elastic shear deformations of the beam members are included in the analyses,
- (iv) Bracing connections are assumed to be rigid, however slip at the bolted connections was taken into account by reducing the effective area of the truss elements used to model the bracings,
- (v) Earthquake excitation is defined in the horizontal direction and all support points are assumed to move in phase,
- (vi) P-Delta effects are included in the analyses,
- (vii) Viscous damping of the structure is considered using a Rayleigh damping model – that is a linear combination of the mass and the stiffness matrices. Damping values from the experiments were used as input for the analytical predictions.

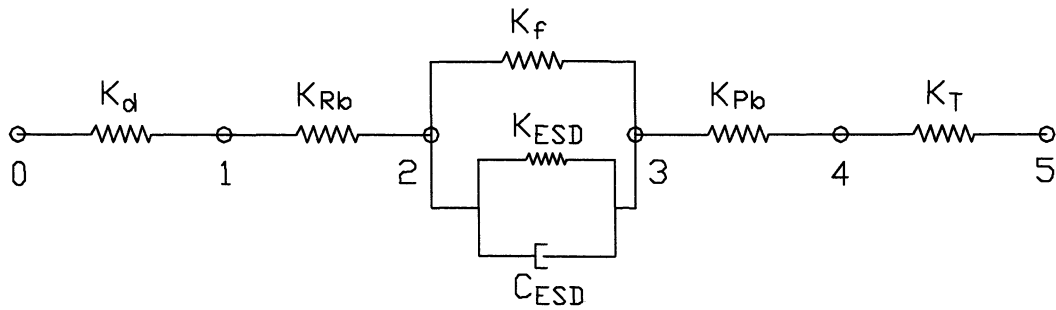


Figure 4-9 Drain-2DX Computational Model of the Tendon System

4.4.2 Modeling of the Structure with the Load Balancing Tendon-Fuse+Damper System

Modeling of the structure with the *load balancing tendon-fuse+damper* system requires one modification to the above list of assumptions and additions as well. These are discussed in what follows.

Rigid floor diaphragm assumption is not valid since prestressing of the tendon system imposes deformations in opposite directions that determine the initial conditions for the dynamic response analysis. Therefore, the previous analytical model was modified to have four translationally and rotationally independent nodes on each floor level.

The *load balancing tendon-fuse+damper* system has six elements in series/parallel arrangement as shown in figure 4-9. These elements are used to model; a) tendon (#9 bar) that transfers the *fuse+damper* system's force to the 3rd floor exterior joints K_T , b) the flexibility due to pull-beam deformation K_{Pb} , c) tension only ESD devices and fuse-bars, d) the flexibility due to reaction-beam deformation K_{Rb} , and e) a dummy element with high axial stiffness (EA) K_d . Additional masses are assigned to the joints 1-5 due to the self-weight of the connected elements. *Load balancing tendon-fuse+damper* system is modeled using ESD elements (defined in Section 2) and special link elements (fuse-bars) that act only in tension and become slack under compressive deformations. Moreover, the elongated (yielded) fuse-bar becomes ineffective in tensions upon reloading of the structure until it is deformed to its new length. Although all of the elements shown in the figure should be modeled as truss elements that can only transmit axial forces (the pull and reaction-beams and the dummy elements), these are actually modeled using beam-column elements that have very small rotational stiffness (low EI). This is mainly because

of the fact that two or more truss elements when connected in series can cause numerical instability, especially in static loading cases. In fact, a single analysis requires two steps: a) non-linear static analysis, b) non-linear dynamic analysis. In the static analysis part, a set of nodal loads are applied at joint 1 with controlled loading steps until the correct (experimental) initial prestress level is achieved in the tendon elements. The dynamic analysis then commences with the initial conditions attained at the end of the previous static analysis. Hence, the dummy beam-column element with high axial rigidity (EA) serves to “lock-in” the initial prestress level.

SECTION 5

SHAKING TABLE TEST RESULTS

5.1 INTRODUCTION

This section presents the experimental and analytical study that investigates the effectiveness of Elastomeric Spring Dampers (ESD) used to mitigate the seismic response of steel structures. In this study, well-known ground motions were used to investigate the performance of a one-quarter scale-model steel-moment frame structure.

The advantage of utilizing ESD devices in retrofitting conventional non-ductile reinforced concrete frame structures was previously investigated both experimentally and analytically by Pekcan et al. (1995). However, one of the major differences between reinforced concrete and steel structures is that linear behavior is expected in the latter, whereas bilinear elastic behavior exists in the former. Thus steel structures generally possess greater flexibility and lower inherent equivalent viscous damping than reinforced concrete structures. Larger interstory drifts can be expected which in turn causes distress to both structural and non-structural elements.

A total of seven different configurations were tested; however, emphasis is given to those with the supplemental systems. Prior to shaking table tests, ESDs and sample fuses were tested to determine their properties. In the following subsections experimental results are presented along with the analytical predictions obtained from the enhanced DRAIN-2DX computational model described in Section 2. In presenting the shaking table test results major emphases are placed on the overall response of the test structure subjected to simulated ground motions as well as the corresponding response of the *load balancing tendon-fuse+damper* system itself. Further details of the properties of the ESD devices and fuse-bars, and experimental setup are discussed in the following.

5.2 DISCUSSION OF PREVIOUS RELATED WORK

Because steel moment frame structures did not perform particularly well in the recent 1994 Northridge earthquake, it is necessary for the profession to investigate both direct and indirect means of mitigating inherently faulty welded steel beam-column connection designs that

were designed prior to the 1994 Northridge earthquake. Direct methods principally involve strengthening and/or enhancing the ductility of the welded beam-column connections. Much research sponsored by SAC has been directed to this end (SAC, 1995). It is the premise of the research presented here that indirect methods of mitigation should be investigated as an alternative or supplement to direct strengthening. Indirect methods embrace supplemental damping and/or bracing. This research investigated a system that employs strengthening through post-tensioned bracing coupled with a class of supplemental damping.

Since the 1994 Northridge earthquake, there have been a considerable number of studies on the effects of near-source ground motions on flexible buildings. This type of ground shaking, which is generally accompanied by large velocity and displacement pulses, has a greater damage potential than those adopted in current design codes. Thus, the adequacy of present codes has been questioned and opened to discussion.

There are on-going studies in United States to form an International Building Code by mainly combining the three recently used building codes, namely, the Uniform Building Code (UBC), the Building Officials and Code Administrators Code (BOCA) and the Standard Building Code (SBC). Various documents such as "Tentative Requirements of SEAONC (Seismology Committee of the Structural Engineers Association of Northern California)", "National Earthquake Hazard Reduction Program (NEHRP) Recommended Provisions for Seismic Regulations for New Buildings (FEMA, 1995)" and "NEHRP Guidelines for Seismic Rehabilitation of Buildings (ATC, 1995)" provide some insight to recent developments in earthquake engineering and protective systems. These documents categorize some of the energy dissipating protective systems and prescribe analysis procedures such as equivalent linear procedures, nonlinear dynamic analysis etc. for buildings that incorporate such systems. Although widely recognized, the near-source ground motions and their damage potential especially on flexible buildings has not yet been addressed. In one recent study (Hall et al., 1995), it was pointed out that the displacement pulses at or near the natural period of vibration of the structure may cause severe damage to the structure as excessive interstory drifts are to be expected. If such pulses occur during the first cycle of the response, maximum response is generally not a function of the damping in the structure. Furthermore, it can easily be shown that maximum deformation is attained at the end of the pulse. Therefore, the effect of damping in reducing the maximum response will be minimal since the dissipated energy will only be about

one-fourth of that expected in one full cycle of response. This becomes an important issue in the design of structures with energy dissipation systems that rely merely on the added damping. For pulse-like ground motions, such as those mentioned above, damper-only systems will damp out the response after the initial peak response achieved but may only be of marginal value in mitigating the peak response.

Therefore, it follows that some additional and/or alternative means of damping is needed to arrest the impulse response. In this part of this study, a *load balancing tendon-fuse+damper* system has been adopted where sacrificial yielding fuse-bars are used in parallel to ESD devices. The fuse-bars provide a high initial stiffness and limit displacements. However, the damping devices are still effective to attenuate the remaining motion following the first large peak. The system tested in this experimental study was designed to work only in tension. This has the advantage of being light-weight (no buckling problems are encountered), relatively unobtrusive and easy to install.

5.3 PROPERTIES OF THE ESD DEVICES AND FUSE-BARS USED IN THE EXPERIMENTAL STUDY

The ESDs tested in the experimental study were off-the-shelf devices. These devices were tested under displacement-controlled sinusoidal motions at various frequencies and amplitudes. Some selected force-displacement plots are shown in figure 5-1. These specimen tests were used to identify the parameters in the mathematical model that was defined in Section 2 (equation 2-1) and repeated here for convenience:

$$F_D = K_2x + \frac{(K_1 - K_2)x}{\sqrt{1 + \left(\frac{K_1x}{P_y}\right)^2}} + C_D \operatorname{sgn}(\dot{x}) \left| \dot{x} \frac{x}{x_{\max}} \right|^\alpha \quad (5-1)$$

in which x = the damper displacement, K_1 = the initial stiffness, K_2 = elastomeric stiffness after the pre-stress has been overcome, P_y = damper static pre-stress force, C_D = the damper constant, \dot{x} = the damper velocity, x_{\max} = the damper stroke capacity, and α is a positive real exponent. For the devices used in this study the following average values were identified from individual tests and used in subsequent analytical modeling:

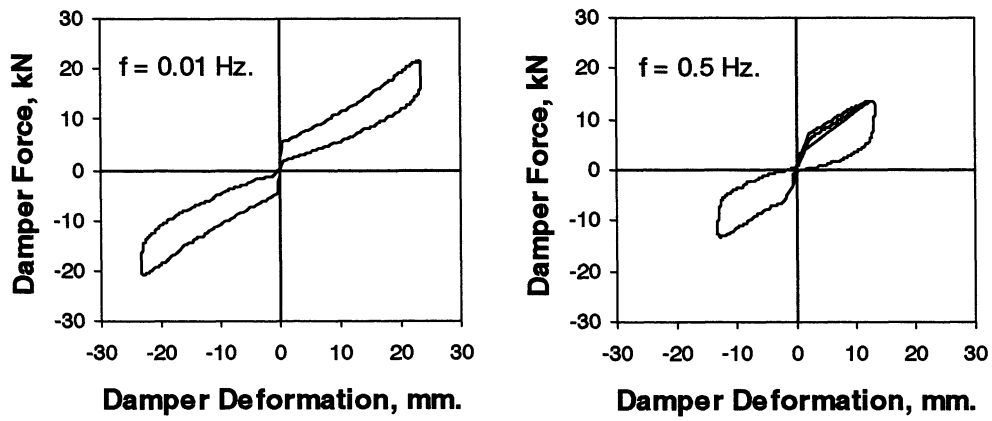


Figure 5-1 Selected ESD Specimen Tests

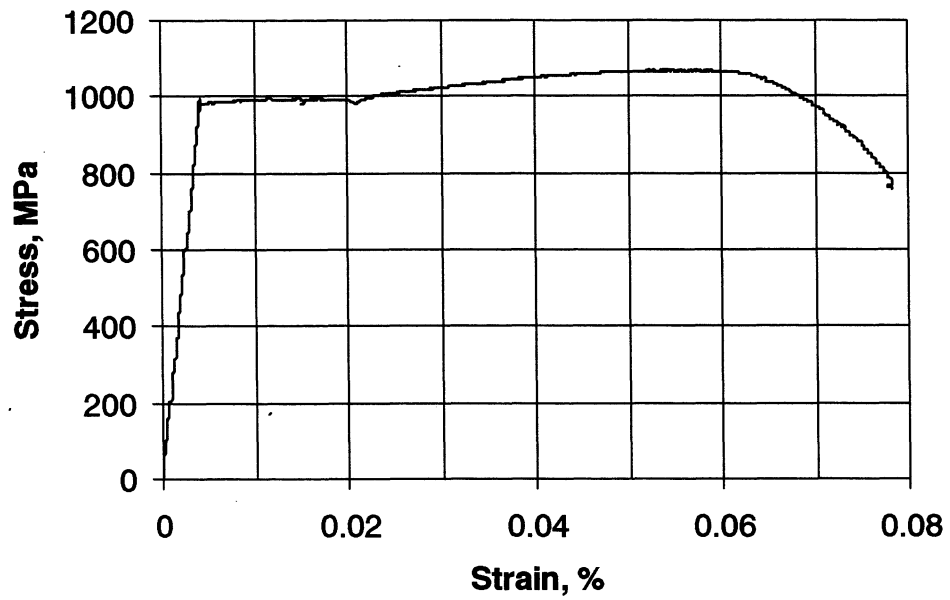


Figure 5-2 Average Stress-Strain Relationship of Fuse-Bars

$K_1 = 25.0 \text{ kN/mm}$, $K_2 = 0.6 \text{ kN/mm}$, $P_y = 2.78 \text{ kN}$, $x_{max} = 25.4 \text{ mm}$,

$C_D = 1.09 \text{ kN}/(\text{mm}/\text{sec})^{0.35}$, and $\alpha = 0.35$, giving

$$F_D = 0.6x + \frac{(25.0 - 0.6)x}{\sqrt{1 + \left(\frac{25.0x}{2.78}\right)^2}} + 1.09 \text{sgn}(\dot{x}) \left| \dot{x} \frac{x}{25.4} \right|^{0.35}$$

Replaceable high strength, $\phi 12 \text{ mm}$ threaded rods were machined to have 7 mm diameter over a fuse length of 152 mm . The stress-strain curve for the fuse-bars is shown in figure 5-2. The fuse-bars had average yield strength of $f_y=950 \text{ MPa}$, and ultimate strength of $f_{su}=1069 \text{ MPa}$. The strain at the offset of strain hardening was $\epsilon_{sh}=0.021$ and that of at the ultimate stress was $\epsilon_{su}=0.054$. Young Modulus was found to be $E=200 \text{ GPa}$ and post yield modulus $E_{sh}=2600 \text{ MPa}$.

5.4 SHAKING TABLE TEST RESULTS

This subsection first compares the structural dynamic characteristics obtained from the various white noise tests that use different setup configurations. These results demonstrate some of the stiffness characteristics of the test structure and effects of the supplementary tendon system. Secondly, response behavior under minor simulated ground motions is discussed in detail referring to the specific experimental results of various braced frame configurations next. Finally, comparative experimental results of the structure tested with and without the *load balancing tendon-fuse+damper* system are given in tables and discussed. When comparing the various structural responses, different PGA levels of the applied ground motions should also be kept in mind.

5.4.1 Comparison of Structural Dynamics Characteristics of Various Configurations

This subsection summarizes the structural dynamics properties of various tested configurations: a) structure without tendon system/with various brace configurations, b) structure with tendon system and top three stories braced, and c) Structure with tendon system and moment frame. One pair of white noise tests was conducted on the structure for each configuration tested in order to identify the mode shapes and corresponding natural periods of vibrations. Dynamic properties of the test structure were then determined from the story level

Table 5-1 Mode Shapes of the Moment Frame

	Modal Amplitude (values in parentheses are analytical)					
	1	2	3	4	5	6
$\xi, \%$	2.78	1.26	0.96	0.20	0.57	0.17
f, Hz	2.44 (2.44)	7.91 (7.63)	14.1 (13.5)	20.0 (19.8)	25.4 (26.1)	29.3 (30.8)
6	1.000 (1.000)	-0.981 (-0.995)	0.815 (0.817)	-0.432 (-0.615)	0.401 (0.409)	-0.094 (-0.180)
5	0.942 (0.925)	-0.391 (-0.392)	-0.480 (-0.392)	0.673 (0.909)	-1.000 (-0.977)	0.400 (0.542)
4	0.786 (0.793)	0.382 (0.401)	-1.000 (-1.000)	0.090 (0.222)	0.943 (0.858)	-0.658 (-0.839)
3	0.627 (0.611)	0.952 (0.967)	-0.093 (-0.200)	-0.823 (-0.998)	-0.038 (-0.084)	0.838 (1.000)
2	0.419 (0.393)	1.000 (1.000)	0.891 (0.892)	0.249 (0.124)	-0.644 (-0.766)	-1.000 (-0.983)
1	0.196 (0.160)	0.528 (0.516)	0.697 (0.812)	1.000 (1.000)	0.901 (1.000)	0.603 (0.718)

transfer functions. Transfer functions for the k^{th} floor were calculated as the ratio of the Fourier Transforms of the k^{th} floor acceleration time history to that of input acceleration at the rigid foundation. Approximate viscous damping ratios were calculated by using the Half Power (Band-Width) Method (Clough and Penzien, 1993). It must be noted here that not all of the six modes of vibrations could be identified accurately for the braced and damped frame configurations from the frequency domain analysis.

The frequency domain analysis results reported herein identify the characteristic response parameters under low-level amplitude ground motions. In fact, as discussed in the next subsections, the experimental model structure showed slightly different response characteristics in case of moderate to high-level input ground motions.

A comparison of story level transfer functions is shown in figure 5-3 for the braced frame configurations. Stiffening effect of braces can be seen, as the natural frequency becomes higher. Mode shapes that could be identified from the transfer functions are shown in figure 5-4. Three modes of vibration could be identified for the configuration in which both top and bottom three stories were braced (B20). Similarly, B40 configuration had its higher modes dampened as well.

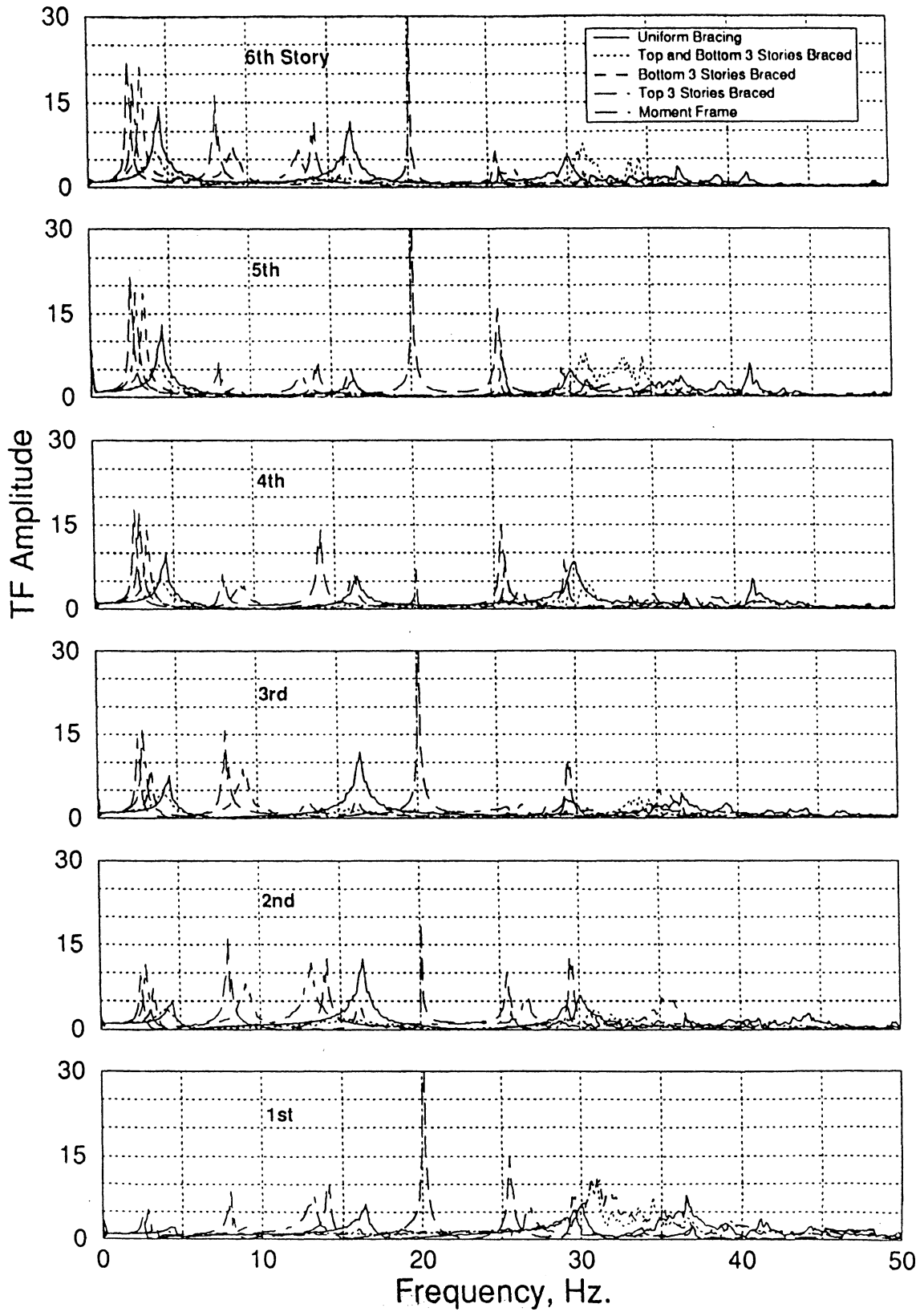
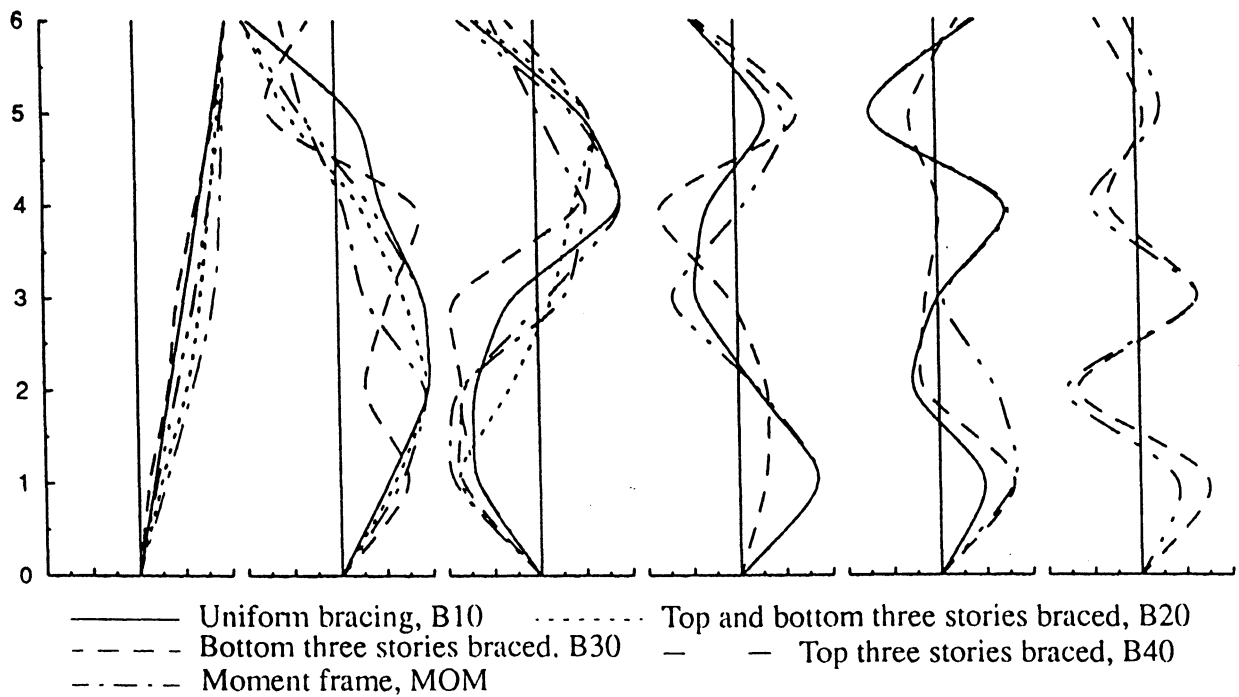


Figure 5-3 Comparison of story level transfer functions obtained from white noise experiments – Braced configurations and moment frame



B10	$[4.39 \ 16.31 \ 29.98 \ 36.72 \ 41.02 \ N/A] Hz$	B40	$[2.73 \ 13.09 \ 26.66 \ N/A \ N/A \ N/A] Hz$				
	$\begin{bmatrix} 1.00 & -0.93 & -0.66 & -0.47 & 0.43 & N/A \\ 0.88 & 0.26 & 0.56 & 0.47 & -1.00 & N/A \\ 0.69 & 0.47 & 1.00 & -0.35 & 0.90 & N/A \\ 0.52 & 0.95 & -0.34 & -0.49 & -0.03 & N/A \\ 0.34 & 1.00 & -0.71 & 0.20 & -0.34 & N/A \\ 0.15 & 0.52 & -0.72 & 1.00 & 0.62 & N/A \end{bmatrix}$		$\begin{bmatrix} 1.00 & -0.57 & -0.46 & N/A & N/A & N/A \\ 0.98 & -0.35 & 0.02 & N/A & N/A & N/A \\ 0.92 & 0.09 & 0.55 & N/A & N/A & N/A \\ 0.87 & 0.26 & 0.34 & N/A & N/A & N/A \\ 0.61 & 1.00 & -0.94 & N/A & N/A & N/A \\ 0.28 & 0.69 & -1.00 & N/A & N/A & N/A \end{bmatrix}$				
	B20		$[4.00 \ 14.94 \ 30.57 \ N/A \ N/A \ N/A] Hz$	MOM	$[2.44 \ 7.91 \ 14.06 \ 20.02 \ 25.39 \ 29.30] Hz$		
			$\begin{bmatrix} 1.00 & -0.98 & -0.61 & N/A & N/A & N/A \\ 0.93 & -0.53 & 0.71 & N/A & N/A & N/A \\ 0.81 & 0.27 & 0.39 & N/A & N/A & N/A \\ 0.70 & 0.74 & 0.17 & N/A & N/A & N/A \\ 0.56 & 1.00 & -0.32 & N/A & N/A & N/A \\ 0.22 & 0.61 & -1.00 & N/A & N/A & N/A \end{bmatrix}$		$\begin{bmatrix} 1.00 & -0.98 & 0.82 & -0.43 & 0.40 & 0.09 \\ 0.94 & -0.39 & -0.48 & 0.67 & -1.00 & -0.40 \\ 0.79 & 0.38 & -1.00 & 0.09 & 0.94 & 0.66 \\ 0.63 & 0.95 & -0.09 & -0.82 & -0.04 & -0.83 \\ 0.42 & 1.00 & 0.89 & 0.24 & 0.64 & 1.00 \\ 0.20 & 0.53 & 0.70 & 1.00 & 0.90 & -0.60 \end{bmatrix}$		
			B30		$[3.22 \ 8.98 \ 16.11 \ 25.59 \ 30.86 \ 34.96] Hz$		
					$\begin{bmatrix} 1.00 & -0.28 & 0.29 & 0.39 & -0.25 & 0.42 \\ 0.88 & -0.94 & -0.67 & -0.96 & 0.37 & -0.19 \\ 0.64 & 1.00 & -0.54 & -0.35 & -0.07 & 0.42 \\ 0.42 & 0.54 & 1.00 & -0.49 & 0.14 & -0.82 \\ 0.33 & 0.23 & 0.82 & 0.20 & 0.23 & 0.88 \\ 0.10 & 0.87 & 0.91 & 1.00 & -1.00 & -1.00 \end{bmatrix}$		

Figure 5-4 Comparison of identified mode shapes—Braced configurations and moment frame

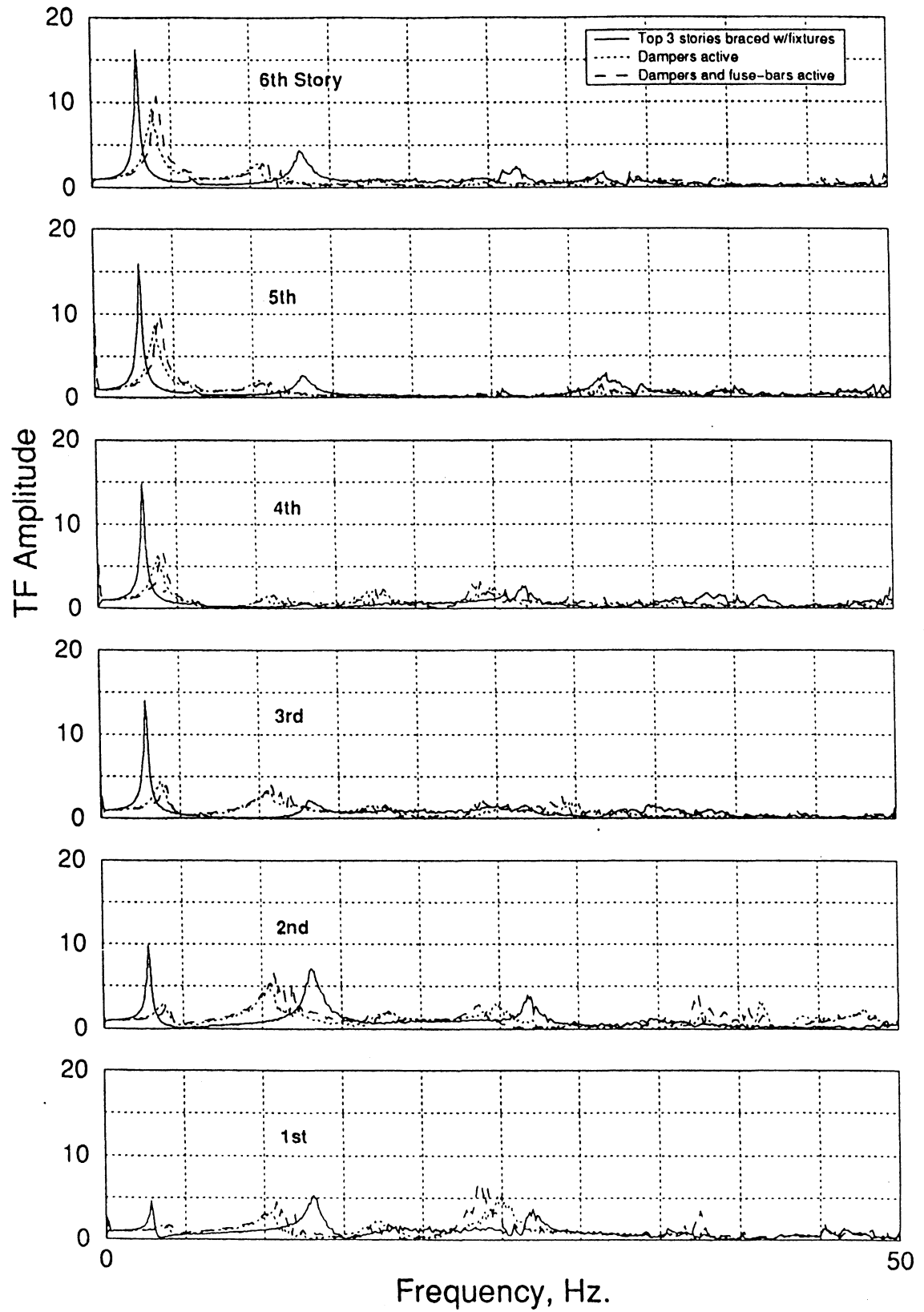
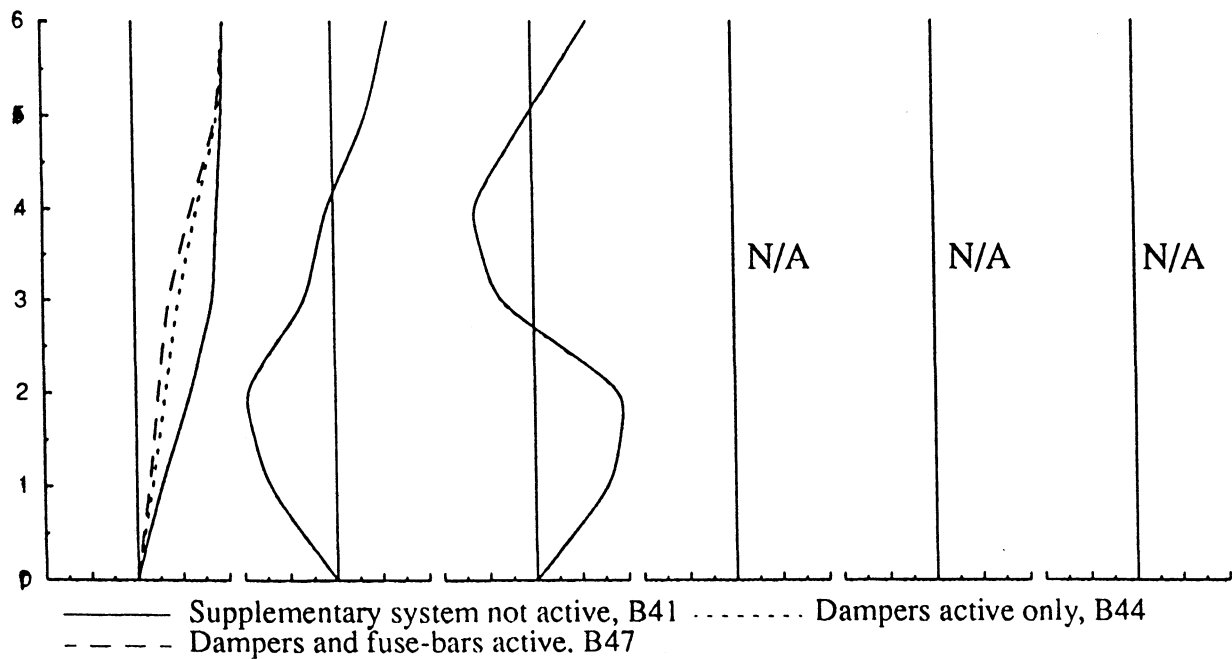


Figure 5-5 Comparison of story level transfer functions obtained from white noise experiments – Top three stories braced with supplementary system



B41	$[2.73 \ 12.99 \ 26.66 \ N/A \ N/A \ N/A] Hz$	B47	$[4.00 \ N/A \ N/A \ N/A \ N/A \ N/A] Hz$
	$[1.00 \ 0.62 \ 0.62 \ N/A \ N/A \ N/A]$		$[1.00 \ N/A \ N/A \ N/A \ N/A \ N/A]$
	$[0.98 \ 0.39 \ -0.05 \ N/A \ N/A \ N/A]$		$[0.93 \ N/A \ N/A \ N/A \ N/A \ N/A]$
	$[0.91 \ -0.08 \ -0.68 \ N/A \ N/A \ N/A]$		$[0.63 \ N/A \ N/A \ N/A \ N/A \ N/A]$
	$[0.86 \ -0.32 \ -0.42 \ N/A \ N/A \ N/A]$		$[0.37 \ N/A \ N/A \ N/A \ N/A \ N/A]$
	$[0.60 \ -1.00 \ 1.00 \ N/A \ N/A \ N/A]$		$[0.24 \ N/A \ N/A \ N/A \ N/A \ N/A]$
B44	$[0.27 \ -0.74 \ 0.84 \ N/A \ N/A \ N/A]$		$[0.15 \ N/A \ N/A \ N/A \ N/A \ N/A]$
	$[3.71 \ N/A \ N/A \ N/A \ N/A \ N/A] Hz$		
	$[1.00 \ N/A \ N/A \ N/A \ N/A \ N/A]$		
	$[0.94 \ N/A \ N/A \ N/A \ N/A \ N/A]$		
	$[0.69 \ N/A \ N/A \ N/A \ N/A \ N/A]$		
	$[0.48 \ N/A \ N/A \ N/A \ N/A \ N/A]$		
	$[0.32 \ N/A \ N/A \ N/A \ N/A \ N/A]$		
	$[0.18 \ N/A \ N/A \ N/A \ N/A \ N/A]$		

Figure 5-6 Comparison of identified mode shapes – Top three stories braced with supplementary system

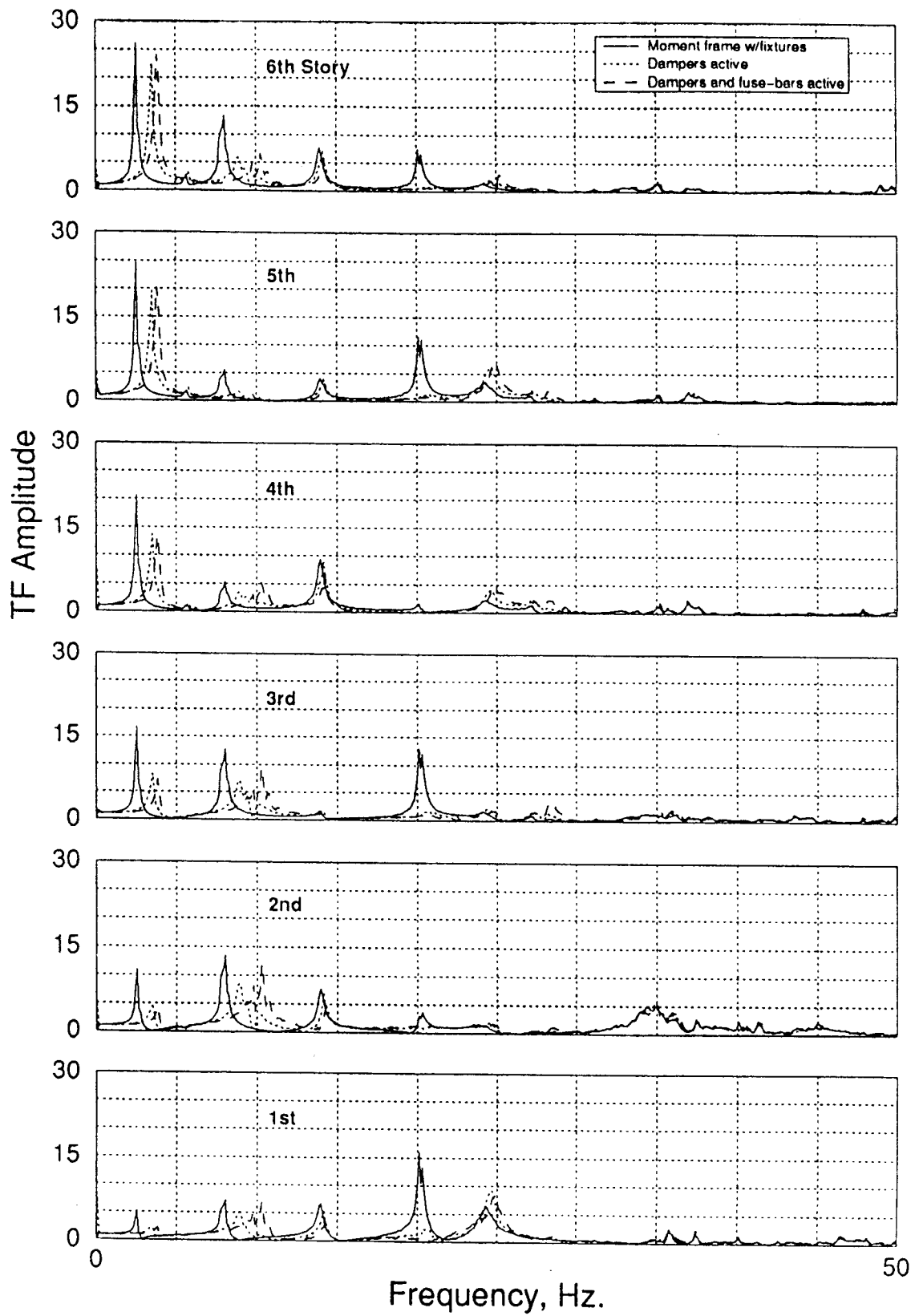
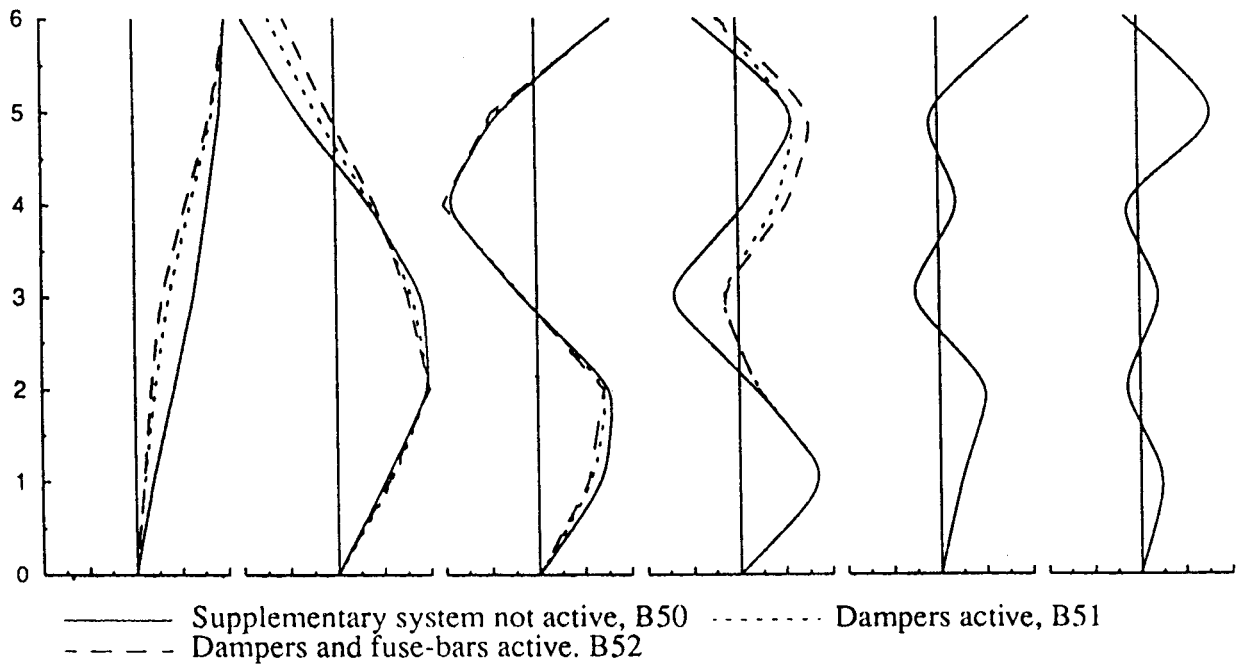


Figure 5-7 Comparison of story level transfer functions obtained from white noise experiments – Moment frame with supplementary system



B50	$[2.44 \ 7.91 \ 13.87 \ 20.02 \ 24.22 \ 35.06] //z$	B52	$[3.71 \ 10.16 \ 14.16 \ 24.80 \ N/A \ N/A] //z$
	$\begin{bmatrix} 1.00 & -0.99 & 0.82 & -0.45 & 1.00 & -0.13 \\ 0.94 & -0.40 & -0.44 & 0.73 & -0.21 & 1.00 \\ 0.79 & 0.38 & -1.00 & 0.10 & 0.25 & -0.22 \\ 0.63 & 0.94 & -0.18 & -0.82 & -0.36 & 0.27 \\ 0.42 & 1.00 & 0.82 & 0.18 & 0.56 & -0.20 \\ 0.19 & 0.52 & 0.72 & 1.00 & 0.22 & 0.31 \end{bmatrix}$		$\begin{bmatrix} 1.00 & -0.53 & 0.82 & 0.19 & N/A & N/A \\ 0.84 & -0.07 & 0.48 & 0.86 & N/A & N/A \\ 0.56 & 0.44 & 1.00 & 0.56 & N/A & N/A \\ 0.29 & 0.77 & 0.16 & 0.21 & N/A & N/A \\ 0.17 & 1.00 & 0.71 & 0.19 & N/A & N/A \\ 0.10 & 0.56 & 0.54 & 1.00 & N/A & N/A \end{bmatrix}$
B51	$[3.42 \ 8.79 \ 14.06 \ 24.51 \ N/A \ N/A] //z$		
	$\begin{bmatrix} 1.00 & -0.69 & -0.82 & -0.21 & N/A & N/A \\ 0.86 & -0.21 & 0.47 & 0.66 & N/A & N/A \\ 0.61 & 0.40 & 1.00 & 0.44 & N/A & N/A \\ 0.37 & 0.83 & 0.16 & -0.22 & N/A & N/A \\ 0.22 & 1.00 & -0.76 & 0.20 & N/A & N/A \\ 0.10 & 0.59 & -0.60 & 1.00 & N/A & N/A \end{bmatrix}$		

Figure 5-8 Comparison of identified mode shapes – Moment frame with supplementary system

Moreover, the model in this configuration can be approximated as a SDOF structure as can be seen from its first mode dominant behavior. Analytical and experimental mode shapes, natural frequencies and modal viscous damping ratios are compared for the moment frame (B50) in table 5-1 to demonstrate the accuracy of the analytical model described in the previous subsections.

Transfer functions obtained from white noise experiments conducted on B41, B44 and B47 configurations are compared in figure 5-5. Mode shapes and corresponding natural periods of vibrations are given in figure 5-6.

These experiments were performed after the prestress was applied to the tendon system. Therefore, results also indicate the initial effects of the prestress load on the stiffness of the model structure. The structure's properties were identical to that of the B41 configuration before the prestress load was applied. As can be seen from figures 5-5 and 5-6, the structure's stiffness was slightly increased due to tendon prestress. The increase in stiffness is explained as follows. When prestress is not used, only one set of tendons can be activated at a time. This set of tendon will tend to stiffen the structure due to bracing action. However, if tendons are prestressed, both set of tendons will contribute to the stiffening of the structure. Only when a compressive-like tendon force exceeds the prestress force will the tendon become slack and in turn reduce the stiffness of the structural system to a level similar to the non-prestressed case. Transfer function amplitude was reduced by about 50% in the first mode of vibration at the 6th floor level. It is interesting to note that natural frequency of second mode vibration was reduced (longer period). This result was attributed to the fact that during the ground motion experiments on the B41 configuration top three story brace connections were further loosened due to slip. Hence, the model structure had a lower apparent natural frequency in this mode.

Similar comparisons are made for the structure without the top three story braces but with the tendon system attached as in the previous configurations. Two white noise tests were conducted before and after each configuration change, after the prestress was applied to the system. Story level transfer functions are compared for the three configurations, namely B50, B51 and B52, in figure 5-7 and the identified mode shapes are shown in figure 5-8. Stiffening and added damping due to the tendon system are evident from the figure. However, reduction in the transfer function amplitude especially in the first mode is marginal in the top three stories, which implies that effectiveness of the tendon system is less on the top stories.

**Table 5-2 Comparison of 1st Mode Natural Periods and Viscous Damping Ratios
Braced Configurations**

Configuration	Natural Period, sec.		Damping Ratio, %	
	White Noise	Ground Motion	White Noise	Ground Motion
B10	0.23	0.24	4.7	6.0
B20	0.25	0.27	9.5	7.5
B30	0.31	0.32	3.2	4.4
B40	0.37	0.38	3.0	2.7
MOM (B50)	0.41	0.41	2.8	2.3

Table 5-3 Summary of Experimental Response – Braced Configurations

Ground Motion	Config.	PGA (g)	Base Shear/Weight (kN)	OTM (kN.m)	Roof Displ.(mm)	Max (ISD) ¹ (%)
El Centro	B10	0.130	0.208	177	6.0	0.164 (2)
	B20	0.121	0.215	198	6.5	0.208 (2)
	B30	0.084	0.147	134	6.5	0.197 (3)
	B40	0.108	0.227	180	9.9	0.339 (2)
	MOM	0.074	0.212	180	12.8	0.328 (2)
Taft	B10	0.115	0.150	156	4.4	0.129 (2)
	B20	0.101	0.145	134	4.5	0.142 (2)
	B30	0.077	0.155	122	6.1	0.186 (3)
	B40	0.108	0.323	249	14.7	0.470 (2)
	MOM	0.067	0.185	183	12.4	0.295 (2)
Hachinohe	B10	0.075	0.102	89	2.8	0.087 (2)
	B20	0.082	0.105	93	2.9	0.109 (2)
	B30	0.088	0.134	97	4.3	0.098 (2,3)
	B40	0.079	0.125	110	6.2	0.219 (3)
	MOM	0.063	0.154	142	10.0	0.260 (3)

¹ Story at which the maximum response was recorded

These discussions provide a brief insight into the structure's behavior under low-level ground shaking. In the following subsections, qualitative comparisons are also given between the results discussed above and those obtained from the relatively high-level ground motion experiments.

5.4.2 Tests on the Structure with Various Bracing Configurations

Experiments of five different braced/unbraced configurations were conducted for the following purposes: a) to validate the accuracy of the computational Drain-2DX model, b) to allow analytical as well as experimental response comparisons with the configuration having the supplemental dampers/fuses (i.e. B4# and B5# configurations in figure 4-8).

Story weights used in the analytical model were 27.6 kN on the 6th, 5th and 4th stories, 27.3 kN on the 3rd and 26.4 kN on the 2nd and 1st stories. Mode shapes and natural periods of vibration were identified from both white noise and simulated ground motion experiments. Due to low amplitudes and high damping owing the braced frame configurations not all six modes of vibrations could be identified accurately using the frequency domain analysis. Moreover, results of ground motion experiments revealed the fact that brace connections were not rigid and allowed considerable slip at the bolted joints. Hence, during the simulated ground motion experiments, the model had in general higher "apparent" natural period of vibrations than those identified from white noise tests. This additional source of flexibility was taken into account in the analytical model by reducing the effective area of the brace elements by 20% to 80% in some cases as the amount of slip increased from one experiment to another.

First mode natural frequencies and damping ratios as obtained from both white noise and ground motion test for the braced configurations tested are summarized in table 5-2. As can be seen from the table, the test structure had lower natural frequencies (higher periods) in case of simulated ground motion tests. As can be seen from table 5-2, the model structure had higher stiffness and viscous damping ratios for the braced configurations. It must be noted here that B40 configuration had properties similar to the moment frame. Top three-story bracing had a marginal effect on the first mode properties, however damped out the higher modes. As mentioned above, the simulated ground motion tests were performed at varying peak acceleration levels. However, for a specific ground motion, identical input signals could not be generated due to difficulties induced by shaking table-structure interaction at certain frequencies

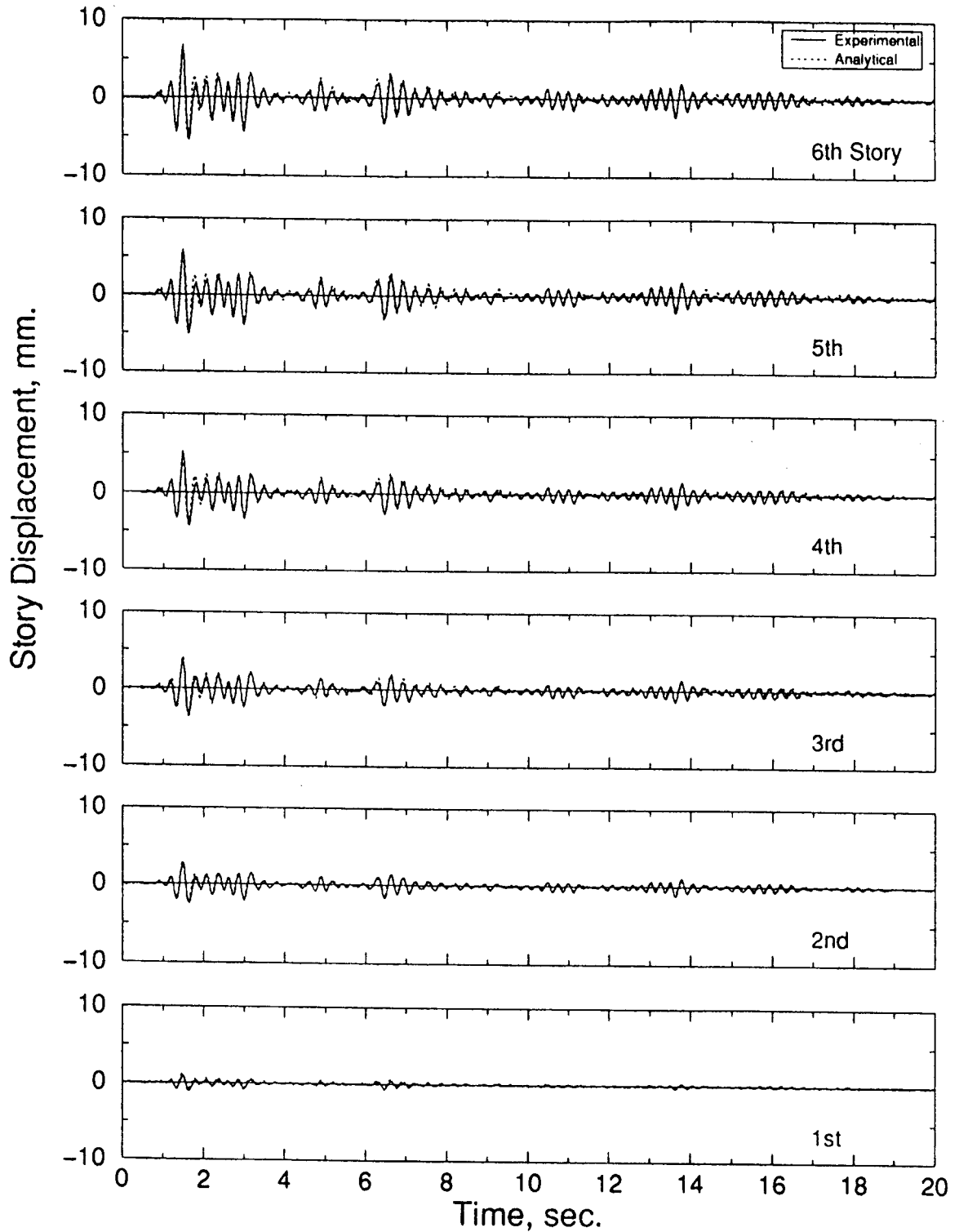


**Figure 5-9 Experimentally observed and analytically predicted displacement time histories:
 B20EL12
 Damping System: none
 Bracing: upper and lower three stories braced
 Earthquake: El Centro, PGA=0.12g**

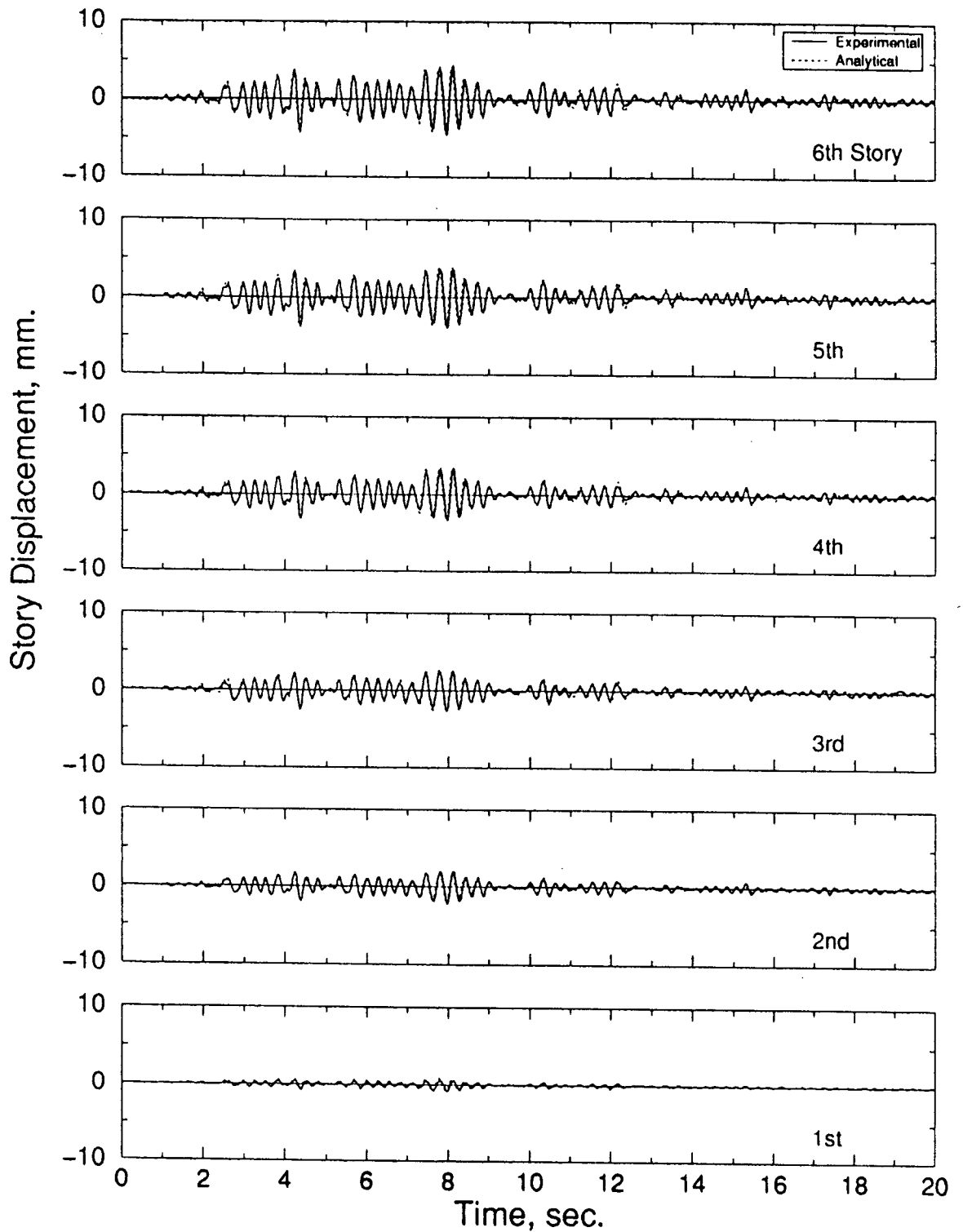


Figure 5-10 Experimentally observed and analytically predicted displacement time histories: B20TA12
Damping System: none
Bracing: upper and lower three stories braced
Earthquake: Taft, PGA=0.12g

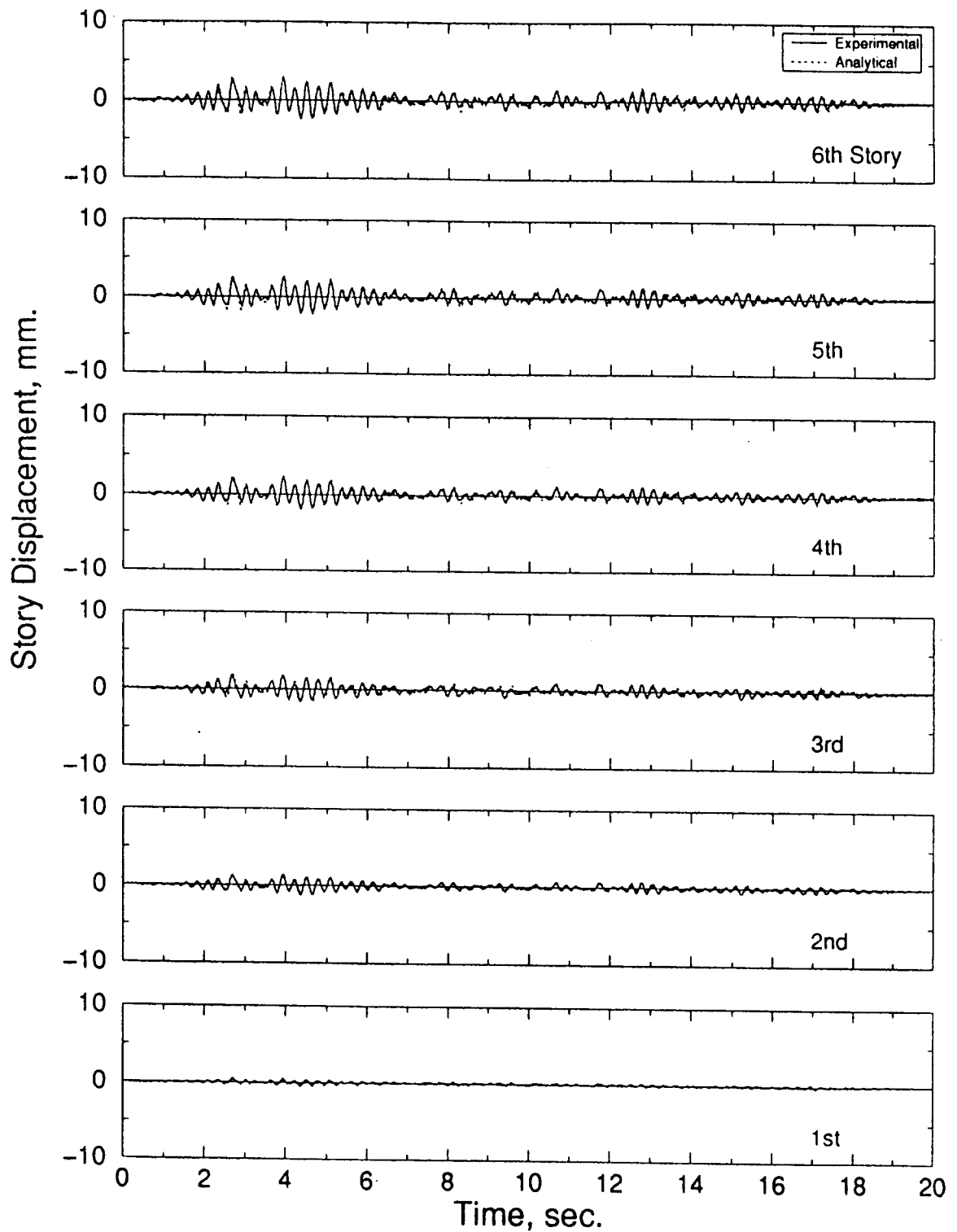


Figure 5-11 Experimentally observed and analytically predicted displacement time histories: B20HA08
Damping System: none
Bracing: upper and lower three stories braced
Earthquake: Hachinohe, PGA=0.08g

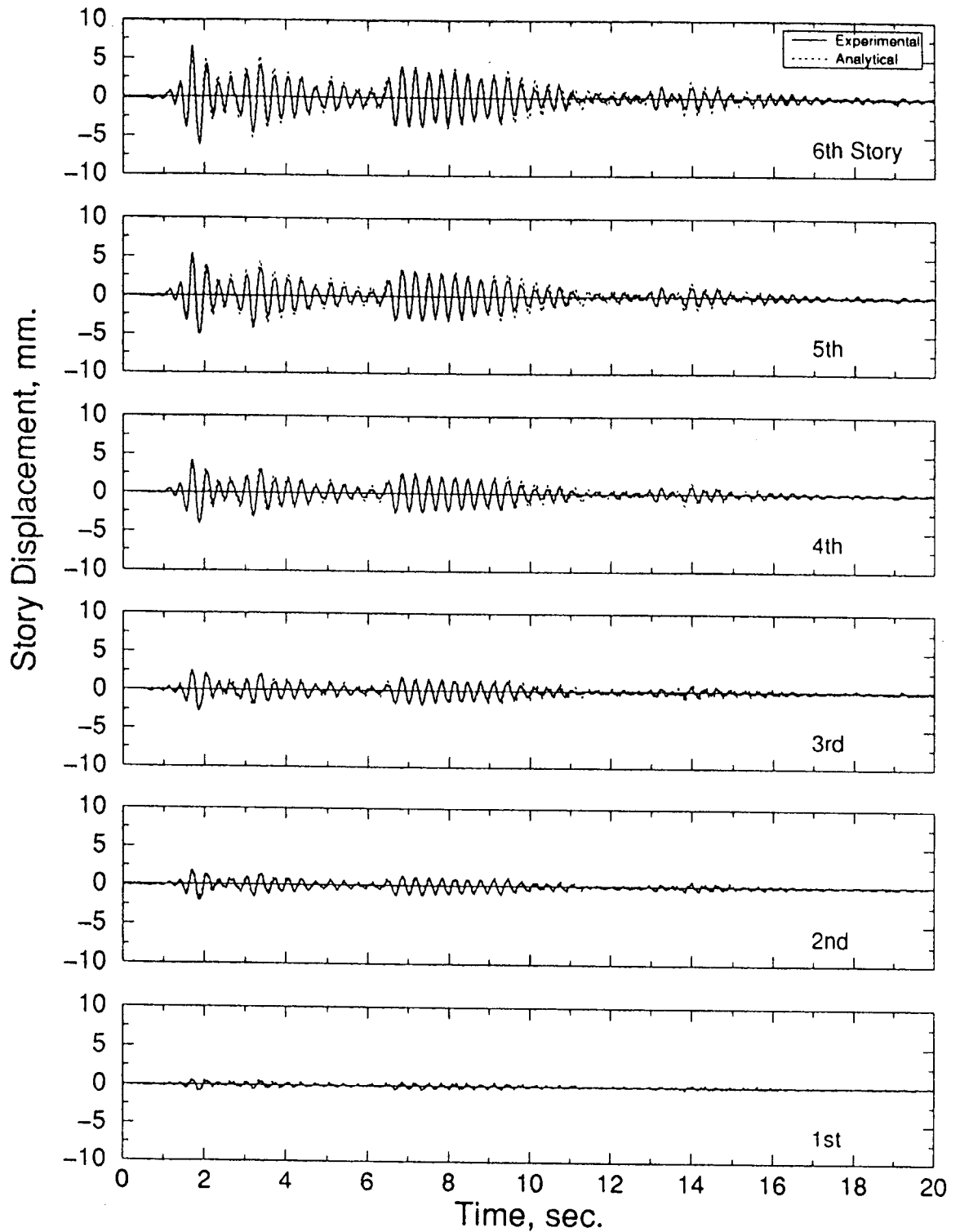


Figure 5-12 Experimentally observed and analytically predicted displacement time histories: B30EL08
Damping System: none
Bracing: lower three stories braced
Earthquake: El Centro, PGA=0.08g

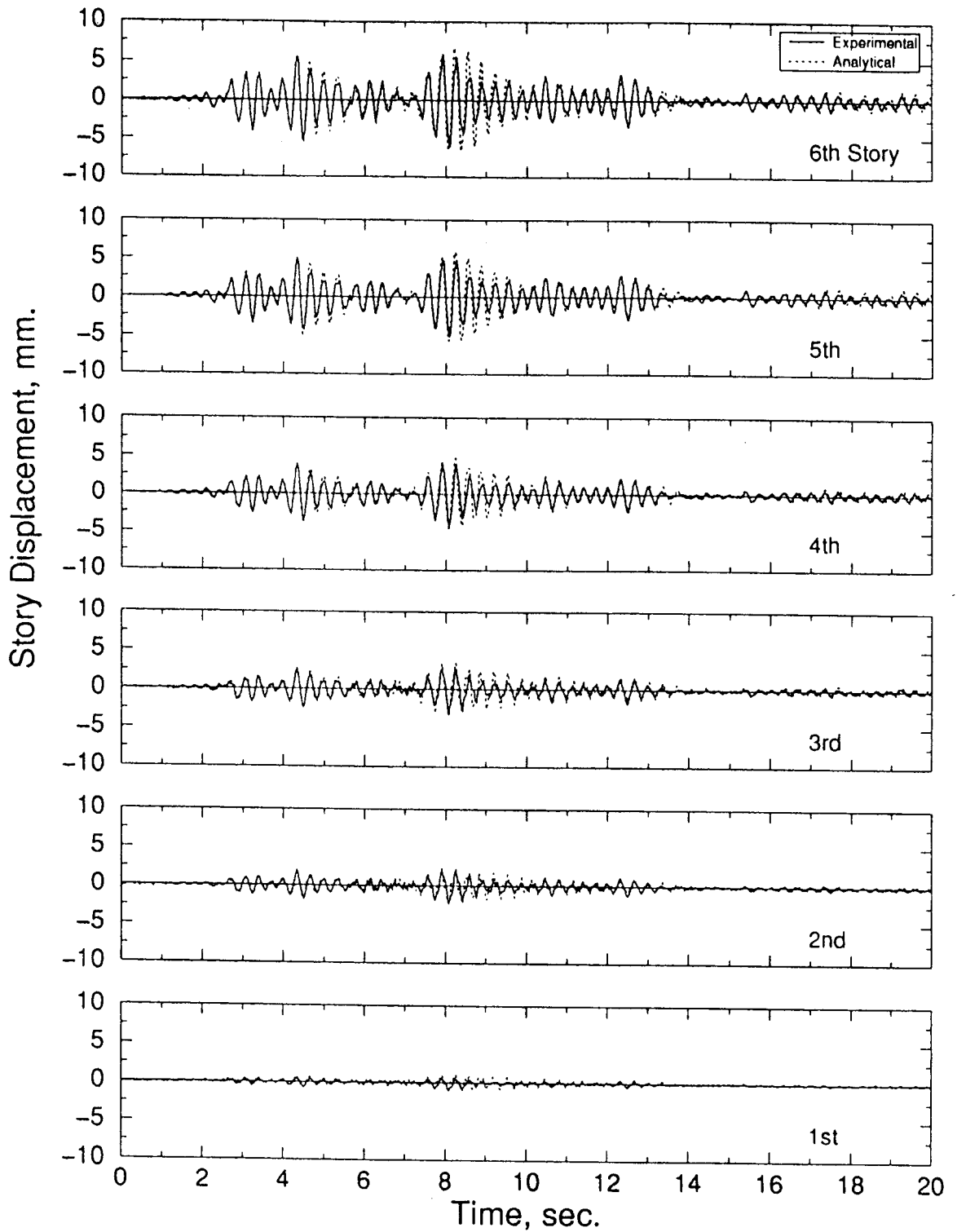


Figure 5-13 Experimentally observed and analytically predicted displacement time histories: B30TA08
Damping System: none
Bracing: lower three stories braced
Earthquake: Taft, PGA=0.08g

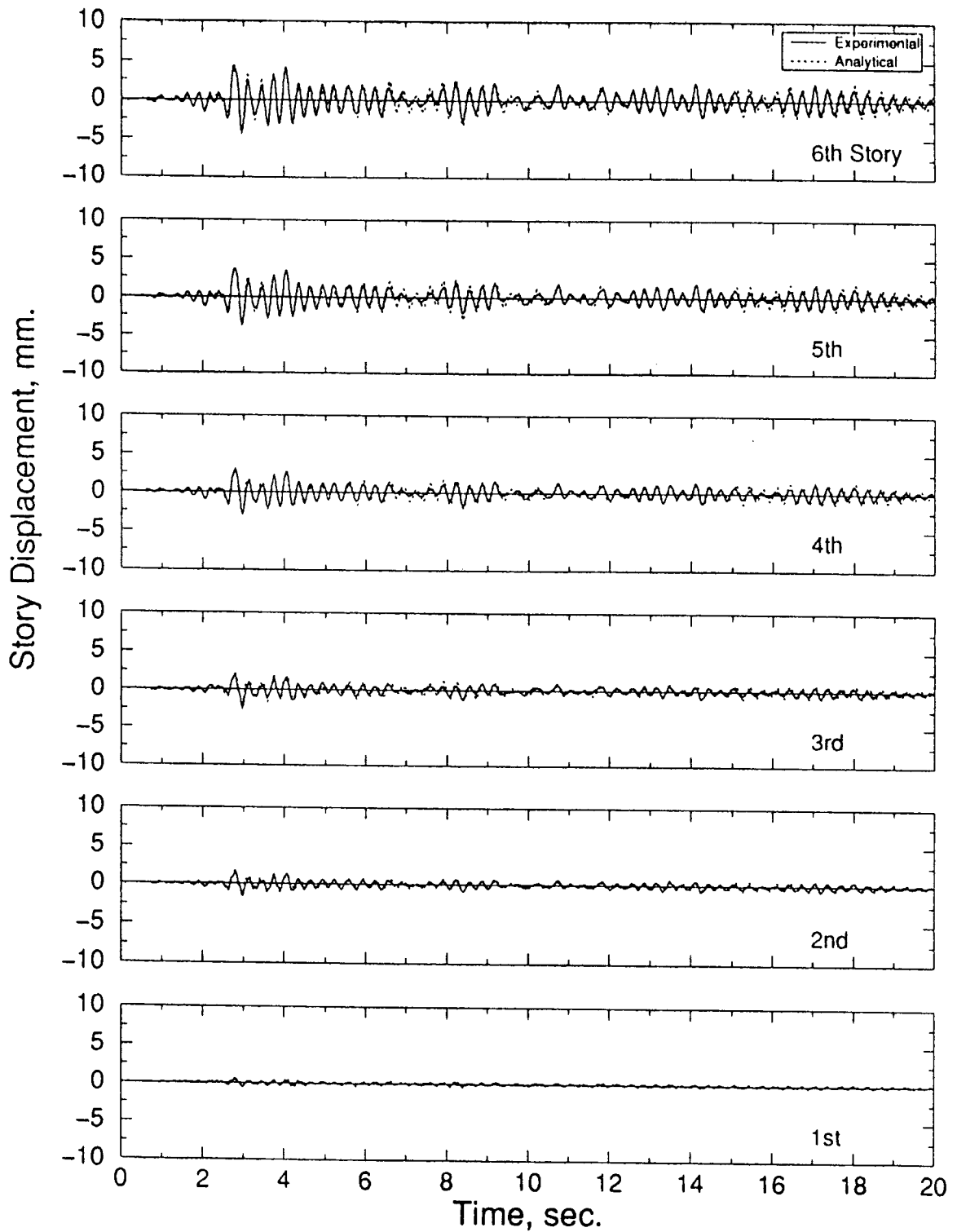


Figure 5-14 Experimentally observed and analytically predicted displacement time histories: B30HA08
Damping System: none
Bracing: lower three stories braced
Earthquake: Hachinohe, PGA=0.08g

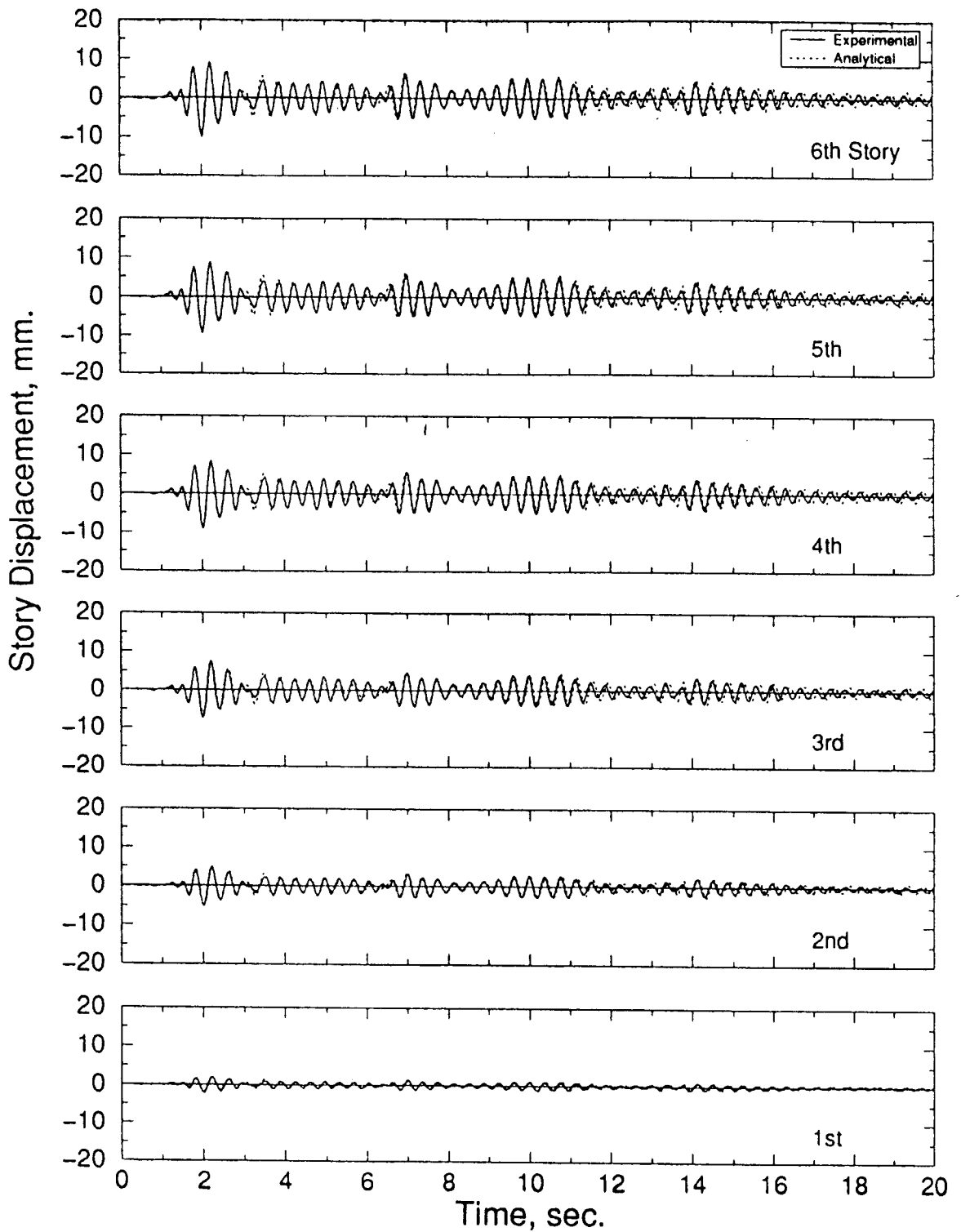


Figure 5-15 Experimentally observed and analytically predicted displacement time histories: B40EL12
Damping System: none
Bracing: upper three stories braced
Earthquake: El Centro, PGA=0.12g

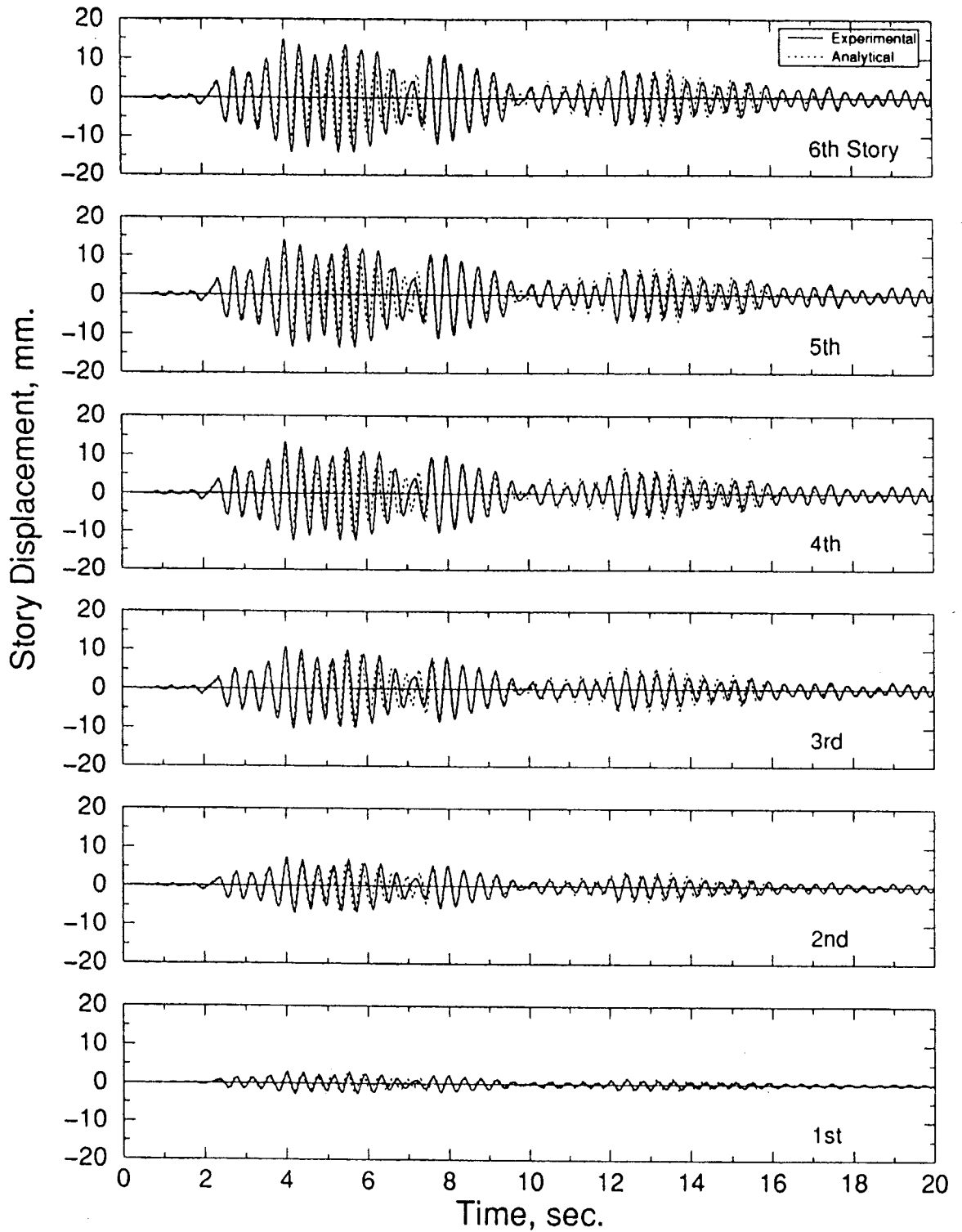


Figure 5-16 Experimentally observed and analytically predicted displacement time histories: B40TA12
Damping System: none
Bracing: upper three stories braced
Earthquake: Taft, PGA=0.12g

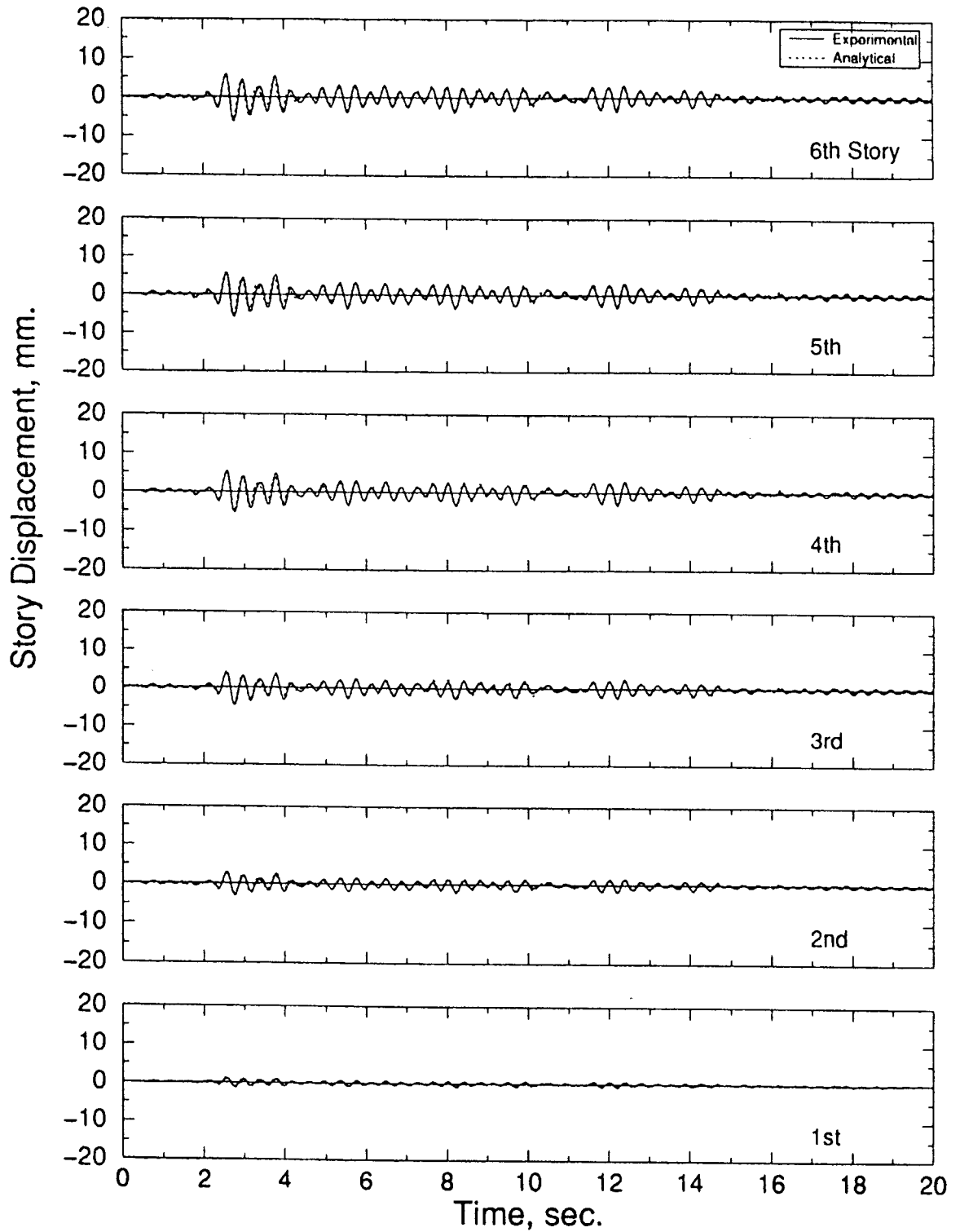
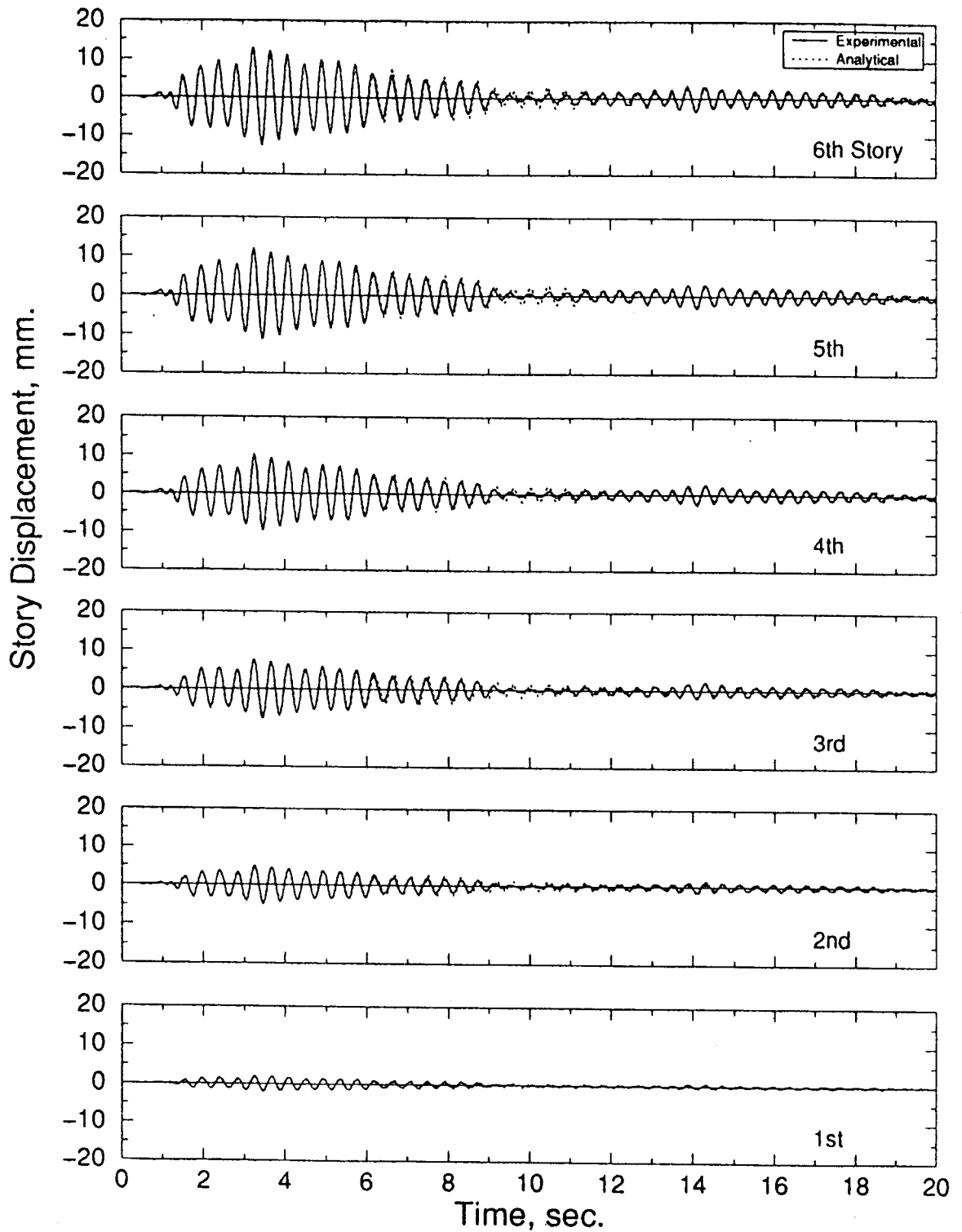


Figure 5-17 Experimentally observed and analytically predicted displacement time histories: B40HA08

Damping System: none

Bracing: upper three stories braced

Earthquake: Hachinohe, PGA=0.08g



**Figure 5-18 Experimentally observed and analytically predicted displacement time histories: MOMEL08
Damping System: none
Bracing: none
Earthquake: El Centro, PGA=0.08g**

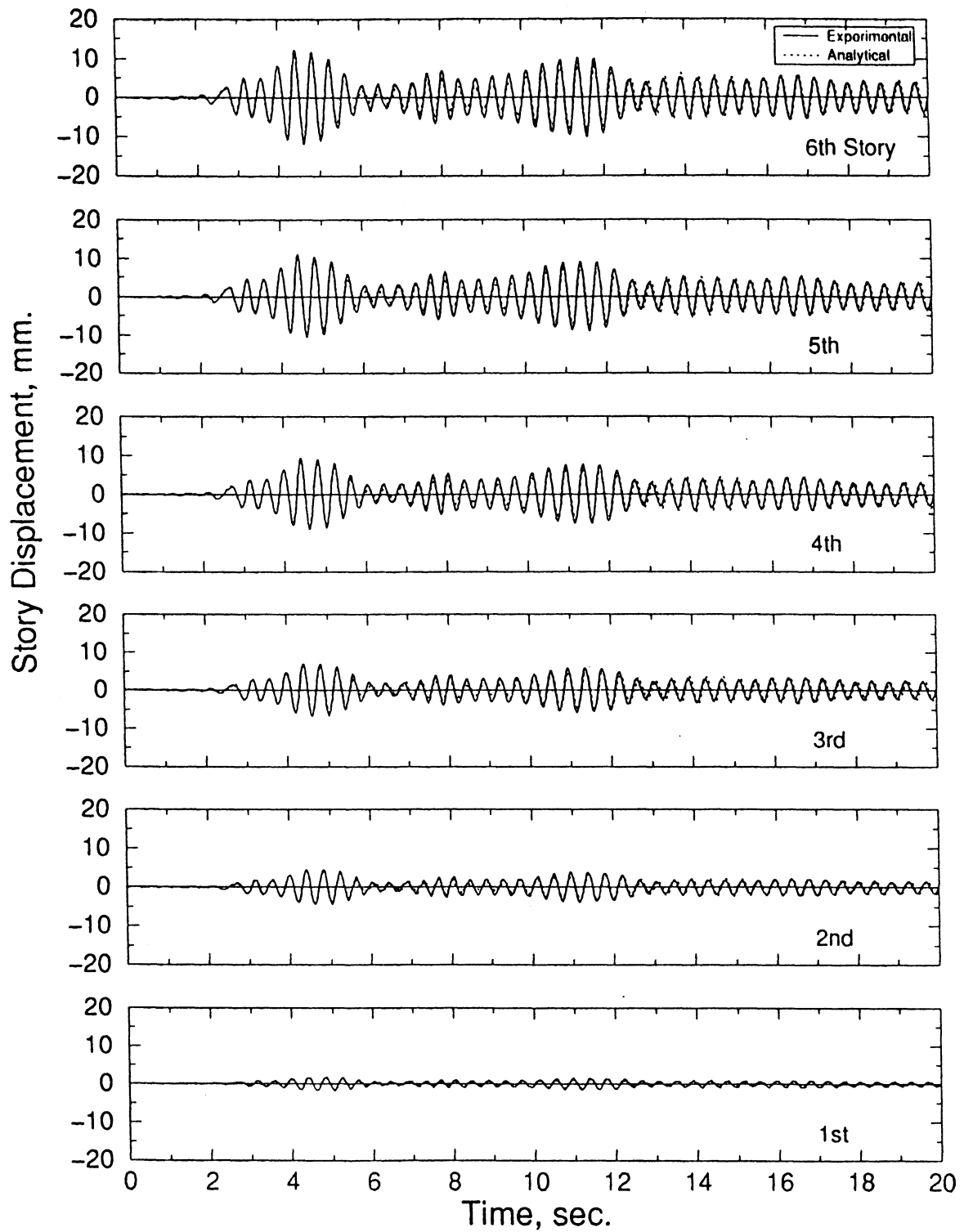


**Figure 5-19 Experimentally observed and analytically predicted displacement time histories: MOMTA08
Damping System: none
Bracing: none
Earthquake: Taft, PGA=0.08g**

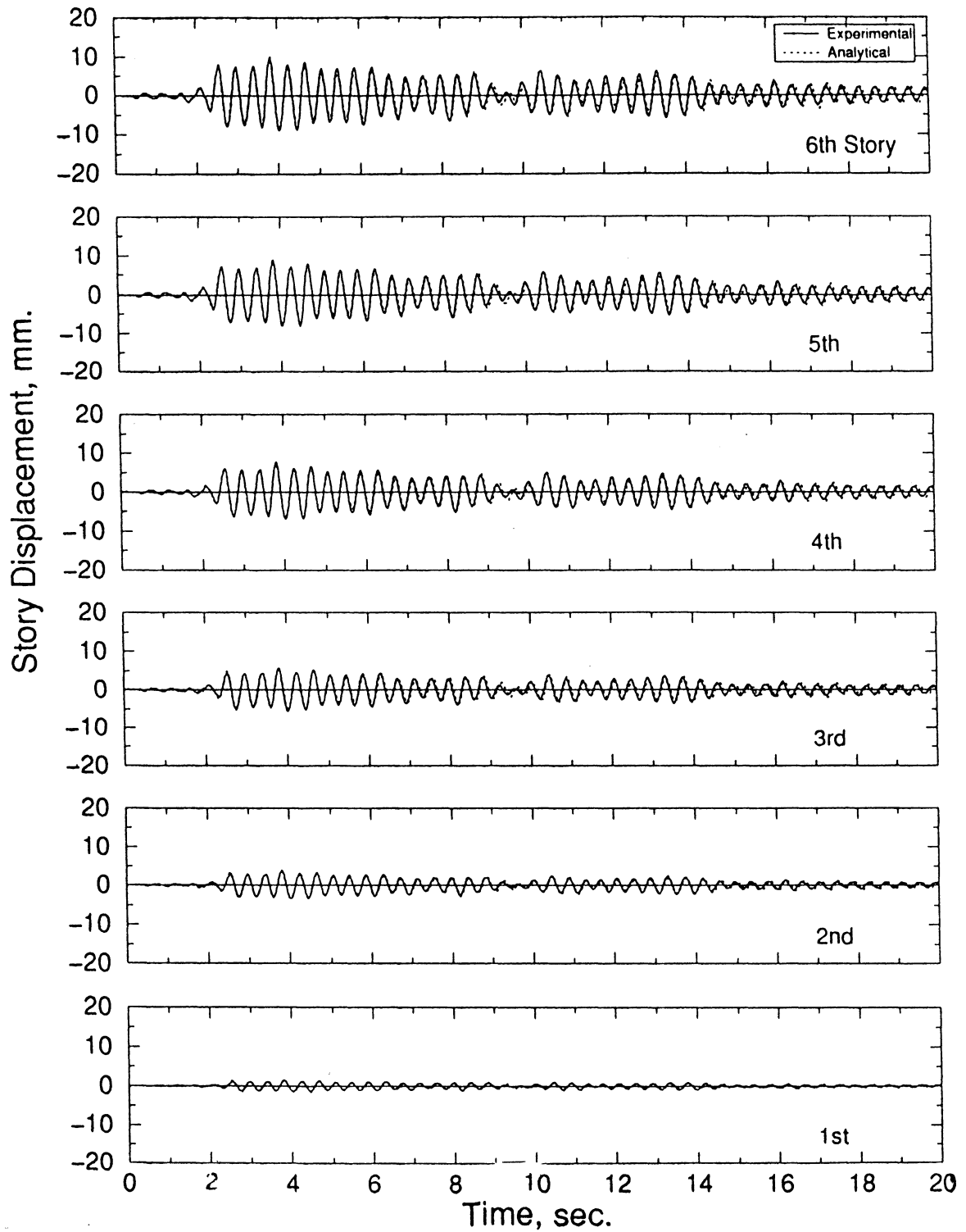


**Figure 5-20 Experimentally observed and analytically predicted displacement time histories: MOMHA08
Damping System: none
Bracing: none
Earthquake: Hachinohe, PGA=0.08g**

— Uniform brace (B10) Top and lower three stories braced (B20)
 - - - Lower three braced (B30) - - - Top three braced (B40) - - - Moment Frame (MOM)

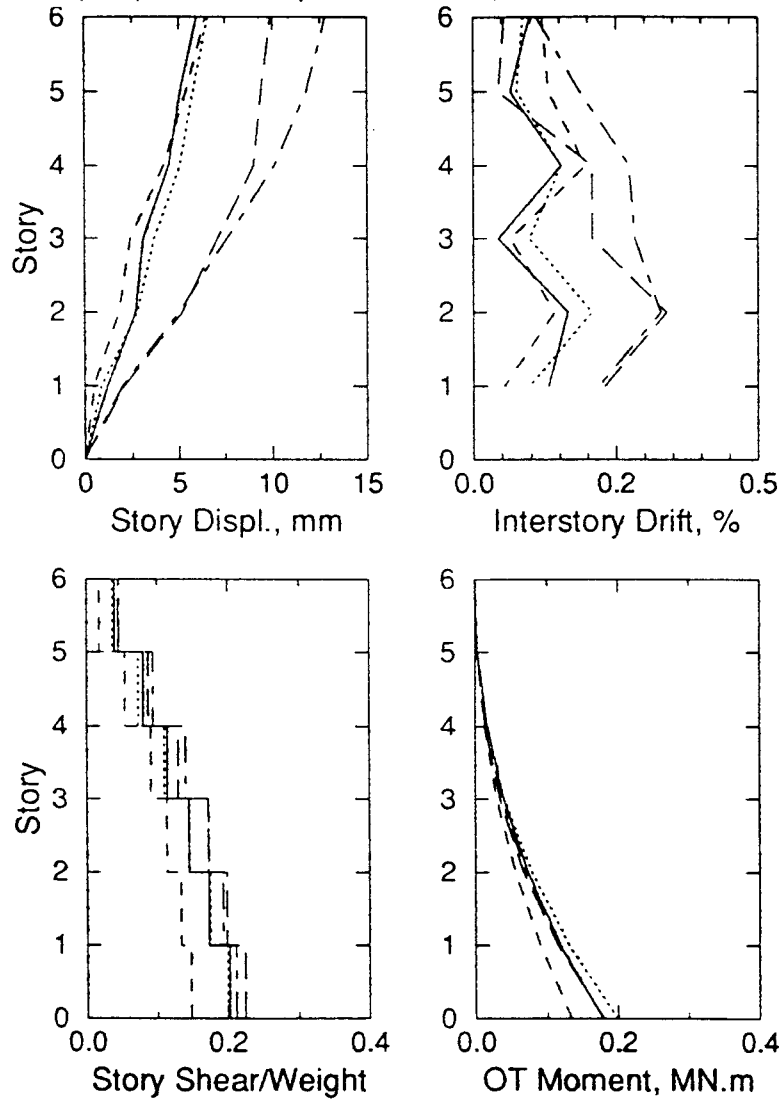


Figure 5-21 Maximum response envelopes for the braced and moment frame configurations subjected to El Centro ground motion at various PGA levels

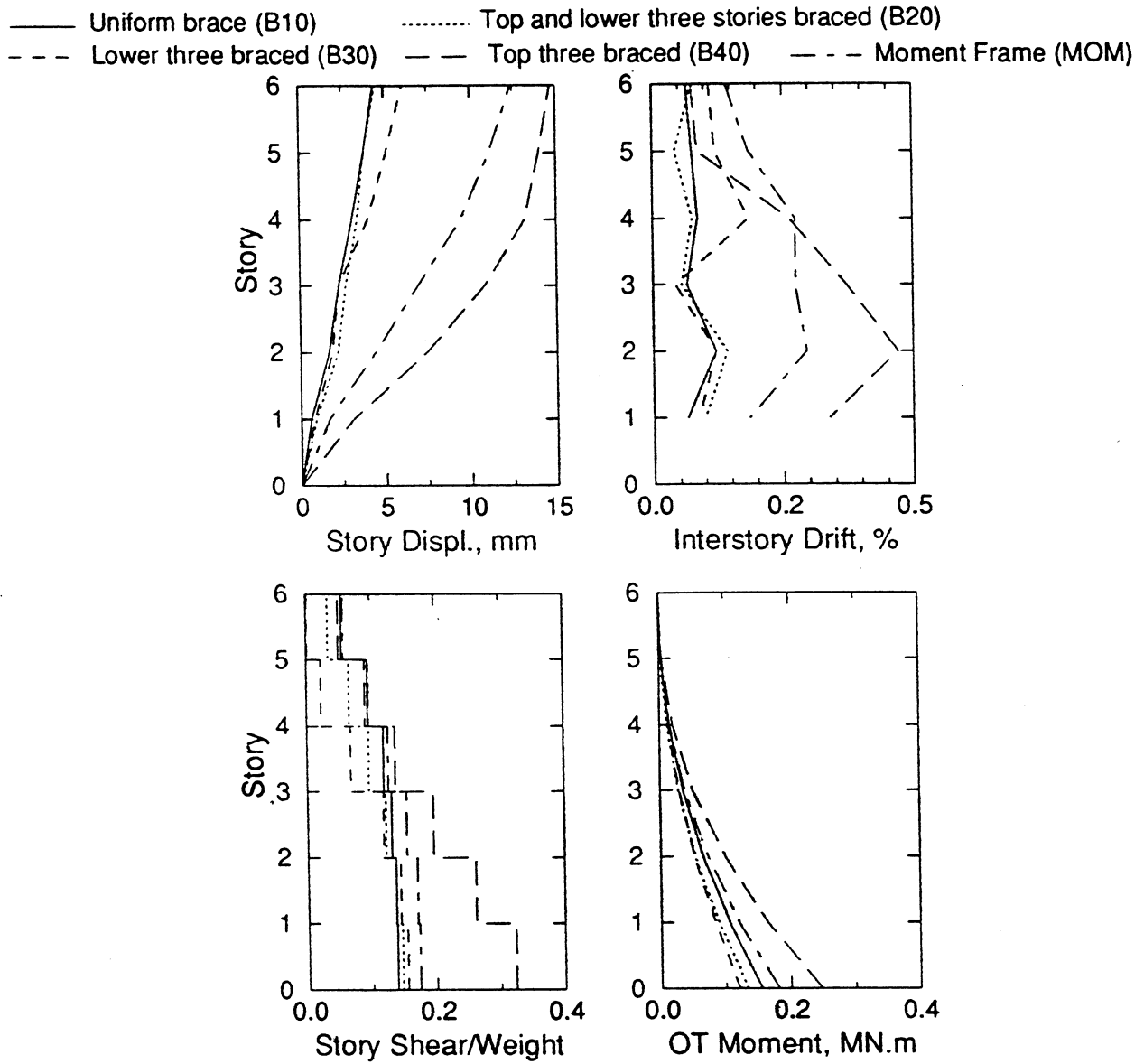


Figure 5-22 Maximum response envelopes for the braced and moment frame configurations subjected to Taft ground motion at various PGA levels

— Uniform brace (B10) Top and lower three stories braced (B20)
 - - - Lower three braced (B30) - - - Top three braced (B40) - - - Moment Frame (MOM)

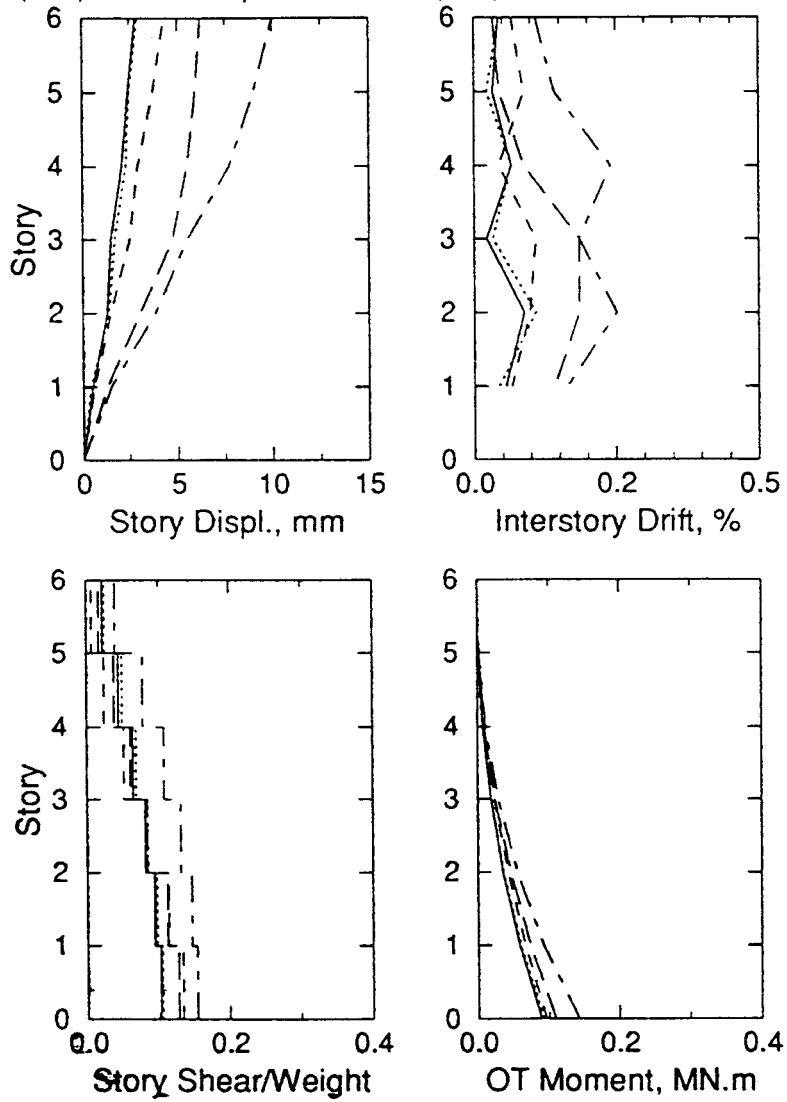


Figure 5-23 Maximum response envelopes for the braced and moment frame configurations subjected to Hachinohe ground motion at various PGA levels

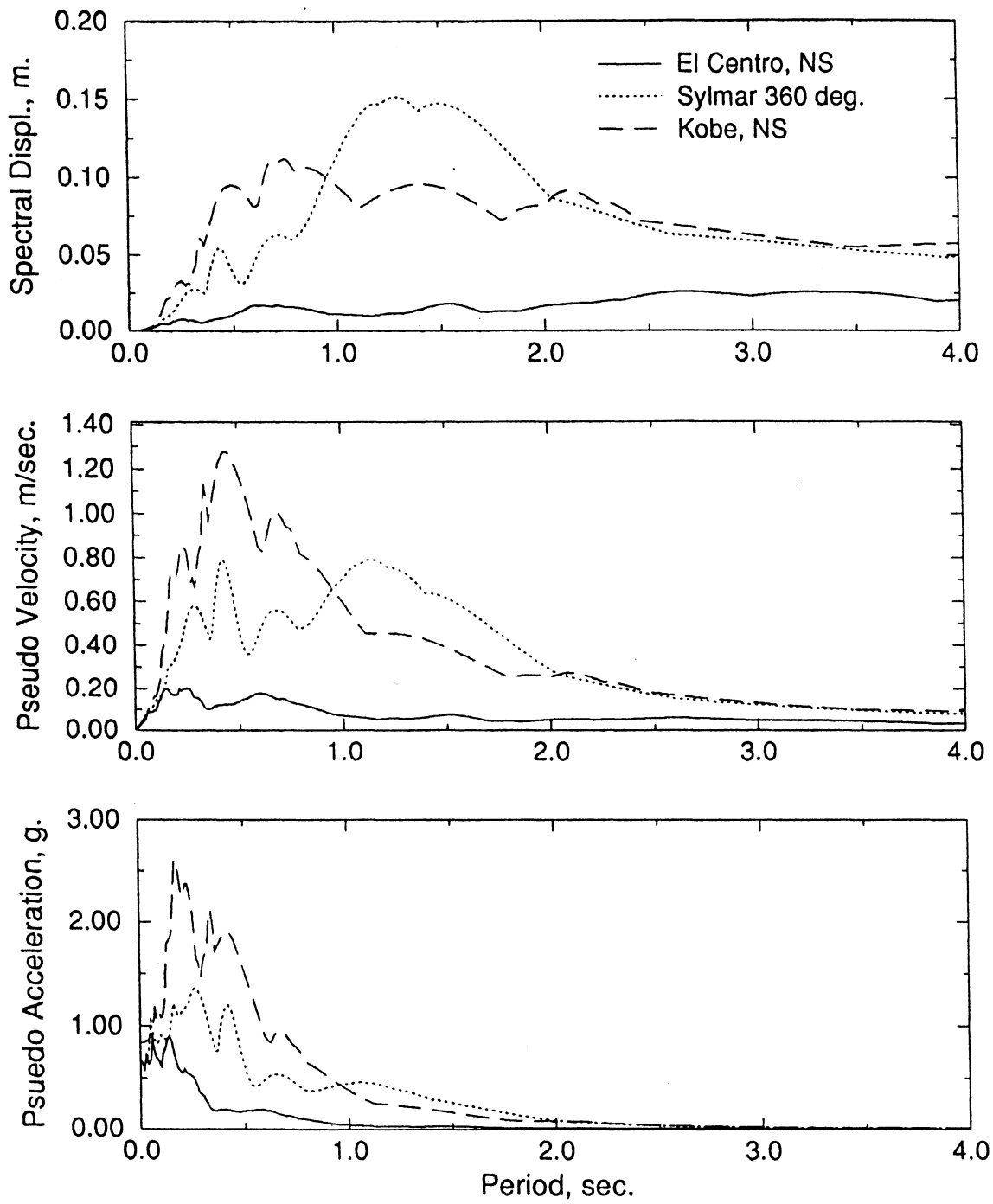


Figure 5-24 Five percent displacement, velocity and acceleration spectra for time-scaled El Centro, Kobe and Sylmar ground motions

Despite the differences, recorded responses for various configurations are still comparable.

A summary of the experimental results is given in table 5-3 which includes the peak table accelerations and the maximum response of the structure in terms of base shear per total weight (162.9 kN), overturning moment at the base (OTM), roof displacement and interstory drift (ISD, Story height = 914 mm). Experimental and analytical story displacement time histories are plotted on figures 5-9 through 5-20. Excellent agreement between the experimental and analytical results can be observed. A comparison of the maximum response profiles for the three ground motions is plotted on figure 5-21 through 5-23.

5.4.3 Tests on the Structure with ESDs and Fuse-Bars

Three ground motions namely, 1940 Imperial Valley- El Centro NS, 1994 Northridge – Sylmar County Hospital 360 deg., and 1995 Great Hanshin – Kobe were used at varying PGA levels from 0.19g to 0.51g in the rest of the experimental program. The latter two records were chosen since they had high early ground velocity /displacement pulses that in turn cause early peak response of flexible structures. Five percent elastic response spectra for the above-mentioned time scaled ground motions are plotted on figure 5-24. The model structure had natural periods of vibration ranging from 0.25 to 0.40 sec., placing it on the response spectra within a critical period range from impulse response point of view. Two previously tested configurations, B40 and B50 (MOM) (figure 4-8), were retrofitted with the tension-only *load balancing* system (figure 4-1). Each configuration was first tested with six dampers only (three on each side of the model structure) in order to investigate the effectiveness of the ESDs in reducing the response of the structure. Two pairs of specially machined fuse-bars (one pair on each side) were then installed in parallel with the ESDs. Experimental results for the two structural configurations are given in the following subsections.

5.4.3.1 Top Three Stories Braced (B4# Configurations)

A set of ground motion experiments was performed on the test structure with the top three stories braced together with the *load balancing tendon-fuse+damper* system. The tendons were connected to connection plates at the third floor level. This anchoring location was chosen since this linear tendon layout was considered an adequate approximation to the optimum (draped) shape for the test structure. Mode shapes and natural periods of vibrations for each

**Table 5-4 Comparison of 1st Mode Natural Periods and Viscous Damping Ratios
Top 3 stories braced – Tendon system active**

Configuration	Natural Period, sec.		Damping Ratio, %	
	White Noise	Ground Motion	White Noise	Ground Motion
B41	0.37	0.39	3.6	5.2
B44	0.27	0.33 ~ 0.38	7.1	6.9 ~ 10.1
B47	0.25	0.26 ~ 0.28	6.3	4.4 ~ 5.5

Table 5-5 Summary of Experimental Response–Top 3 stories braced-Tendon system active

Ground Motion	Config.	PGA (g)	Pre-stress (kN) ¹	Base Shear/Weight (kN)		OTM (kN.m)	Displacement (mm)		Max (ISD) ² (%)
				Total	Col.		6 th fl.	3 rd fl.	
El Centro	B41	0.110	-	0.178	0.178	163	9.6	7.2	0.299 (2)
	B44	0.306	11.4/12.1	0.401	0.183	421	19.0	11.6	0.481 (2)
	B47	0.418	58.4/53.1	0.554	0.059	615	20.3	9.0	0.623 (4)
Sylmar	B41	0.175	-	0.207	0.207	203	11.7	8.9	0.368 (2)
	B44	0.350	11.3/12.0	0.308	0.189	389	16.3	10.1	0.394 (2)
	B47	0.505	59.2/56.3	0.430	0.021	570	18.2	7.2	0.481 (4)
Kobe	B41	0.168	-	0.316	0.316	266	19.1	13.1	0.540 (2)
	B44	0.265	11.1/11.9	0.404	0.284	384	21.9	13.0	0.678 (4)
	B47	0.431	59.6/56.6	0.506	0.146	560	18.2	6.9	0.558 (4)

¹ Average load cell reading. East/West

² Story at which the maximum response was recorded

configuration were identified using both white noise and simulated ground motion tests. Table 5-4 summarizes the first mode periods of vibrations and viscous damping ratios obtained from the frequency domain analysis for the three different configurations tested namely, dampers/fuse-bars not active (B41), dampers active only (B44), and dampers and fuse-bars active (B47). Maximum response of the structure is summarized in table 5-5 in terms of the base shear coefficient, overturning moment at the base (OTM), roof and 3rd floor displacement, and interstory drift (ISD). After the installation of the *load balancing* tendon system, shaking table tests were conducted at PGA levels of 0.1g to 0.2g before the dampers were activated (B41). This configuration had first mode natural periods of 0.37 sec and 0.39 sec obtained from the white noise test and ground motion test, respectively. Corresponding viscous damping ratios were 3.6% and 5.2%.

It was observed that when compared to the experiments conducted on the B40 configuration, the peak response did not change; only a marginal increase in the viscous damping of the structure was observed. This is attributed to the friction induced at the pull-beam/tendon connection. Some selected displacement time history plots are shown in figures 5-25 through 5-29 for B41 configuration. Note that in general, very good agreement is evident between the experiment and analytical predictions.

Similar experiments were then conducted at similar input levels after the dampers were activated (B42). The *load balancing tendon-fuse+damper* system was not prestressed, mainly due to the existence of certain amount of slack in the system at the connections etc., dampers were engaged only when the relative displacements were high enough to remove the slack. Therefore, responses of the two configurations (i.e. B41 and B42) were essentially the same.

After the low-level trial runs, the *load balancing tendon-fuse+damper* tendon system was prestressed to approximately 12 kN in each direction, therefore prestressing each damper to about 20% beyond their initial pre-load (2.8 kN). Prestress was applied by torquing the anchorage nuts at the pull beam-tendon connection and by observing the change in the individual load cell readings. As can be seen in table 5-4, the first mode natural period of vibration for this configuration was found to be 0.27 sec from the white noise input and 0.33 to 0.38 sec from the ground motion inputs. The difference between those obtained from the ground motion and white noise experiments is again attributed to the slip at the bolted brace connections and the friction

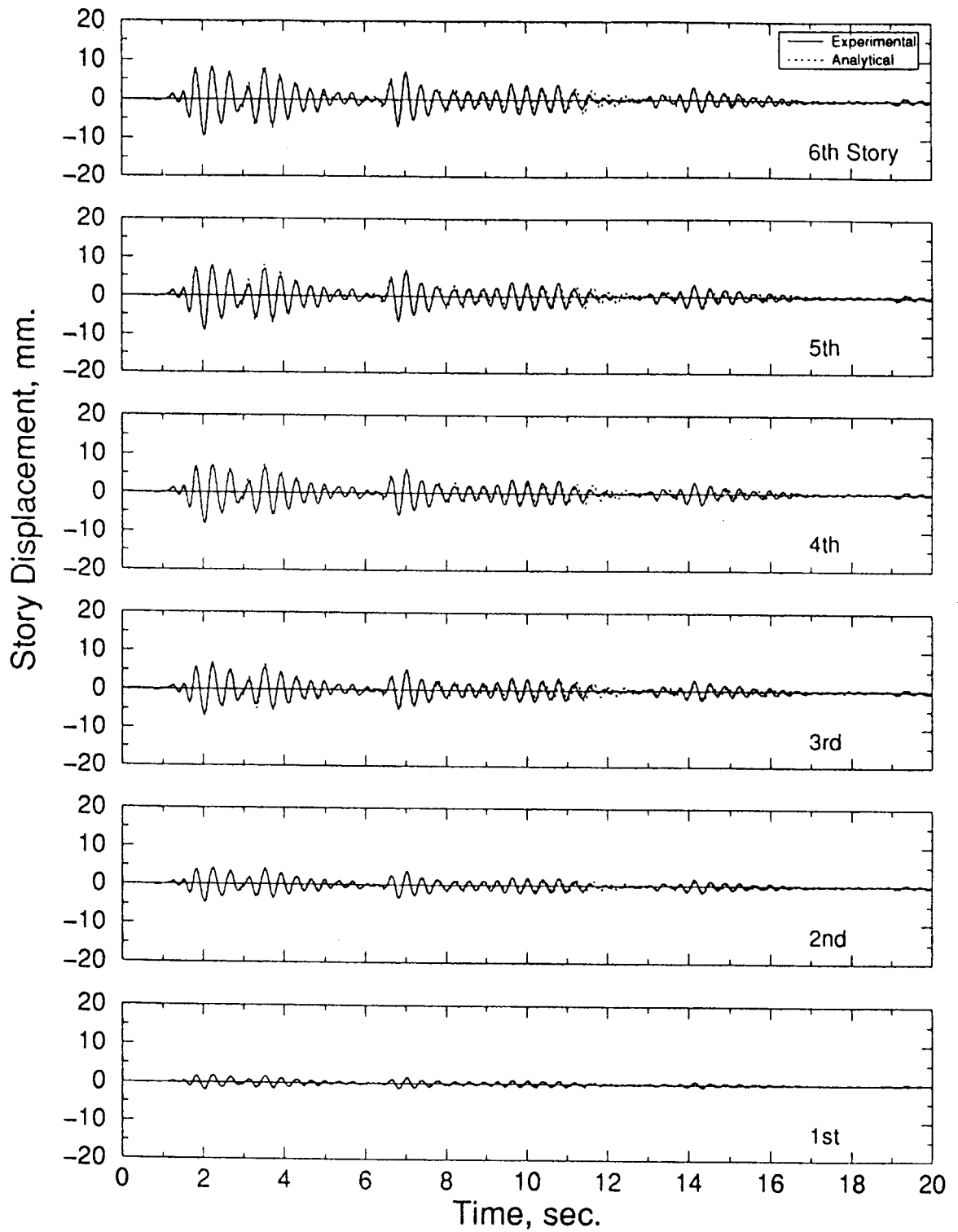


Figure 5-25 Experimentally observed and analytically predicted displacement time histories: B41EL12

Damping System: none (tendons slack)

Bracing: upper three stories braced

Earthquake: El Centro, PGA=0.12g

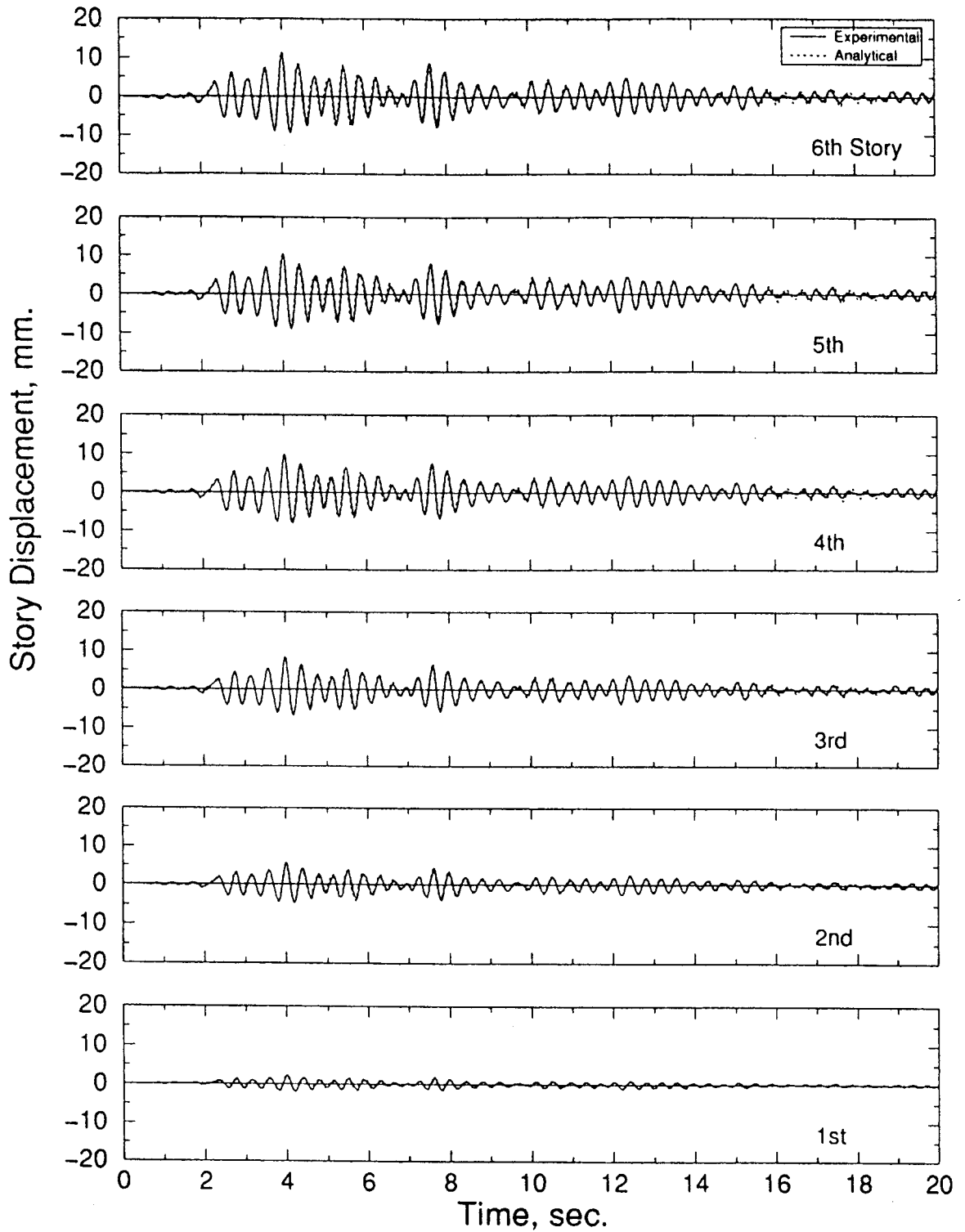


Figure 5-26 Experimentally observed and analytically predicted displacement time histories: B41TA12
Damping System: none (tendons slack)
Bracing: upper three stories braced
Earthquake: Taft, PGA=0.12g

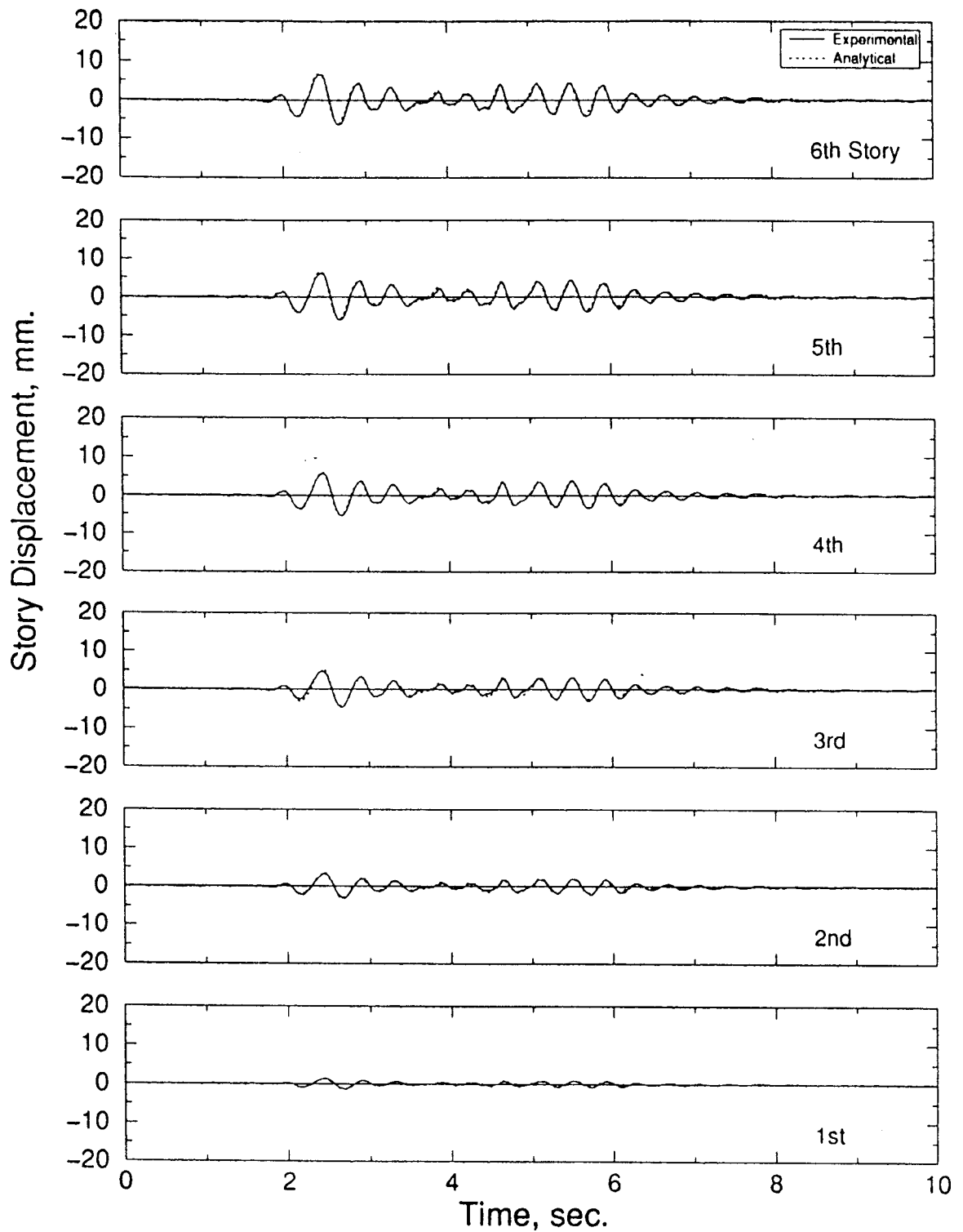


Figure 5-27 Experimentally observed and analytically predicted displacement time histories: B41PA18
Damping System: none (tendons slack)
Bracing: upper three stories braced
Earthquake: Pacoima Dam, PGA=0.18g

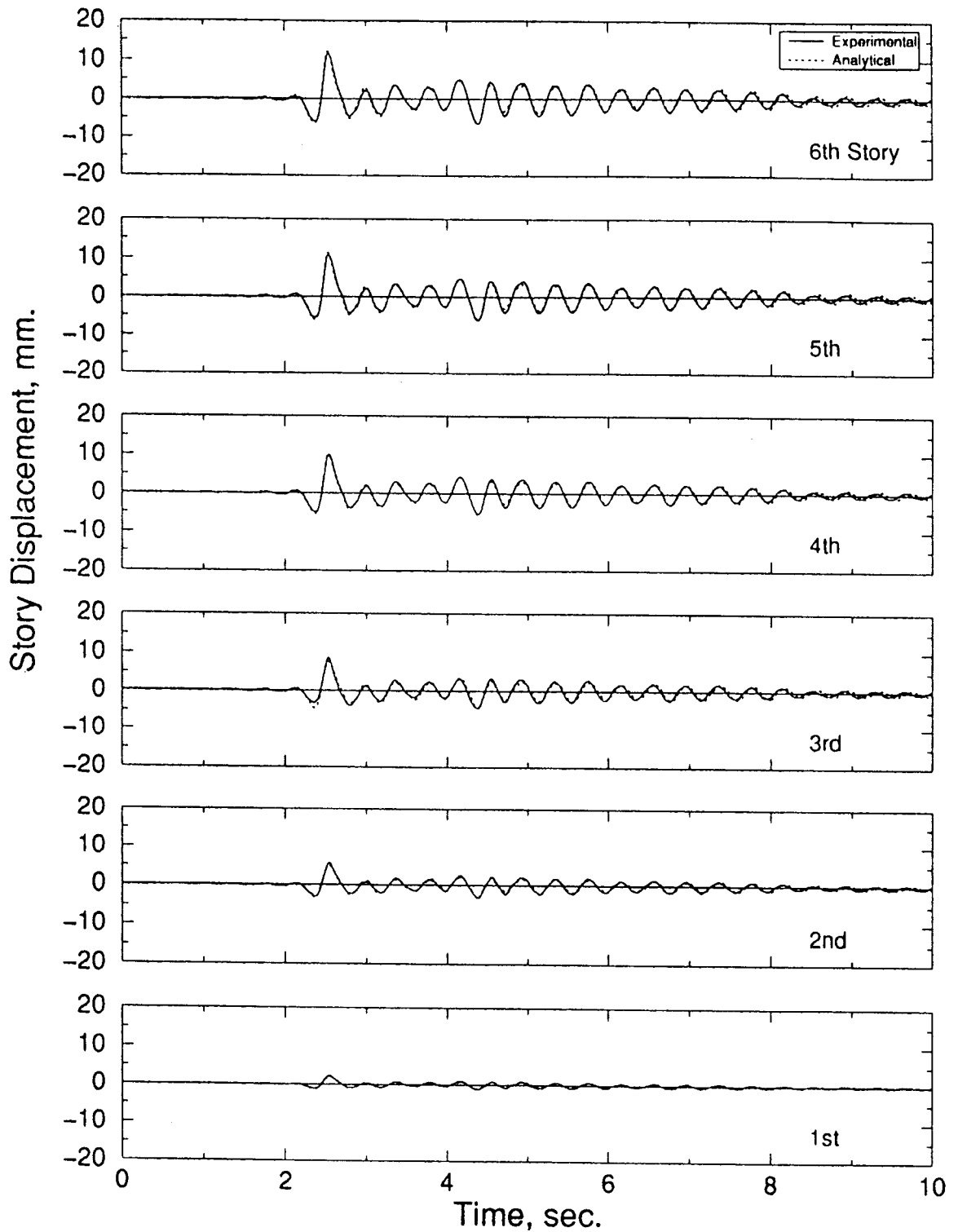


Figure 5-28 Experimentally observed and analytically predicted displacement time histories: B41SY17
Damping System: none (tendons slack)
Bracing: upper three stories braced
Earthquake: Sylmar, PGA=0.17g

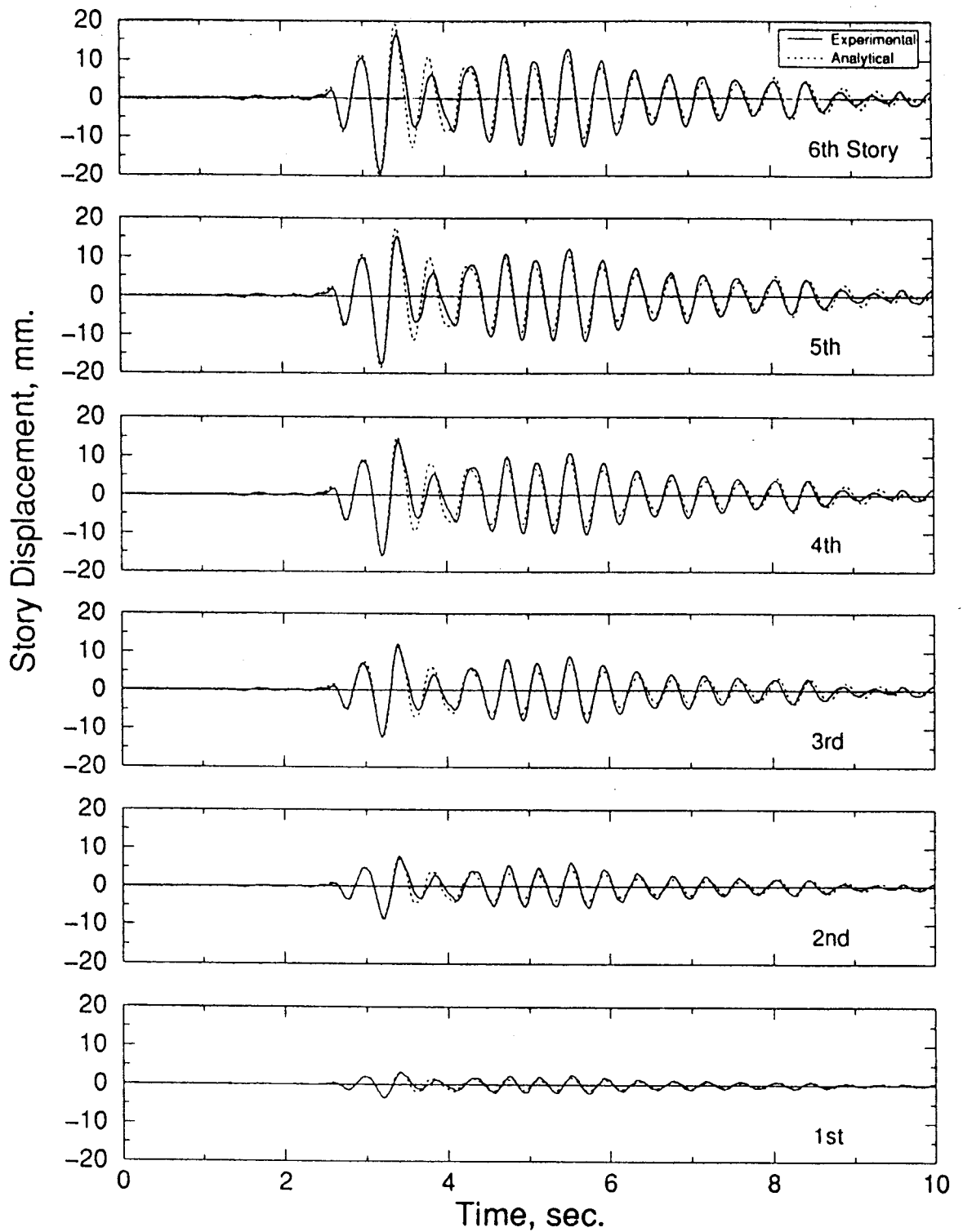


Figure 5-29 Experimentally observed and analytically predicted displacement time histories: B41KO17
Damping System: none (tendons slack)
Bracing: upper three stories braced
Earthquake: Kobe, PGA=0.17g

induced at the tendon connections. Another reason for period lengthening may also be the fact that the tendon system became slack at some instances during the ground motion tests. The viscous damping ratio increased from about 5.0% to 10.0% of critical. High frequency response as well as that of the dominant first mode were damped considerably by the ESD devices under ground motion input. Some selected experimental and analytical story displacement time histories and damper deformation-tendon force relationships are shown in figures 5-30 through 5-45. It was realized that tendon responses on either side of the structure were not symmetric due to unequal initial prestress etc., therefore “average” analytical results are compared with experimental tendon force-deformations as recorded by individual load cells. Good agreement between the experimental and analytical results can be observed.

A comparison of the maximum responses summarized in table 5-5 for B41 and B44 configurations suggests that an increase in peak ground acceleration of approximately two to three times resulted in comparable story displacements at the third and lower stories. Roof displacements did not reduce in comparison with those of third floor mainly due to two reasons: the damper-tendon system was not directly effective in the upper stories (4th, 5th and 6th floor levels), and slip at the bolted brace connections further increased after each test. Overturning moments at the rigid base increased in proportion to the total story shears. Maximum recorded interstory drifts were either reduced or stayed the same considering the level of the PGA that the structure was subjected to in B41 and B44 configurations, respectively.

Fuse bars were installed between the reaction beam (fixed end) and pull-beam as shown in figure 4-1. The *load balancing tendon* system was then further prestressed to a higher level. Approximately 60 kN was applied in each direction, therefore prestressing each damper to about their initial preload (2.8 kN) level while prestressing each fuse-bar to about 60-65% of their yield strength. Prestressing was done in two steps: 1) torque was applied to anchorage nuts at the pull beam-tendon connection until a total of 12 kN tendon force was read in each direction. 2) each fuse-bar was then torqued until a total load cell reading of 60 kN achieved in each direction. The same fuse-bars were used for all three consecutive experiments (B47) as there was minor yielding hence loss of prestress in the system. As can be seen from table 5-4, the first mode natural period of vibration was found to be 0.25 sec. from the white noise input and 0.26 sec. to 0.28 sec. from the ground motion inputs. Slight shortening of calculated natural period renders

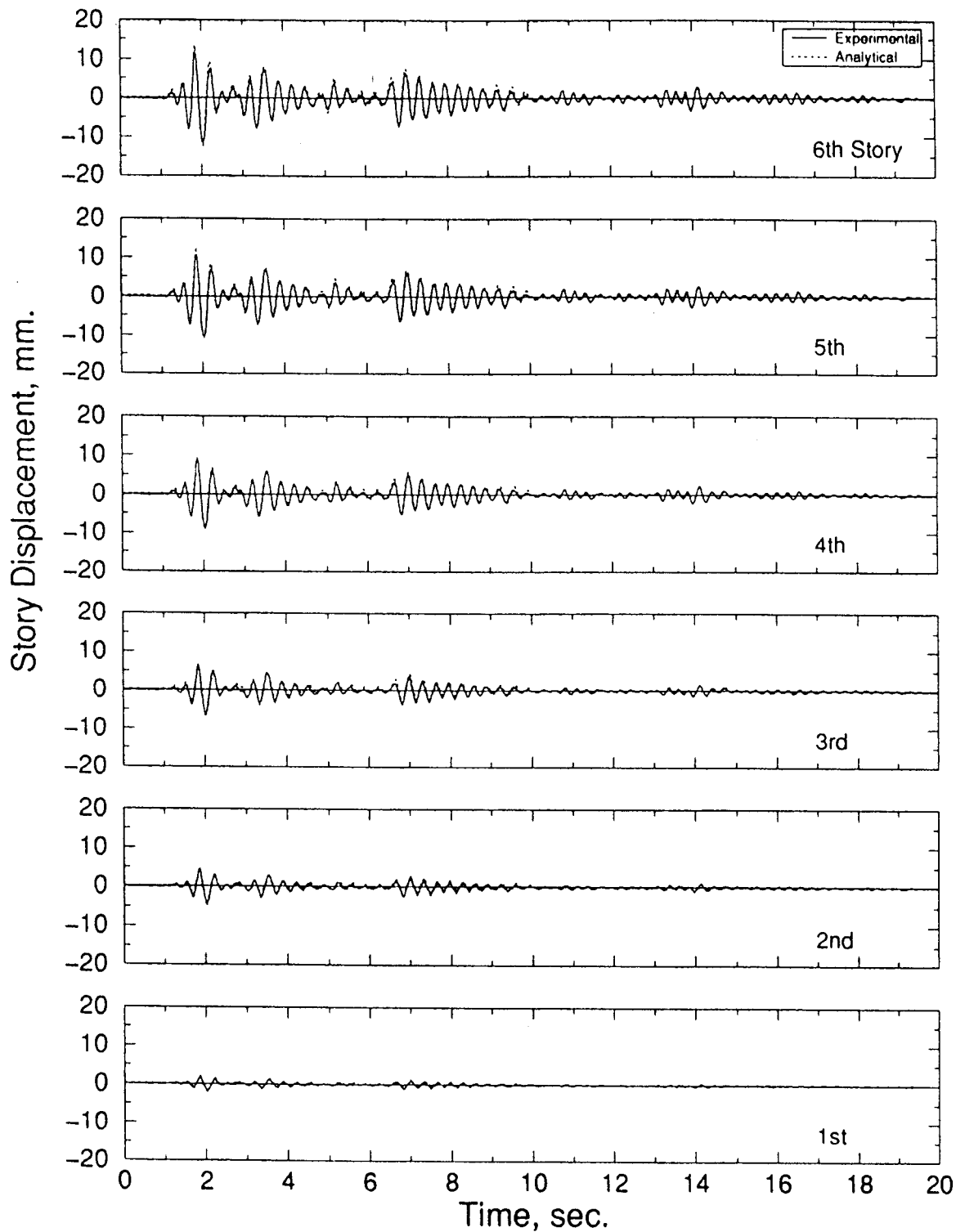


Figure 5-30 Experimentally observed and analytically predicted displacement time histories: B43EL20
Damping System: dampers only
Bracing: upper three stories braced
Earthquake: El Centro, PGA=0.20g

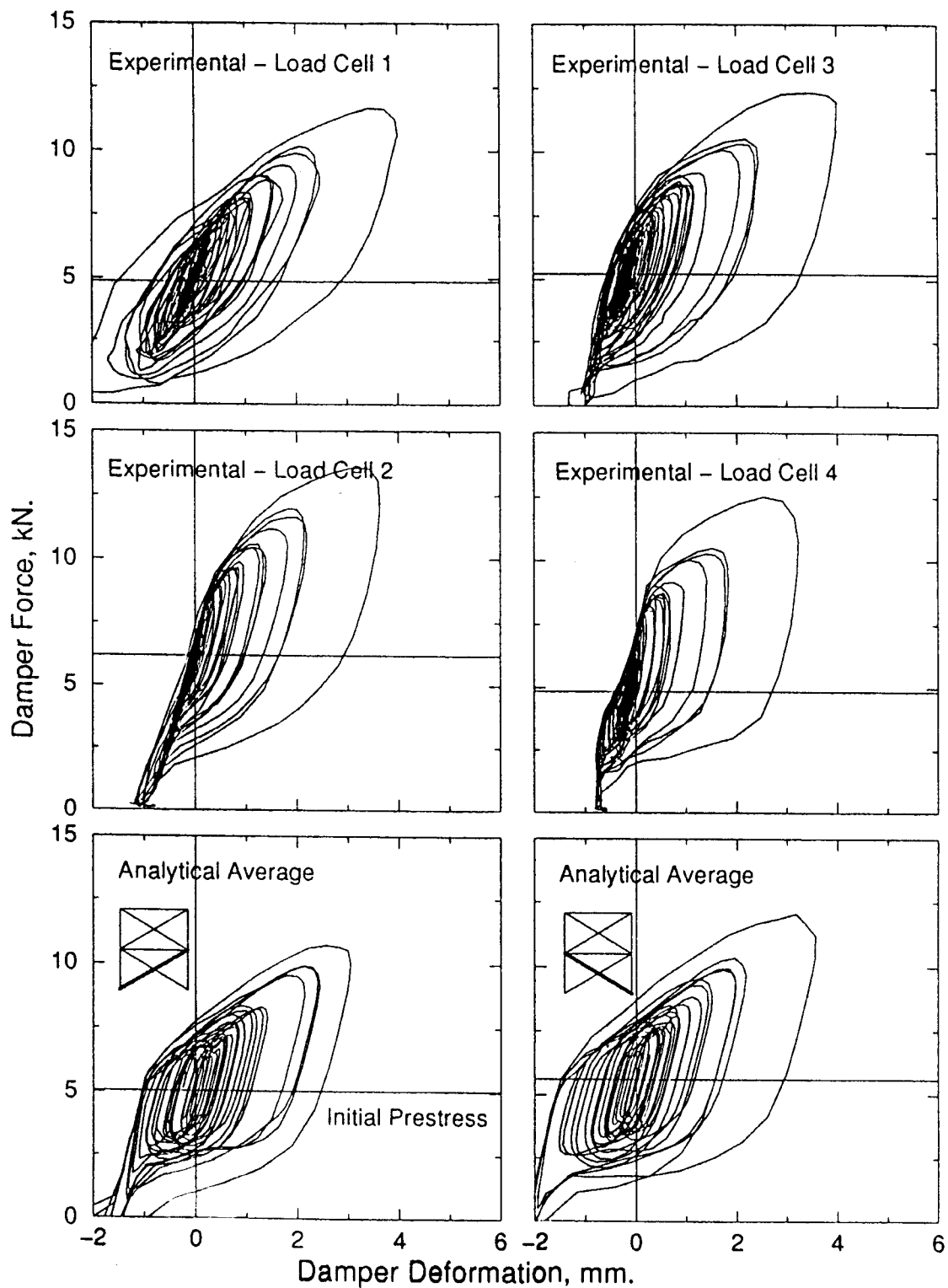


Figure 5-31 Experimentally observed and analytically predicted average tendon force-deformation: B43EL20
Damping System: dampers only
Bracing: upper three stories braced
Earthquake: El Centro, PGA=0.20g

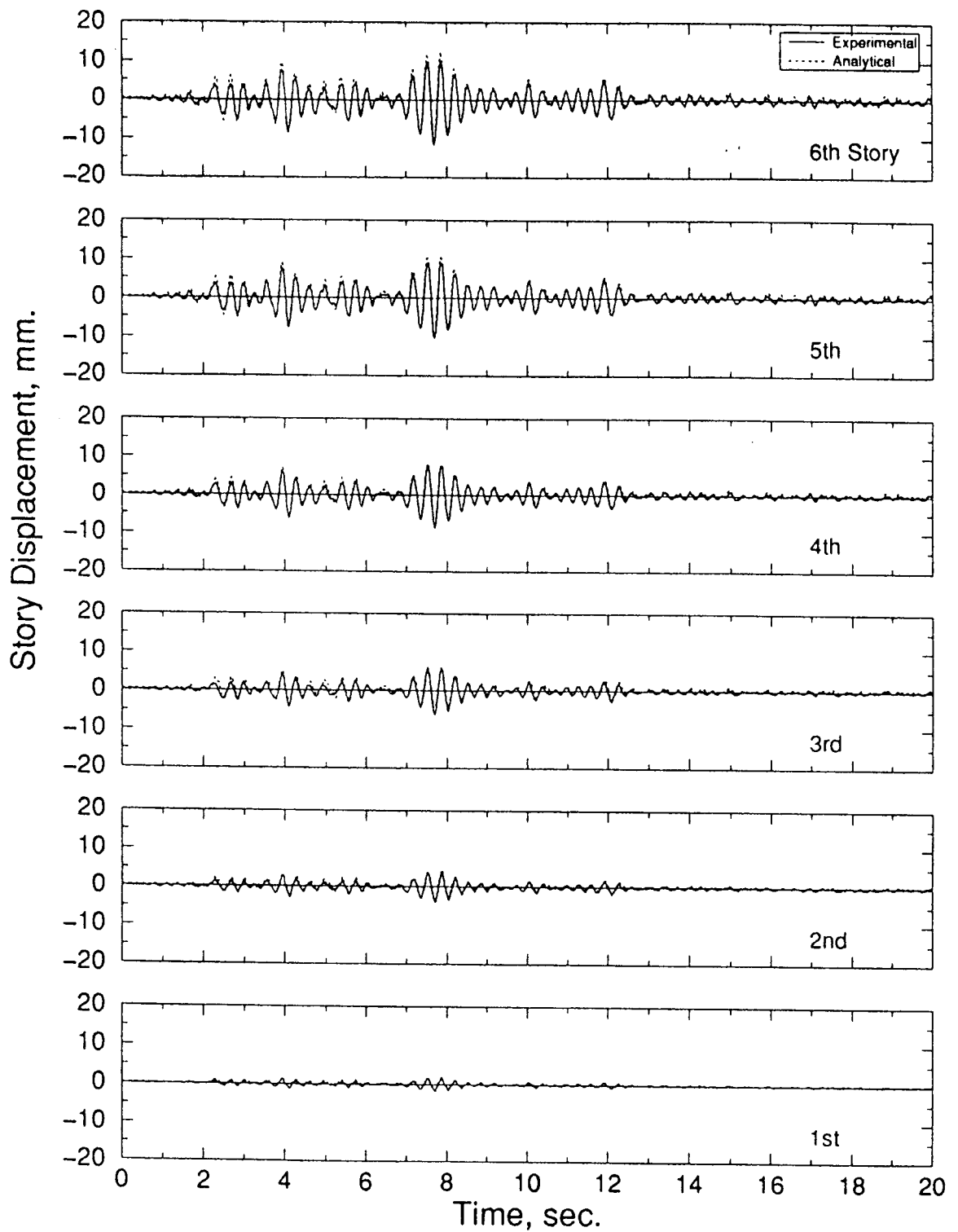


Figure 5-32 Experimentally observed and analytically predicted displacement time histories: B43TA20
Damping System: dampers only
Bracing: upper three stories braced
Earthquake: Taft, PGA=0.20g

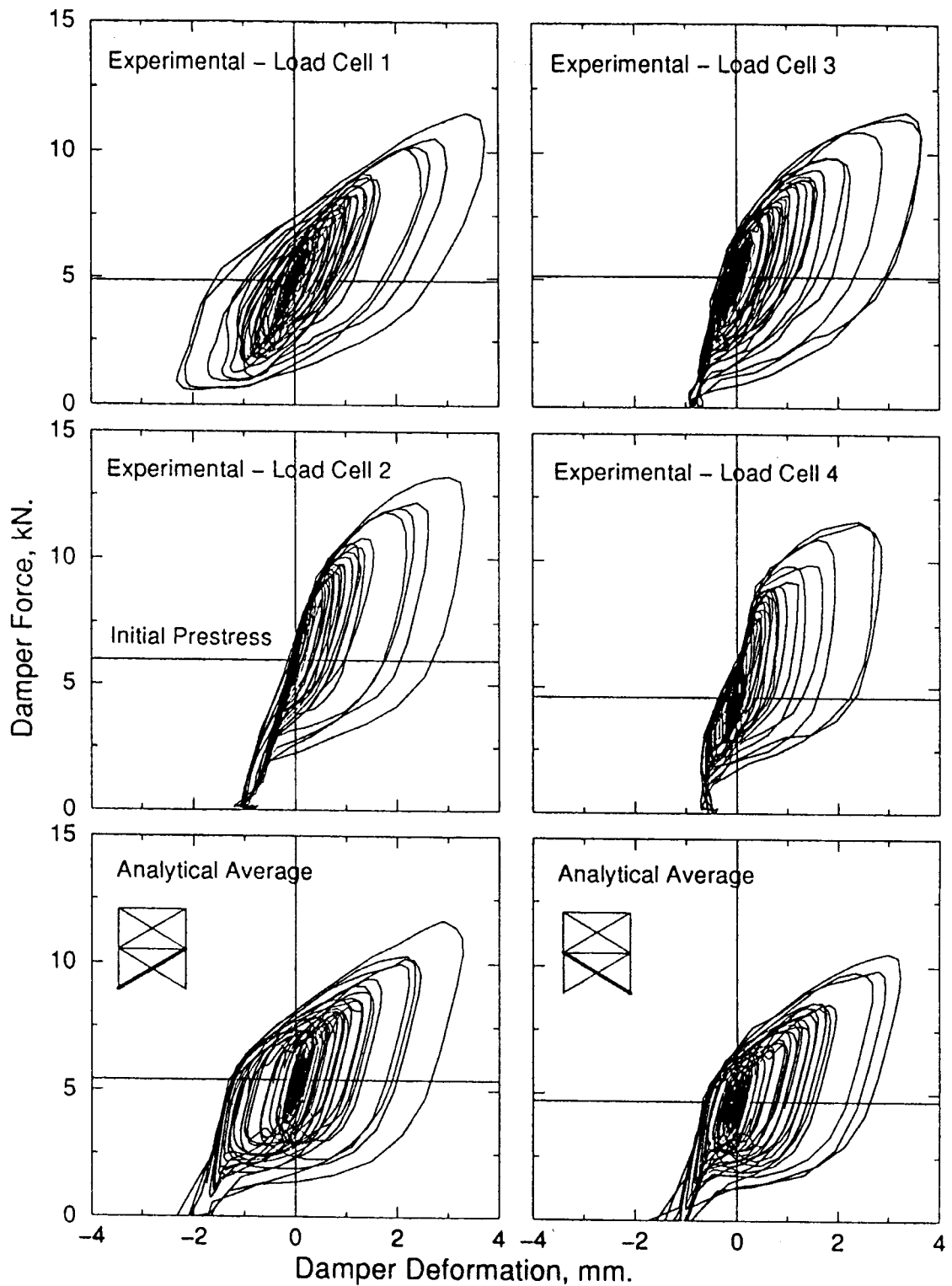


Figure 5-33 Experimentally observed and analytically predicted average tendon force-deformation: B43TA20

Damping System: dampers only
Bracing: upper three stories braced
Earthquake: Taft, PGA=0.20g

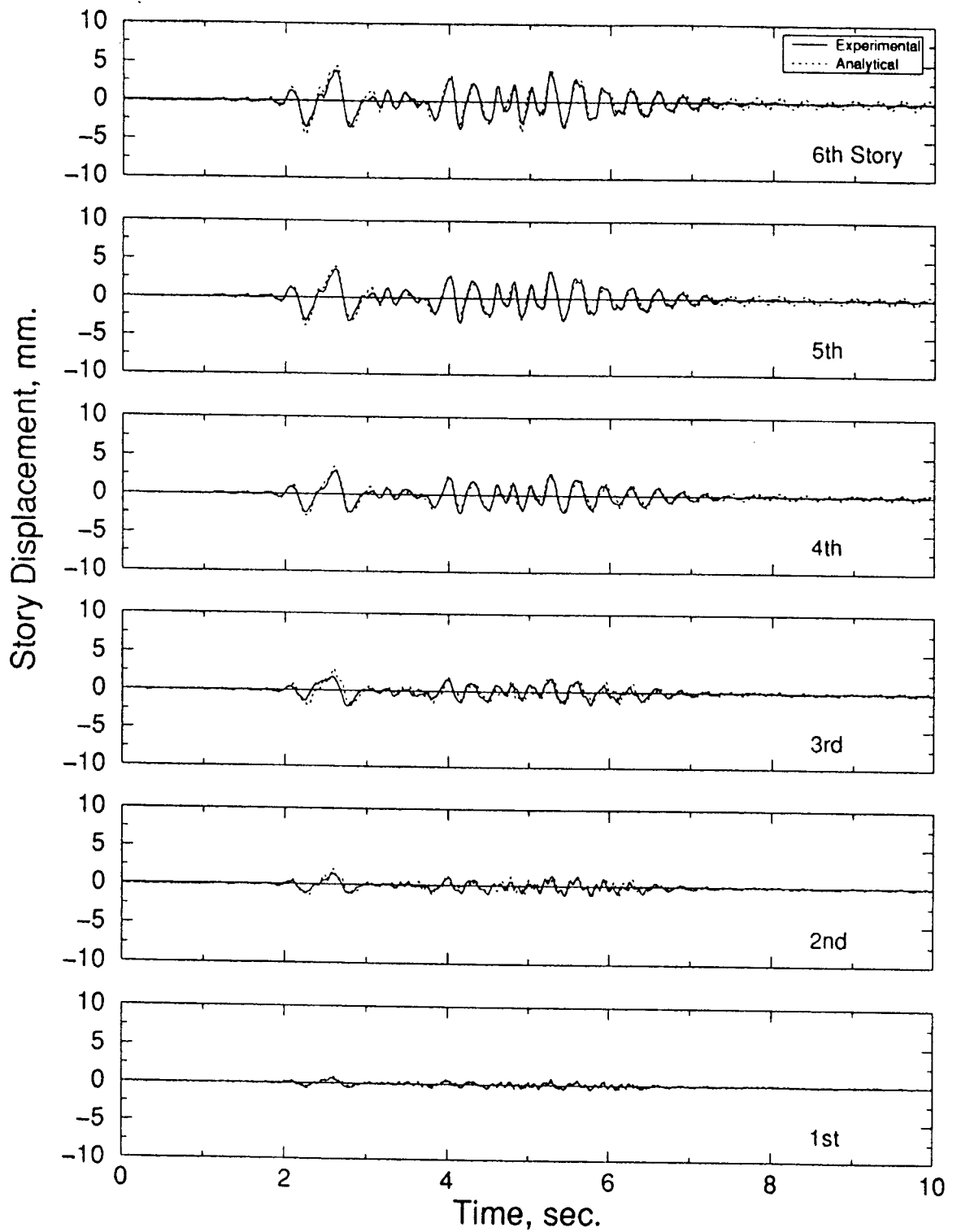


Figure 5-34 Experimentally observed and analytically predicted displacement time histories: B43PA20
Damping System: dampers only
Bracing: upper three stories braced
Earthquake: Pacoima Dam, PGA=0.20g

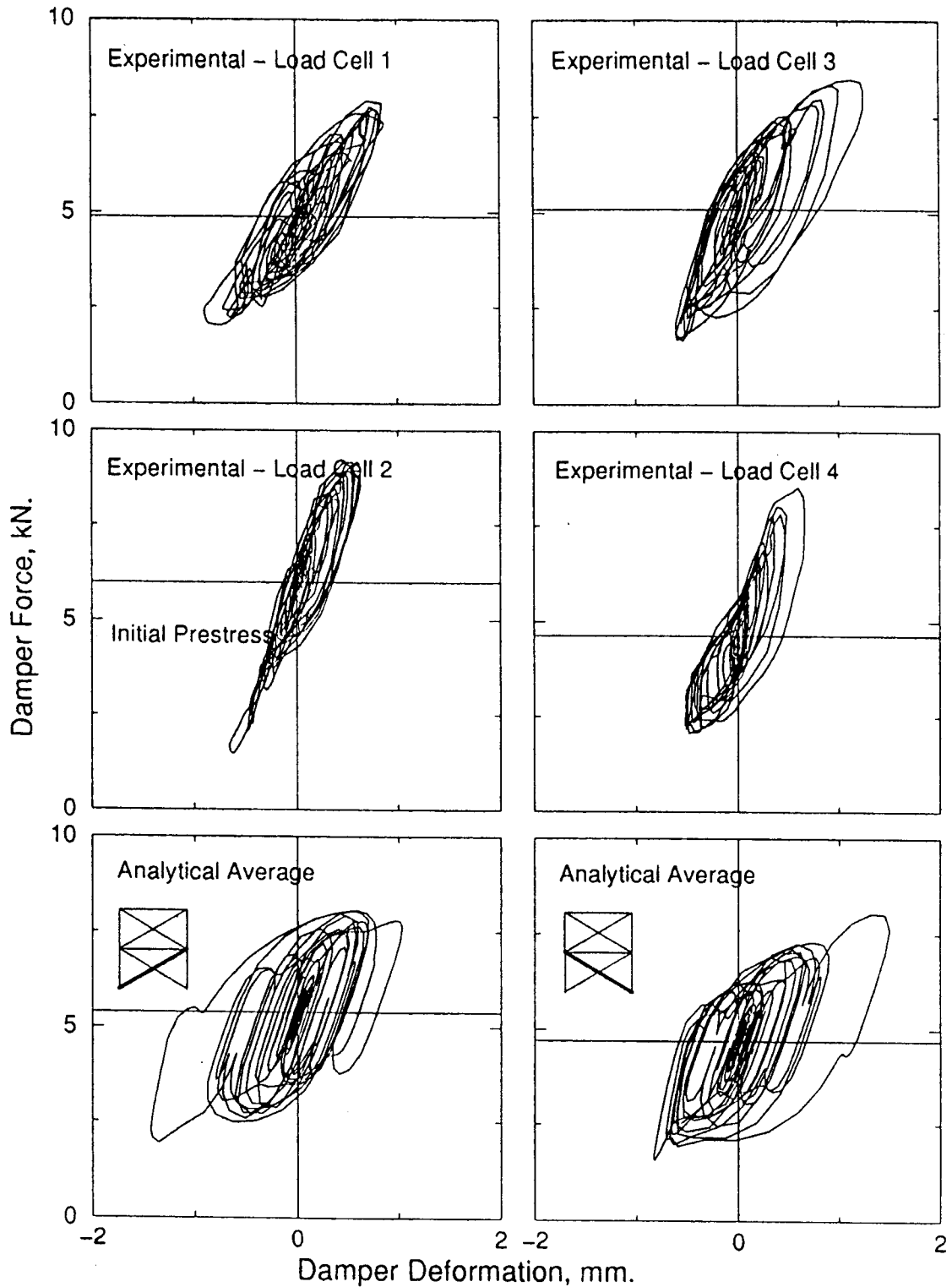


Figure 5-35 Experimentally observed and analytically predicted average tendon force-deformation: B43PA20
Damping System: dampers only
Bracing: upper three stories braced
Earthquake: Pacoima Dam, PGA=0.20g

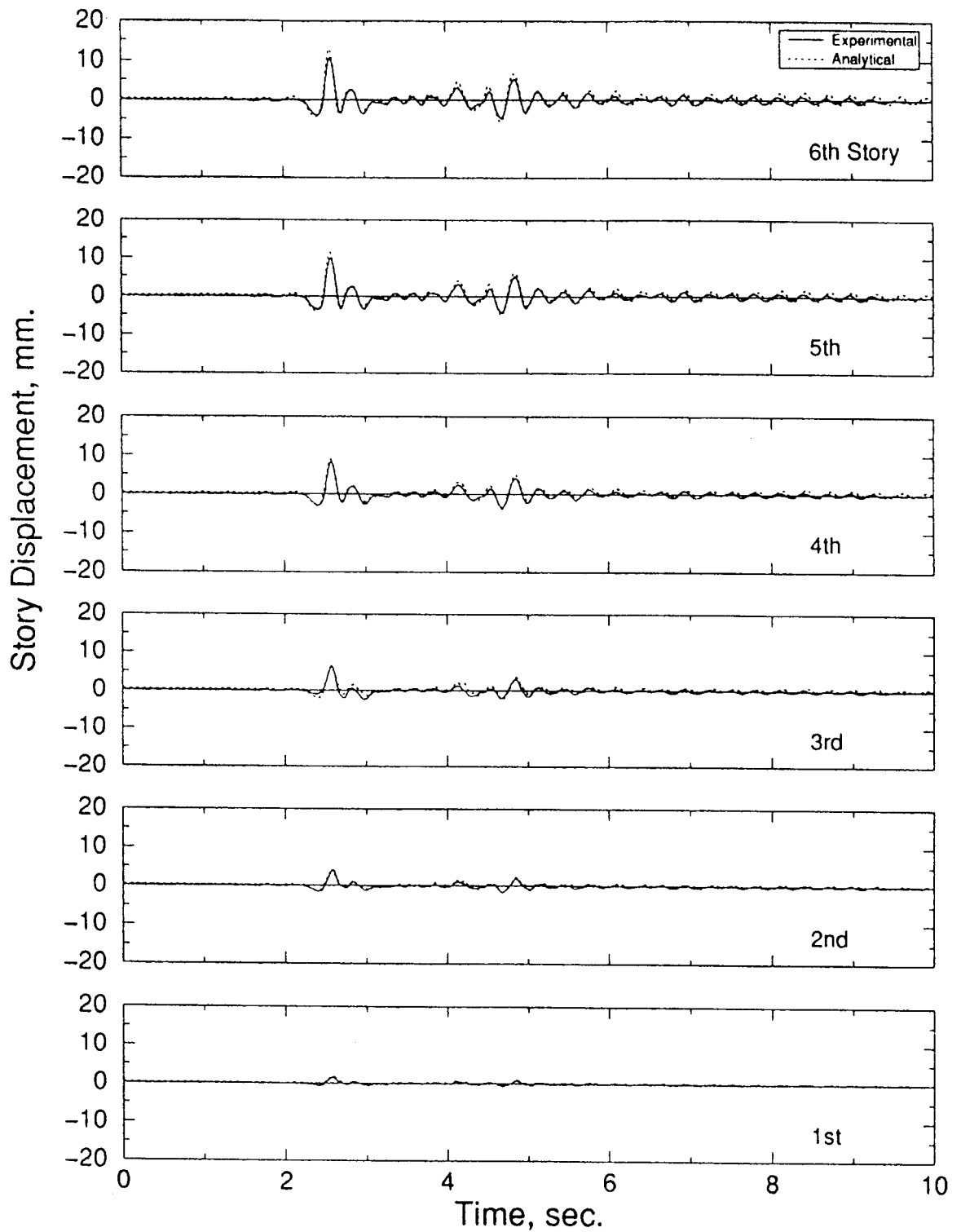


Figure 5-36 Experimentally observed and analytically predicted displacement time histories: B43SY20

Damping System: dampers only

Bracing: upper three stories braced

Earthquake: Sylmar, PGA=0.20g

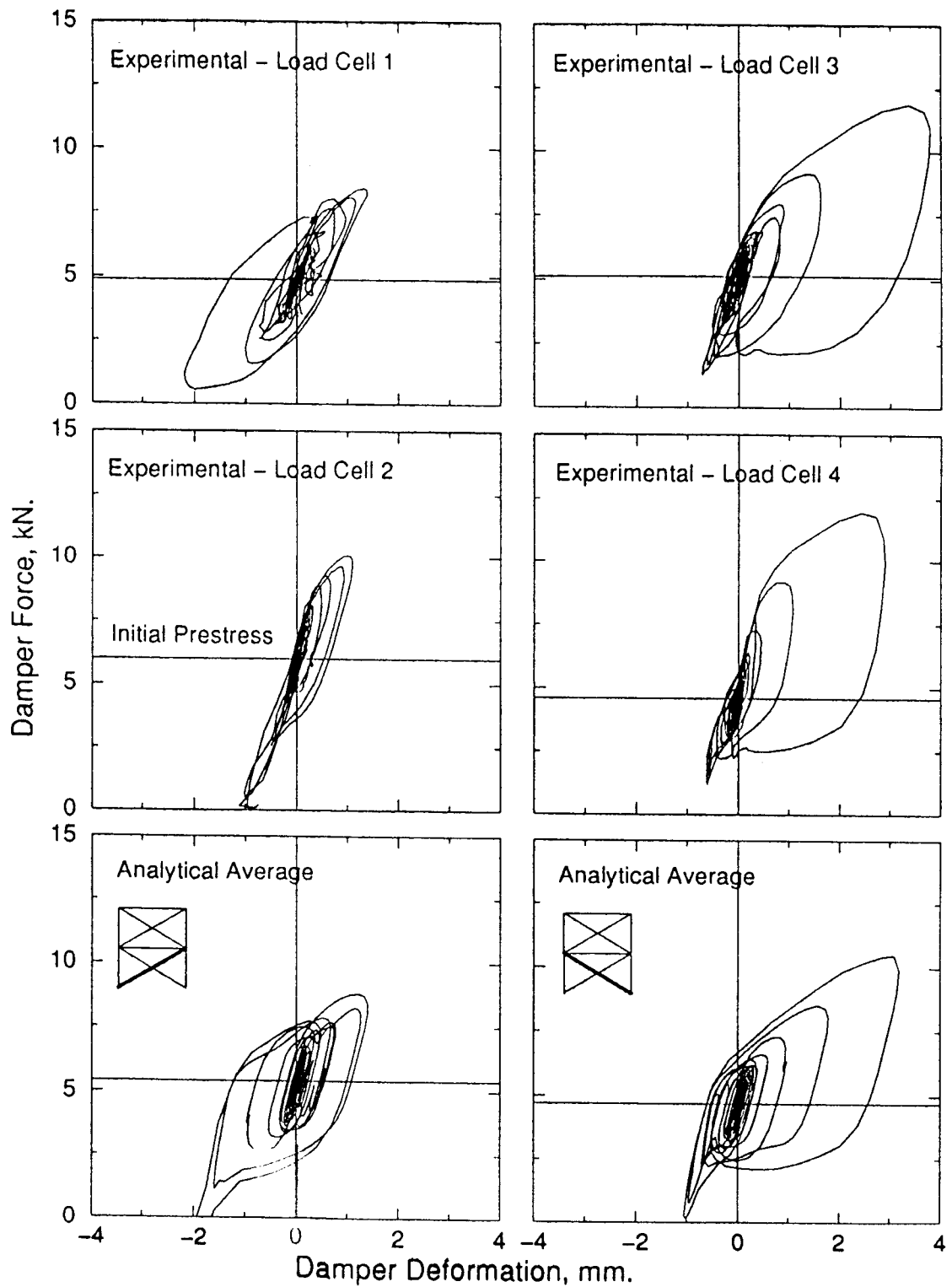


Figure 5-37 Experimentally observed and analytically predicted average tendon force-deformation: B43SY20
Damping System: dampers only
Bracing: upper three stories braced
Earthquake: Sylmar, PGA=0.20g

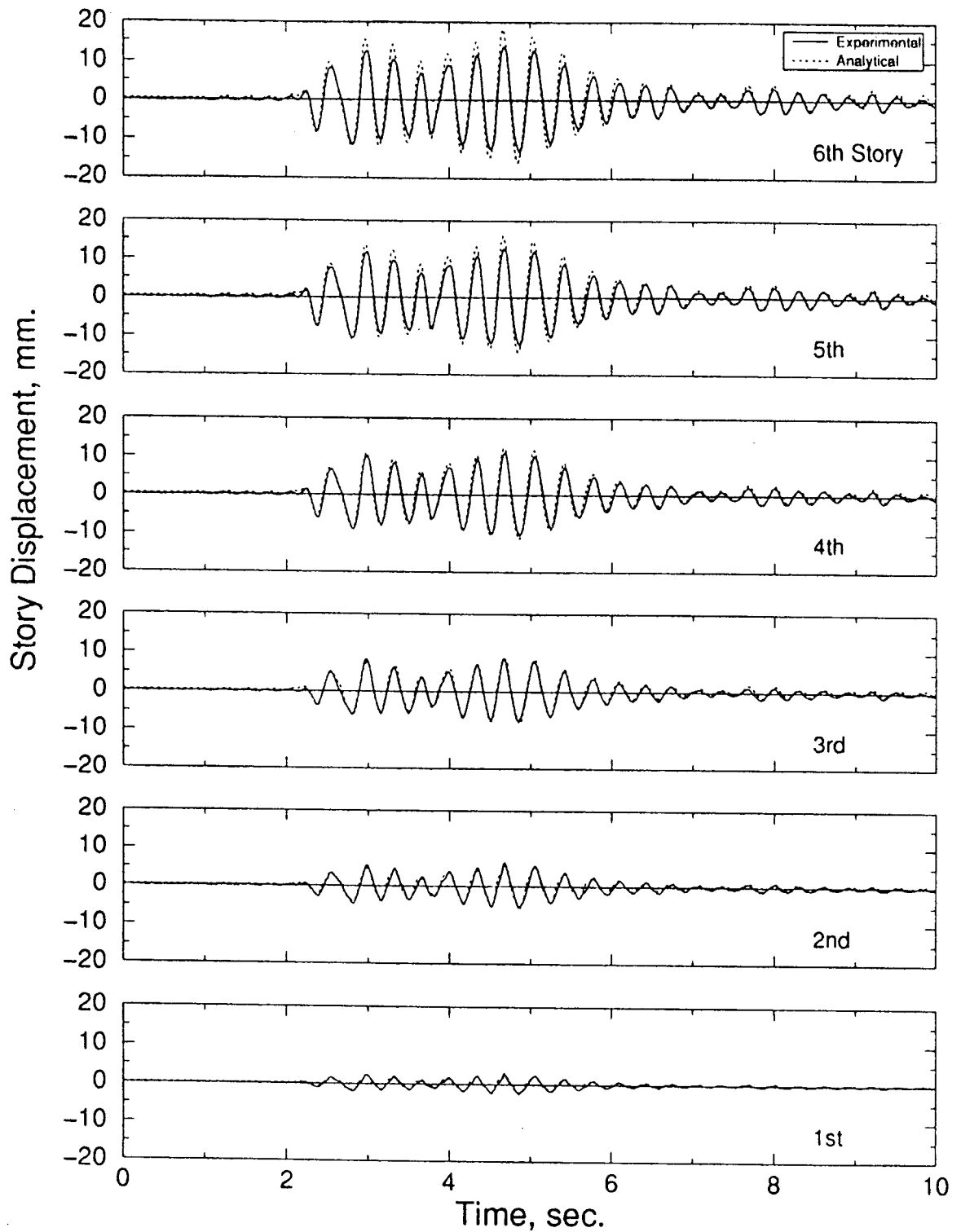


Figure 5-38 Experimentally observed and analytically predicted displacement time histories: B43KO20

Damping System: dampers only

Bracing: upper three stories braced

Earthquake: Kobe, PGA=0.20g

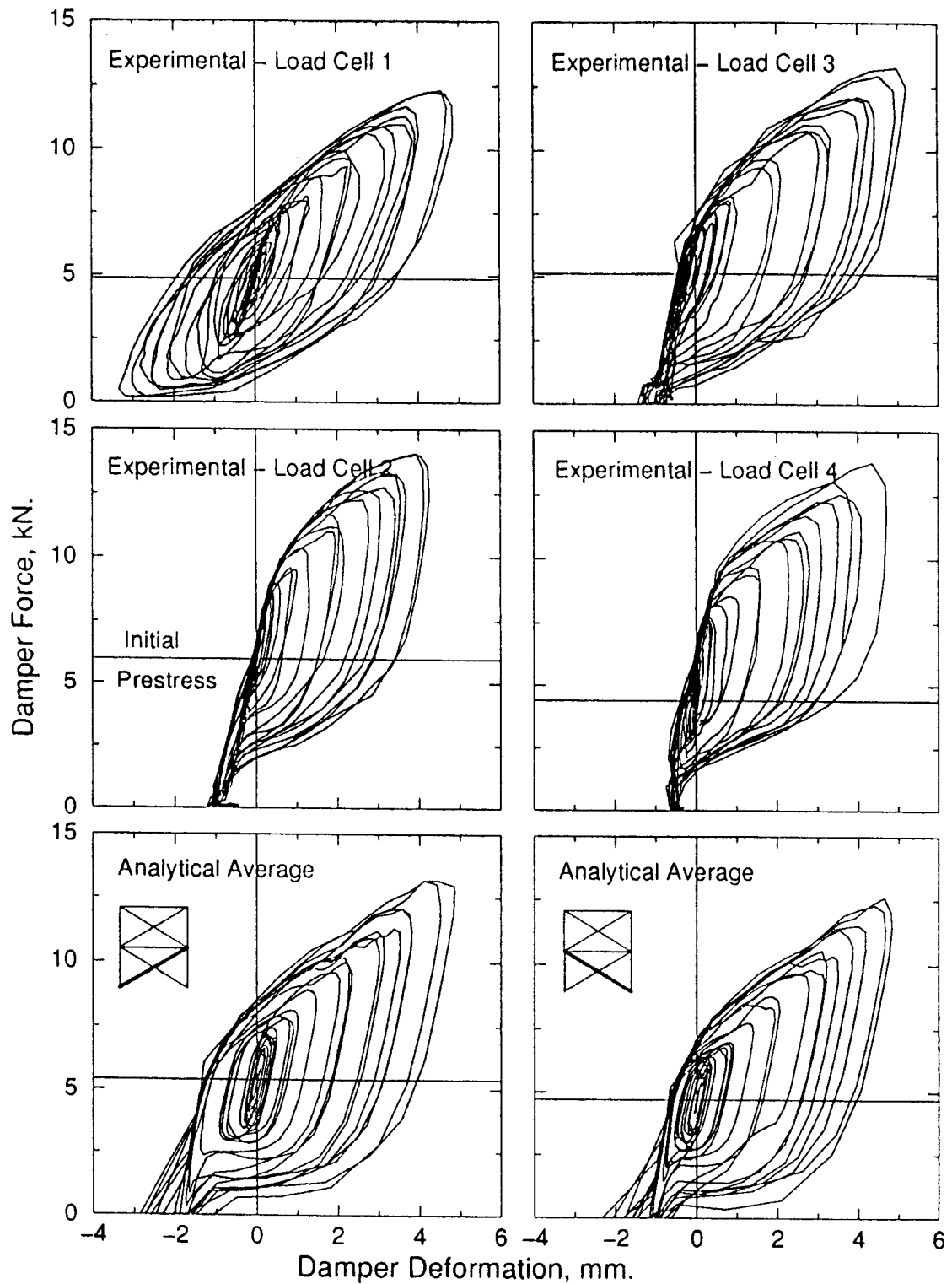


Figure 5-39 Experimentally observed and analytically predicted average tendon force-deformation: B43KO20
Damping System: dampers only
Bracing: upper three stories braced
Earthquake: Kobe, PGA=0.20g

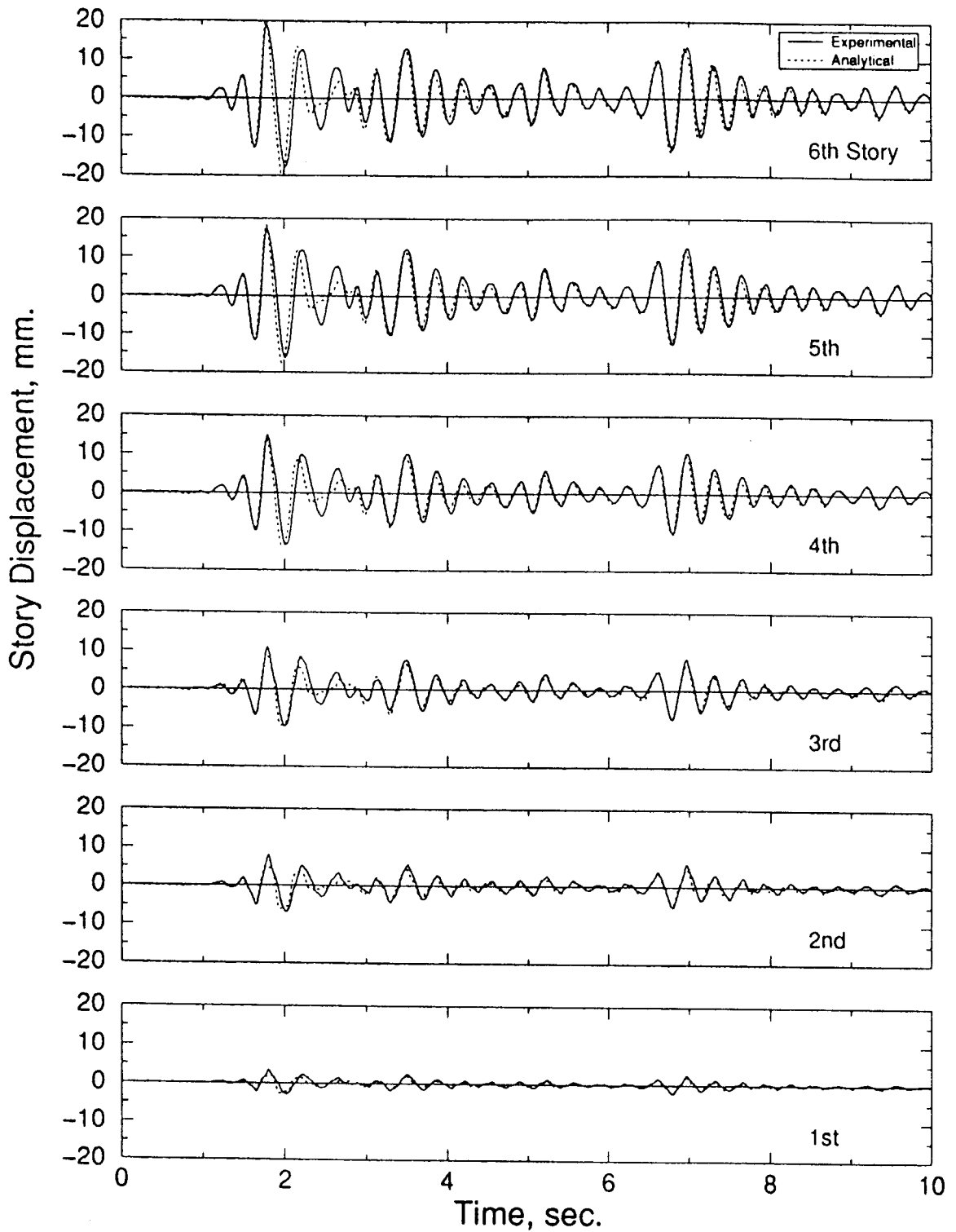


Figure 5-40 Experimentally observed and analytically predicted displacement time histories: B44EL30
Damping System: dampers only
Bracing: upper three stories braced
Earthquake: El Centro, PGA=0.30g

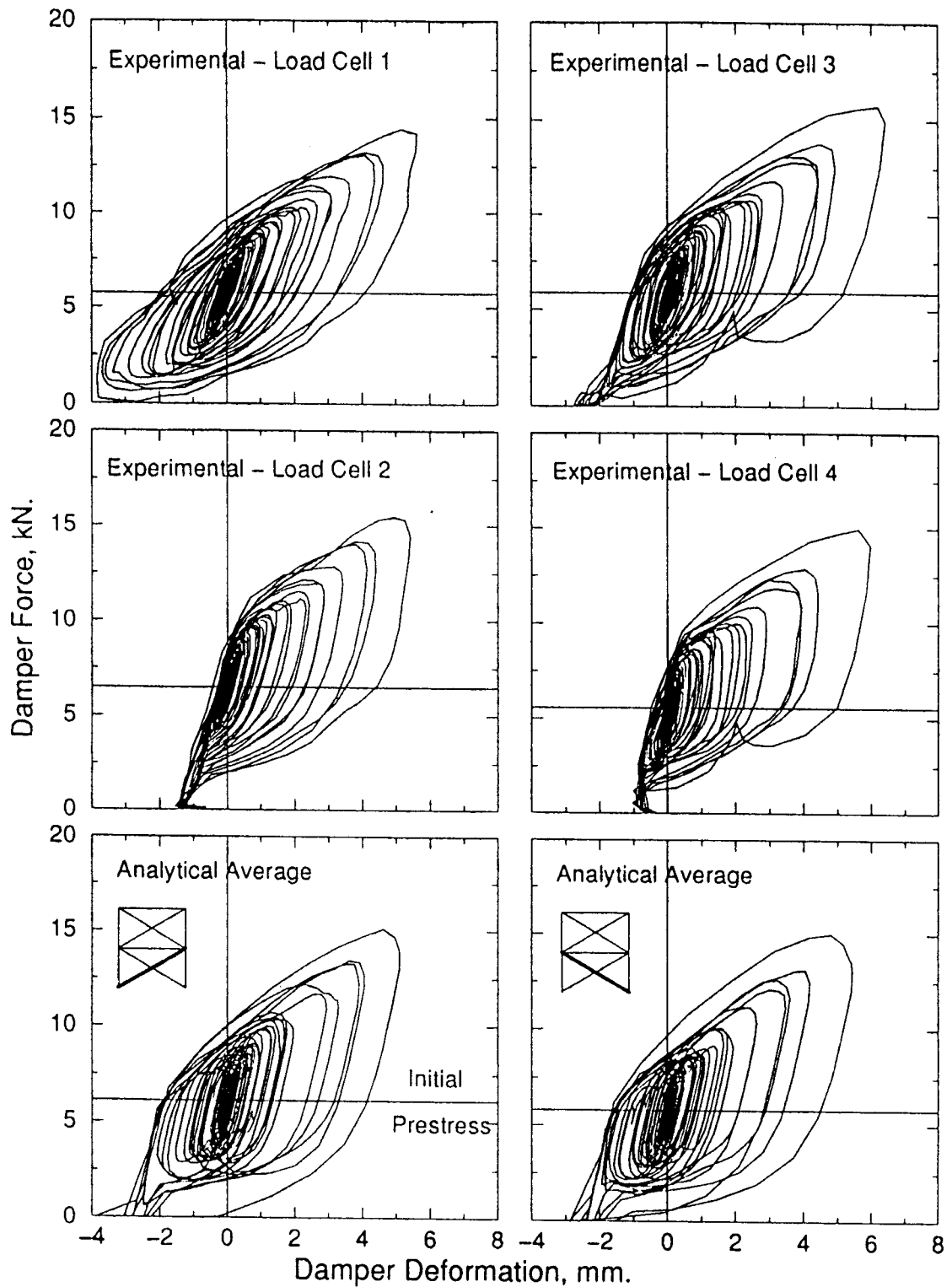


Figure 5-41 Experimentally observed and analytically predicted average tendon force-deformation: B44EL30
Damping System: dampers only
Bracing: upper three stories braced
Earthquake: El Centro, PGA=0.30g

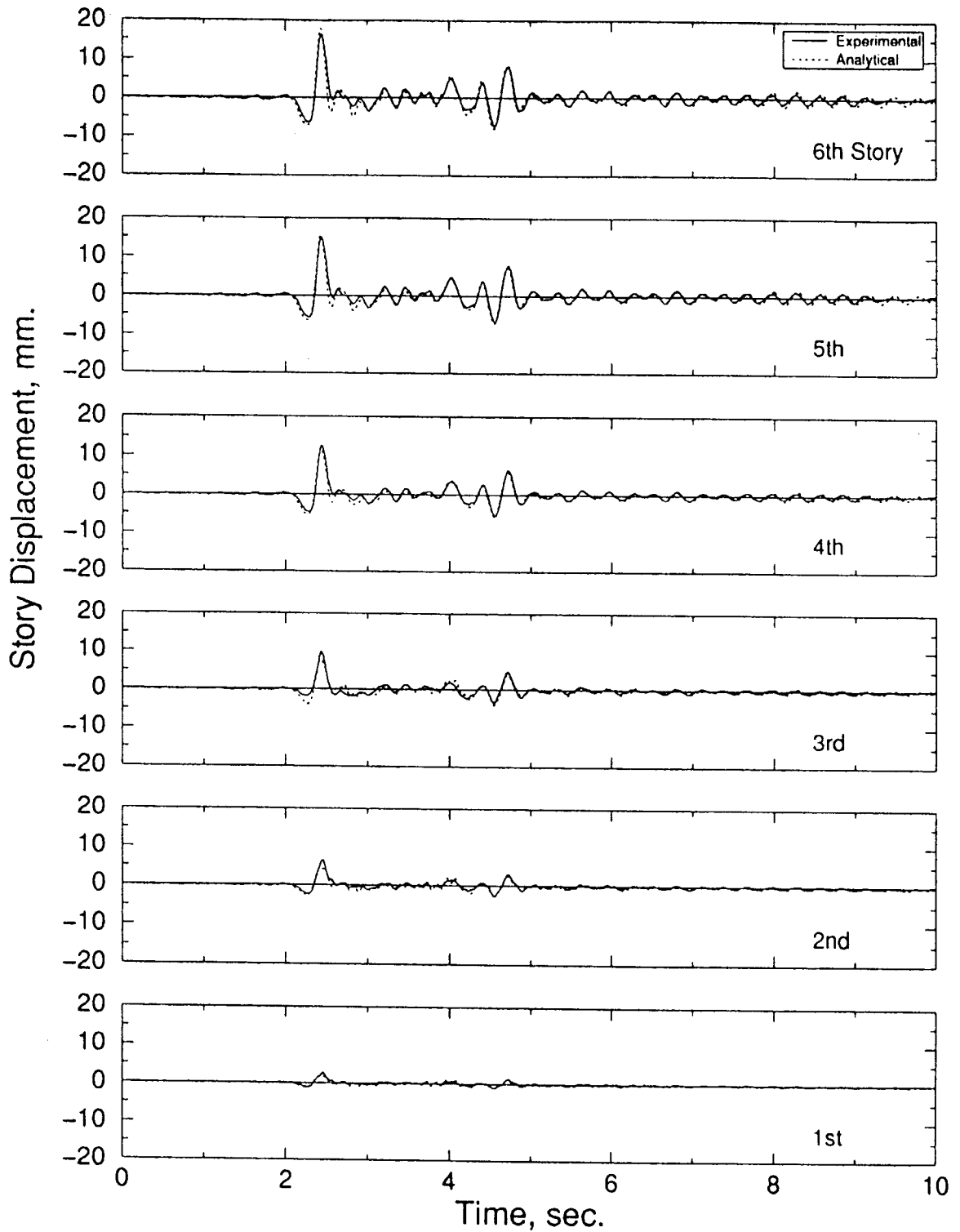


Figure 5-42 Experimentally observed and analytically predicted displacement time histories: B44SY30
Damping System: dampers only
Bracing: upper three stories braced
Earthquake: Sylmar, PGA=0.30g

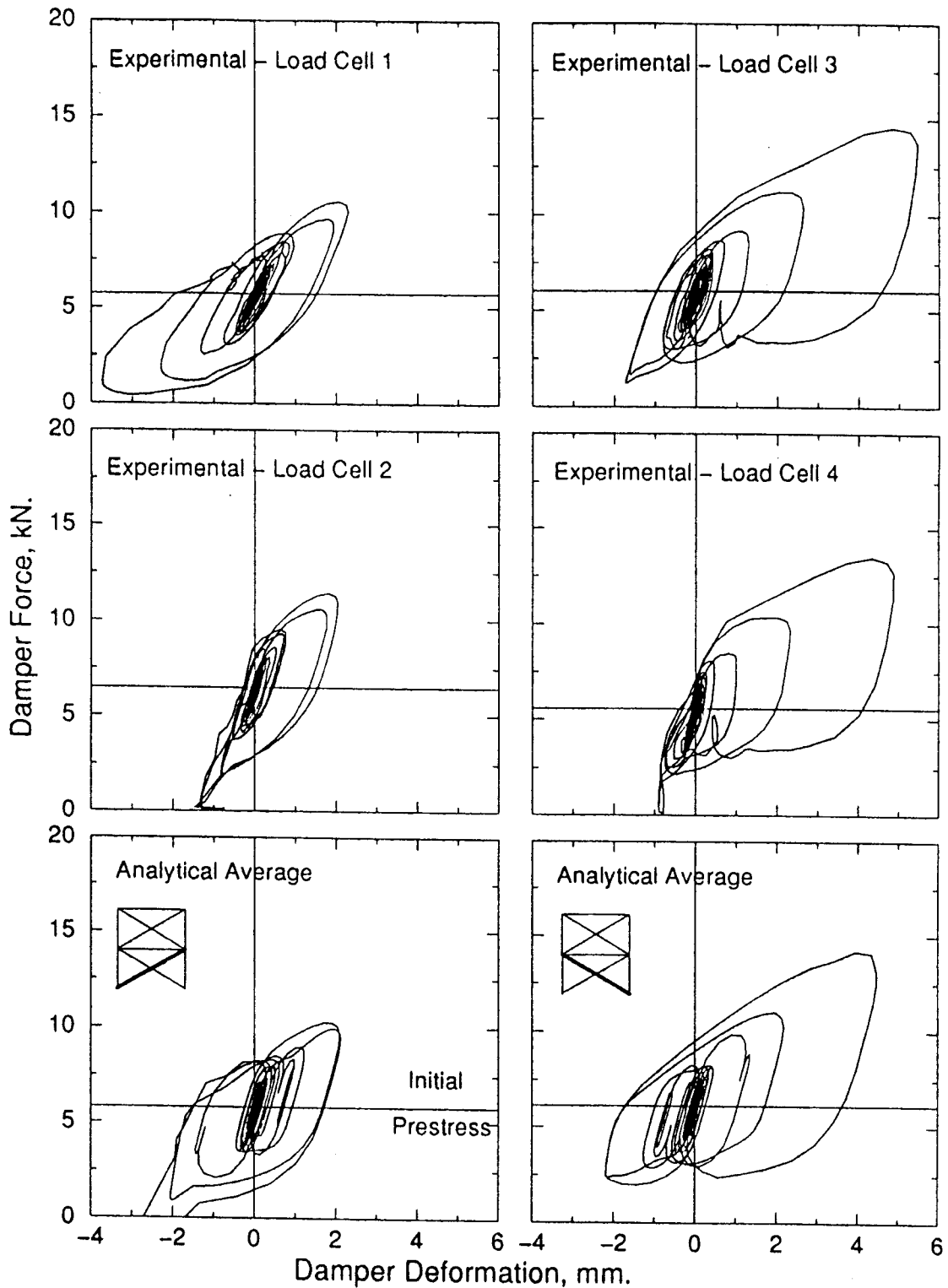


Figure 5-43 Experimentally observed and analytically predicted average tendon force-deformation: B44SY30
Damping System: dampers only
Bracing: upper three stories braced
Earthquake: Sylmar, PGA=0.30g

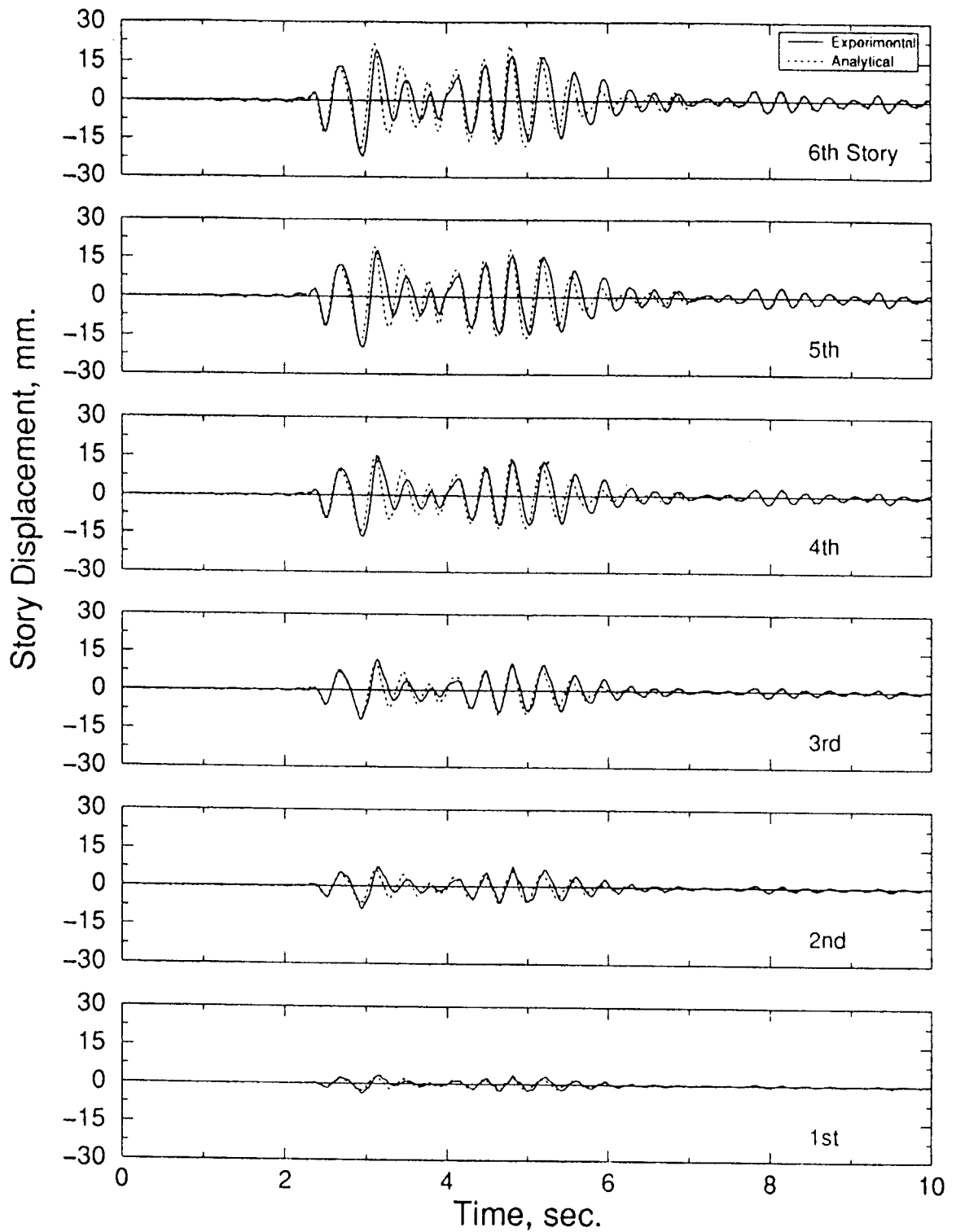


Figure 5-44 Experimentally observed and analytically predicted displacement time histories: B44KO30
Damping System: dampers only
Bracing: upper three stories braced
Earthquake: Kobe, PGA=0.30g

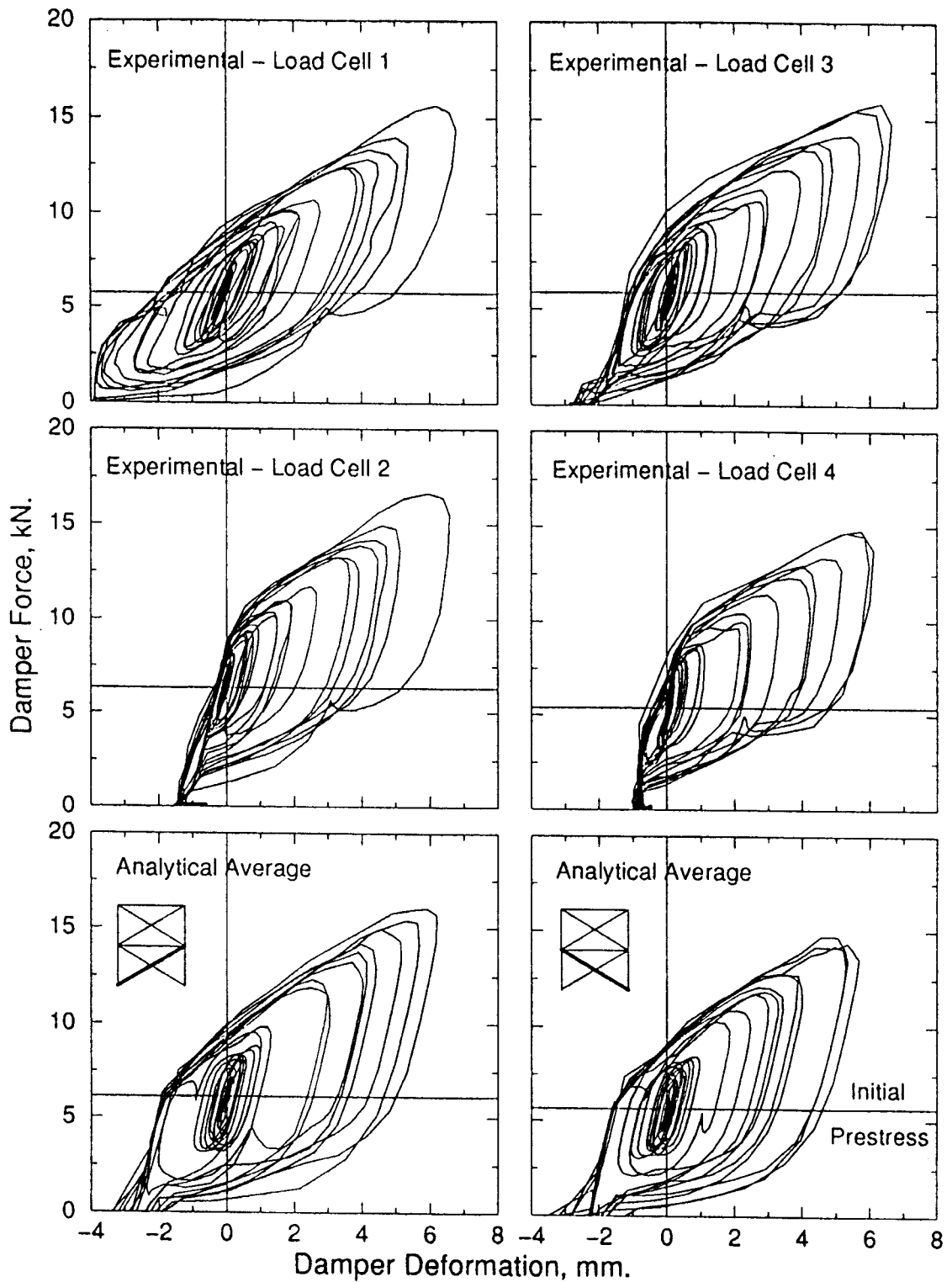


Figure 5-45 Experimentally observed and analytically predicted average tendon force-deformation: B44KO30
Damping System: dampers only
Bracing: upper three stories braced
Earthquake: Kobe, PGA=0.30g

the higher stiffness of the test structure due to the presence of the fuse-bars. An average equivalent viscous damping ratio of 6.3% was obtained from the response to white noise input and 4.4% to 5.5% from the ground motion inputs. These values, when compared to B41 and B44 configurations, are somewhat similar to the former and less than the latter.

Experimental and analytical story displacement time histories and *fuse+damper* system deformation vs. tendon force relationships are plotted in figures 5-46 through 5-51. Maximum recorded responses for B47 configuration are summarized in table 5-5 in comparison with those of B41 and B44. As can be seen from table 5-5, although roof displacement response was improved markedly, the acceleration amplification factor stayed either the same or was only marginally less. However, the response reduction was much better in the lower stories. In fact, these observations suggest that the response was mostly controlled by the stiffening effect of the fuse-bars and not so much by the added damping due to ESD devices. Finally, envelopes of various response profiles are plotted on figure 5-52 through 5-54, which depicts the overall benefits of the *load balancing tendon-fuse+damper* system over the undamped and damper-only system.

5.4.3.2 Moment Frame (B5# Configurations)

Braces in the top three stories were removed to further investigate the effectiveness of the *load balancing tendon-fuse+damper* system on flexible moment frame structures under pulse-like ground motions. One of the major differences between these and the previous configurations was that the former could be identified essentially as a SDOF system due to the nature of the braced top stories. However, the same tendon system layout was used as it still represents a good approximation to the optimum shape that balances the inertial forces. Mode shapes and natural periods of vibrations were identified using the experimental data from both white noise and simulated ground motion tests. First mode periods of vibrations and corresponding viscous damping ratios obtained from the frequency domain analysis for the three different configurations are given in table 5-6. These configurations were; a) dampers/fuse-bars not active (B50), b) dampers active only (B51) and, c) dampers and fuse-bars active (B52). Maximum response of the structure is summarized in table 5-7 in terms of the base shear coefficient, overturning moment at the base (OTM), roof and 3rd floor displacement, and interstory drift

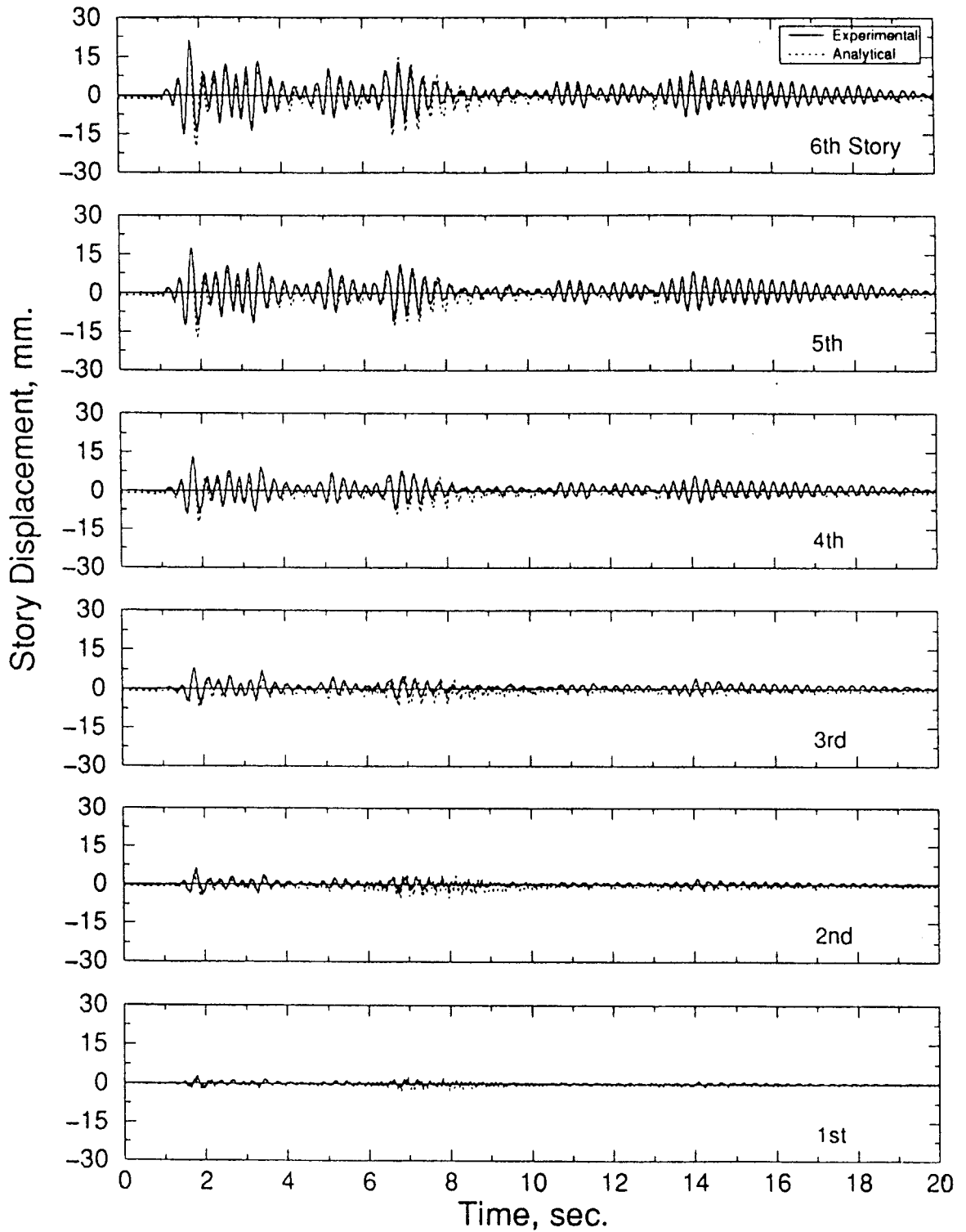


Figure 5-46 Experimentally observed and analytically predicted displacement time histories: B47EL40
Damping System: fuse-bars and dampers
Bracing: upper three stories braced
Earthquake: El Centro, PGA=0.40g

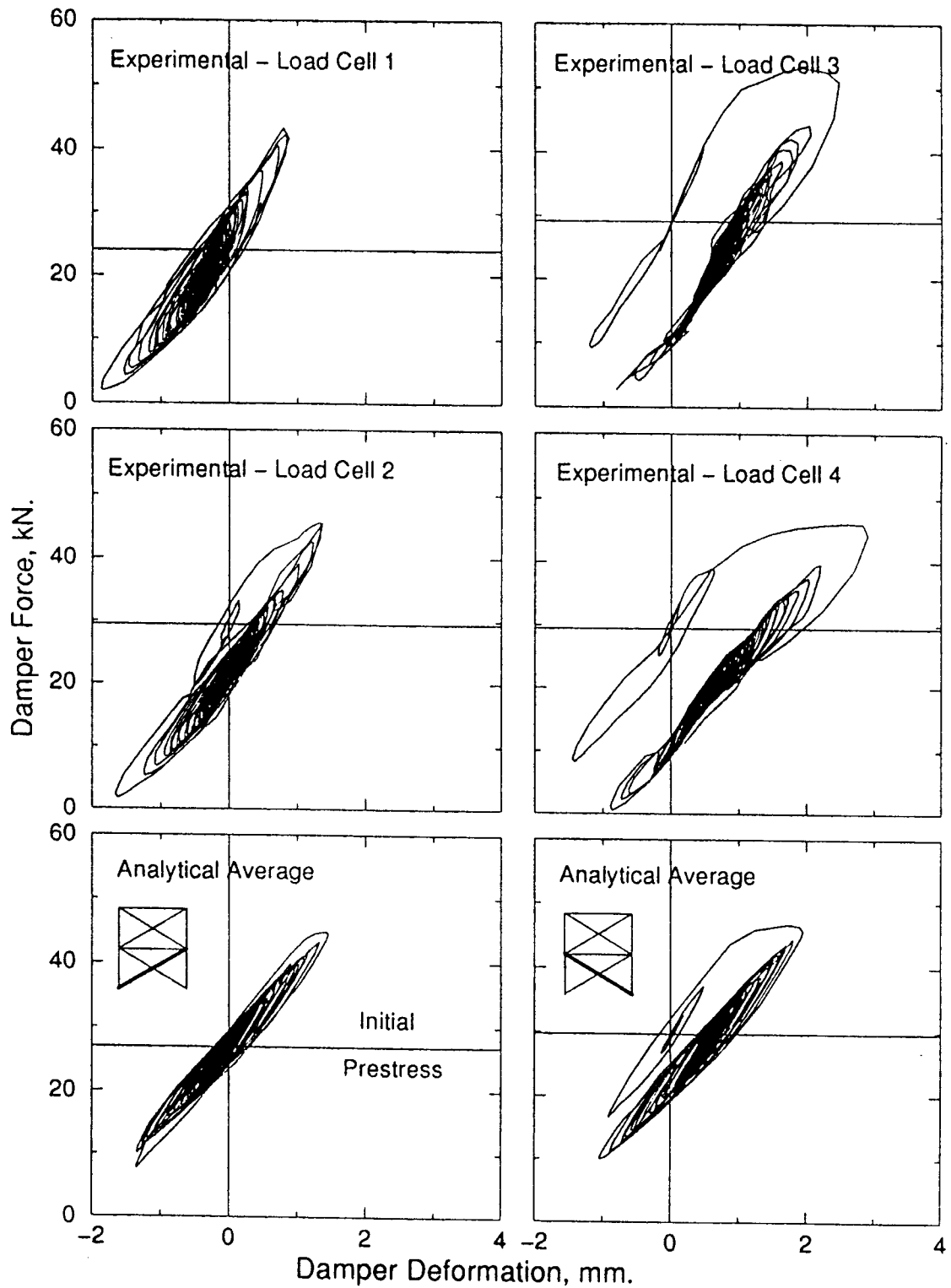


Figure 5-47 Experimentally observed and analytically predicted average tendon force-deformation: B47EL40

Damping System: fuse-bars and dampers

Bracing: upper three stories braced

Earthquake: El Centro, PGA=0.40g

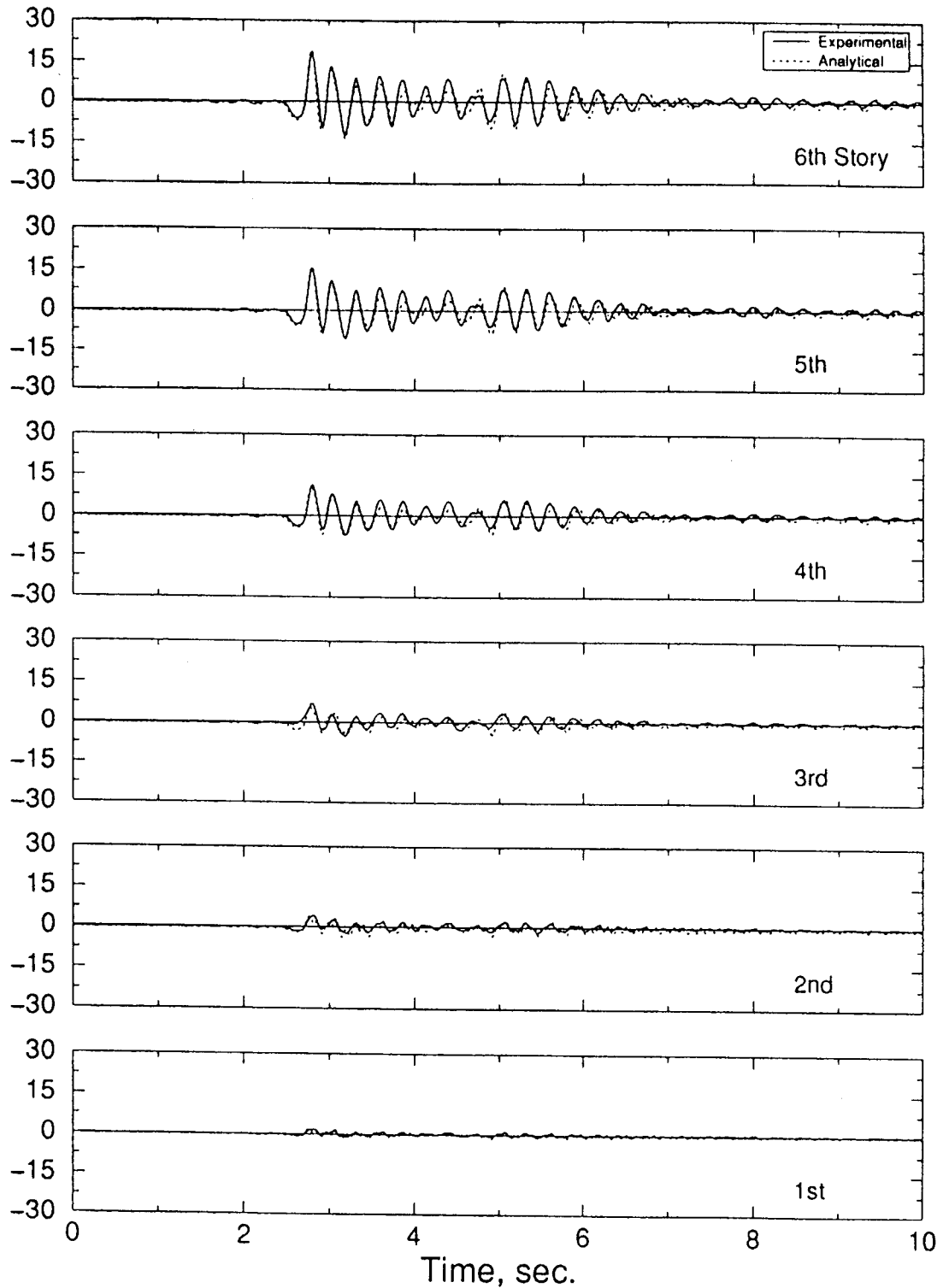


Figure 5-48 Experimentally observed and analytically predicted displacement time histories: B47SY40
Damping System: fuse-bars and dampers
Bracing: upper three stories braced
Earthquake: Sylmar, PGA=0.40g

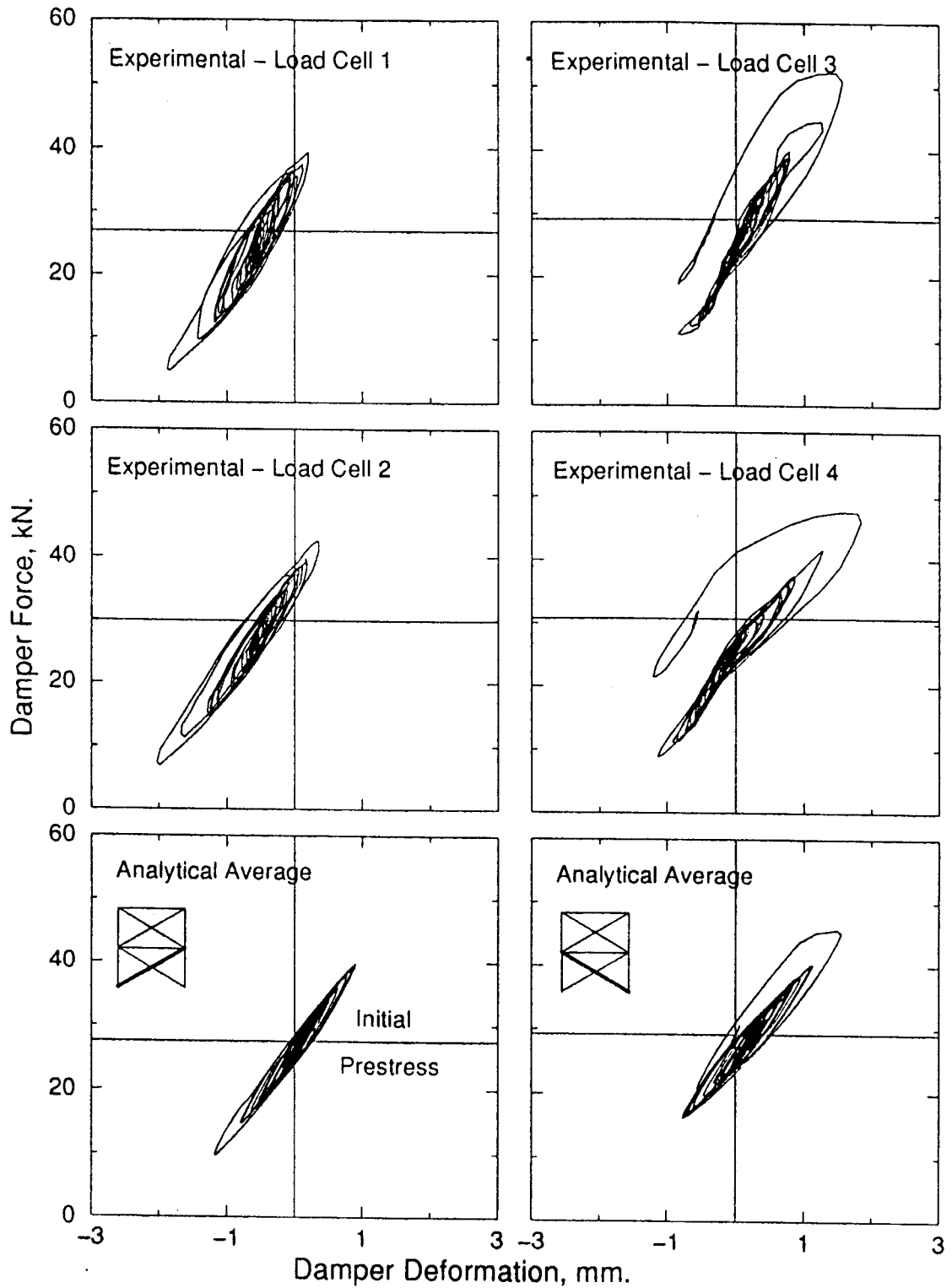


Figure 5-49 Experimentally observed and analytically predicted average tendon force-deformation: B47SY40
Damping System: fuse-bars and dampers
Bracing: upper three stories braced
Earthquake: Sylmar, PGA=0.40g

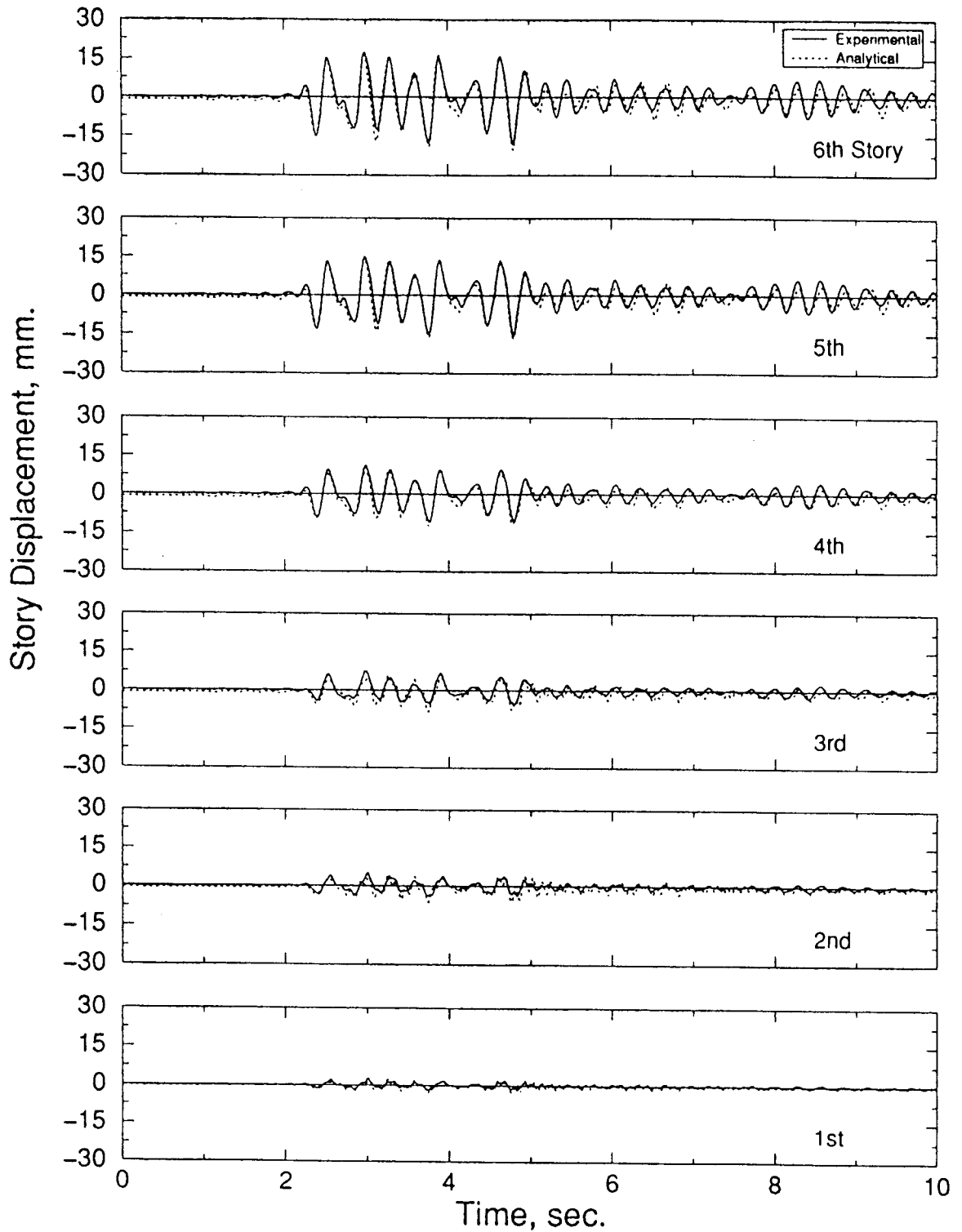


Figure 5-50 Experimentally observed and analytically predicted displacement time histories: B47KO40
Damping System: fuse-bars and dampers
Bracing: upper three stories braced
Earthquake: Kobe, PGA=0.40g

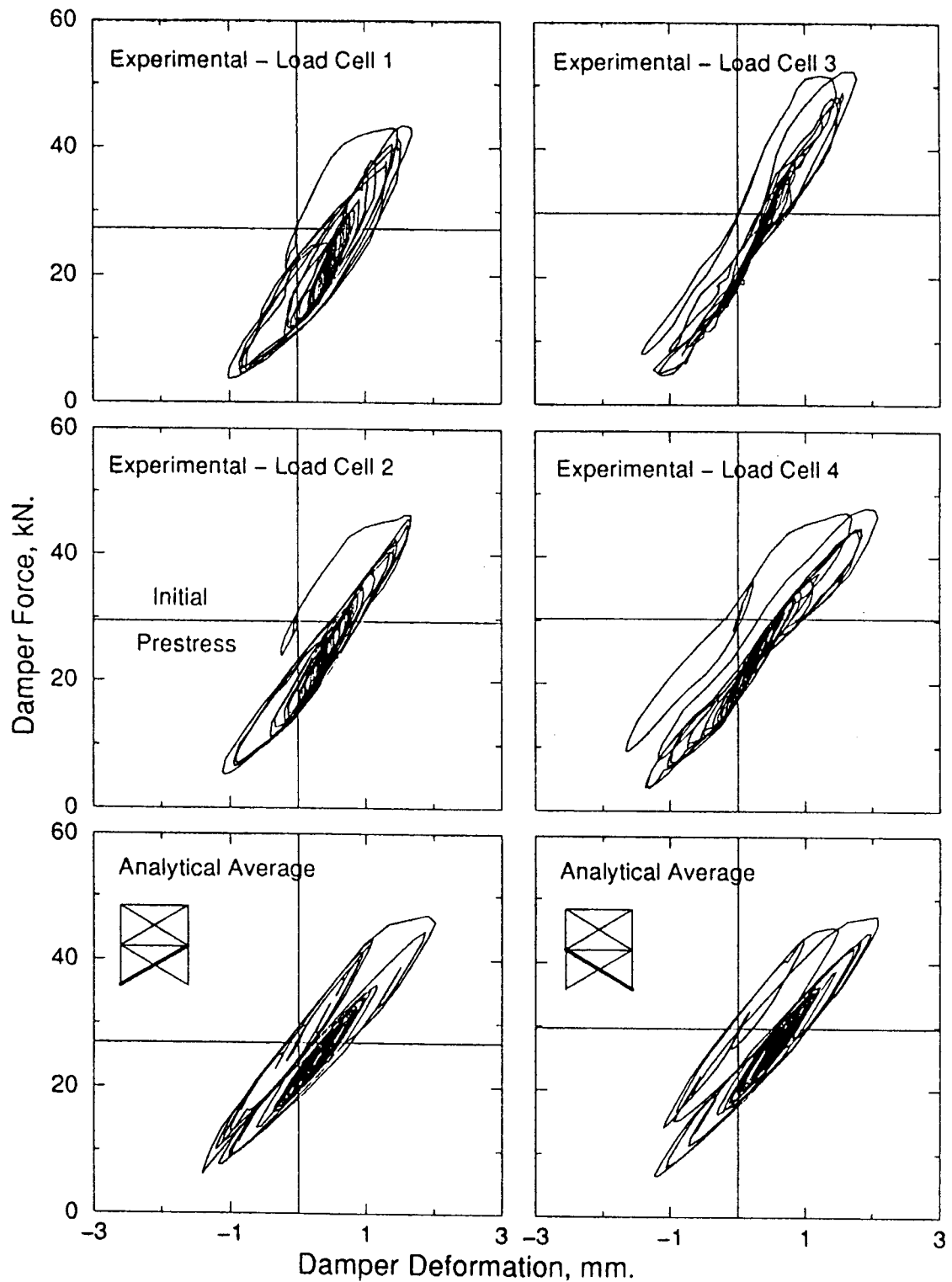


Figure 5-51 Experimentally observed and analytically predicted average tendon force-deformation: B47KO40
Damping System: fuse-bars and dampers
Bracing: upper three stories braced
Earthquake: Kobe, PGA=0.40g

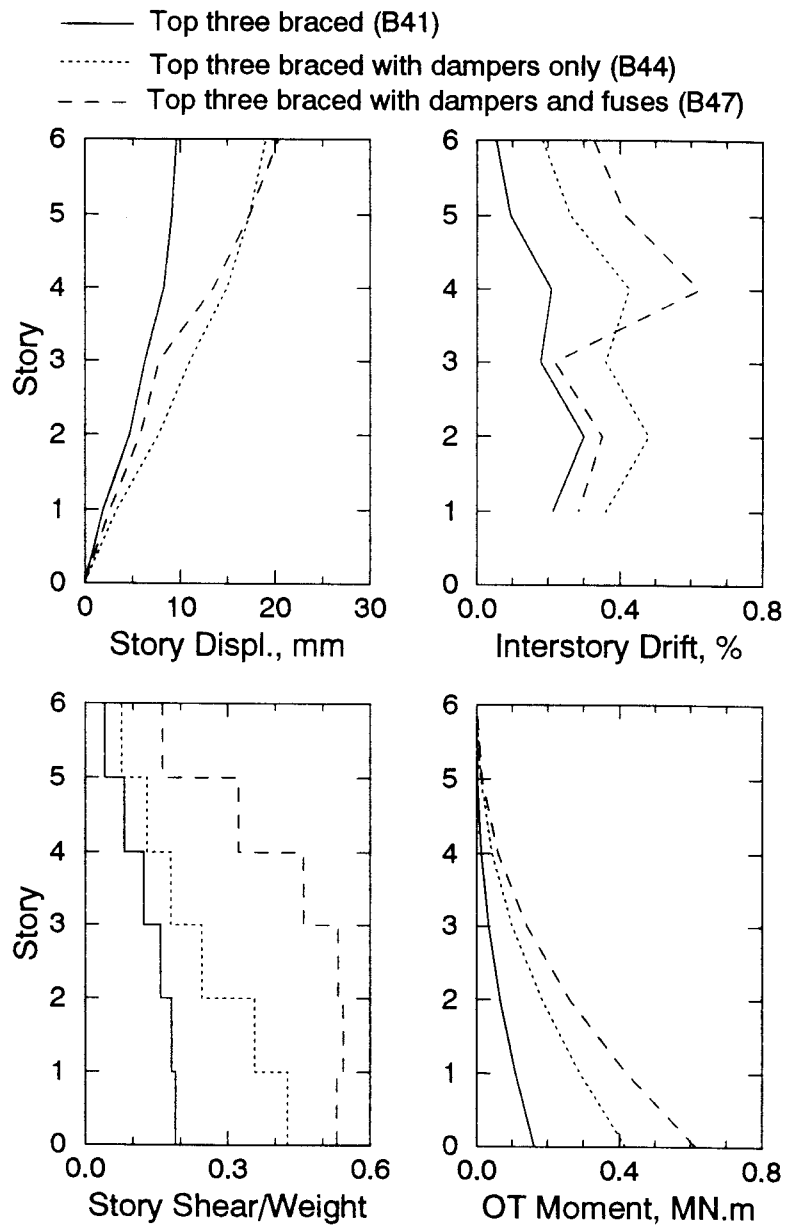


Figure 5-52 Maximum response envelopes for the structure with top three stories braced and supplementary system active configurations subjected to El Centro ground motion at various PGA levels

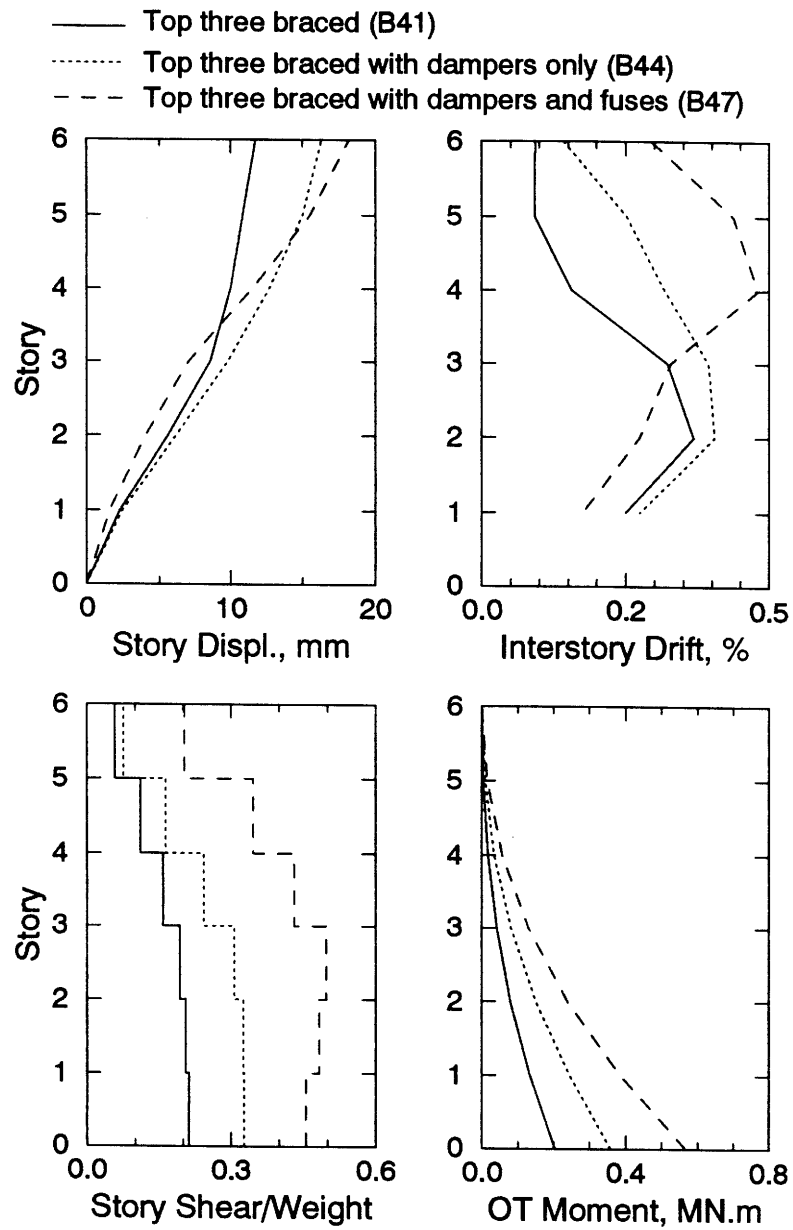


Figure 5-53 Maximum response envelopes for the structure with top three stories braced and supplementary system active subjected to Sylmar ground motion at various PGA levels

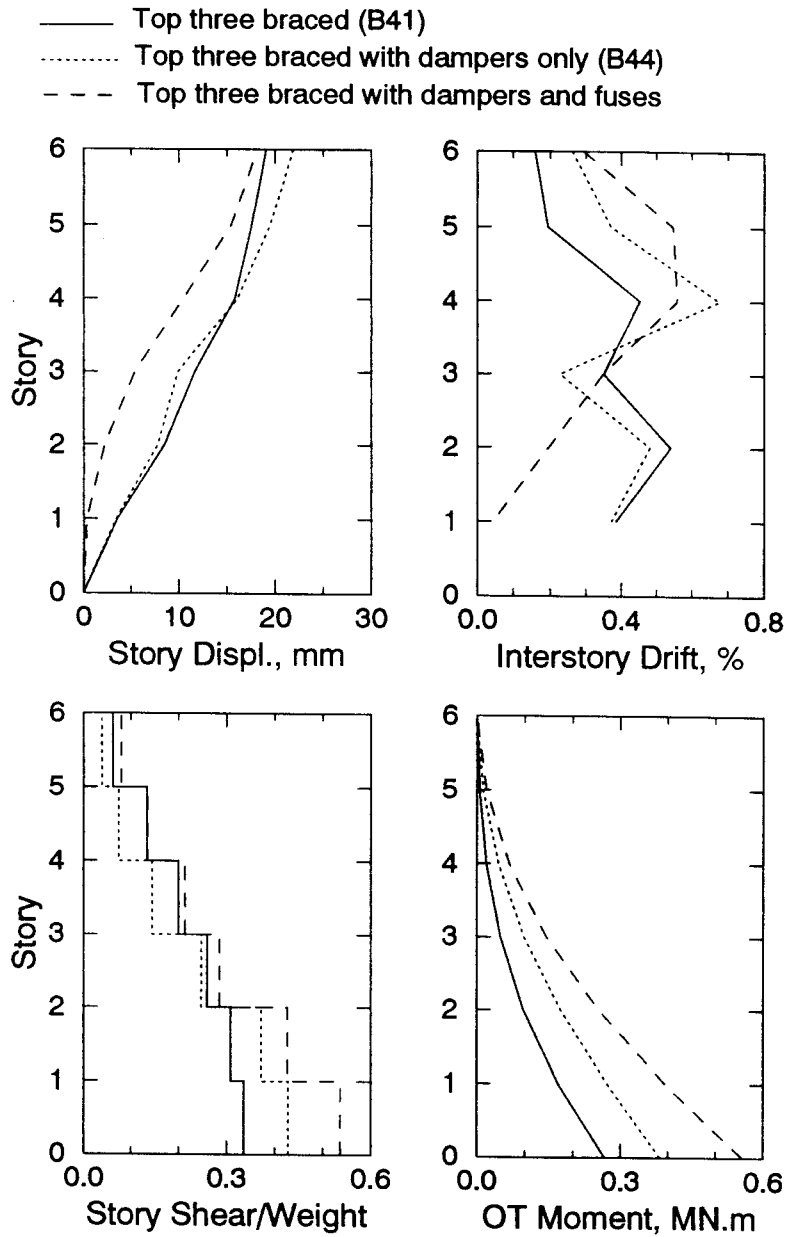


Figure 5-54 Maximum response envelopes for the structure with top three stories braced and supplementary system active subjected to Kobe ground motion at various PGA levels

(ISD). It must be noted here that the B52 configuration could not be tested under Sylmar and Kobe ground motions because of an unfortunate malfunction of the shaking table that terminated all experimentation. Therefore, only one experimental data set is available for the *load balancing tendon-fuse+damper* system on the moment frame.

Preliminary simulated ground motion experiments were conducted on the moment frame at a PGA level of 0.17g before the activation of the damping system (B50). This configuration had a first mode natural period of vibration of 0.41 sec. as obtained from both white noise and ground motion tests. Corresponding viscous damping ratio was 2.4% that is slightly higher than that of the MOM configuration (tables 5-2 and 5-6). This increase in the viscous damping ratio was again attributed to the presence of the friction between the tendon and the pull-beam. However, peak responses are comparable to those obtained from the previous tests (MOM).

Experiments were carried out on the damped structure. The tendon system was prestressed to about 15 kN which corresponded to about 150% of the initial pre-load (2.8 kN) on the ESD devices. Prestress was applied by torquing anchorage nuts at the pull-beam/tendon connection and by observing the change in the individual load cell readings. Since the prestressing was performed on one tendon at a time, the prestress level differed by as much as 1 kN on either side of the test structure. However, the difference was considered to be negligible from the torsional response point of view. In fact, no torsional response was observed during this series of experiments.

As can be seen in table 5-6, the first mode natural period of vibration for this configuration was found to be 0.29 sec. from the white noise input and 0.33 to 0.35 sec. from the ground motion inputs. Equivalent viscous damping ratio was increased from about 2.4% to 9.0% when compared to undamped configuration. The benefit of the ESD devices (B51) configuration can also be seen in the same figure in comparison to B50 configuration, i.e. high frequency response as well as the first mode was damped out by the ESD devices. Experimental and analytical story displacement time histories and damper deformation-tendon force relationships are plotted in figures 5-55 through 5-60 for the three simulated ground motion experiments. Very good agreement between the experimental and analytical results can be observed.

Table 5-6 Comparison of 1st Mode Natural Periods and Viscous Damping Ratios Moment Frame - Tendon system active

Configuration	Natural Period, sec.		Damping Ratio, %	
	White Noise	Ground Motion	White Noise	Ground Motion
B50	0.41	0.41	2.4	2.4
B51	0.29	0.33 ~ 0.35	3.0	6.5 ~ 9.0
B52	-	0.26	-	9.7

Table 5-7 Summary of Experimental Response – Moment Frame – Tendon system active

Ground Motion	Config.	PGA (g)	Pre-stress (kN) ¹	Base Shear/Weight (kN)		OTM (kN.m)	Displacement (mm)		Max (ISD) ² (%)
				Total	Col.		6 th fl.	3 rd fl.	
El Centro	B50	0.172	-	0.485	0.485	457	33.1	19.9	0.819 (2)
	B51	0.332	14.2/15.0	0.456	0.302	467	26.7	13.0	0.699 (4)
	B52	0.307	68.9/60.2	0.416	0.018	550	25.5	7.7	0.842 (4)
Sylmar	B50	0.162	-	0.214	0.214	215	14.4	8.4	0.354 (3)
	B51	0.456	14.3/15.3	0.338	0.192	456	24.9	11.5	0.591 (4)
	B52	-	-	-	-	-	-	-	-
Kobe	B50	0.164	-	0.464	0.464	483	34.2	20.2	0.819 (2)
	B51	0.397	14.1/15.0	0.572	0.387	574	35.6	17.1	0.809 (2)
	B52	-	-	-	-	-	-	-	-

¹ Average load cell reading. East/West

² Story at which the maximum response was recorded

In general, maximum-recorded responses were reduced by as much as two times considering the PGA levels that the structure was subjected to in B50 and B51 configurations. However, maximum ISDs stayed about the same and were recorded at the 4th story for B51 configuration. This was expected as the tendon force (damping force) was directly applied at the 3rd floor. A remarkable reduction in the maximum total column shear as well as in the total base shear can be observed in table 5-7. Overturning moments at the rigid base either increased in proportion to the total story shear or stayed the same.

A new set of fuse-bars was then installed in parallel with the ESD dampers as mentioned in previous subsections. The *load balancing tendon-fuse+damper* system was then prestressed to approximately 69 kN in each direction as described above. This total prestress load was distributed between the ESD devices and the fuse-bars such that ESD devices were subjected to an initial force of about 5% beyond their pre-load level whereas fuse-bars were at 65-70% of their yield strength. As mentioned before only one test could be conducted because of the shaking table malfunction. The first mode natural period of vibration was found to be 0.26 sec. with an equivalent viscous damping ratio of 9.7%. Further reductions in maximum-recorded 3rd story displacement can be seen in table 5-7 for this experiment. Experimental and analytical story displacement time histories and *fuse+damper* system deformation vs. tendon force relationships are plotted in figure 5-61 and 5-62. Maximum response profiles are shown in Figures 5-63 through 5-65, which presents the overall benefits of the *load balancing tendon-fuse+damper* system in controlling the earthquake response of the flexible frame structures.

5.5 SUMMARY AND CONCLUSIONS

Shaking table tests were conducted on a 1/4 scale, six story-flexible steel moment frame with and without supplemental ESD devices. An enhanced version of the non-linear time history analysis program DRAIN-2DX was used to analytically compare predicted response with the experimental behavior of the structure. The analytical predictions compared very well with the experimental results. The efficacy of a practical and accurate analytical tool is thought to be encouraging for future analytical-parametric studies as well as for design verification studies.

In the experimental study, results for seven ground motions are reported: namely 1952 Kern County -Taft N21E, 1968 Tokachi-Oki - Hachinohe NS, 1971 San Fernando - Pacoima Dam S16E and S74W, 1940 Imperial Valley - El Centro NS, 1994 Northridge - Sylmar County

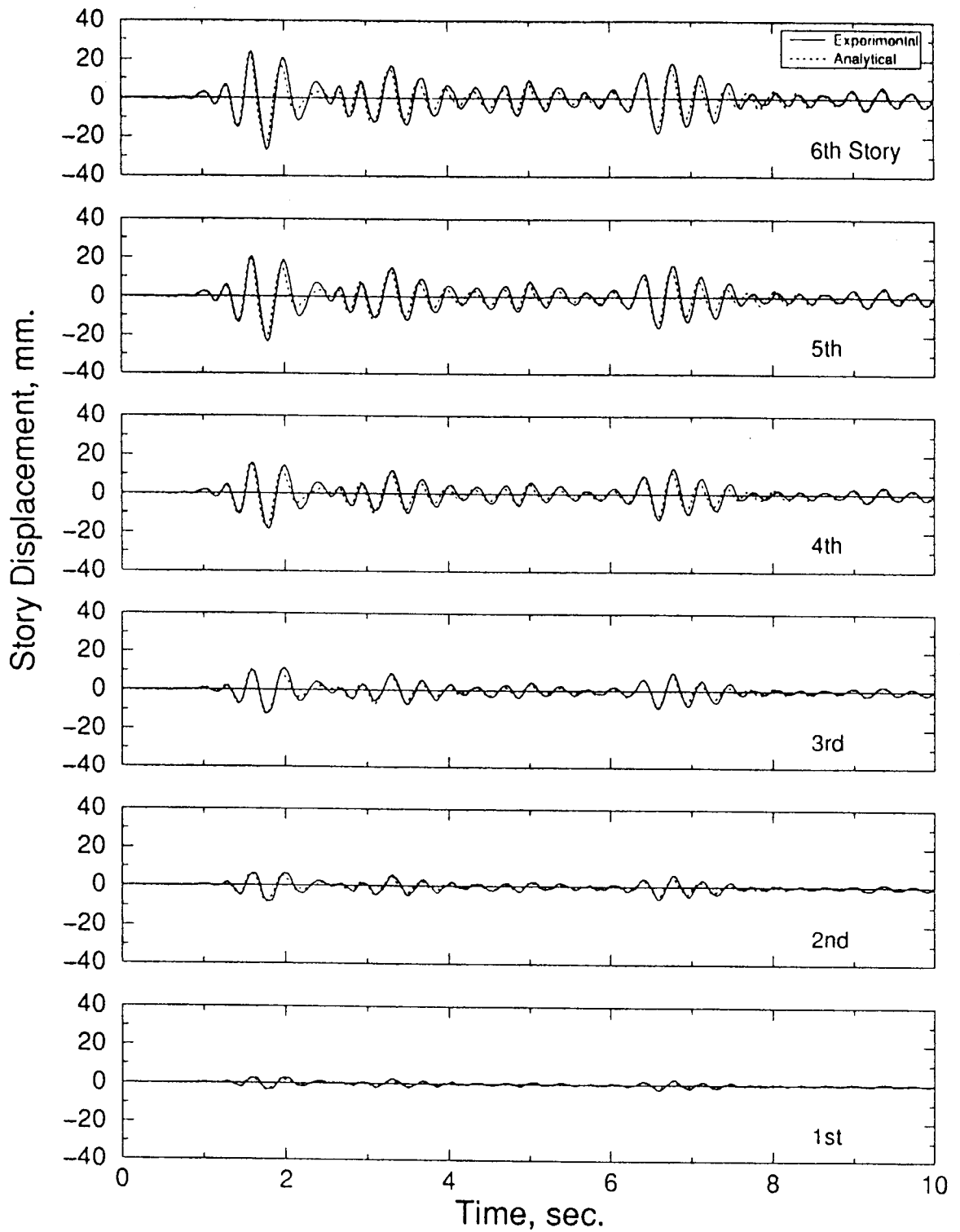


Figure 5-55 Experimentally observed and analytically predicted displacement time histories: B51EL40
Damping System: dampers only
Bracing: none
Earthquake: El Centro, PGA=0.40g

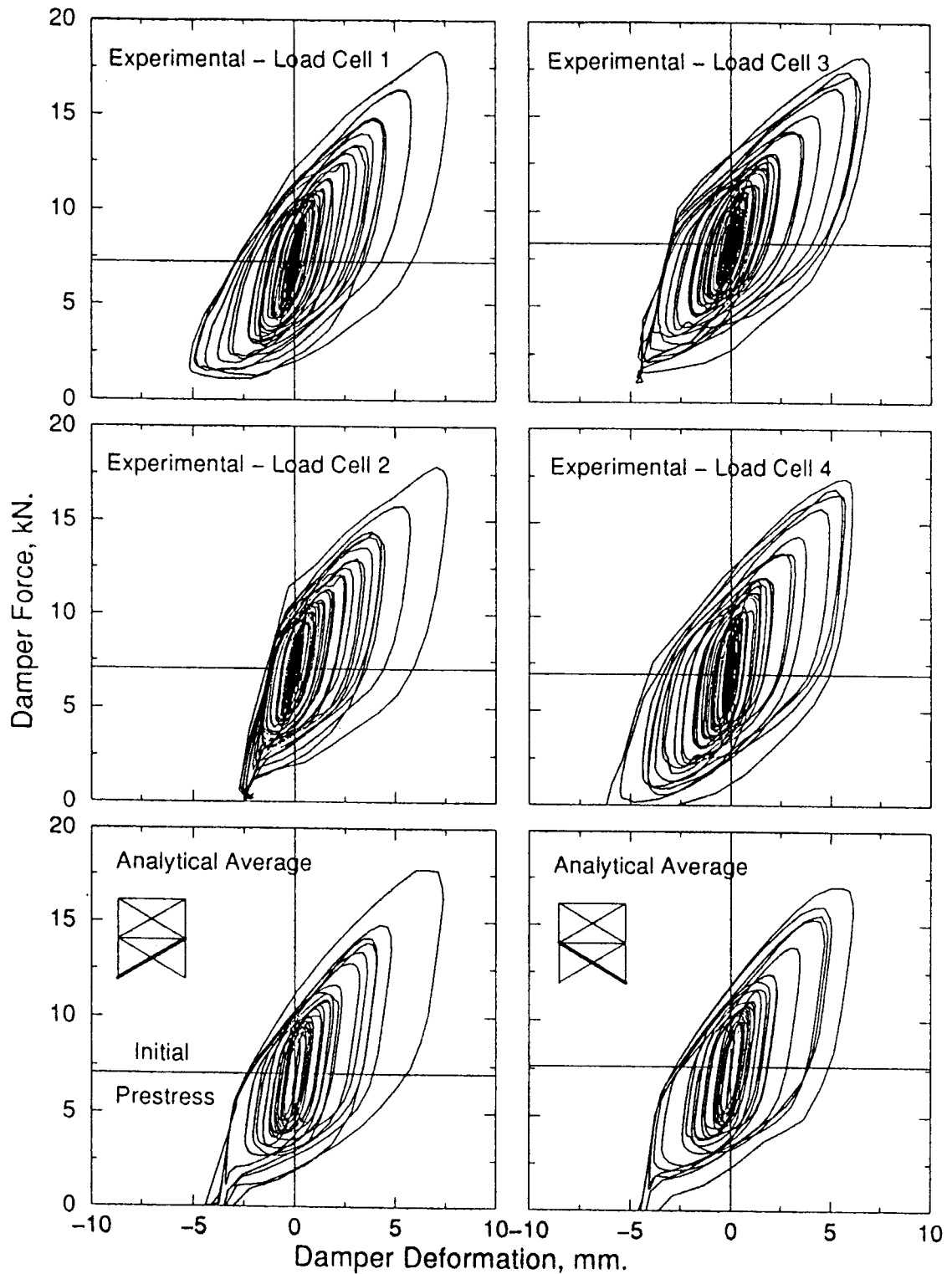


Figure 5-56 Experimentally observed and analytically predicted average tendon force-deformation: B51EL40
Damping System: dampers only
Bracing: none
Earthquake: El Centro, PGA=0.40g

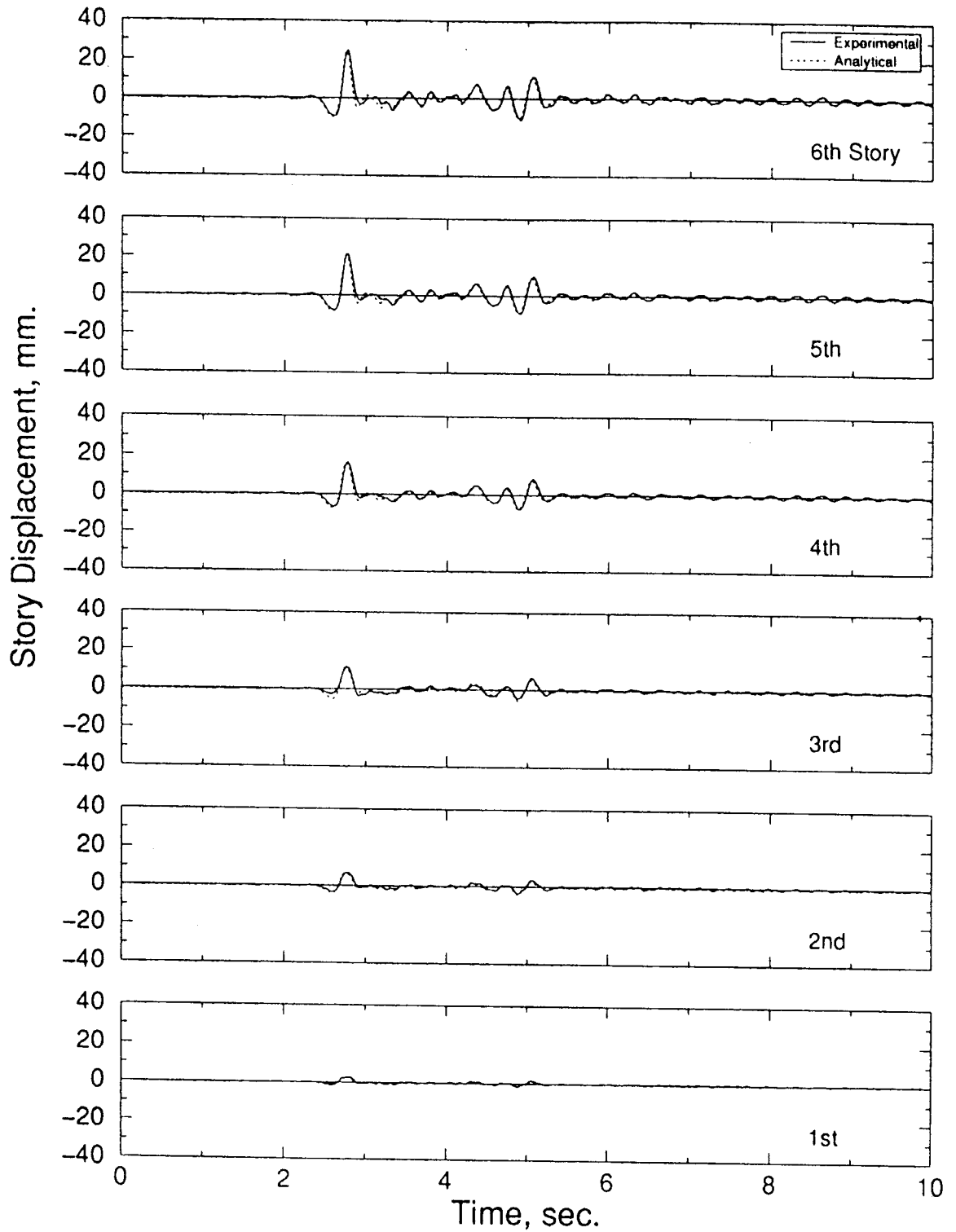


Figure 5-57 Experimentally observed and analytically predicted displacement time histories: B51SY40
Damping System: dampers only
Bracing: none
Earthquake: Sylmar, PGA=0.40g

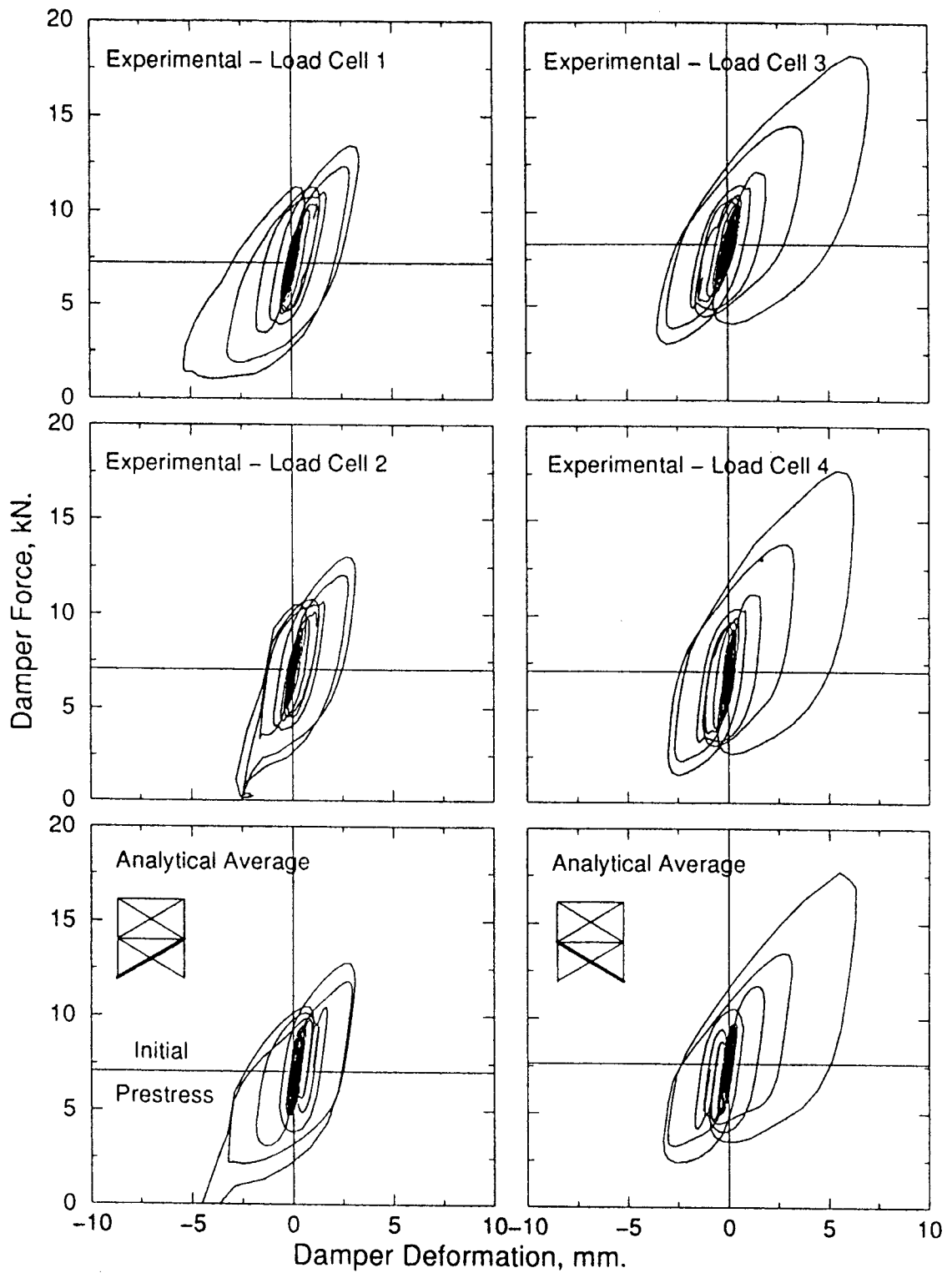
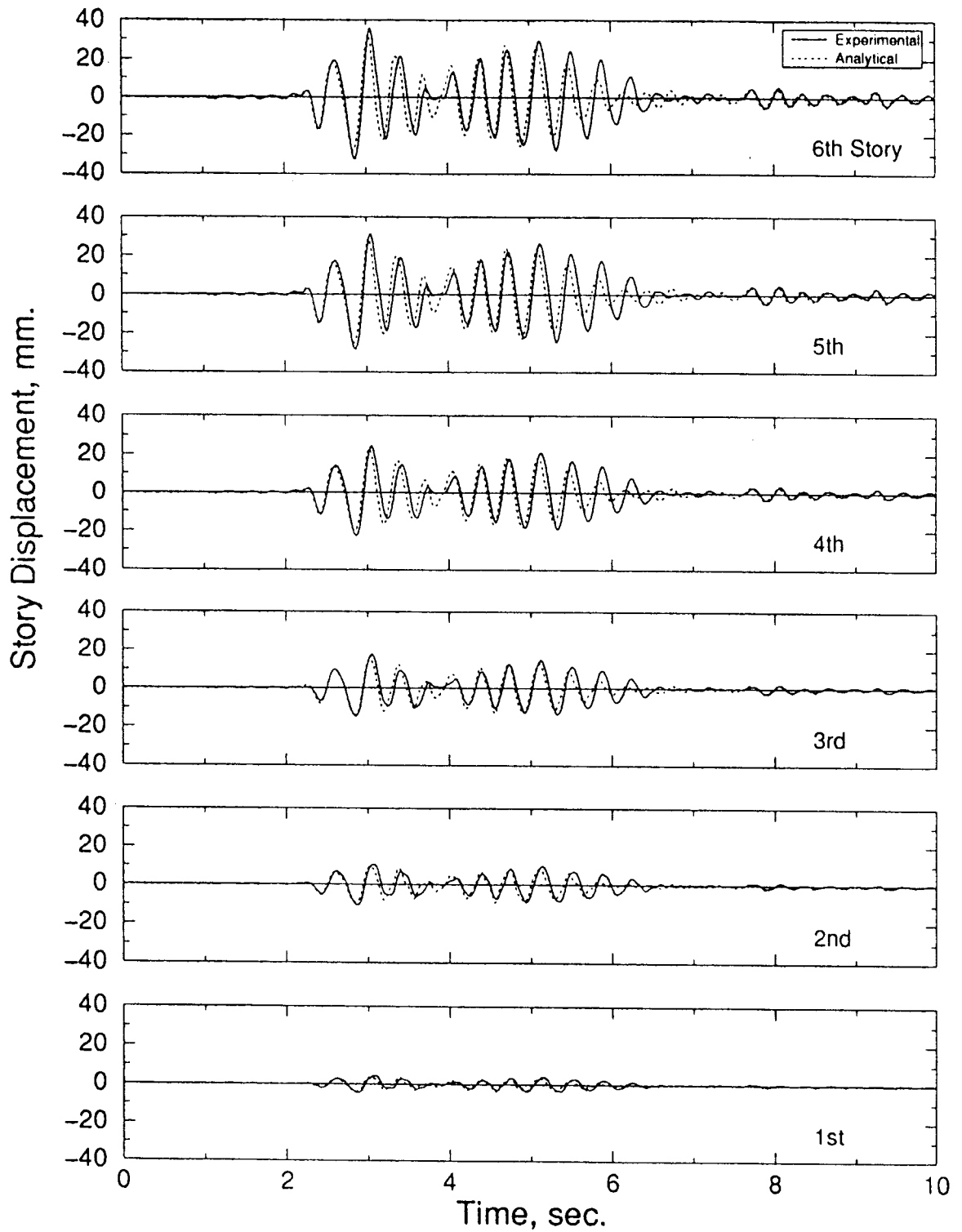


Figure 5-58 Experimentally observed and analytically predicted average tendon force-deformation: B51SY40
Damping System: dampers only
Bracing: none
Earthquake: Sylmar, PGA=0.40g



**Figure 5-59 Experimentally observed and analytically predicted displacement time histories: B51KO40
 Damping System: dampers only
 Bracing: none
 Earthquake: Kobe, PGA=0.40g**

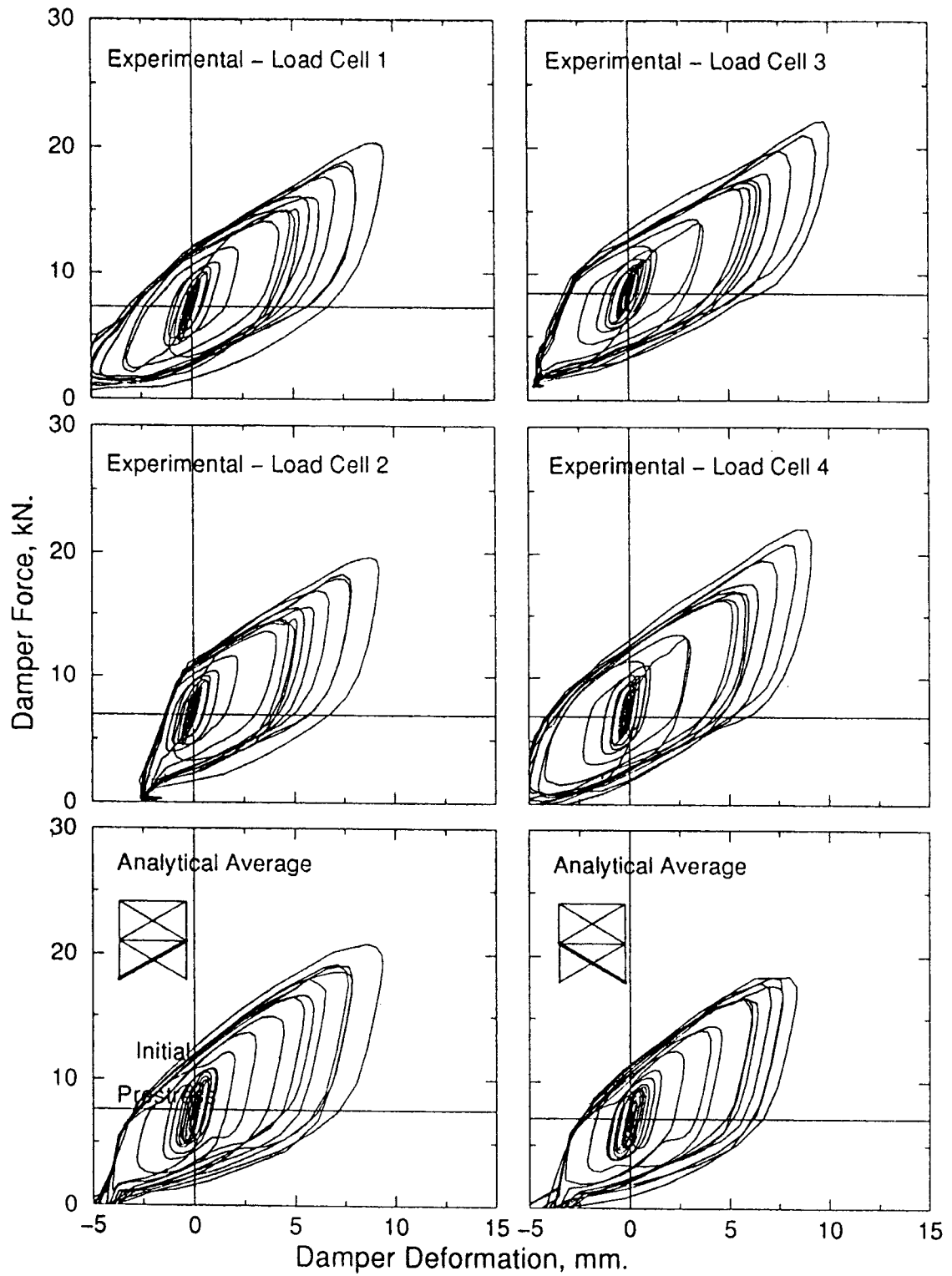


Figure 5-60 Experimentally observed and analytically predicted average tendon force-deformation: B51KO40
Damping System: dampers only
Bracing: none
Earthquake: Kobe, PGA=0.40g

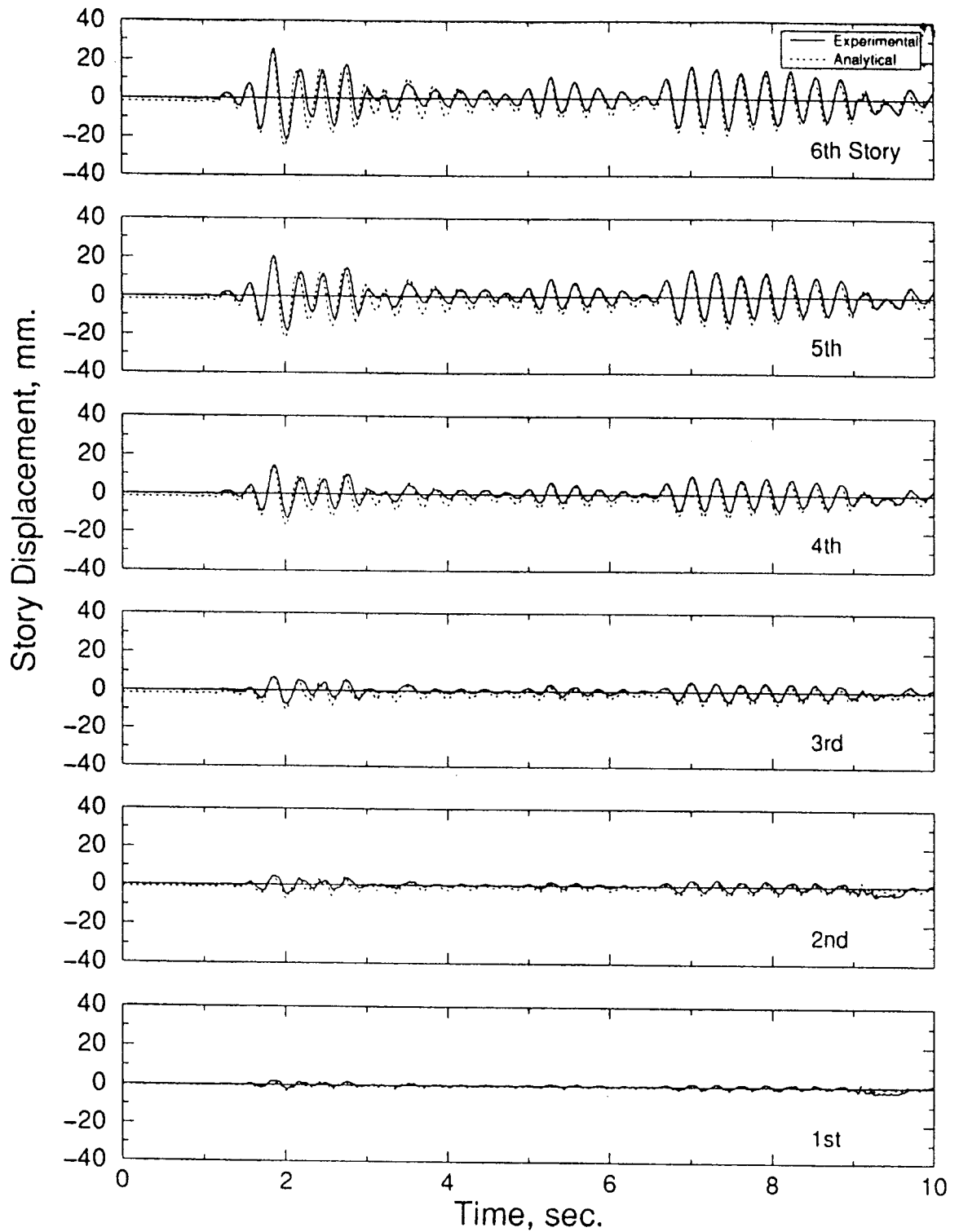


Figure 5-61 Experimentally observed and analytically predicted displacement time histories: B52EL40
Damping System: fuse-bars and dampers
Bracing: none
Earthquake: El Centro, PGA=0.40g

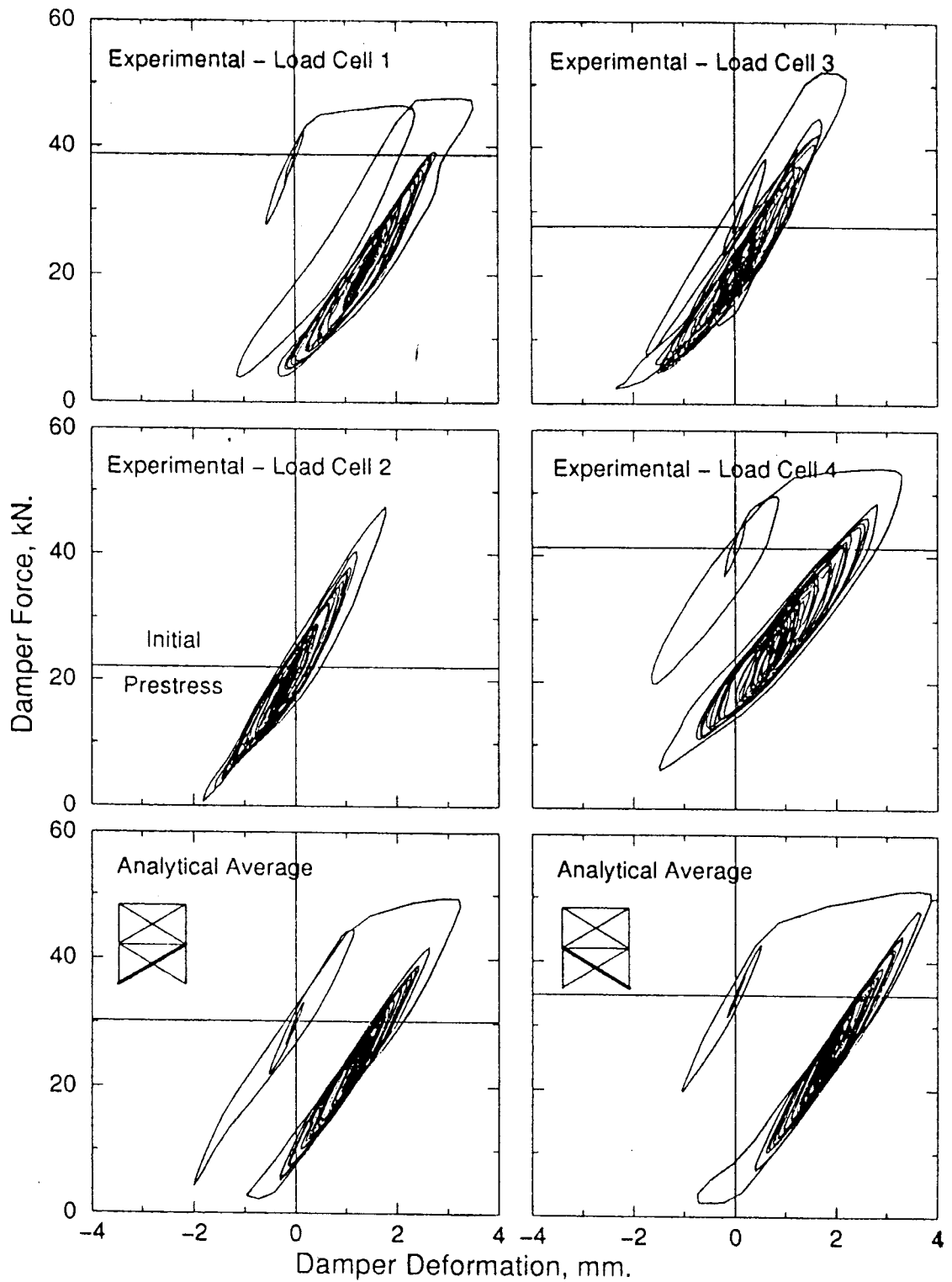


Figure 5-62 Experimentally observed and analytically predicted average tendon force-deformation: B52EL40
Damping System: fuse-bars and dampers
Bracing: none
Earthquake: El Centro, PGA=0.40g

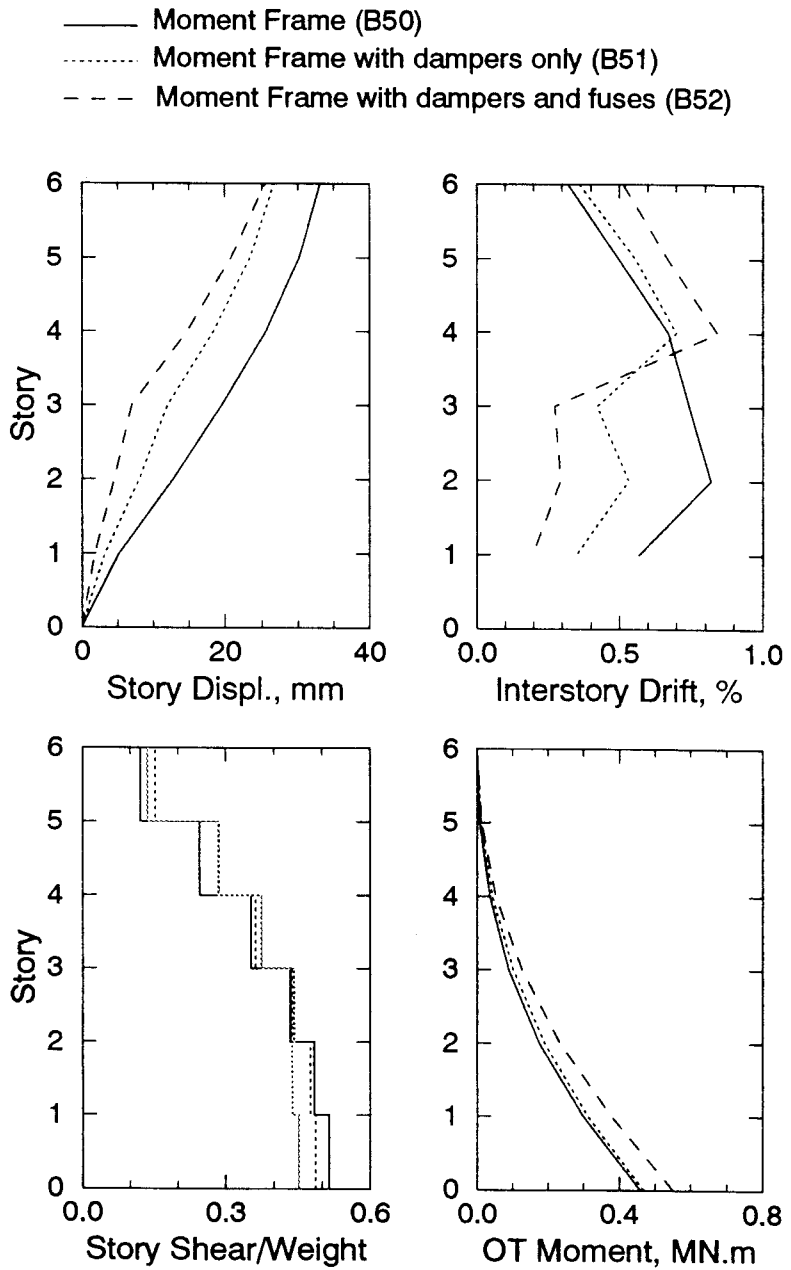


Figure 5-63 Maximum response envelopes for the moment frame structure and supplementary system active subjected to El Centro ground motion at various PGA levels

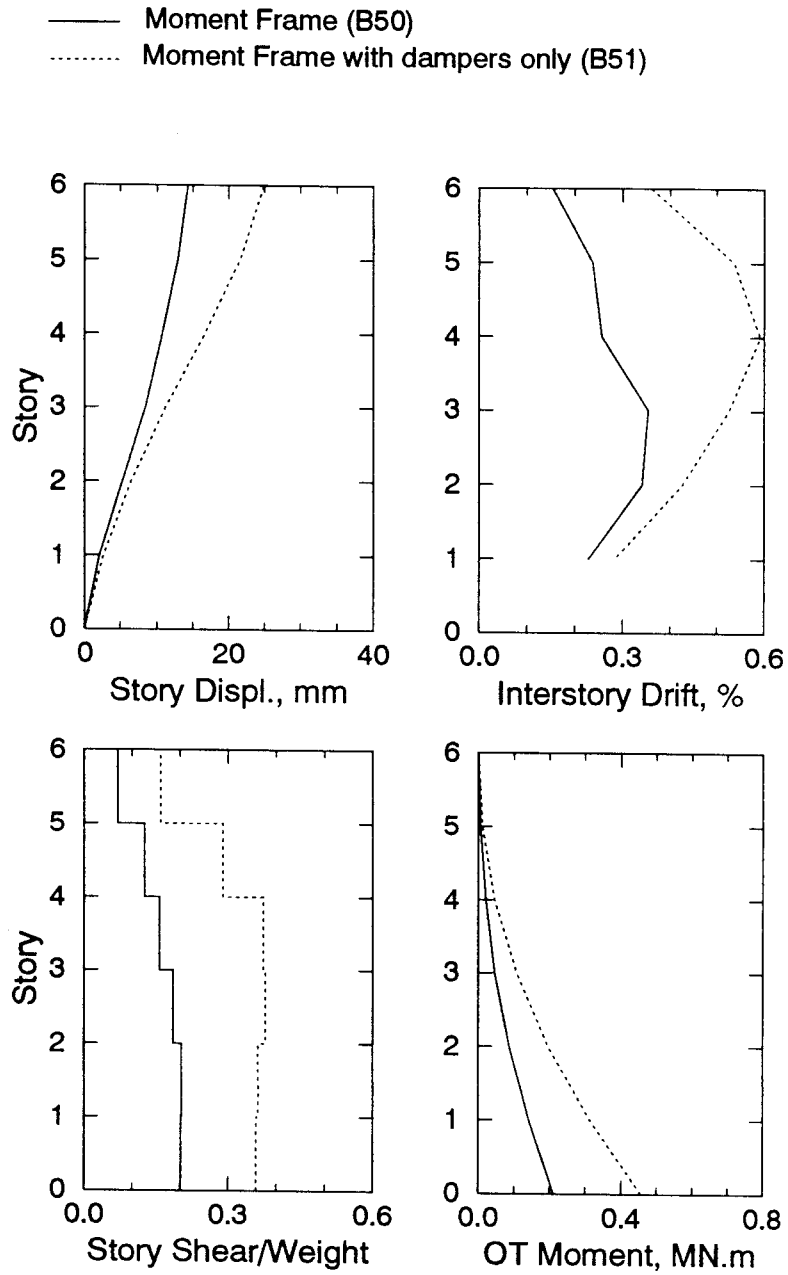


Figure 5-64 Maximum response envelopes for the moment frame structure and supplementary system active subjected to Sylmar ground motion at various PGA levels

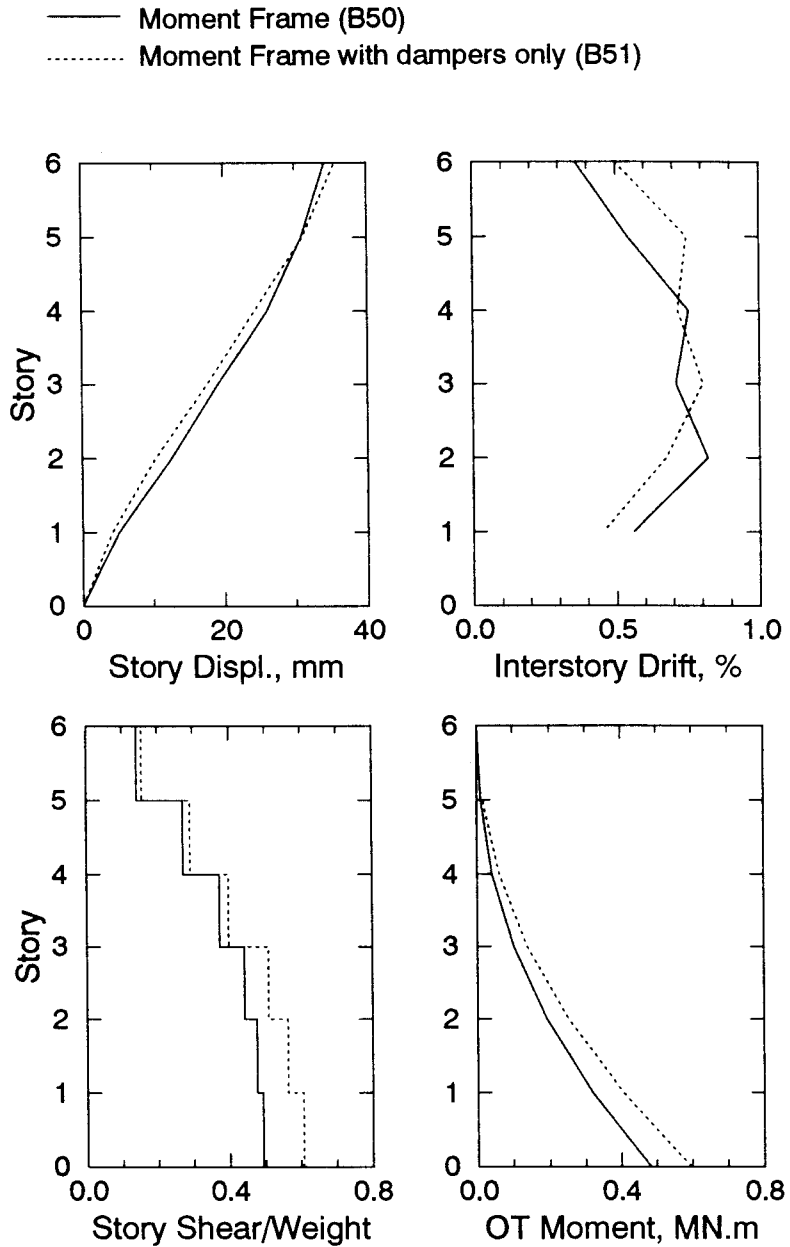


Figure 5-65 Maximum response envelopes for the moment frame structure and supplementary system active subjected to Kobe ground motion at various PGA levels

360 deg., and 1995 Great Hanshin - Kobe at various PGA levels. One of the major objectives of performing this experimental study was to investigate the effectiveness of an innovative supplemental *load balancing tendon-fuse+damper* damping system in mitigating the response of flexible building structures under pulse-type ground motions. Therefore, only the latter three ground motions formed the basis for experimental and analytical comparisons between different configurations. The computational model was used to predict the response of the structure at PGA levels of 0.4 to 0.5g in two different configurations: ESD devices only and bare frame (no supplemental system, with or without top story bracing). These predictions were compared to experimental response of the structure with the *load balancing tendon-fuse+damper* system.

Among the parameters investigated that have primary effect on the overall response are: a) bracings, b) ESD devices alone, c) *fuse+damper* system, d) tension only system and, e) prestress level. It must be noted that only one specific tendon configuration was tested. This configuration is by no means the optimum system in which the tendon layout should follow a specific shape that optimally balances the inertial forces. However, the tendon layout used in the shaking table tests is thought to best approximate the optimum layout. Therefore, this experimental study should be considered as the first step in investigating ways of overcoming a very important problem in both retrofitting and designing flexible structures

Based on the experimental and analytical results reported in the previous sections, the following conclusions are drawn:

1. ESD devices alone as well as *load balancing tendon-fuse+damper* system reduced the overall seismic response of the structure. Initial peak response due to pulse-type input motions are controlled better by the *load balancing tendon-fuse+damper* system. This observation is consistent with the fact that dampers were only partially effective during the early impulse response.
2. Added damping by either ESD devices alone or in the combined *fuse+damper* system was small mainly because of the relatively small deformations in the supplemental system. However, it is well known that high damping does not always mean improved response. In fact, for flexible structures even small amounts of added damping can reduce the structural response to acceptable limits. This is especially important in design and retrofit applications where optimum solutions are desired from both engineering and economical point of view.

3. Tension-only working tendon systems may be criticized as follows. When the tension is applied in later loading cycles (when the tendons are slack due to fuse yielding) the loading may be applied abruptly and may cause high accelerations through the height of the structure. A further concern is that the structure lacks redundancy. These drawbacks of tension-only systems can be overcome by prestressing the supplemental system together with the steel tendon. Depending on the initial prestress level, prestress helps delay, if not outright prevent, the systems' becoming slack. Thus, initial prestressing would eliminate, or at least significantly reduce the problems associated with the sudden loading of the supplemental system, as long as there is no appreciable creep or relaxation in the system. Furthermore, *load balancing tendon-fuse+damper* systems can be designed for and installed on the gravity load carrying-interior frames in all directions to achieve a redundant system.
4. When the supplemental system is prestressed to a level which is less than the preload in the elastomeric spring dampers (i.e $F < P_y$), the prestress force is transferred by a steel only system. In such cases there will be no creep losses in the system.
5. High strength steel tendons can provide the building with lateral strength very efficiently, making prestressed *load balancing tendon-fuse+damper* system an attractive alternative when lack of strength and stiffness are the main deficiencies of an existing building, especially against pulse-type earthquake loading. Increase in stiffness usually means increase in the story shear forces, however, as can be seen from the experimental results: although story shears stayed at about the same levels, total column shears were significantly reduced. In real prototype applications, shear forces can be safely transferred to the foundation level by the tendons and they can be attached to a specially designed anchorage built apart from the main structure. Moreover, tendons could be stressed and then encased in fireproof concrete filled ducts.
6. Fuse-bars were very effective in reducing the peak response at least to a level where the original structure responded at 2-3 times lower PGA inputs. As can be seen from the experimental results, fuse-bars yielded at high deformations. It is a common understanding that yielding in tension reduces the amount of initial prestress in the system. However, it does not necessarily lead to the total loss of the prestress. Therefore, fuse-bars can be allowed to yield without completely losing the prestress

force. In such cases, ESD devices act as a backup system and lock the prestress. This is consistent with the experimental observations as no prestress losses were recorded during the shaking table experiments.

SECTION 6

DISCUSSION OF STRUCTURAL RESPONSE AND COMPARATIVE EVALUATION

6.1 INTRODUCTION

This section is intended to provide an overall discussion on the structural response observed during the shaking table tests that were previously reported herein. Effects of the configurations tested on the behavior of the test structure are discussed referring to key response parameters. Analytical predictions are used to study the behavior under severe ground shaking since such input ground motions would cause catastrophic failure of the undamped structure. It is believed that the DRAIN-2DX model has been validated in the previous sections as an accurate computational tool. Accurate analytical models therefore allow comparative studies to be performed. Experimental response of the frames with “*load balancing tendon-fuse+damper system*” is compared with analytical predictions of the “dampers only” and “bare frame” cases for the same ground motion input. In doing so, El Centro, Sylmar and Kobe earthquakes, scaled to 0.419g (0.307g for the moment frame case), 0.505g and 0.432g PGAs respectively, were utilized as the comparative benchmark motions.

6.2 DISCUSSION OF STRUCTURAL RESPONSE AND ANALYTICAL EVALUATION

Experimental and analytical results are given in the previous sections. Assumptions adopted for the analytical modeling and analysis procedures for various cases are also described in detail. It was shown that analytical simulations can reproduce the experimentally observed behavior very closely. Hence, the above-mentioned analytical models are extensively used with confidence, to predict and to study the behavior of the test structure under other severe ground motions. It must be noted that three ground motions, namely, 1940 Imperial Valley - El Centro, 1994 Northridge - Sylmar County Hospital and 1995 Great Hanshin – Kobe are used in this comparative analytical study.

It is well known that even a slight increase in the damping value may be significantly beneficial for flexible building structures with small inherent viscous damping. However, pulse-type ground motions can result in early peak response that make it practically impossible to control by using regular damping systems, especially the latter two records which have a high

intensity over a relatively short duration. Such behavior is a unique feature of near-field ground motions. In general, near-field motions produce high acceleration, velocity and displacement responses over the long period range. Under such earthquake loading, excessive deformations may accumulate in the lower stories of flexible (long period) building structures which in turn may cause structural collapse. However, the *load balancing tendon-fuse+damper* system can be used to improve the stiffness characteristics by properly designing the sacrificial fuse-bars that will arrest the excessive displacements by improving lateral stiffness. ESD devices can be thought of a back-up system that will continue to function (after the fuse-bars have done their job) to damp out the rest of the response.

Experimental results have shown that the response of the structure is significantly improved by using the supplemental *load balancing tendon-fuse+damper* system. ESD devices when used alone as the damping system, produced response reductions that were less than but still comparable to those attained with the *load balancing tendon-fuse+damper* system in general. The peak response was controlled better by the *load balancing tendon-fuse+damper* system. However, PGA levels were selected such that the structure stayed elastic at all times. Therefore, it is realized that cases in which the moment frame structure would yield/collapse should be analytically investigated.

Another important parameter that affects the overall response is the amount of the initial prestress. Although it is evident from the experimental results that the response can be reduced by increasing the level of prestress, the effect of prestress should be further investigated with respect to the yield strength of the fuse-bars. Initial prestress is desirable for mainly three reasons: a) it removes any unwanted slack in the tendon system, b) it provides increase in lateral stiffness, c) the prestress doubles the effectiveness of the X-bracing, as both systems work together while the tension force is maintained. Depending on the initial prestress, fuse-bars may either yield early in the response history or stay elastic, which may or may not be desirable.

Experimental response of frames with *load balancing tendon-fuse+damper* system is compared with the analytical predictions of “dampers only” and “moment frame only” cases for the above mentioned ground motions. Top story displacement time histories, maximum story displacement, interstory drift, story shear and overturning moment envelopes are compared on

Table 6-1 Comparison of Maximum Responses – Upper Three Stories Braced

Ground Motion		El Centro (0.419g)			Sylmar (0.505 g)			Kobe (0.432 g)		
		D+F ¹	D ²	B ³	D+F	D	B	D+F	D	B
Configuration										
Top Displ. ⁴ (mm)		20.3 (51%)	27.5 (34)	41.8	18.2 (47)	23.8 (31)	34.3	18.2 (67)	39.9 (28)	55.5
B.S. ⁴ (kN)	Total	43.2 (15)	47.8 (6)	50.7	37.1 (1)	32.9 (13)	37.6	43.7 (17)	66.4 (-26)	52.9
	Column	5.13 (90)	33.2 (35)	50.7	1.77 (95)	18.0 (52)	37.6	12.6 (76)	44.6 (16)	52.9
OTM ⁴ (kN.m)		620 (-8)	520 (9)	570	570 (-7)	480 (9)	530	560 (14)	740 (-14)	650

¹ Dampers and fuses – Experimental

² Dampers only – Analytical,

³ Braced (top three stories) moment frame – Analytical

⁴ Values in parentheses are per cent reductions with respect to “B” configuration

Table 6-2 Comparison of Maximum Responses – Bare Frame Only

Ground Motion		El Centro (0.307 g)		
Configuration		D+F ¹	D ²	B ³
Top Displ. ⁴ (mm)		25.5 (40)	27.4 (35)	42.4
B. S. ⁴ (kN)	Total	35.9 (32)	45.2 (15)	52.9
	Column	1.57 (97)	30.0 (43)	52.9
OTM ⁴ (kN.m)		550 (-2)	520 (4)	540

¹ Dampers and fuses – Experimental

² Dampers only – Analytical

³ Bare-moment frame – Analytical

⁴ Values in parentheses are per cent reductions with respect to “B” configuration

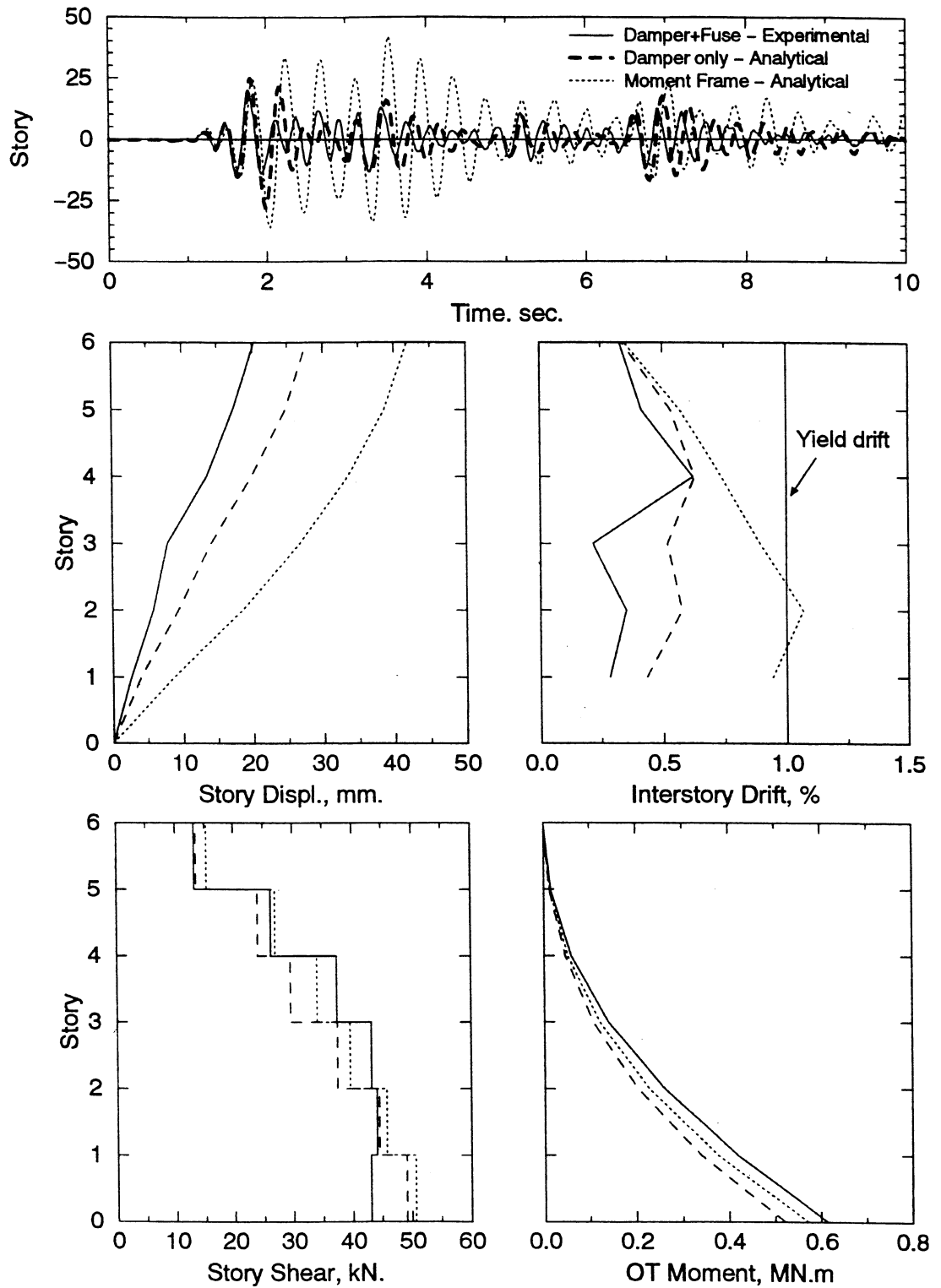


Figure 6-1 Comparison of response of the test structure subjected to severe ground motions (top three stories braced and damper only cases obtained analytically) – El Centro, PGA=0.419

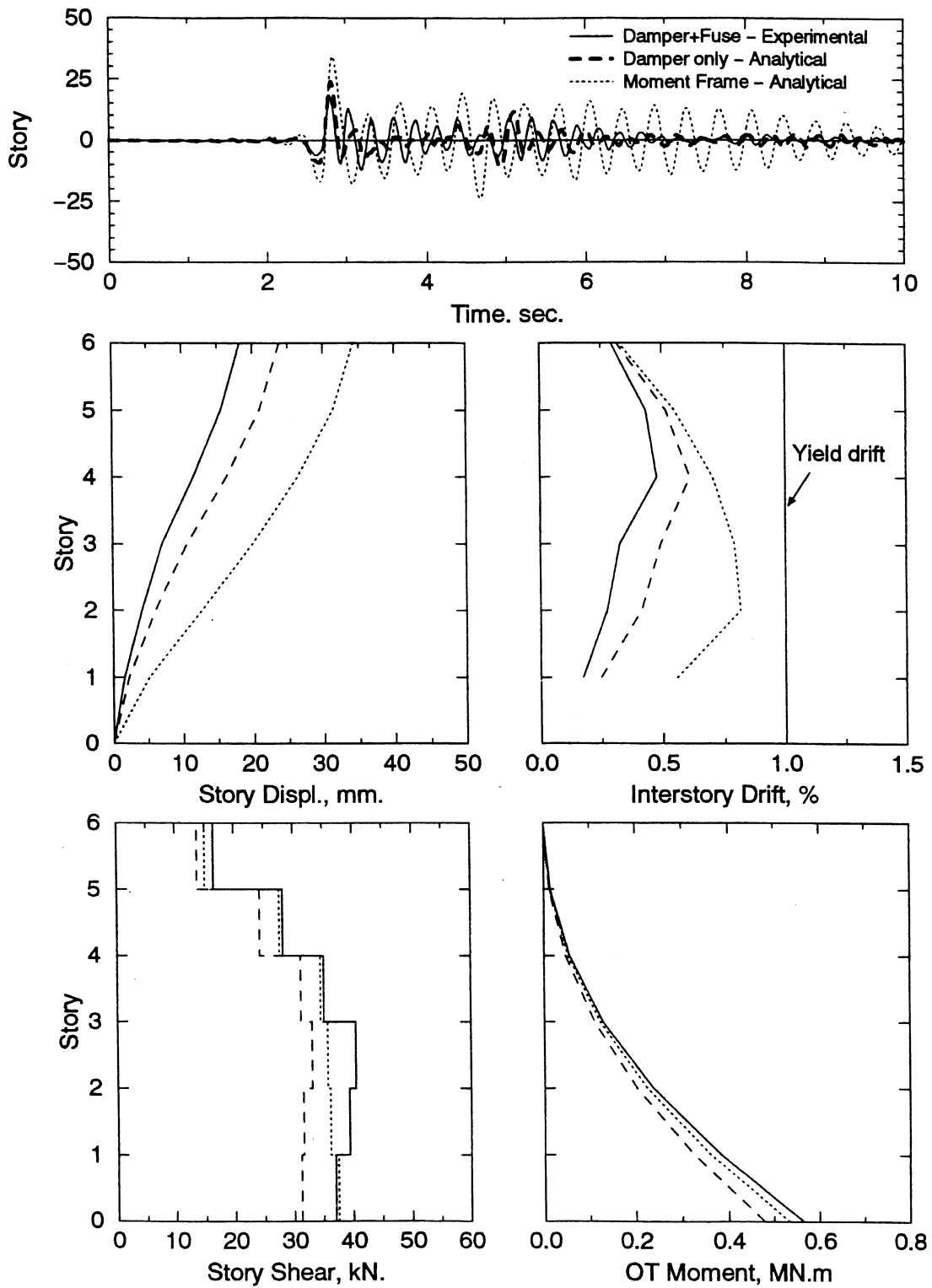


Figure 6-2 Comparison of response of the test structure subjected to severe ground motions (top three stories braced and damper only cases obtained analytically) – Sylmar, PGA=0.505

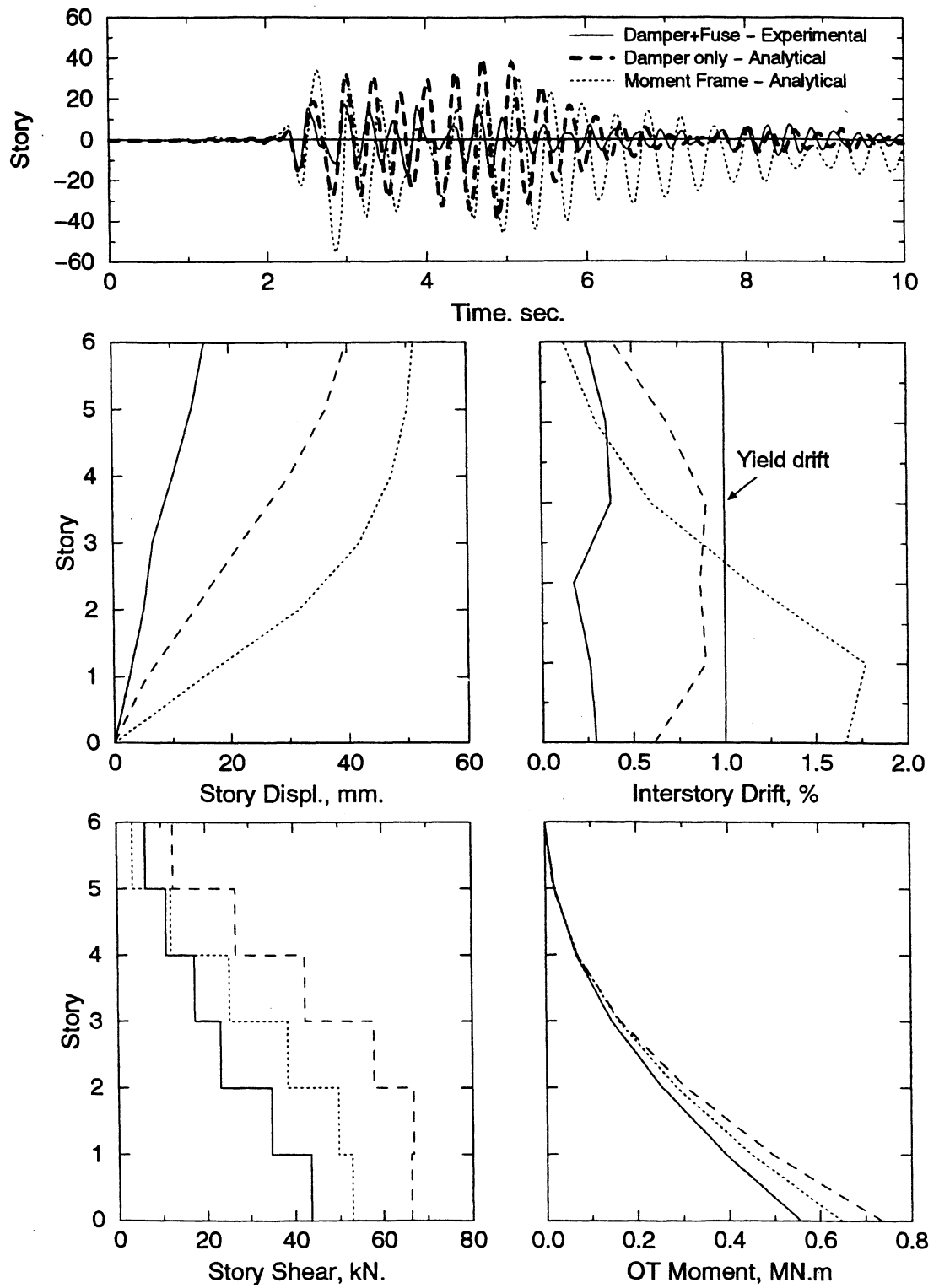


Figure 6-3 Comparison of response of the test structure subjected to severe ground motions (top three stories braced and damper only cases obtained analytically) – Kobe, PGA=0.432

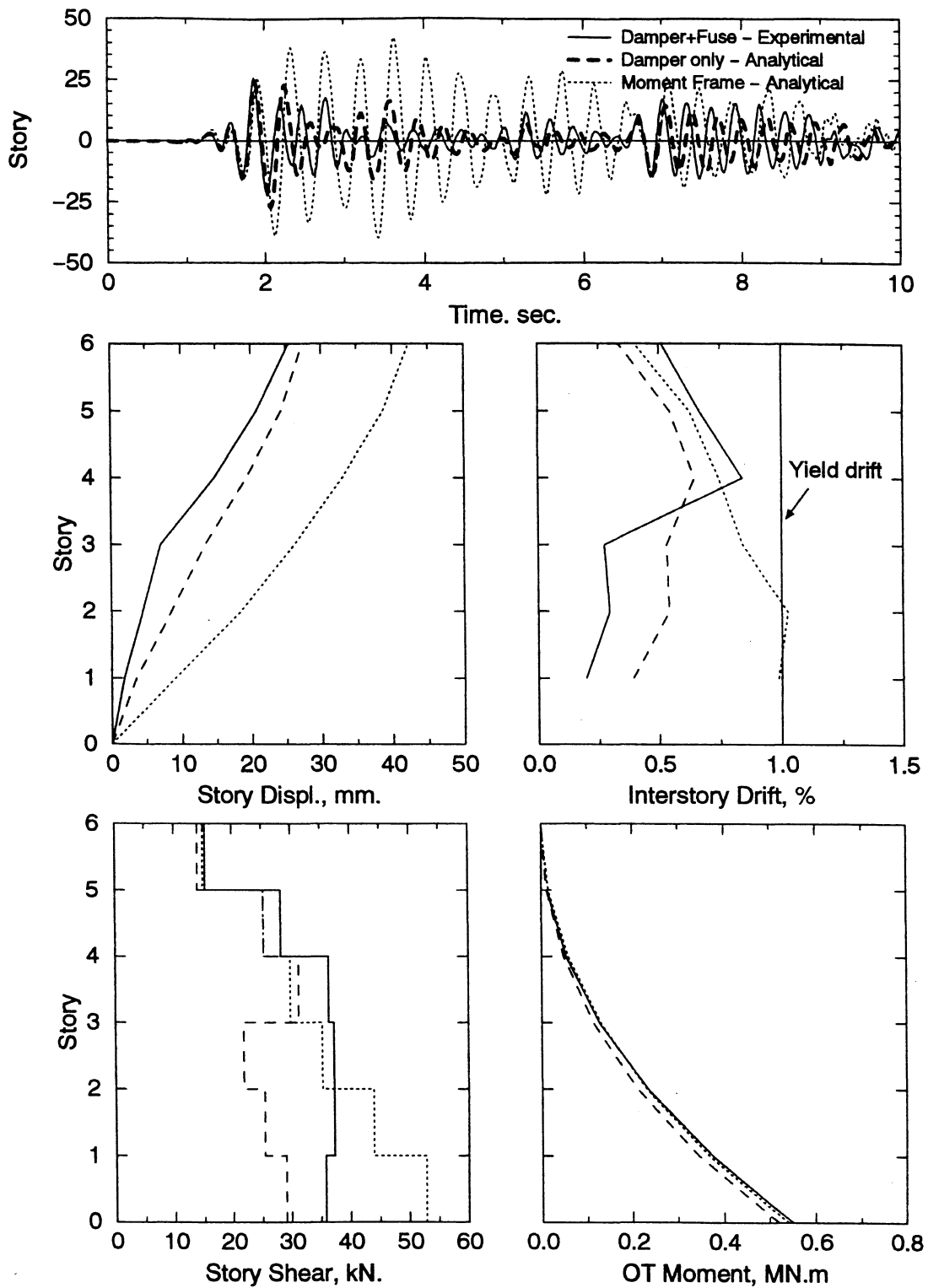


Figure 6-4 Comparison of response of the test structure subjected to severe ground motions (moment frame and damper only cases obtained analytically) – El Centro, PGA=0.307

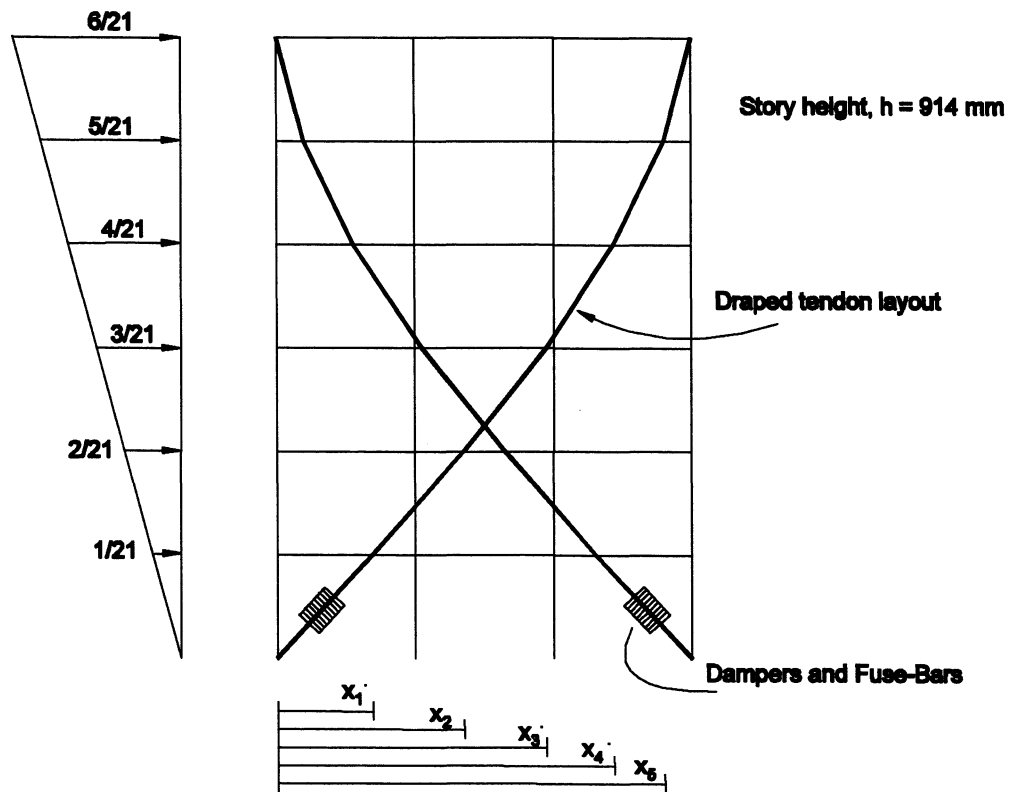
figures 6-1 through 6-4. Various peak responses are summarized on tables 6-1 and 6-2. Top floor displacement reductions were as high as 67% in case of Kobe earthquake. Interstory drifts are reduced as well, however both story displacement and interstory drift envelope plots suggest that stories where dampers are not “directly” effective (i.e. upper three stories) should be braced. Story shear response was marginally improved whereas overturning moments slightly increased. It must be noted here that the moment frame would suffer excessive yielding in all cases. Collapse is to be expected with a soft first story mechanism due to high deformation demands in the Kobe earthquake (figure 5-39). In general, early peak as well as rest of the response was reduced significantly. Finally, the same initial prestress levels recorded during the experiments were used in the simulations as well.

6.3 EFFECT OF TENDON PROFILE

Although the experiments described in this section possessed a straight tendon-fuse+damper profile, it is of interest to investigate (for this model) the improved effectiveness of a more precise load balancing tendon profile. On other words: what is the improved effectiveness of the tendon system if a draped profile is adopted compared to the straight profile used in these experiments? In an attempt to answer this question the results of a series of analytical studies are presented for the 1940 Imperial Valley - El Centro NS and 1995 Great Hanshin – Kobe ground motion records.

The optimum tendon layout is determined using the relationships given in Section 3 and shown in figure 6-5. Corresponding tendon layout geometry is tabulated in figure 6-5. Initial prestress levels are set to be equal to the corresponding experimental values as previously given.

The results of the analyses with the *load balancing draped tendon* system are compared with the analytical predictions of approximate straight tendon with “dampers” and “fuses+dampers” cases for the above mentioned ground motions. Top story displacement time histories, maximum story displacement, interstory drift, story shear and overturning moment envelopes are compared in figures 6-6 to 6-9. Although a considerable reduction in the maximum story deformations is evident in the upper stories, the reduction is marginal at the lower stories when compared to the straight tendon case. A similar observation can be made for the interstory drifts. This result was expected, since the straight tendon is not effective in the upper stories as previously mentioned. However, story-overturning moments as well as story



Location	X - coordinate (mm)
X_1	844
X_2	1648
X_3	2371
X_4	2974
X_5	3416

Figure 6-5 Load Balancing Draped Tendon Profile used in the Analytical Study

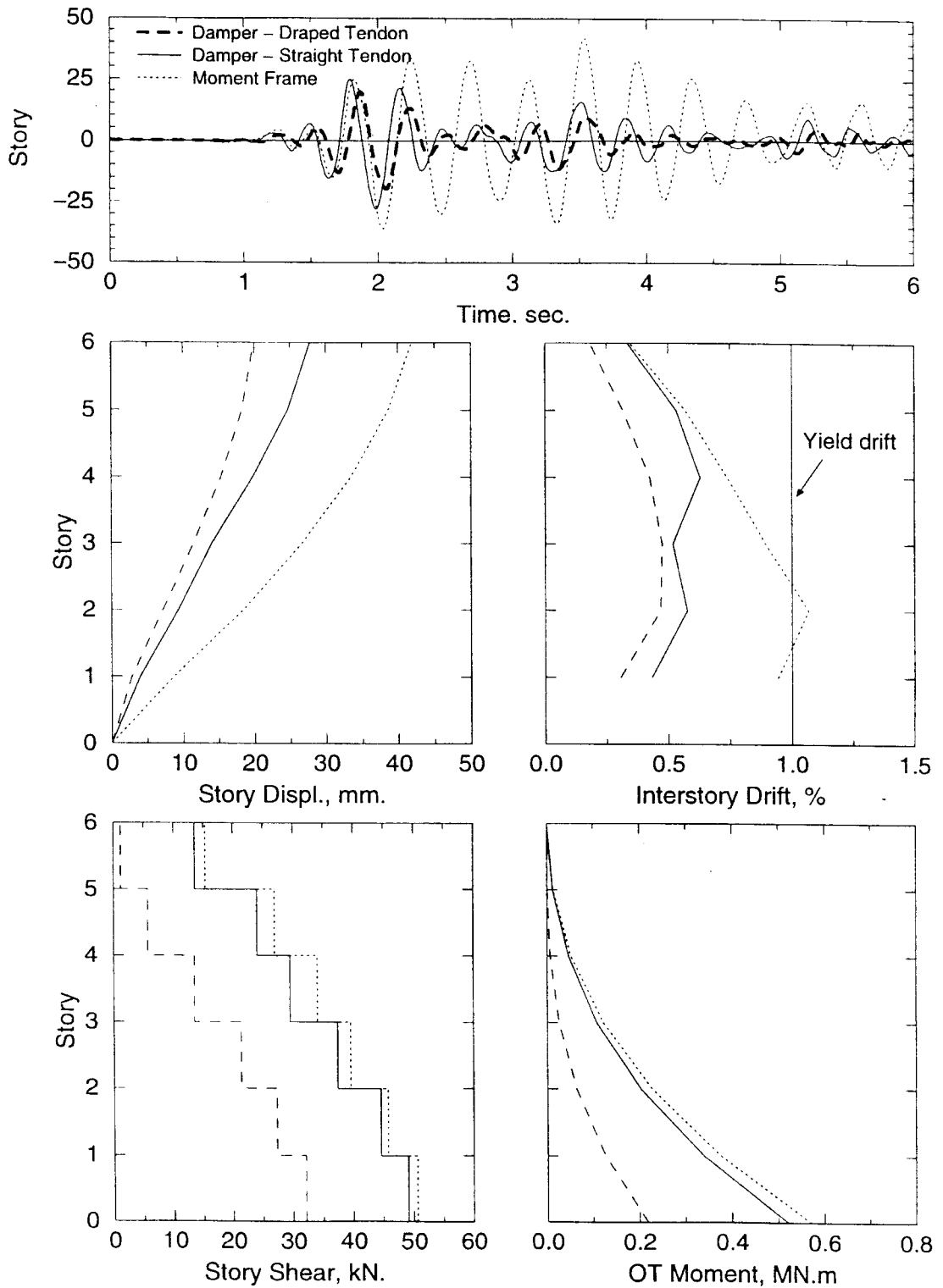


Figure 6-6 Comparison of response of the test structure retrofitted with straight and draped tendon profile with dampers only and subjected El Centro, PGA=0.307

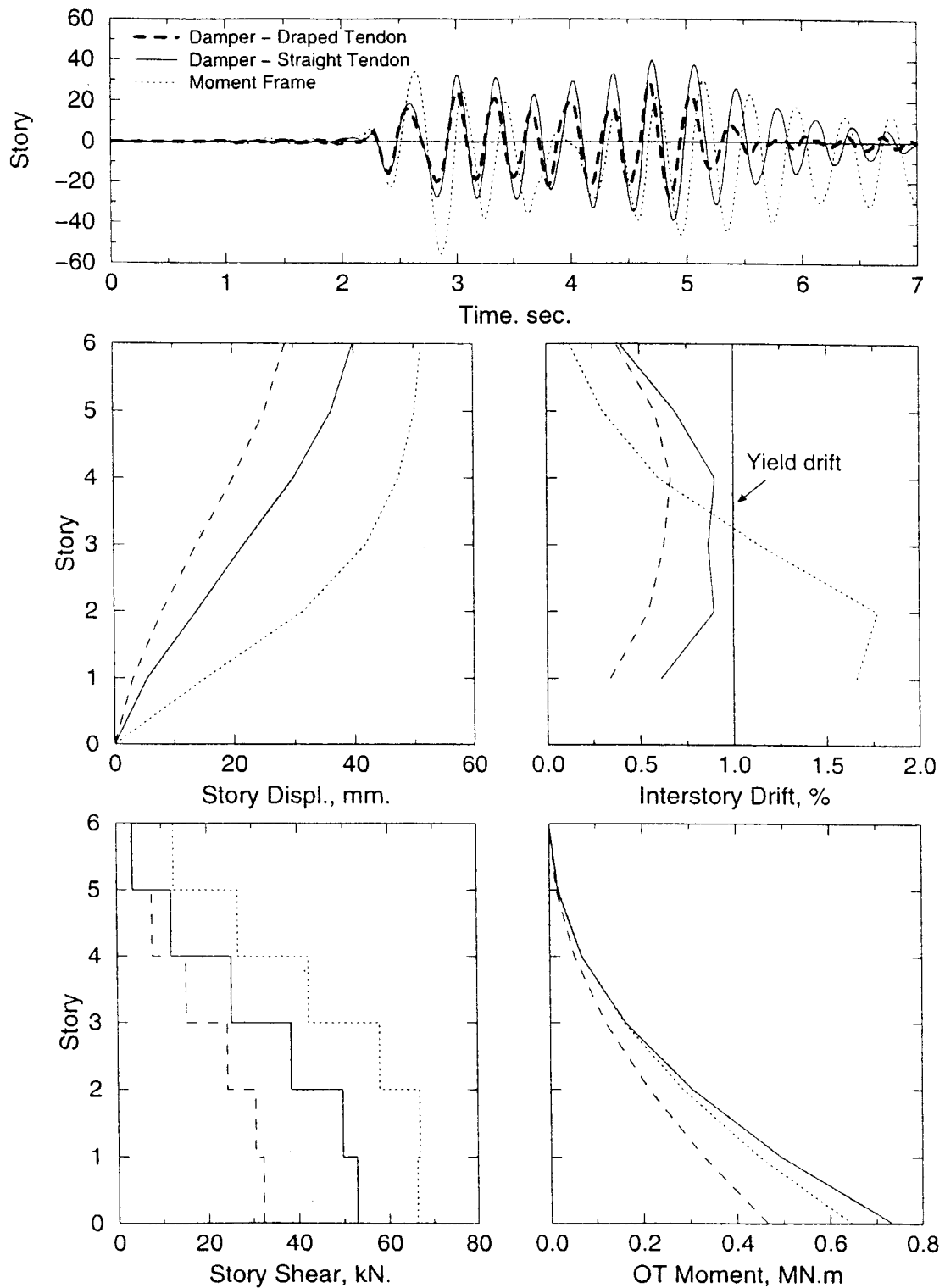


Figure 6-7 Comparison of response of the test structure retrofitted with straight and draped tendon profile with dampers only and subjected to Kobe, PGA=0.432

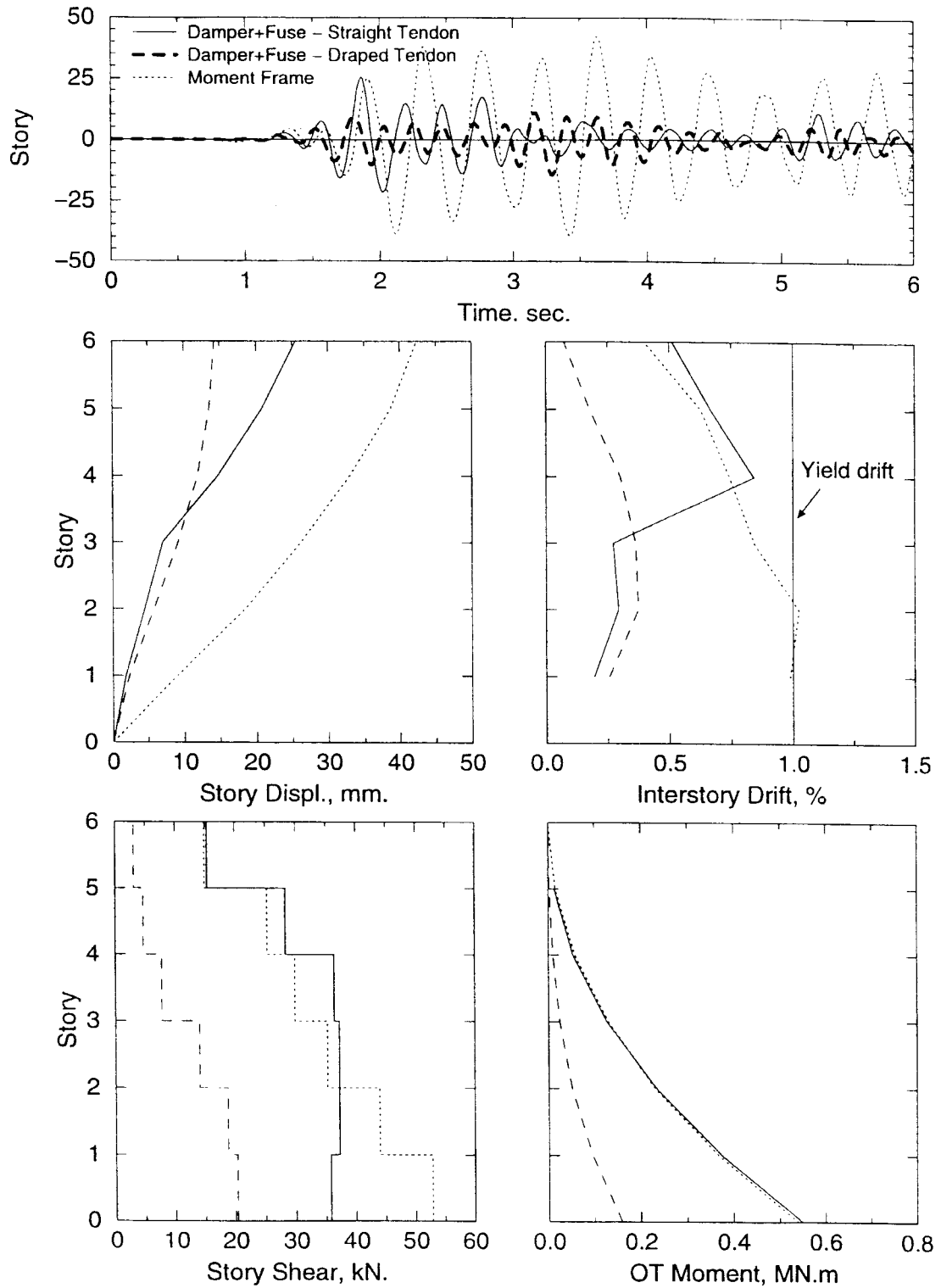


Figure 6-8 Comparison of response of the test structure retrofitted with straight and draped tendon profile with dampers+fuses and subjected to El Centro, PGA=0.307

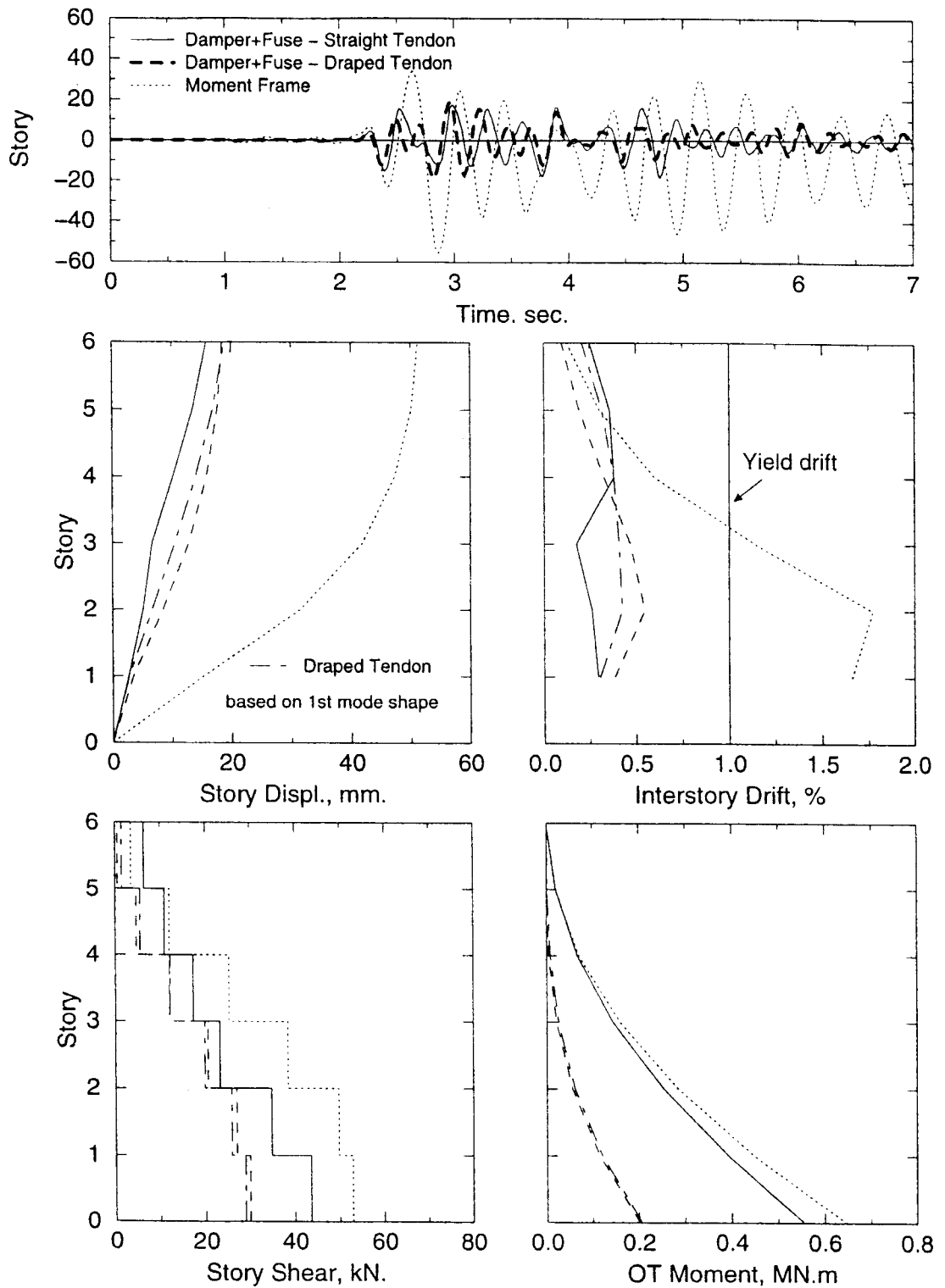


Figure 6-9 Comparison of response of the test structure retrofitted with straight and draped tendon profile with dampers+fuses and subjected to Kobe, PGA=0.432

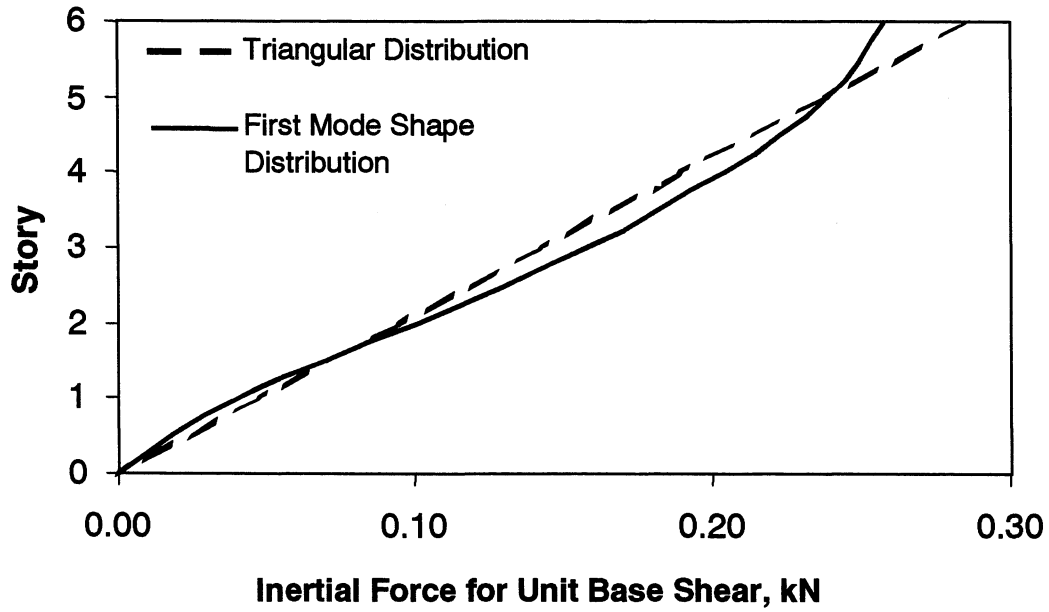


Figure 6-10 Balanced Inertial Loads Based on the Triangular Distribution and Proportional to the 1st Mode Shape for Unit Base Shear

shears are drastically reduced due to the more precise load balancing nature of the draped tendon layout.

It was found that the first mode shape of the structure with the draped tendon profile is very close to that of the moment frame. Normalized (for unit base shear) first mode shape is plotted on figure 6-10 together with the normalized-balanced triangular load pattern described above. It can be seen from the figure that the inertial loads are somewhat under-balanced by the triangular distribution at the 3rd and 4th floor levels. This observation agrees with the analytical results presented in figures 6-6 to 6-9, as the interstory drift response is greater at these levels. Therefore, a tendon layout, which balances the inertial loads that are proportional to the first mode shape, is determined and the analyses are repeated for Kobe and El Centro ground motions. The results of the case for Kobe with dampers and fuses are presented on figure 6-9 with dot-dashed lines. As can be seen from the figure interstory drifts are controlled better which results in a uniform profile. However, no improvement was observed in the other cases.

6.4 SUMMARY AND CONCLUSIONS

The enhanced DRAIN-2DX computational model provides reliable predictions for the behavior of flexible moment frame structures as was pointed out in the previous sections. Therefore, further dependable analytical studies can be carried out to investigate the effect of various parameters in the design of the presented *load balancing tendon-fuse+damper* system.

Analytical studies have shown the effectiveness of the load balancing draped tendon profile in reducing the overturning moments as well as story shears. It is evident from the experimental as well as analytical results that, in the upper stories where the supplemental system is not directly effective, bracings should be used, as the upper story deformations tend to amplify. Hence, this “whipping action” must be considered in the design.

Initial prestressing can significantly modify the distribution of internal forces (bending moments and axial forces) of structural elements. Depending on the prestress level, the magnitude of the induced forces due to prestressing may reach values that approach the capacity of the members. Therefore, this consideration may impose limitations to the level of initial prestress and should be carefully considered in the design and particularly in retrofit applications. However, several column-strengthening techniques exist which may be easily applied in such

cases. Moreover, gravity load carrying-interior frames usually have sufficient reserve axial capacity to accommodate these additional compressive loads.

SECTION 7

SUMMARY, CONCLUSIONS AND RECOMMENDATIONS

7.1 EXECUTIVE SUMMARY

The study reported herein consisted of two major stages: i) concept development, ii) concept verification. In the first stage, design/retrofit alternatives were developed from a performance-based engineering point-of-view. The conceptual development was based on fundamental structural engineering principles. The second stage involved both an experimental and analytical investigation of the seismic response of a typical steel moment frame model structures retrofitted with a special type of seismic energy dissipation device, namely, elastomeric spring damper (ESD). Also tested was a load balancing system composed of a combined supplemental system in which ESD devices were used in parallel with sacrificial fuse-bars for improved stiffness. The experiments were intended to provide experimental data, which then were used to verify/improve alternative design concepts. Each of the above-mentioned stages is summarized in what follows.

Computational Modeling

The component tests performed on the ESDs revealed their mechanical properties. A simple two-component nonlinear computational model was then developed to model the velocity dependent force-deformation behavior of these devices. The model consists of a bilinear element that captures the stiffness characteristics of the elastomer and the preload in the device. The second component is velocity dependent (semi-viscous) element, which simulated the distinct re-centering capability of ESDs. Hence, the component tests were used in the development as well as in the calibration of the computational model.

The model was incorporated into the nonlinear time history analysis program DRAIN-2DX. Two solution methods were introduced namely, a one-step correction method and an iterative solution method. In the former, device response was calculated based on the current deformations in the structure and considered as pseudo forces in the next time step of the time history analysis. This solution method had its drawbacks in which the unbalanced forces that are carried over from the previous time step may cause numerical instability when in large systems

and with excessive structural yielding. In order to improve and avoid numerical instability, an iterative solution technique was employed. The computational model was modified by adding a spring element in series with the spring-damper element. Hence, a differential force-deformation relationship was formulated for the improved model. The differential equation for the device force was solved using a Runge-Kutta method. The time history analysis program (DRAIN-2DX) was then modified to iteratively solve the system equations of motion. Consequently, these models were utilized in analytically identifying the structural response observed in the subsequent experimental studies.

Concept Development of Design/Retrofit Alternatives

Two design and/or retrofit alternatives were introduced: “Damper-Truss Solution (DTR)” and a “Load Balancing Prestressed Tendon Fuse+Damper Solution (PTFD).” The former approach was thought as an extension to present practice of using story-by-story cross-braced damper configuration. The size of each damper was determined based on the story shear at the corresponding story level. The second solution approach was based on the concept of load balancing which is widely employed in prestressed concrete beam technology. The system is designed to work in tension only and is composed of two major components: a prestressed tendon with high axial stiffness and a supplementary damping/stiffness system located, e.g. at the foundation level. The layout is piecewise continuous and draped in the shape of overturning moment diagram induced by the assumed inertial forces at each floor level.

The supplemental system consists of energy dissipators (preferably with a preload capability) and sacrificial fuse-bars with a prescribed initial stiffness and displacement ductility. The damping forces generated in the supplemental system are transferred to the floor slabs opposing inertial loads. The prestressed tendon layout is preferably designed to counteract the inertial forces hence to reduce the overturning moments; a draped tendon results. However, a linear tendon profile may be used as a simplification of the lateral load balancing concept.

Experimental Verification

A sets of shaking table experiments were conducted on a 1/4 scale – 6-story steel moment frame structure. The physical model was tested on the shaking table at the University at Buffalo, SUNY.

A total of seven different retrofit configurations were tested on the model steel structure with braces, with and without the supplemental system (PTFD). In this experimental study, instead of a draped tendon configuration (which would ideally follow the shape of the overturning moment diagram), a straight tendon layout was used. This layout was considered to be a reasonable approximation to the optimal draped layout. Aspects of using tension-only systems were investigated forming the basis for further analytical studies.

This study provided valuable experimental databases that were used to validate the computational modeling strategies. The experiments served not only in the verification of the design/retrofit concepts that are developed elsewhere (Pekcan et al. , 1998) but also in the improvement and identification of possible drawbacks.

7.2 CONCLUSIONS

The important conclusions drawn and observations made are listed under in what follows.

1. Elastomeric Spring Dampers (ESD) reduced the overall seismic response of the tested structures while reducing the peak responses as well.
2. ESD show high initial stiffness characteristics until the preload in the device is overcome after which the elastomeric stiffness prevails. When these devices are used especially as damper braces, this contributes to the overall structural system stiffness. However, experimental results have shown that the energy dissipation contribution of the devices more than compensated for the effects of the increased stiffness.
3. High initial stiffness is considered to be beneficial under minor ground motions as well as wind loading. In fact, stiffening of the structure leads to further reduction of deformations but at the expense of increased acceleration response.
4. In designing a supplemental system for building structures, the altered load-path compared to the bare structure must be carefully traced and addressed in both design and retrofit applications. In all of the cases, it is evident that a truss action is desirable in the combined structural-supplemental damping system.
5. While the self-centering characteristics of ESD devices should eliminate any permanent deformations in yielding structures, it also has a positive contribution in reducing the maximum response along with added damping.
6. Tension-only tendon systems may be open to criticism. This is because when tension is applied in second and subsequent loading cycles the loading may be applied abruptly and may

cause high accelerations through the height of the structure. A further concern is that the structure lacks redundancy. These drawbacks of a tension-only system can be overcome by prestressing the supplemental system with the use of high-strength steel tendons. Depending on the initial prestress level, it may help delay the system in becoming slack. Thus, initial prestressing might eliminate or at least significantly reduce the problems associated with sudden loading of the supplemental system. Load-balancing tendon-fuse+damper systems can be designed for and installed on the gravity load carrying-interior frames in all directions to achieve a redundant system.

7. Tension-only supplemental systems can be effectively implemented in the design of flexible frame structures as an economical feasible solution. However, it must be noted here that the supplemental system should be initially prestressed up to a prescribed level and that the devices should have preload in order to accommodate the applied prestressed forces.

8. The load-balancing technique in the seismic design/retrofit of buildings proved to be promising as the seismic response was reduced considerably even by the approximate straight tendon solution implemented in the experimental study.

9. Improved response due to presence of sacrificial fuse-bars was evident compared to damper-only tendon system. High initial stiffness of the fuse-bars provided increased capacity while at larger deformations damping due to yielding was supplemented by the dampers hence reduced the response.

10. Although the system was initially prestressed to avoid the tendons becoming slack and cause undesirably high accelerations due to sudden loading during the ground shaking, floor accelerations were amplified especially at the upper stories where the tendon forces were not directly effective.

11. Flexibility of the prestressed tendon and its anchorages should be carefully considered in the design of such systems since it has a direct effect on the effectiveness of the supplemental system.

12. Unequal prestress in the tendons on either side of the frame structure must be avoided since this will cause undesirable torsional response of the structure.

13. When the supplemental system is prestressed to a level which is less than the preload in the elastomeric spring dampers (i.e $F < P_y$), the prestress force is transferred by a steel only system. In such cases there will be no creep losses in the system.

7.3 FUTURE RESEARCH RECOMMENDATIONS

1. Both the experimental and the analytical studies reported in this report suggest that load-balancing approach is a promising retrofit and design alternative in mitigating the seismic response of building structures. However, since the basic concept has emanated from the fundamentals of structural engineering, it is believed that the method can be employed equally well in other engineered structures (such as bridges etc.) but some modifications to the design theory may be needed. For example tension-only straight tendons with or without supplemental systems can be used to transfer the inertial loads on the superstructure of a bridge to the substructure by-passing the supporting bearings. In fact, the efficacy of this approach was recently investigated analytically by Ye (1998). However, experimental studies should be undertaken to further validate the approach and investigate the effect of various configuration details on the seismic response of such structures.
2. As was mentioned previously, determination of the optimum tendon layout for building structures is not an easy task for especially tall-flexible structures for which the higher mode effects may be significant. However, it is believed that if the higher mode effects are eliminated by other means such as bracing etc., a prestressed-draped tendon system can be effectively employed in seismic design/retrofit.
3. Three-dimensional response of structures with load balancing tendons may pose important problems if it is not carefully considered in the design. Fuse-bars are designed to yield under a major ground motion shaking. Hence, after the first major peak response, stiffness characteristics and distribution in the structure will be modified due to yielding of the fuse-bars. This difference in stiffness is likely to promote torsional response. Therefore, the overall supplemental system should be designed to accommodate the undesired torsional effects. Moreover, three-dimensional non-linear analysis tools should be developed and used in the analytical investigations of this phenomenon.

SECTION 8


REFERENCES

- Al-Hussaini, T.M., Zayas, V.A., Constantinou, M.C., (1994), "Seismic Isolation of Multi-Story Frame Structures Using Spherical Sliding Isolation Systems," *Technical Report NCEER-94-0007*, National Center for Earthquake Engineering Research, SUNY at Buffalo, March.
- Chopra. A.K., (1995), "Dynamics of Structures", Prentice Hall, Inc.
- Clough, R.W., Penzien, J., (1993), "Dynamics of Structures," McGraw-Hill, Inc., 2nd Edition, New York, USA.
- Constantinou, M.C., Symans, M.D., Tsopelas, P., and Taylor, D.P., (1993), "Fluid Viscous Dampers in Application of Seismic Energy Dissipation and Seismic Isolation," *Proceeding of Seminar on Seismic Isolation, Passive Energy Dissipation, and Active Control, ATC 17-1*, Vol.2, pp. 581-592.
- FEMA 273, (1997) "NEHRP Guidelines for the Seismic Rehabilitation of Buildings," *Federal Emergency Management Agency*.
- FEMA 274, (1997) "NEHRP Commentary on the Guidelines for the Seismic Rehabilitation of Buildings," *Federal Emergency Management Agency*.
- Gluck, N., Reinhorn, A.M., Gluck, J., and Levy, R., (1996), "Design of Supplemental Dampers for Control of Structures," *Journal of Structural Engineering, ASCE*, Vol. 122, No.12, pp.1394-1399.
- Hall, J.F., Heaton, H.T., Marvin, W.H. and Wald, D.J., (1995), "Near-Source Ground Motion and its Effects on Flexible Buildings," *Earthquake Spectra*, Vol. 11, No. 4, pp. 569-605, November 1995.
- Lin, T.Y., (1955), "Design of Prestressed Concrete Structures", 2nd Edition, John Wiley & Sons.
- Menegotto, M., and Pinto, P.E., (1973), "Method of Analysis for Cyclically Loaded Reinforced Concrete Plane Frames Including Changes in Geometry and Non-elastic Behavior of Elements Under Combined Normal Forces and Bending", *IABSE Symposium on the*

Resistance and Ultimate Deformability of Structures Acted on by Well-Defined Repeated Loads, Lisbon.

- Mokha, A.S., Constantinou, M.C., and Reinhorn, A.M., (1990), "Experimental Study and Analytical Prediction of Earthquake Response of Sliding Isolation System with a Spherical Surface," *Technical Report NCEER-90-0020*, National Center for Earthquake Engineering Research, SUNY at Buffalo, October.
- Newmark, N.M., (1959), "A method of Computation for Structural Dynamics," *Journal of Structural Engineering Mechanics Division, ASCE*, Vol. 85, No. EM3, pp.67-94.
- Newmark, N.M., and W.J. Hall, (1982), "Earthquake Spectra and Design," *Earthquake Engineering Research Institute*, Oakland, California.
- Park, Y.J., Reinhorn, A.M., and Kunnath, S. K., (1987), "IDARC 2D: Inelastic Damage Analysis of Reinforced Concrete Frame - Shear-Wall Structures", Technical Report NCEER-87-0008, State University of New York at Buffalo.
- Park, Y.J., and Ang, A.H.S., (1985), "Mechanistic Seismic Damage Model for Reinforced Concrete," *Journal of Structural Engineering, ASCE*, Vol.111, No.4, pp. 722-739.
- Pekcan G., Mander, J.B., Chen, S.S., (1995), " Experimental Performance and Analytical Study of a Non-Ductile Reinforced Concrete Frame Structure Retrofitted with Elastomeric Spring Dampers,". *Technical Report NCEER-95-0010*, National Center for Earthquake Engineering Research, SUNY at Buffalo, July.
- Pekcan G., Mander, J.B., Chen, S.S., (1998), "Fundamental Considerations in the Design of Supplemental Damping Systems for Building Structures," (submitted) "will replace by NCEER #2 --- still submitted.
- Prakash, V., Powell, G.H., Filippou, F.C., (1992), "Drain-2DX: Base Program User Guide," *Report No. UCB/SEMM-92/29*, University of California at Berkeley, December.
- Reinhorn, A.M., Soong, T.T., Lin, R.C., Wang, Y.P., (1989), "1:4 Scale Model Studies of Active Tendon Systems and Active Mass Dampers for Aseismic Protection," *Technical Report NCEER-89-0026*, National Center for Earthquake Engineering Research, SUNY at Buffalo, November.


- Reinhorn, A.M., Li, C., Constantinou, M.C., (1995), "Experimental and Analytical Investigation of Seismic Retrofit with Supplemental Damping, PART I: Fluid Viscous Damping Devices," *Technical Report NCEER-95-0001*, National Center for Earthquake Engineering Research, SUNY at Buffalo, January.
- Rosenbrock, H.H, (1963), "Some General Implicit Process for the Numerical Solution of Differential Equations," *Computer Journal*, Vol. 5, No. 4, pp. 329-330, January.
- SAC, (1995), *Interim Guidelines: Evaluation, Repair, Modification and Design of Steel Moment Frames*, Report No. SAC-95-02, California, USA.
- SEAONC, Structural Engineers Association of Northern California, (1993), "Tentative Seismic Design Requirements for Passive Energy Dissipation Systems," draft, San Francisco, California.
- Shen, K.L., and Soong, T.T., (1996), "Design of Energy Dissipation Devices Based on Concept of Damage Control," *Journal of Structural Engineering*, Vol. 122, No.1, pp. 76-82.



MULTIDISCIPLINARY CENTER FOR EARTHQUAKE ENGINEERING RESEARCH

A National Center of Excellence in Advanced Technology Applications

University at Buffalo, State University of New York
Red Jacket Quadrangle ■ Buffalo, New York 14261-0025
Phone: 716/645-3391 ■ Fax: 716/645-3399
E-mail: mceer@acsu.buffalo.edu ■ WWW Site: <http://mceer.buffalo.edu>



University at Buffalo *The State University of New York*

ISSN 1520-295X